P-09-62

Oskarshamn site investigation

HLX28 large-scale confirmatory multiple-hole tracer test and hydraulic interference test

Pernilla Thur, Calle Hjerne, Jan-Erik Ludvigson,
Tomas Svensson, Rune Nordqvist

Geosigma AB

July 2010

Svensk Kärnbränslehantering AB
Swedish Nuclear Fuel
and Waste Management Co

Box 250, SE-101 24 Stockholm
Phone +46 8 459 84 00

ISSN 1651-4416
SKB P-09-62

Oskarshamn site investigation

HLX28 large-scale confirmatory multiple-hole tracer test and hydraulic interference test

Pernilla Thur, Calle Hjerne, Jan-Erik Ludvigson
Tomas Svensson, Rune Nordqvist

Geosigma AB

July 2010

Keywords: HLX28, HLX32, HLX37, HLX38, KLX11A, KLX19A, KLX20A, KLX27A, Tracer test, Dilution test, Pumping test, Hydraulic interference test, Transport parameters, Hydrogeological model, AP PS 400-08-016.

Abstract

A large-scale tracer- and hydraulic interference test as well as several groundwater flow measurements have been conducted within the Oskarshamn site investigation area. The aims of the tests were to partially verify the hydrogeological model of the Oskarshamn investigation area and, if possible, to determine transport properties for some major flow paths in the area.

Pumping was carried out in borehole HLX28 for 125 days between January and May 2009, with a flow rate of 300 L/min. Groundwater flow measurements were performed in ten borehole sections before and after start of pumping. Non-sorbing tracers were injected in six isolated sections in six different surrounding boreholes. The straight-line distance from the injection sections to the pumping borehole varied between 122 m and 702 m. The injections were performed through an exchange procedure without excess pressure.

Groundwater flow rate responses to pumping in HLX28 were in general rather weak. Only four of the ten sections displayed an increase in the flow rate with more than a factor of two during pumping in HLX28. No clear correlation between the flow response due to pumping and the distance from HLX28 was found, which might indicate a heterogeneous system. The groundwater flow measurements were useful as indicators of connectivity and for design of the tracer test.

Clear tracer breakthrough was observed from tracer injections in HLX32:2, HLX37:1 and HLX38:3. No increased levels of tracers could be detected prior to pump stop from tracer injections in KLX11A:3 and KLX20A:5. In the case of KLX27A:6, it was difficult to firmly determine whether tracer breakthrough had occurred or not. An advection-dispersion model for a single pathway was used for evaluation of tracer breakthrough. Calculated mass balance apertures are relatively large considering estimated values of transmissivity and results from previous tracer tests.

Hydraulic responses to pumping were detected in 63 out of 266 observation sections. In 53 of these sections, the responses were classified as clear and in 10 sections as weak. Transient evaluation was made for 61 sections. The transmissivity of the pumping section in HLX28 was estimated to be $3.0 \cdot 10^{-4}$ m^2/s.

The hydraulic responses to the pumping show a tendency to be stronger north of HLX28 than in other directions. In particular, the zone ZSMNS001C appears to act as a hydraulic barrier since no sections located to the west of the zone responded during the test. Sections corresponding to ZSMNW042A in the vicinity of HLX28 showed responses, although not significantly stronger than other sections in the area. Data indicates that ZSMNW042A and also to some degree ZSMNS059A, may act as hydraulic barriers, although this is not indicated as clearly as for ZSMNS001C. Tracer breakthrough data indicate that all three of the zones ZSMNS001C, ZSMNW042A and ZSMNS059A were involved in the transport of tracers from injection sections to HLX28.

Sammanfattning

Ett storskaligt hydrauliskt interferenstest i kombination med spårförsök och grundvattenflödesmätningar har genomförts inom platsundersökningsområdet i Oskarshamn. Syftet vara att partiellt verifiera den hydrogeologiska modellen över Oskarshamns undersökningsområde och om möjligt bestämma transportegenskaper för några mer betydande transportvägar i området.

Pumpning utfördes i borrhål HLX28 under 125 dygn mellan januari och maj 2009 med ett flöde av 300 L/min. Grundvattenflödesmätningar gjordes i tio utvalda borrhålssektioner både före och efter pumpstart i HLX28. Icke-sorberande spårämnen injicerades i sex borrhålssektioner i sex olika borrhål. Avståndet från injiceringssektionerna till HLX28 var mellan 122 och 702 m. Injiceringarna utfördes genom utbyte utan pålagt tryck.

Responsen på pumpningen i HLX28 med avseende på grundvattenflöde var generellt sett relativt svag. Endast fyra av tio sektioner uppvisade en flödesökning med faktor 2 eller mer under pumpningen i HLX28. Ingen tydlig korrelation mellan flödesrespons och avstånd till HLX28 kunde hittas vilket skulle kunna indikera ett heterogent system. Grundvattenflödesmätningarna var användbara som indikatorer på konnektivitet och för design av spårförsöket.

Ett tydligt spårämnesgenombrott i HLX28 från injiceringarna HLX32:2, HLX37:1 och HLX38:3 kunde konstateras. Ingen förhöjd koncentration av spårämne som injicerats i KLX11A:3 och KLX20A:5 kunde detekteras under pumpningen. Avseende KLX27A:6 var det svårt att med säkerhet avgöra om spårämnesgenombrott skett eller ej. En advektion-dispersionsmodell för en enskild flödesväg användes för utvärderingen av spårförsöket. Massbalansaperturen beräknad från utvärderingen var stor med hänsyn till den beräknade transmissiviteten och resultat från tidigare genomförda spårförsök.

Hydraulisk respons på pumpningen i HLX28 kunde konstateras i 63 av 266 observationssektioner. För 53 av dessa sektioner var responsen klassad som tydlig och för 10 sektioner som svag. 61 sektioner användes vid transient utvärdering. Transmissiviteten för pumphålet HLX28 utvärderades till $3.0 \cdot 10^{-4}$ m^2/s.

Den hydrauliska responsen vid pumpning visar en tendens till att vara tydligare norrut än i andra riktningar. Noteras bör att ZSMNS001C verkar vara en tydlig hydraulisk barriär eftersom inga sektioner väster om zonen visar någon respons. Sektioner kopplade till ZSMNW042A i närheten av HLX28 visar respons, dock inte mycket tydligare än andra sektioner i området. Zon ZSMNW042A och till viss del även ZSMNS059A uppvisar tendenser till att vara hydrauliska barriärer, dock inte lika tydligt som ZSMNS001C. Spårämnesgenombrott indikerar att alla tre av zonerna ZSMNS001C, ZSMNW042A och ZSMNS059A var involverade i transporten från injiceringssektionerna till HLX28.

Contents

1 Introduction

This document reports the results from the combined hydraulic interference and tracer test in the Laxemar sub-area. The test is one of the activities performed within the site investigation at Oskarshamn. All of the work was carried out in accordance with activity plan AP PS 400-08-016. In Table 1-1 controlling documents for performing this activity are listed. The activity plan and the method descriptions are SKB's internal controlling documents. The data obtained from the activity are reported to the Sicada database, where they are traceable by the activity plan number.

The field work was performed from June to July 2008 and from January to May 2009. The field work involved pumping in HLX28 together with pressure registration in surrounding boreholes, tracer dilution tests and a cross-hole tracer test. A map of the investigation area in Laxemar with borehole locations is shown in Figure 1-1.

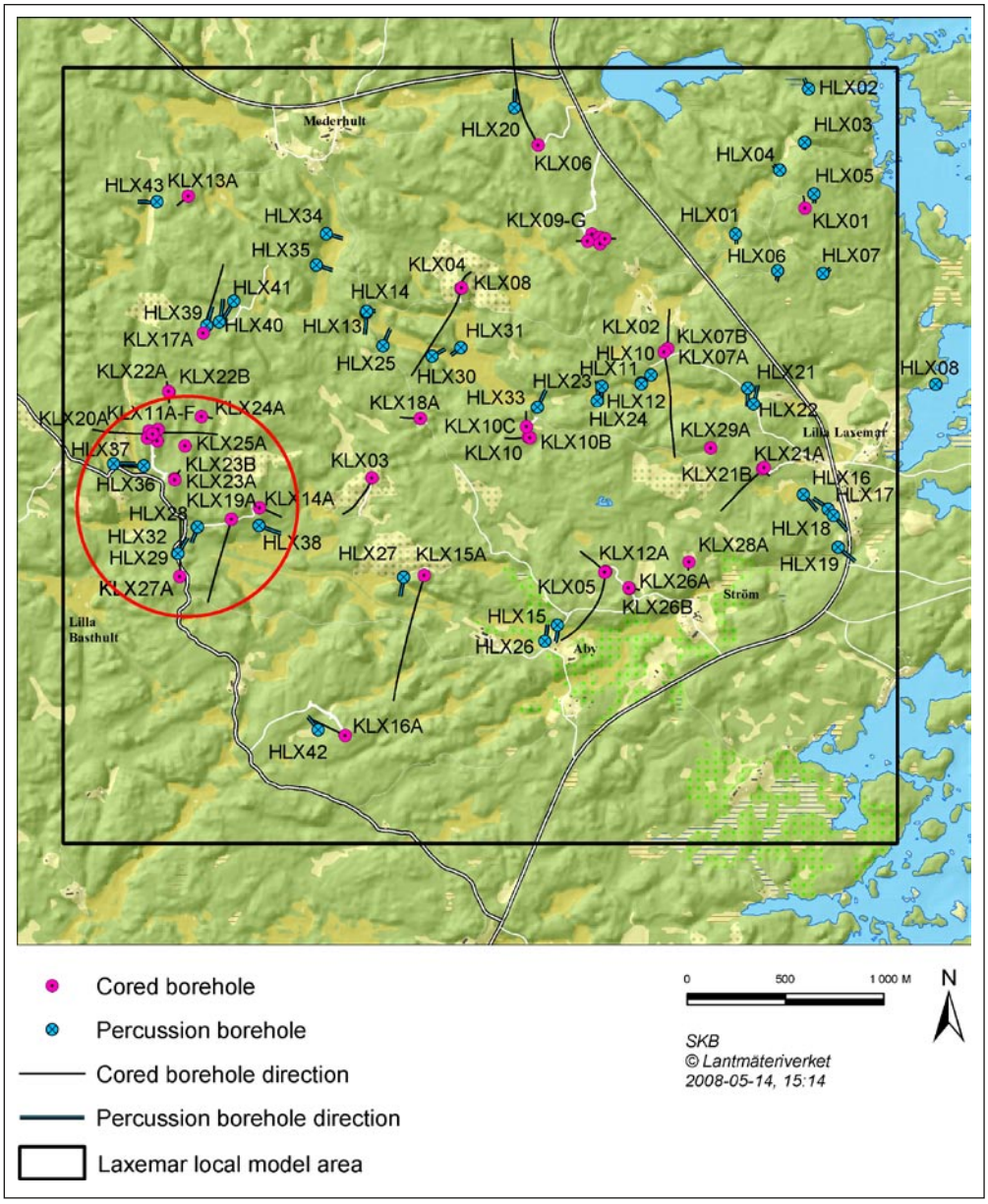

Figure 1-1. *The Laxemar site investigation area and the boreholes involved in the tests. The pumping borehole HLX28 and the boreholes used for the tracer tests are situated in the western part of the area (inside the red circle).*

Table 1-1. Controlling documents for performance of the activity.

Activity plan	**Number**	**Version**
Storskaligt långtidspumptest och spårförsök i Laxemar	AP PS 400-08-016	1.0
Method descriptions	**Number**	**Version**
Metodbeskrivning för flerhålsförsök	SKB MD 530.006	1.0
Metodinstruktion för analys av injektions- och enhålspumptester	SKB MD 320.004	1.0
Metodbeskrivning för interferenstester	SKB MD 330.003	1.0
System för hydrologisk och metrologisk datainsamling. Vattenprovtagning och utspädningsmätning i observationshål.	SKB MD 368.010	1.0

2 Objective and scope

The primary objective of the combined hydraulic interference and tracer test was to verify the hydrogeological model of the Oskarshamn candidate area and secondly, if possible, determine transport properties for some major flow paths in the area.

The activity can be divided into two main parts; one part concerns hydraulic parameters and the hydrogeological model (the pumping test and the interference test) and the second part concerns transport characteristics (the tracer test). One of the aims is to combine the evaluations of these two parts and results from other previous investigations in the area.

2.1 Tests performed

The tests performed within this activity comprise groundwater flow measurements (natural conditions and during pumping) and a tracer test combined with a hydraulic interference test. Additionally, water samples were taken for chemical analysis. A compilation of the tests performed within this activity is shown in Table 2-1. The execution of the tests is described in detail in Section 4.4.

During pumping, the withdrawal rate (constant flow rate) and the pressure response in HLX28 were registered. Pressure responses to the pumping in surrounding boreholes were monitored using HMS (Hydro Monitoring System). Tracers were injected into permanently installed sections in HLX32, HLX37, HLX38, KLX11A, KLX20A and KLX27A and the pumped water from HLX28 was analysed for tracer breakthrough. Water samples from the injection sections were also collected and analysed in order to monitor the tracer concentration in those sections.

2.1.1 Groundwater flow measurements

Prior to the tracer test, groundwater flow measurements were conducted in ten sections in seven boreholes during two separate campaigns. No pumping was performed during the first campaign so these dilution tests are considered representative for natural conditions. The second campaign was performed in conjunction with the pumping start in HLX28 in January 2009, and thus includes both natural conditions and during pumping, in order to investigate the effect of pumping in HLX28 on the groundwater flow rates.

2.1.2 Interference tests

The interference test was performed by pumping in HLX28 for c 125 days. The pressure was monitored before, during and after the pumping period in the borehole sections listed in Appendix 1. During the pumping, the withdrawal rate and the pressure response in HLX28 were registered. Pressure responses to the pumping in surrounding boreholes were monitored using HMS (Hydro Monitoring System). During the test the flow rate was maintained at c 300 L/min after an initial period of regulation to obtain a suitable flow rate.

Table 2-1. Tests performed within the activity

Test	Borehole	Start date	Stop date
Water sampling for chemical analysis (four occasions)	HLX28	2008-06-11	2009-05-26
Groundwater flow measurement (natural conditions) first campaign	[1]	2008-07-01	2008-07-09
Groundwater flow measurement (natural conditions and during pumping) second campaign	[1]	2009-01-13	2009-01-30
Pumping test	HLX28	2009-01-20	2009-05-26
Interference test	HLX28 (pumping hole) [2]	2009-01-20	2009-05-26
Tracer sampling	HLX28	2009-02-10	2009-05-24
Tracer injection	[3]	2009-02-10	2009-02-12

[1] HLX32:2 HLX37:1 HLX38:3 KLX11A:3 KLX11A:7 KLX19A:3 KLX20A:2 KLX20A:5 KLX27:1 KLX27A:6.
[2] Observation sections, see Appendix 1.
[3] HLX32:2 HLX37:1 HLX38:3 KLX11A:3 KLX20A:5 KLX27A:6.

2.1.3 Tracer test

The tracers were injected in selected borehole sections, with permanently installed equipment, after more than 20 days after the pump start in HLX28 in order for relatively stationary conditions to develop. The pumped water in HLX28 was sampled and analysed for tracer breakthrough. Sampling in HLX28 started before the injections in order to obtain background values of the tracers. Water samples from the injection sections were also collected and analysed. Motives for selection of the six tracer injection sections are given in Section 4.2.

2.2 Borehole information

The reference point of the boreholes is always top of casing (ToC). The Swedish National coordinate system (RT90 2.5 gon V 0:-15) is used in the x-y-plane together with RHB70 in the z-direction. Northing and Easting refer to the top of the boreholes at top of casing. All section positions are given as length along the borehole, i.e. meter borehole length (mbl) and not vertical distance from ToC. Distances from the borehole sections to HLX28 given in this report are calculated as the Euclidian (shortest straight line) distance using the x, y and z coordinates for the midpoint of each section.

2.2.1 Pumping borehole

Table 2-2. Selected technical data for the pumping borehole.

Borehole	Coordinate Northing (m)	Easting (m)	Elevation (m)	Inclination (degrees)	Bearing (degrees)	Secup (mbl)	Seclow (mbl)
HLX28	6365861.70	1546834.47	13.42	59.49	201.38	6	154

2.2.2 Dilution and tracer injection borehole sections

Selected data for the borehole sections used for groundwater flow measurements and tracer injection are given in Table 2-3. All sections listed in Table 2-3 were used for groundwater flow measurements.

Table 2-3. Selected data for borehole sections used for groundwater flow measurements and tracer injection.

Borehole	Section	Secup (mbl)	Seclow (mbl)	Section volume (L)	T (m^2/s)	Distance to HLX28 (m)	Used for tracer test
HLX32	2	20.00	30.00	33.4	6.9E–06 [1)]	122	Y
HLX37	1	150.00	199.80	164.6	4.9E–05 [2)]	486	Y
HLX38	3	28.00	40.00	38.9	5.6E–05 [3)]	349	Y
KLX11A	3	573.00	586.00	50.2	1.5E–05 [4)]	702	Y
KLX11A	7	256.00	272.00	32.2	2.6E–05 [4)]	563	N
KLX19A	3	509.00	517.00	41.5	1.0E–06 [5)]	420	N
KLX20A	2	260.00	293.00	55.6	2.1E–06 [6)]	663	N
KLX20A	5	103.00	144.00	48.2	8.2E–06 [6)]	591	Y
KLX27A	1	640.00	650.56	50.1	3.6E–06 [7)]	519	N
KLX27A	6	220.00	259.00	64.6	4.0E–07 [7)]	198	Y

[1)] /Rohs et al. 2007/.
[2)] /Harrström et al. 2008/.
[3)] /Rohs 2006/.
[4)] /Väisäsvaara et al. 2007/.
[5)] /Kyllönen et al. 2007/.
[6)] /Kristiansson 2007/.
[7)] /Pöllänen et al. 2008/.

2.2.3 Interference test borehole sections

The pressure was measured in all boreholes connected to the HMS system at Laxemar. The pressure changes were monitored in core-drilled boreholes and percussion-drilled boreholes, in rock as well as in soil monitoring wells. The borehole sections monitored for hydraulic responses from the pumping in HLX28 are listed in Appendix 1, which also lists calculated straight line distance to HLX28.

3 Equipment

3.1 General

Each borehole used as injection borehole was permanently instrumented with 2-9 inflatable packers isolating 3-10 borehole sections. Drawings of the instrumentation in core and percussion boreholes are presented in Figure 3-1.

All isolated borehole sections are connected to the HMS-system for pressure monitoring. In general, the sections planned to be used for tracer tests are equipped with three polyamide tubes. Two of the tubes are for injection, sampling and circulation in the borehole section and one is for pressure monitoring.

The pressure monitoring was made using pressure transducers in standpipes connected to each section in the borehole, see Figure 3-1. All data were collected by means of pressure transducers connected to different types of data loggers. In order to calibrate registrations from the data loggers, manual levelling of all sections was made, normally once every month. The logger data were converted to water levels by means of a linear calibration equation, and subtraction of the air pressure since all transducers give the absolute pressure. The ground water levels are given in metres above sea level (m.a.s.l.).

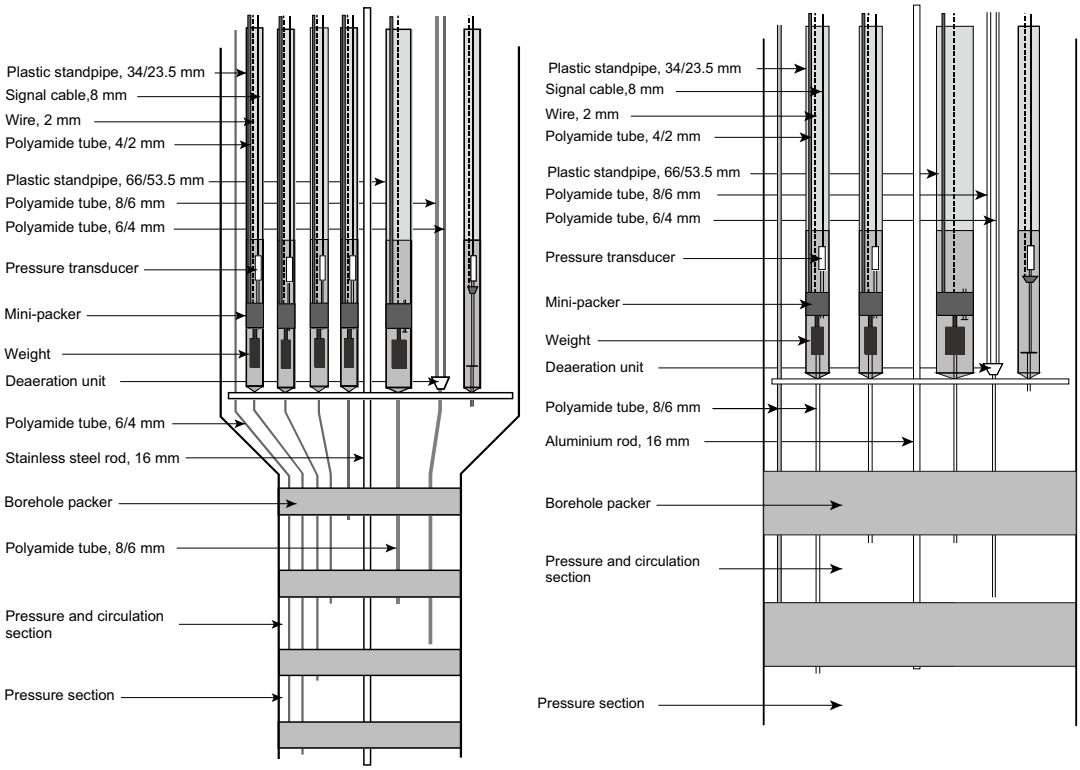

Figure 3-1. *Explanatory sketch of permanent instrumentation in core boreholes (left) and percussion boreholes (right) with circulation sections.*

3.2 Groundwater flow measurements

A schematic drawing of the dilution tracer test equipment is shown in Figure 3-2. The basic idea is to create an internal circulation in the borehole section. The circulation makes it possible to obtain a homogeneous tracer concentration within the borehole section and to sample the tracer outside the borehole in order to monitor the dilution of the tracer.

Circulation was controlled by a down-hole pump with adjustable capacity and measured by a flow meter. Tracer injections were made with a peristaltic pump and sampling was performed by continuously extracting a small volume of water from the system through another peristaltic pump (constant leak) to a fractional sampler. The circulation unit and the sampling equipment are also shown in Figure 3-3. The equipment and test procedure is described in detail in SKB MD 368.010, SKB internal document, see Table 1-1.

The tracer used in the groundwater flow measurements was Amino-G Acid, from Aldrich-Chemie.

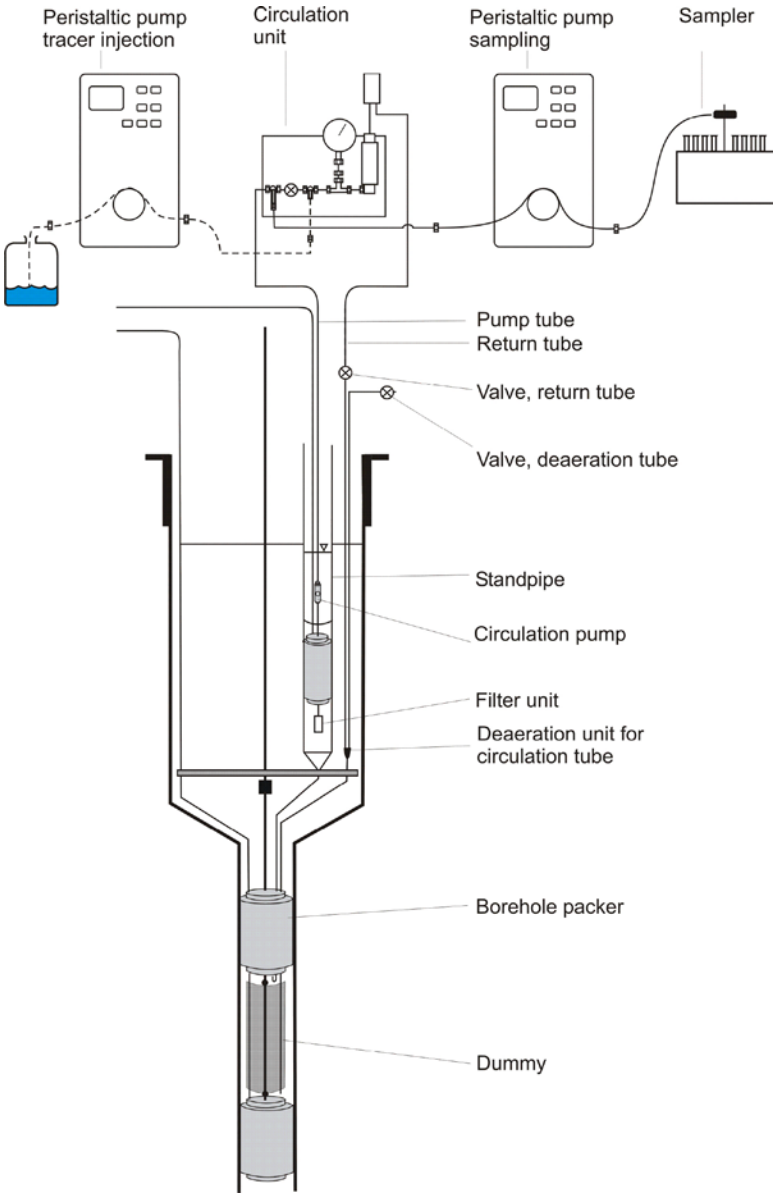

Figure 3-2. *Schematic drawing of the equipment used in tracer dilution measurements.*

Figure 3-3. *Circulation unit, peristaltic pump and fractional sampler used for the groundwater flow measurements and the tracer test.*

3.3 Tracer test

The tracer test was performed with one equipment set-up for the pumping borehole, HLX28, and one set-up for each of the injection sections. The principal experimental layout is shown in Figure 3-4. The equipment used for the tracer injection section was basically the same, although slightly altered, as for the groundwater flow measurements. A schematic view of the injection procedure and the equipment is shown in Figure 3-5.

The injections were performed, through a fluid exchange procedure, without excess pressure. The tracer injection was accomplished by using a pump at the surface, pumping the tracer solution from 25 L containers, whereas the circulation pump in the borehole was used to pump water from the section. The pumped water was collected in 25 L containers, which were weighed and analysed for tracer concentration.

Samples were collected from the withdrawal borehole HLX28 using two automatic programmable samplers. One of the samplers consists of 24 magnetic valves and a control unit allowing selection of time period between openings/samples and open duration (to get an appropriate sample volume), see Figure 3-6. Samples were collected in 125 ml plastic (HDPE) bottles. The other sampler producing 500 ml samples is supplied with 24 bottles and was only used as a back-up sampler. When the regular magnetic valve sampler functioned well, the sampled water in the 500 ml bottles was discarded.

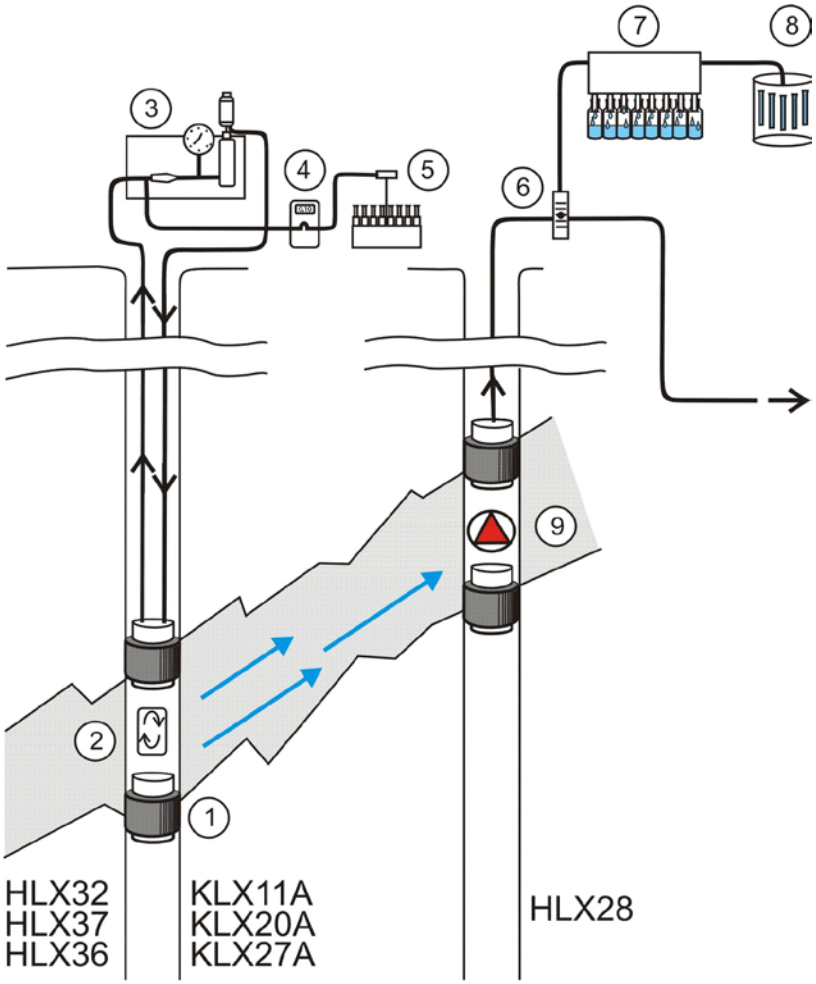

1. Packer
2. Circulation pump
3. Circulation unit
4. Peristaltic pump for sample withdrawal
5. Fractional sampler
6. Flow meter connected to logger
7. Automatic sampler
8. Automatic sampler
9. Pump

Figure 3-4. *Layout of the tracer test.*

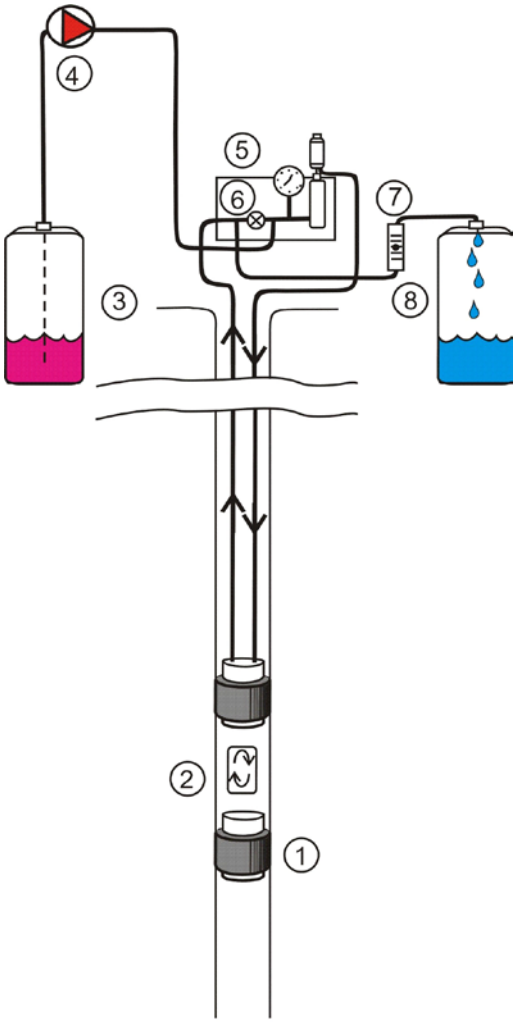

1. Packer
2. Circulation pump
3. Tracer
4. Injection pump
5. Circulation unit
6. Closed valve
7. Flow meter
8. Water pumped from section

Figure 3-5. *Schematic view of equipment used for the tracer injections.*

3.3.1 Tracers used

Six different tracers were used, one for each injection section. Five of the tracers consisted of DTPA-complexes of the rare earth metals (lantanoids); Europium (Eu), Terbium (Tb), Gadolinium (Gd), Dysprosium (Dy) and Holmium (Ho). The sixth tracer was Rhenium (Re), which was prepared by dissolving the salt ReCl in water. In addition, Amino-G (c 1 ppm) was added to all tracer solutions to enable quick analyses and monitoring of the increase/decrease of tracer concentration in the injection sections during and after the injection. The DTPA-complexes will, for convenience, be referred to as Eu, Tb, Gd, Dy and Ho further on in this report. In Table 3-1 the tracer used in each borehole is presented together with the initial concentration (C_{00}) of the tracer solutions in the containers.

The DTPA-complexes were prepared at the Geosigma laboratory in Uppsala by mixing DTPA, NaOH, the chloride salt of each metal and, if needed, some HCl to correct the pH and also in some cases NaCl to obtain a density close to that of the borehole water. The tracer solutions were stored in 25 L containers.

Figure 3-6. The automatic sampling equipment (24 magnetic valves) at the withdrawal borehole HLX28.

Table 3-1. Tracers used.

Borehole	Section	Tracer	C_{00} (g/l)
HLX32	2	Gd	0.294
HLX37	1	Dy	5.72
HLX38	3	Re	0.255
KLX11A	3	Tb	0.159
KLX20A	5	Ho	3.18
KLX27A	6	Eu	0.541

3.4 Pumping and interference test

The pumping equipment in HLX28 consisted primarily of the following parts:

- A submersible pump (Debe FN23 with a capacity of 350 L/min at 40 m depth) connected to the surface with a PEM63-hose.
- Pressure transducer in the borehole above the pump, connected to the HMS system.
- A flow rate control valve at the surface together with a flow meter connected to the HMS system. The flow rate was adjusted manually when needed.

The discharged water was led to a nearby creek via a plastic hose. Before discharge, some of the water was led into the container at HLX28 from which water samples were taken with a tube sampler.

A number of sections in surrounding boreholes were used as observation sections. All sections included in the interference test are part of the SKB hydro monitoring system (HMS), in which pressure is recorded continuously.

4 Execution

4.1 General

The work involved planning and scoping calculations, field work, analyses of collected samples, data handling, evaluation and modelling.

All activities were carried out in accordance with the method descriptions SKB MD 368.010 and SKB MD 530.006 (SKB internal documents), see Table 1-1.

4.2 Scoping calculations

In order to optimise the test in terms of tracer injection method, injection times, pumping rates, tracers, etc scoping calculations were performed during the planning stage.

The scoping and planning of the test was focused on three key issues: injection method, travel time and tracer to be used. Since several injection sections may be used, the chosen injection method must be practical enough to be used at multiple locations at the same time or be rather short in terms of time. Due to the large scale of the test, the dilution from the injection to the pumping section will be considerable. For that reason, the dynamic ranges of the tracers have to be large in order to detect breakthrough. Further, the travel time from the injection section to HLX28 has to be reasonably short. The conditions for the present test are similar to the large scale tracer tests performed within the Forsmark site investigation area during the summer of 2007 /Lindquist et al. 2008a/. Hence, the methods and experiences from the previous tracer test were used to a large degree in the planning and scoping of the present tests.

4.2.1 Injection method

As in /Lindquist et al. 2008a/, the chosen method for tracer injection was injection by exchange of water. The method is rather easy to perform as the tracer solution with the ideal initial concentration C_0 is injected while the existing section water is pumped out with the same flow rate. After exchange of at least one section volume, the borehole section is circulated (i.e. continuously mixed) and the concentration decays as the tracer is transported away by the ambient groundwater flow. The exchange method only requires the equipment used for groundwater flow rate measurements and some containers for the injection solution and for collection of return water.

4.2.2 Pumping flow rate

The duration of the test was originally planned to be 3–4 months. In order to ensure a tracer breakthrough in HLX28, a high flow rate in the section was preferable. On the other hand, the flow rate should be constrained so that the total expected drawdown in HLX28 would not exceed 40 m. Based on previous estimates of transmissivity in HLX28, a pumping flow rate of 300 L/min was considered appropriate.

4.2.3 Travel time and dilution

The borehole sections used for the groundwater flow measurements, see Table 2-3, were considered as potential tracer injection sections. The travel time from each potential injection section to HLX28 were estimated using the AD-1 model (see Section 4.6.4) and assumptions of mean residence time, t_m [T], Peclet number, Pe [-], and tracer recovery. The tracer recovery was assumed to be 100% in the scoping calculations. Two values of Pe were used, 2 and 5. The mean residence time, t_m, was estimated using Equation 4-1 and Equation 4-2:

$$\delta_m = \frac{Qt_m}{\pi (r^2 - r_w^2)} \qquad \text{Equation 4-1}$$

$$\delta_m = 0.19 \cdot T^{0.26} \qquad \text{Equation 4-2}$$

where Q is the average pumping rate [L^3/T], r is the travel distance [L], r_w is the borehole radius [L], T is the hydraulic transmissivity [L^2/T] and δ_m is mass balance aperture [L]. Equation 4-2 used in this study is an early and preliminary result from the study presented in /Hjerne et al. in prep/. Hence, it differs slightly from the final relationship between δ_m and T presented in /Hjerne et al. in prep/.

The results from the groundwater flow measurements, as presented in Section 5.2, were used to calculate the input function for the simulations.

The results from the simulations are presented in Table 4-1 in terms of maximum concentration and elapsed time for maximum concentration. The assumed travel distance used in the scoping calculations deviates slightly from the distances presented in Table 2-3, due to different point of application when calculating the distances. However, this should not affect the scoping simulations in any major way. It should also be noted that the assumed distances are equal to the straight line distance which probably is a large underestimate in many of the cases.

The criteria used for selection of borehole section for tracer injection was relatively low dilution and short travel time. The flow response due to pumping as presented in Section 5.2 was also considered when selecting borehole section for the tracer test. The borehole sections selected for tracer injection are indicated with red colour in Table 4-1.

4.2.4 Tracers

The expected dilution from the injection sections to the pumping borehole was quite high, as seen in Table 4-1, which means that the solubility needs to be high and the background level needs to be rather low for the tracers. DTPA-complexes of the rare earth metals (lantanoids) Europium (Eu), Terbium (Tb), Gadolinium (Gd), Dysprosium (Dy) and Holmium (Ho) have in previous tracer tests been used successfully and fulfil the requirements of high solubility and low background levels. The tracer Rhenium (Re) also fulfils these requirements.

The six tracers were optimized for the different injection sections with respect to expected dilution, costs, available amount, solubility and background level so that the maximum concentration in HLX28 should be significantly above the expected background level if the assumptions made in Section 4.2.3 are valid. The selection of tracer for each borehole section is given in Table 4-5.

4.3 Preparations

Equipment function checks were performed in the field before tracer injections. All equipment was found to be functioning well.

All of the tracer solutions were prepared at the Geosigma laboratory in Uppsala and stored in 25 L containers.

Table 4-1. Calculated maximum concentrations and times to maximum concentrations for different assumptions of dispersivity and injections section while pumping 300 L/min in HLX28.

Borehole: section	Assumed travel distance, r (m)	Estimated mean travel time, t_m (h)	Pe=2 Max conc C/C_0	Time to max conc (h)	Pe=5 Max conc C/C_0	Time to max conc (h)
HLX32:2	125	22	1.40E–05	47	1.70E–05	43
HLX37:1	459	497	1.00E–05	390	3.10E–05	130
HLX38:3	346	292	1.90E–06	490	2.30E–06	480
KLX11A:3	704	856	1.90E–06	590	2.50E–06	750
KLX11A:7	561	626	4.50E–07	1,400	5.20E–07	1,300
KLX19A:3	430	157	8.30E–07	530	9.00E–07	430
KLX20A:2	662	449	3.50E–06	430	4.50E–06	500
KLX20A:5	588	509	3.20E–06	320	4.10E–06	420
KLX27A:1	526	328	2.00E–06	560	2.40E–06	550
KLX27A:6	206	28	1.6.E–05	70	1.80E–05	60

4.4 Execution of field work

4.4.1 Groundwater flow measurements

The groundwater flow measurements were performed before the tracer test. The time periods for the measurements at the first and second campaign are presented in Table 4-2 and Table 4-3. During the second campaign, the pumping of HLX28 started (see Table 4-4), making the second campaign include both a period of natural conditions and a period of pumping. The duration of the period with natural gradient ranged from 140 to 164 hours, and the corresponding time during the period with pumping gradient from 145 to 242 hours.

The tests were made by injecting a tracer (Amino-G, 1,000 mg/L) in the selected borehole section and allowing the natural groundwater flow to dilute the tracer. The tracer was injected during a time period equivalent to the time it takes to circulate one section volume. The injection/circulation flow ratio was set to 1/1,000, implying that the start concentration in the borehole section would be about 1 mg/L. The tracer solution was continuously circulated and sampled using the equipment described in Section 3.2.

All samples intended for analysis of Amino-G was buffered with c 1% Titrisol buffer solution (pH 9). Earlier experiences have showed that the buffer prevents decomposition of the dye.

Table 4-2. Groundwater flow measurements, first campaign.

Borehole	Section	Secup (mbl)	Seclow (mbl)	Start date and time	Stop date and time
HLX32	2	20	30	2008-07-02 09:19	2008-07-08 15:30
HLX37	1	150	200	2008-07-01 10:54	2008-07-08 17:27
HLX38	3	28	40	2008-07-01 15:41	2008-07-03 09:33
KLX11A	3	573	586	2008-07-01 10:48	2008-07-08 18:15
KLX11A	7	256	272	2008-07-01 10:39	2008-07-08 18:36
KLX19A	3	509	519	2008-07-01 14:01	2008-07-08 16:26
KLX20A	2	260	293	2008-07-01 10:11	2008-07-08 07:03
KLX20A	5	103	144	2008-07-01 09:57	2008-07-08 20:05
KLX27A	1	640	650	2008-07-01 17:51	2008-07-09 10:35
KLX27A	6	220	259	2008-07-01 17:15	2008-07-09 10:57

Table 4-3. Groundwater flow measurements, second campaign.

Borehole	Section	Secup (mbl)	Seclow (mbl)	Start date and time	Stop date and time
HLX32	2	20	30	2009-01-14 09:00	2009-01-30 11:25
HLX37	1	150	200	2009-01-13 15:39	2009-01-26 11:25
HLX38	3	28	40	2009-01-14 11:38	2009-01-30 11:29
KLX11A	3	573	586	2009-01-14 12:48	2009-01-26 11:32
KLX11A	7	256	272	2009-01-14 12:52	2009-01-30 11:42
KLX19A	3	509	519	2009-01-14 10:36	2009-01-30 11:33
KLX20A	2	260	293	2009-01-13 14:25	2009-01-30 11:44
KLX20A	5	103	144	2009-01-13 14:42	2009-01-30 11:44
KLX27A	1	640	650	2009-01-14 13:56	2009-01-30 11:23
KLX27A	6	220	259	2009-01-14 13:57	2009-01-30 11:23

4.4.2 Pumping and interference test

The previously installed sections with packers, dummys and tubing were removed from the pumping borehole HLX28. Pumping equipment was installed in the borehole and lowered to about 70 m below the top of casing (ToC). The borehole was open during the pumping. Dates and times for the pumping are presented in Table 4-4.

All data was reported into the Hydro Monitoring System (HMS). Data were collected automatically or manually from data loggers at each site depending on how the individual boreholes and soil pipes were equipped. The data registration frequency was increased in conjunction to start and stop of the pumping in order to achieve sufficient amount of data for transient test evaluation.

Table 4-4. Date and time data for the pumping in borehole HLX28.

Start date and time of pumping	Stop date and time of pumping	Stop date and time of recovery	Length of pumping period (min)	Length of recovery period (min)
2009-01-20 10:02:10	2009-05-26 09:45:39	2009-06-01 05:59:59	1,81423.5	8,414.3

4.4.3 Tracer test

The tracer injection was carried out as an exchange procedure with the equipment given in Section 3.3. During the exchange procedure, samples for analysis of Amino-G were taken every 10 minutes from the pumped water to monitor the injection procedure. The volume of tracer injected was c 1.5 times the section volume. Hence, the exchange continued for a time that equalled circulation of c 1.5 section volumes. Some data regarding the tracer injections are presented in Table 4-5. After injection the circulation was started and samples were continuously withdrawn from the injection section. The automatic sampling continued for 2 weeks from the injection sections.

The sampling of the pumped water from HLX28 was started prior to the tracer injections in order to collect data on background concentrations. To be sure to detect the first arrivals of the tracers, the sample interval was shorter during the first days of the test. After 10 days the interval between samples was set to 6 hours, and after 30 days to 12 hours.

1% HNO_3 was added to the bottles and tubes for samples to be analysed for metals in order to keep the DTPA-complexes stable and prevent sorption on the plastic bottles.

Table 4-5. Tracer injection information.

Borehole: section	Tracer	Section volume (L)	Volume tracer injected (L)	Injection start YYYY-MM-DD hh:mm	Injection stop YYYY-MM-DD hh:mm	Injection time (min)
HLX32:2	Gd	33.4	49.7	2009-02-10 10:14	2009-02-10 11:27	73
HLX37:1	Dy	165	246.5	2009-02-11 09:30	2009-02-11 13:22	232
HLX38:3	Re	38.9	56.1	2009-02-10 13:26	2009-02-10 14:52	86
KLX11A:3	Tb	50.2	73.1	2009-02-11 15:49	2009-02-11 18:02	133
KLX20A:5	Ho	48.3	71.4	2009-02-12 09:04	2009-02-12 10:49	105
KLX27A:6	Eu	64.6	95.5	2009-02-10 12:10	2009-02-10 14:28	138

4.4.4 Water sampling for chemical analysis

To control the stability of the water quality during the pumping, water sampling for SKB chemical analysis Class 3 was performed at four occasions during the activity. The first sample was taken before pump start in June 2008, with addition of Eu, Tb, Dy, Ho, Gd and Re for background, the second at pump start at the second campaign in January 2009, the third in the middle of the pumping period and the last one at the end. Table 4-6 shows the dates and times of the sampling together with the SKB sample number used for identification in the Sicada database.

Table 4-6. SKB Class 3 water sampling.

Borehole	Date and time of sample	Pumped section (m)	Pumped volume (m^3)	Sample type	Sample ID no
HLX28	2008-06-11 16:54	6–154	0	WC080	15595
HLX28	2009-01-20 10:15	6–154	4	WC080	15822
HLX28	2009-03-11 11:45	6–154	22,000	WC080	15854
HLX28	2009-05-26 10:26	6–154	54,000	WC080	15944

4.5 Data handling/post processing

All samples analysed for Amino-G were analysed at the Geosigma laboratory in Uppsala using a Jasco FP 777 Spectrofluorometer. The samples intended for analysis of metals were sent to ALS Scandinavia laboratory in Luleå.

All data from HMS (pumping and observation sections) was downloaded as .mio-files for further processing.

The results from the laboratory analyses were compiled together with sample date and time for further processing, plotting and calculations.

4.6 Analyses and interpretations

4.6.1 Groundwater flow measurements

In the dilution method, a tracer is introduced and homogeneously distributed into a borehole test section. The tracer is subsequently diluted by the ambient groundwater, flowing through the borehole test section. The groundwater flow rate is calculated from the rate with which the tracer concentration decreases with time, Figure 4-1.

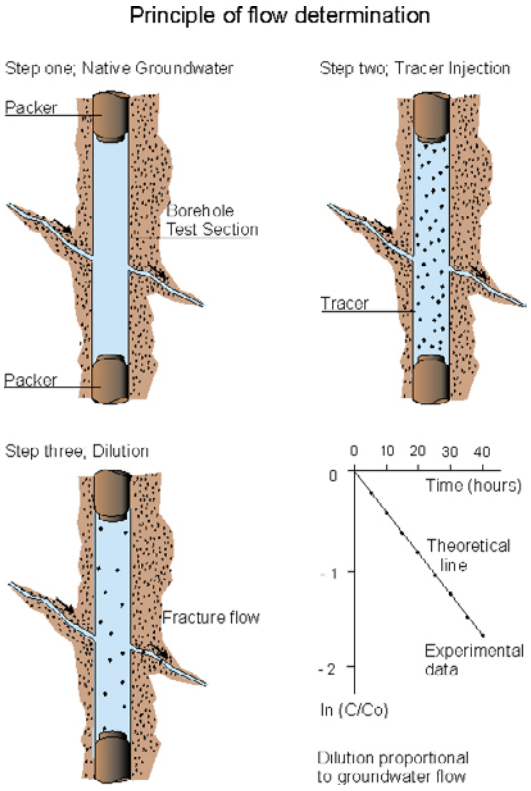

Figure 4-1. *General principles of dilution and flow determination.*

Flow rates were calculated from the decay of tracer concentration versus time through dilution with natural unlabelled groundwater /Gustafsson 2002/. The so-called "dilution curves" were plotted as the natural logarithm of concentration versus time. Theoretically, a straight-line relationship exists between the natural logarithm of the relative tracer concentration (C/C_0, where C_0 is the initial concentration) and time, t [T]:

$$ln\ (C/C_0) = -\ (Q_{bh}/V) \cdot t \qquad \text{Equation 4-3}$$

where Q_{bh} [L^3/T] is the groundwater flow rate through the borehole section and V [L^3] is the volume of the borehole section. By plotting ln (C/C_0) or ln C versus t, and by knowing the borehole volume V, Q_{bh} may then be obtained from the straight-line slope.

The sampling procedure with a constant flow of 4–10 ml/h also creates a dilution of tracer. The sampling flow rate is therefore subtracted from the value obtained from Equation 4-3.

4.6.2 Pumping and interference test

General

Standard methods for constant flow rate interference tests in an equivalent porous medium were used for evaluation of the responses in the observation test sections in accordance with the methodology description for interference tests (SKB MD 330.003 v2.0) and for single-hole tests in the pumping borehole. The response in the pumping borehole HLX28 has been evaluated according to the Instruction for analysis of hydraulic injection and single-hole pumping tests (SKB MD 320.004 v.2.0). The results are reported in Section 5.3 below.

The quantitative transient analysis was performed using the software AQTESOLV Pro v. 4.0 that enables both manual and automatic type curve matching. The transient evaluation was carried out as an iterative process of manual type curve matching and by employing automatic non-linear regression. The quantitative, transient interpretation of the hydraulic parameters of the observation sections (mainly transmissivity and storativity) is normally based on the identified pseudo-radial flow regime and associated flow regimes during the tests.

All pressure data from the observation boreholes presented in this report have, prior to evaluation, been corrected automatically in HMS for atmospheric pressure changes by subtracting the latter pressure from the measured (absolute) pressure. No other corrections of the measured drawdown due to e.g. precipitation, drought periods and/or tidal effects have been made.

Observation boreholes

In the primary qualitative evaluation, data from all observation borehole sections included in the interference test were studied in linear pressure versus time diagrams to identify responding sections. Corresponding diagrams of precipitation etc were also used. Linear diagrams of pressure versus time for all evaluated test sections together with precipitation, barometric pressure and sea water level are presented in Appendix 2. A classification of the strength of the responses in the observation sections is presented in Appendix 1.

Qualitative evaluation of the responses was made for all core-drilled and percussion-drilled boreholes in rock in the Laxemar area monitored in the HMS system, as well as in all soil monitoring wells monitored in the HMS system within a radius of 1 km from HLX28.

The evaluation of the dominating transient flow regimes, pseudo-linear- (PLF), pseudo-radial- (PRF) and pseudo-spherical flow (PSF), and outer boundary conditions, was mainly based on the drawdown responses in logarithmic diagrams. In particular, pseudo-radial flow is reflected by a constant (horizontal) derivative in such diagrams, whereas no-flow- (NFB) and constant head boundaries (CHB) are characterized by an increase and decrease of the derivative, respectively. Based on the qualitative evaluation, relevant models were selected for the transient evaluation of the responses.

In the quantitative evaluation, sections with clear responses were analysed with standard transient methods, mainly regarding transmissivity and storativity /Kruseman and de Ridder 1990/. The responses in the sections were analysed according to a variable flow rate in the pumping borehole.

Observation borehole sections with a very weak and/or uncertain response were only analysed qualitatively. Such borehole sections are not included in the response analysis. The classification of responses in the observation sections are presented in Appendix 1.

Pumping borehole

The evaluation of the single-hole pumping test in HLX28 was made according to the instruction SKB MD 320.004. The storativity, S [-] was calculated according to Equation 4-4 /SKB 2006/ where the transmissivity,T [L^2/T] is in units of m^2/s. The transmissivity and the skin factor were obtained by type curve matching.

$$S=0.0007 \cdot T^{0.5} \qquad \text{Equation 4-4}$$

In addition to the transient analysis, an interpretation based on the assumption of stationary conditions in the pumping borehole was performed.

The wellbore storage coefficient, C_{WBS} (m^3/Pa), in the pumping borehole section can be obtained by assuming a fictive casing radius, r(c) [L], in an equivalent open test system according to Equation 4-5.

$$C_{WBS} = \frac{\pi \cdot r(c)^2}{\rho \cdot g} \qquad \text{Equation 4-5}$$

The radius of influence at a certain time during the test may be estimated from Jacob's approximation of the Theis' well function according to Equation 4-6:

$$r_i = \sqrt{\frac{2.25 \cdot T \cdot t}{S}} \qquad \text{Equation 4-6}$$

where r_i [L] is the radius of influence at time t after start of pumping.

Furthermore, a r_i-index (–1, 0 or 1) is defined to characterize the hydraulic conditions by the end of the test. The r_i-index is defined as shown below. It is assumed that a certain time interval of PRF can be identified between t_1 and t_2 during the test.

- r_i-index = 0: The transient response indicates that the size of the hydraulic feature tested is greater than the radius of influence based on the actual test time ($t_2=t_p$), i.e. the PRF is continuing at stop of the test. This fact is reflected by a flat derivative at this time.
- r_i-index = 1: The transient response indicates that the hydraulic feature tested is connected to a hydraulic feature with lower transmissivity or an apparent barrier boundary (NFB). This fact is reflected by an increase of the derivative. The size of the hydraulic feature tested is estimated as the radius of influence based on t_2.
- r_i-index = –1: The transient response indicates that the hydraulic feature tested is connected to a hydraulic feature with higher transmissivity or an apparent constant head boundary (CHB). This fact is reflected by a decrease of the derivative. The size of the hydraulic feature tested is estimated as the radius of influence based on t_2.

If a certain time interval of PRF cannot be identified during the test, the r_i-indices –1 and 1 are defined as above. In such cases the radius of influence is estimated using the flow time t_p in Equation 4-6 using a value of S estimated from Equation 4-4.

Response analysis and estimation of hydraulic diffusivity

In responding observation sections the response indices and hydraulic diffusivity based on the estimated response time were calculated.

Maximum drawdown, s_p, is in this case taken from the time when the transient evaluation is aborted due to drought and hydraulic boundaries. The response time, dt_L, is defined as the time lag after start of pumping until a drawdown response of 0.1 m respectively 0.01m is observed in the actual observation section.

The pumping flow rate, Q_p [L^3/T], was used in combination with dt_L, r_s and s_p to calculate the response indices, which characterize the hydraulic connectivity between the pumping and the observed sections. The parameters, indices and calculated hydraulic connectivity parameters are shown in tables in Section 5.3.3. Sections with no response can be found in Appendix 1. The response indices were calculated according to Equation 4-7 and Equation 4-8 as follows:

Index 1:
Normalised distance r_s with respect to the response time dt_L (s = 0.1m) [L^2/T].

$$Index\ 1 = \frac{r_s^2}{dt_L}$$ Equation 4-7

Index 2 new:
Normalised drawdown s_p with respect to the pumping rate Q_p, also considering the distance r_s assuming r_0=1 m [T/L^2].

$$Index\ 2\ new = \frac{s_p}{Q_p} \cdot \ln\left(\frac{r_s}{r_0}\right)$$ Equation 4-8

Index 2, according to Equation 4-9, has been calculated in some of the previous response analyses. However, in this investigation Index 2 was not calculated but instead, Index 2_new.

Index 2:
Normalised drawdown s_p with respect to the pumping rate Q_p [T/L^2].

$$Index\ 2 = \frac{s_p}{Q_p}$$ Equation 4-9

The classification of the indices is given in Table 4-7.

All observation data are influenced by natural fluctuations of the groundwater level such as tidal effects and long term trends. These background variations of pressure may sometimes make it difficult to estimate the response time lag in the observation sections. The pressure changes due to tidal effects are different for the observation boreholes and sections.

The calculation of the hydraulic diffusivity T/S from the lag times is based on radial flow according to /Streltsova 1988/ and may be estimated according to Equation 4-10.

$$\frac{T}{S} = \frac{r_s^2}{4 \cdot dt_L \cdot \left(1 + \frac{dt_L}{t_p}\right) \cdot \ln\left(1 + \frac{t_p}{dt_L}\right)}$$ Equation 4-10

The time lag dt_L is in this case defined as the time when the pressure response in an observation section is 0.01 m. The pumping time is included as t_p. The estimates of the hydraulic diffusivity according to Equation 4-10 should be seen as approximate and could be compared with the hydraulic diffusivity calculated as the ratio of T/S from the transient evaluation of the observation sections.

Table 4-7. Classification of response indices.

	Limits	Classification	Colour code
Index 1 r_s^2/dt_L	r_s^2/dt_L > 100 m²/s	Excellent	Red
	10 < r_s^2/dt_L ≤ 100 m²/s	High	Yellow
	1 < r_s^2/dt_L ≤ 10 m²/s	Medium	Green
	r_s^2/dt_L ≤ 1 m²/s	Low	Blue
Index 2 new $s_p/Q_p \cdot \ln(r_s/r_0)$	$(s_p/Q_p) \cdot \ln(r_s/r_0) > 5 \cdot 10^5$ s/m²	Excellent	Red
	$5 \cdot 10^4 < (s_p/Q_p) \cdot \ln(r_s/r_0) \leq 5 \cdot 10^5$ s/m²	High	Yellow
	$5 \cdot 10^3 < (s_p/Q_p) \cdot \ln(r_s/r_0) \leq 5 \cdot 10^4$ s/m²	Medium	Green
	$(s_p/Q_p) \cdot \ln(r_s/r_0) \leq 5 \cdot 10^3$ s/m²	Low	Blue
	s_p < 0.1 m	No response	Grey

4.6.3 Tracer test

The total injected mass of each tracer was determined by weighing the containers before and after the injection and by analysing the concentration in each container. Since the injection was performed as an exchange procedure, the containers with water pumped from the section were also weighed and the water was analysed. The small mass of metal leaving the system through sampling of the injection section was also considered in the estimation of the total mass injected.

To check the analyses and the calculations of injected mass the total mass of tracer in the containers before injection (calculated by weighing and analyses) was compared to the total mass of each tracer that had actually been added.

The sample bottles and tubes were weighed before being sent to the consulted laboratory. The results from the laboratory were re-calculated to account for dilution by acid added to the samples. After this, the concentrations of tracer were plotted against elapsed time from the injection start and the data were checked. Some outliers were removed manually and the correct mean background concentrations of the various tracers were determined. The background was subtracted from the sample concentrations and the breakthrough curves from HLX28 were plotted as normalized mass flux against elapsed time. The normalized mass flux from HLX28 was calculated by multiplying the measured concentrations by the withdrawal rate and dividing with the total injected mass.

No correction for delay in tubes and hoses were made for samples from HLX28 since the flow rate was very high and the pump was placed at a moderate depth in the borehole.

It was assumed that tracer starts entering the fractures (e.g. leave the borehole section) when 0.5 section volumes have been injected. This time was selected as t=0 for the individual injection section and the elapsed time is related to this time in all calculations.

For calculation of the injection function used for modelling some assumptions were made:

- Plug flow is assumed in the injection sections.
- Complete mixing during circulation.
- The groundwater flow in the injection section is constant.

The injection function was estimated by calculating a concentration in the section that is constant during the injection period and then decreases according to the groundwater flow through the section, from the dilution measurements, so the total mass of the injection function equals the estimated total mass injected in the borehole section during the test. The input concentration was then converted into a function of normalized mass flux against time that was used as input for the transport modelling.

4.6.4 Transport models

The tracer tests were evaluated by fitting an advection-dispersion model for a single pathway to the breakthrough curve in the pumping borehole. This model is described by the standard governing equation for one-dimensional advection-dispersive transport with linear equilibrium sorption:

$$D_L \frac{\partial^2 C}{\partial x^2} - v\frac{\partial C}{\partial x} = R\frac{\partial C}{\partial t} \qquad \text{Equation 4-11}$$

where C is concentration [e.g. M/L^3], x is distance along transport path [L], t is time [T], v is the average water velocity [L/T] along the flow path, D_L is the longitudinal dispersion coefficient [L^2/T] and R is the retardation factor.

The following initial and boundary conditions are applied:

$$C(x,0) = 0 \qquad \text{Equation 4-12}$$

$$\frac{\partial C(\infty,t)}{\partial x} = 0 \qquad \text{Equation 4-13}$$

$$-D_L\frac{\partial C}{\partial x} + vC = vC_0 \qquad x = 0 \qquad \text{Equation 4-14}$$

where C_0 is the concentrations of the in-flowing water across the inlet boundary. The above boundary and initial conditions result in a solution for a constant injection of tracer. For a tracer pulse with constant concentration of limited duration (t_{inj}), the resulting tracer concentration may be calculated as:

$C(x,t) = M(x,t) \qquad 0 < t \le t_{inj}$ Equation 4-15

$C(x,t) = M(x,t) - M(x, t - t_{inj}) \qquad t > t_{inj}$ Equation 4-16

where $M(x,t)$ is the solution for a step-input injection with constant injection concentration. A more complex temporal variation in the tracer injection may be calculated in an analogous way by summation of a several such injection periods. A solution to the above equations, for a step input of constant concentration, is given by /Javandel et al. 1984/ as follows:

$$M(x,t) = \frac{1}{2} erfc\left[\frac{Rx - vt}{2(D_L Rt)^{1/2}}\right] + \left[\frac{v^2 t}{\pi D_L R}\right]^{1/2} \exp\left[-\frac{(Rx - vt)^2}{4 D_L R t}\right] - \frac{1}{2}\left[1 + \frac{vx}{D_L} + \frac{v^2 t}{D_L R} + \right] \exp\left[\frac{vx}{D_L}\right] erfc\left[\frac{Rx + vt}{2(D_L Rt)^{1/2}}\right]$$ Equation 4-17

where *erfc* is the complimentary error function.

The advection-dispersion model for a single pathway is herein referred to as the AD-1 model.

The results from AD-1 model evaluation are in this report presented using mean residence time, t_m (= x/v) and Peclet number, Pe (=x/a_L). Since no sorbing tracers were used, the retardation factor, R, was assumed to be 1 for all tracers. Further, the proportionality factor, pf , which describes the fraction of the injected tracer mass that arrives at the sampling section, may be employed as fitting parameters during model evaluation.

Other models used previously for evaluation of similar tracer tests include advection-dispersion in multiple pathways and advection-dispersion with matrix diffusion for one pathway. These models are not applied in this modelling, for description see /Lindquist et al. 2008a/.

4.6.5 Parameter estimation method

Estimated parameter values are obtained by non-linear least-squares regression. The basic non-linear least-squares regression minimises the sum of squared differences between the modelled (Y^M) and the observed (Y^O) variables and may be formulated as:

$\min S = E_R^T W E_R$ Equation 4-18

where E_R is a vector of residuals ($Y^O - Y^M$) and W is a vector of reliability weights on observations.

The specific method for carrying out the regression employed in this study is often referred to as the Marquardt-Levenberg method. This method is a Newton-type optimisation algorithm that finds the parameter values that minimises the sum of squared errors between model and measurement values in an iterative manner. A basic Newton-type search algorithm used may be written as:

$B_{r+1} = B_r + (X_r^T W X_r)^{-1} X_r^T (Y^O - Y_r^M)$ Equation 4-19

where B is a vector of parameter estimates, X is a parameter sensitivity matrix, and the subscripts r and r+1 refer to the iteration number. The Marquardt-Levenberg method is an extension that enhances the convergence properties of the search algorithm by restricting the search direction.

Given an initial parameter estimate (B_r), the model variable vector (Y^M) and the sensitivity matrix (X) are calculated and a new vector of estimates (B_{r+1}) is obtained. Equation 4-18 is then repeated until a local optimal solution is found. The local minimum is defined by some convergence criterion, for example when parameter estimates are essentially identical between iterations. Finding a local minimum does not guarantee that the global minimum is found. When this appears to be a problem, several sets of initial estimates may be tried. When some knowledge about the parameters to be estimated and the physical system is already available, the initial estimates are often good enough for ensuring that a global minimum is found.

An important element of the above procedure is the matrix containing the parameter sensitivities. Parameter sensitivity is defined as the partial derivative of the dependent (simulated) variable with respect to a parameter. A sensitivity matrix contains one row for each observation and one column for each estimated parameter, as in the following example with three observations and two parameters.

$$\mathbf{X} = \begin{pmatrix} \frac{\partial y_1}{\partial b_1} & \frac{\partial y_1}{\partial b_2} \\ \frac{\partial y_2}{\partial b_1} & \frac{\partial y_2}{\partial b_2} \\ \frac{\partial y_3}{\partial b_1} & \frac{\partial y_3}{\partial b_2} \end{pmatrix} \qquad \text{Equation 4-20}$$

Parameter sensitivities may be used to determine the precision of the estimated parameter values. Two diagnostic measures are given below regarding parameter uncertainty that may be obtained as a result of regression /Cooley 1979/.

The *standard errors* of parameter estimates are obtained by taking the square roots of the diagonals in the parameter covariance matrix, which is given by:

$$s^2(X^T W X)^{-1} \qquad \text{Equation 4-21}$$

with s^2 being the error variance:

$$s^2 = \frac{\sum_{i=1}^{N} w_i \, (y_i^O - y_i^M)^2}{N - P} \qquad \text{Equation 4-22}$$

where N is the number of measurements, P the number of parameters to be estimated and w_i the weight on observation i.

The linear correlation $r(p_1,p_2)$ between two parameters with values of p_1 and p_2, respectively, is given by:

$$r(p_1, p_2) = \frac{Cov(p_1, p_2)}{\sqrt{Var(p_1) Var(p_2)}} \qquad \text{Equation 4-23}$$

where the variance and covariance terms are elements of the $s^2(X^T W X)^{-1}$ matrix. The correlation is a measure of the inter-dependence between two parameter estimates, and correlation values range between –1 and 1. Values close to either –1 or 1 mean that a change in one parameter value may be compensated for by a similar change in another parameter value to maintain the same fit (sum of squares) between model and measurements. The standard errors and parameter correlation values are the main diagnostic measures used in this analysis when examining the parameter estimation results from evaluation of the tracer tests.

4.6.6 Other derived transport parameters

In accordance with the SKB method description for two-well tracer tests (SKB MD 530.006), some further transport parameters are derived, mainly based on the average residence time, t_m, determined from the model evaluation described above. The derived parameters are:

- mass balance aperture (fracture aperture)
- hydraulic fracture conductivity
- flow porosity

The mass balance aperture, δ_m [L], is determined from:

$$\delta_m = \frac{Q t_m}{\pi (r^2 - r_w^2)} \qquad \text{Equation 4-24}$$

where Q is the average pumping rate [L^3/T], r is the travel distance [L] and r_w is the borehole radius [L].

The hydraulic fracture conductivity, K_{fr} [L/T] is calculated using:

$$K_{fr} = \ln\left(\frac{r}{r_w}\right)\frac{\left(r^2 - r_w^2\right)}{2t_m\Delta h} \qquad \text{Equation 4-25}$$

where Δh is the head difference [L] between the injection and pumping sections. The flow porosity, ε_f is determined from:

$$\varepsilon_f = \frac{K}{K_{fr}} \qquad \text{Equation 4-26}$$

where K is the hydraulic conductivity of the packed-off section. In this report, K is determined from a steady-state evaluation of the single hole test /Moye 1967/.

4.7 Nonconformities

The groundwater flow measurements, the tracer test and the interference test were carried out according to the plan except for the following nonconformities:

- The water level in HLX37:1 was at the time of tracer injection so low that the water could not be circulated. Hence, the tracer injection could not be performed with exchange of water as planned. Instead, the tracer solution was injected in the borehole section and followed by injection of c 180 L of water without tracer. Consequently, no sampling or groundwater flow measurements could be performed during the tracer injection.
- The analyses of Gadolinium (Gd), carried out early during the tracer test at the ALS laboratory, show large divergence between batches of samples due to insufficient corrections for disturbance from other elements. However, the last batch of samples analysed, covering the entire tracer test, was not considered to be affected by insufficient correction. This batch is also the only one used for reporting, modelling and evaluation of the tracer test.
- The analysed values for Gd in the injection containers agree poorly with the recipe that was used for preparation of the injection solution. Due to the uncertainty about the Gd analyses, see above, it was judged that the recipe used was more accurate than the laboratory analyses of Gd. The theoretical concentration from the recipe has therefore been used for further calculations and evaluation.
- Prior to the start of pumping, there was a failed attempt to start the pump that caused a small pressure disturbance in the pumping borehole HLX28. This was due to a faulty electric connection, causing a considerable reduction in pump capacity. Pumping with reduced capacity occurred for c 1 minute.
- In borehole section HLX36:1 and KLX11E, the water level decreased below the position of the pressure transmitter. Hence, pressure data is not representative for parts of the test period.
- Data for KLX14A:2 in conjunction with pumping start in HLX28 are not available due to a defect pressure transmitter. A new pressure transmitter was installed 2009-01-21.
- The pumping in HLX28 was interrupted three times during the pumping period. Interruptions occurred 2009-02-07 c 14:48–17:09, 2009-05-22 c 19:16–21:04 and 2009-05-24 c 12:41–15:03. All three interruptions were caused by interruptions in the power supply. The pumping was resumed as soon as power was restored.
- Pressure data were taken from HMS shortly after the completion of the interference test in order to carry out evaluation and reporting within a reasonable time frame. The data, or at least parts of the data, used for evaluation within the present report were therefore not processed with the usual quality assurance made within the HMS. Hence, some data may have been altered in HMS after the extraction for this report. However, generally no or only very small changes in data are made within the quality assurance of HMS. It is assumed that such small changes would not affect the overall result presented in this report in any major way.

5 Results

5.1 Nomenclature and symbols

The nomenclature and symbols used for the results of the single-hole- and interference test are according to the Instruction for analysis of single-hole injection- and pumping tests (SKB MD 320.004) and the method description for interference tests (SKB MD 330.003), respectively (both are SKB internal controlling documents). The same applies for nomenclature and symbols used for the results from groundwater flow measurements and tracer tests which are carried out according to the method descriptions SKB MD 368.010 and SKB MD 530.006 respectively (SKB internal controlling documents). Additional symbols used are explained in the text.

Since the pressure in the boreholes are given in terms of groundwater levels in HMS, the terms pressure, groundwater level and hydraulic head are used as synonyms to explain the hydraulic conditions in the boreholes.

5.2 Groundwater flow measurements

The results of the groundwater flow measurements are presented in Table 5-1. An example of a tracer dilution curve is shown in Figure 5-1. All tracer dilution graphs are presented in Appendix 3 and Appendix 4. The groundwater levels during the entire test period are shown in Appendix 2, see also Table 4-2 and Table 4-3.

After tracer injection in the tracer test, the dilution of tracers in the injection sections were measured in the same way as during the groundwater flow measurements with Amino-G, except in HLX37:1 (see Section 4.7). They were interpreted in the same way and the tracer dilution graphs are presented in Appendix 5.

The largest flow responses, in terms of mL/min, due to the pumping in HLX28 were found in HLX37:1, KLX20A:5, KLX27A:6 and KLX11A:3. For HLX32:2, the highest flow rate was found during the last measured period after the tracer injection period. For KLX11A:3 and KLX20A:5, the flow rates instead decrease with time.

Table 5-1. Measured groundwater flow in the investigated sections and comparison between the two different measurements of groundwater flow during pumping in HLX28.

Borehole: section	Measured flow (ml/min)			
	Undisturbed conditions		During pumping in HLX28	
	First campagn	Second campagn	Prior to tracer test (Amino-G)	During tracer test (with tracer)
HLX32:2	8.3	7.1	7.7	4.2/20*
HLX37:1	2.5	1.8	27	No data available
HLX38:3	4.6	0.95	1.3	2.5
KLX11A:3	2.6	1.1	7.1	2.5
KLX11A:7	0.70	0.38	0.23	No tracer test
KLX19A:3	0.61	0.37	0.32	No tracer test
KLX20A:2	0.69	5.2	5.4	No tracer test
KLX20A:5	6.3	6.4	17	18/8.0*
KLX27A:1	0.32	0.07	1.3	No tracer test
KLX27A:6	4.2	4.6	7.6	11

* period 1/period 2.

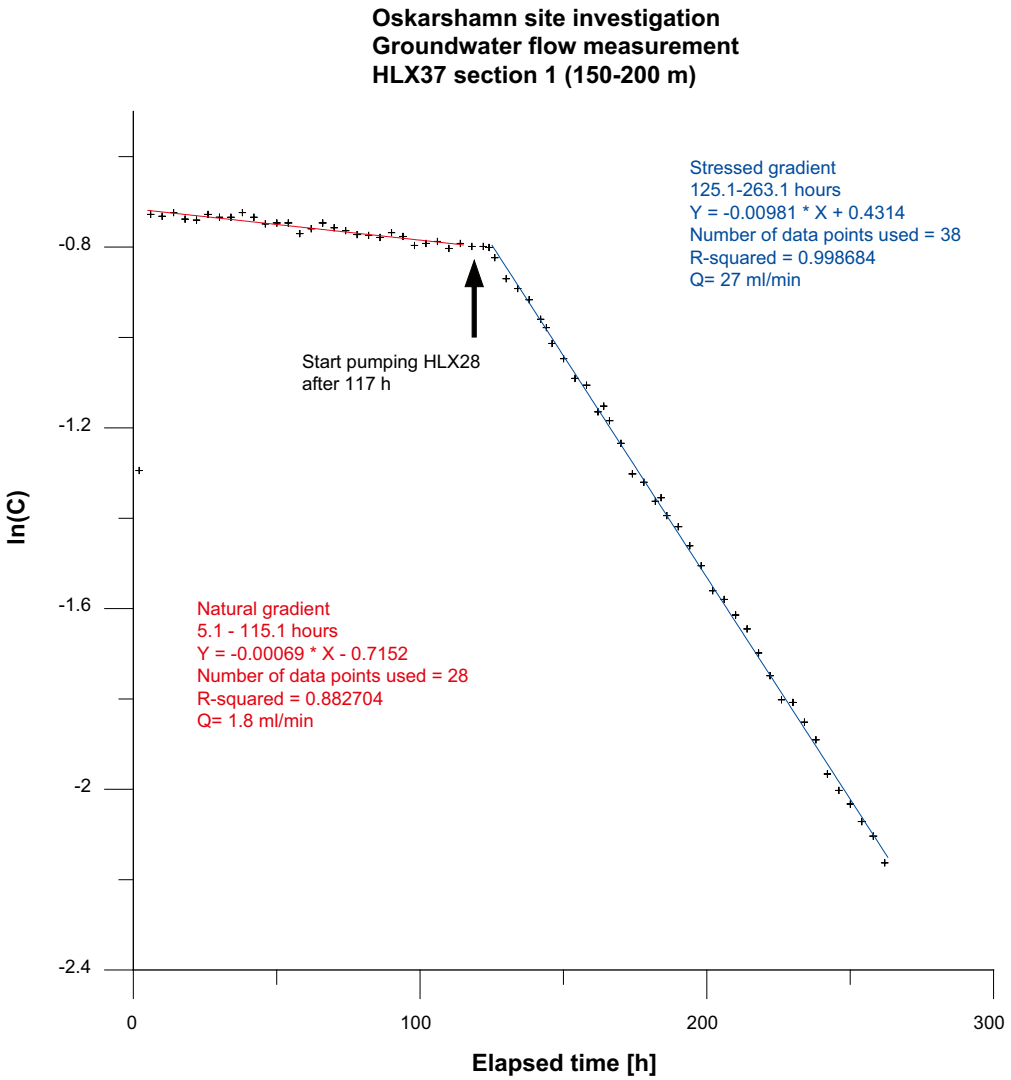

Figure 5-1. *Example of a tracer dilution graph (logarithm of concentration versus time) for borehole HLX37, section 1, including straight-line fits during both natural and pumped conditions.*

5.3 Pumping and interference test

5.3.1 General

The flow period of the interference test in HLX28 lasted from 2009-01-20 to 2009-05-26 (181,423 min). The subsequent recovery period was recorded but not analysed in this case. It was decided by the activity leader to evaluate the interference test in HLX28 based on data only up to 2009-04-30 24:00:00 during the flow period. The beginning of the recovery period was in some cases used to deduce if the actual observation section responded to the pumping in HLX28 or not, e.g. in weakly responding sections. The exact start and stop times of the flow and recovery period are shown in Table 4-4.

Measurements of precipitation, air pressure and sea water level during the interference test period are shown in Figure A2-1 and A2-2. The flow rate and pressure in the pumping borehole are shown in Figure A2-3. Linear diagrams of the groundwater level versus time (HMS diagrams) in all observation boreholes together with comments on the test data, are presented section by section in Figures A2-4 through A2-21 in Appendix 2. The test diagrams showing transient evaluation are shown in Appendix 6. The locations of the boreholes in the Laxemar area, including the pumping borehole HLX28, are shown in Figure 1-1.

According to Figure A2-1, none or little precipitation occurred during the beginning of the flow period. However, heavy precipitation occurred 2009-02-21 to 2009-02-22 and later on, which temporarily caused approximate steady-state groundwater head conditions, see Appendix 2. Subsequently, a drought period, starting at about 2009-04-01, caused a natural trend of decreasing groundwater levels in the area. This trend was interrupted by heavy rainfall at the end of April. By the end of the flow period, the head in the pumping borehole HLX28 had decreased significantly due to apparent outer no-flow boundary conditions in combination with the naturally decreasing head trend.

The transient evaluation of the flow period was based on responses up to c 25,000 min (2009-02-06), before the short pump stop at 2009-02-07, due to the presence of drought periods, precipitation and effects of no-flow boundaries at longer times. During the period up to 25,000 min, little precipitation occurred. No corrections of the head data due to drought periods, or other corrections of the data, were considered necessary during this period. Finally, there were no effects of apparent hydraulic boundaries up to this time.

In several observation sections located relatively close to the pumping borehole HLX28, e.g. in HLX32, KLX14A and KLX19A, a slightly increasing head trend was observed shortly after start of pumping in HLX28. This resulted initially in an apparently negative drawdown, see Figure 5-2 although this is not fully explained. Prior to the pumping start, the head was quite stable so it is not an effect of an on-going trend. Nor were any effects related to equipment, such as change of scanning interval, found that may explain this phenomenon. Instead, it seems like the increasing head in some sections is a hydraulic effect, possibly reinforced by the short failed attempt to start the pump just before the real pump start, see Section 4.7, which is shown in Figure 5-3.

The increasing head behaviour causes slightly higher apparent response times in these sections (see Section 5.3.3). However, the influence of this effect on the estimated hydraulic parameters from the transient evaluation is negligible.

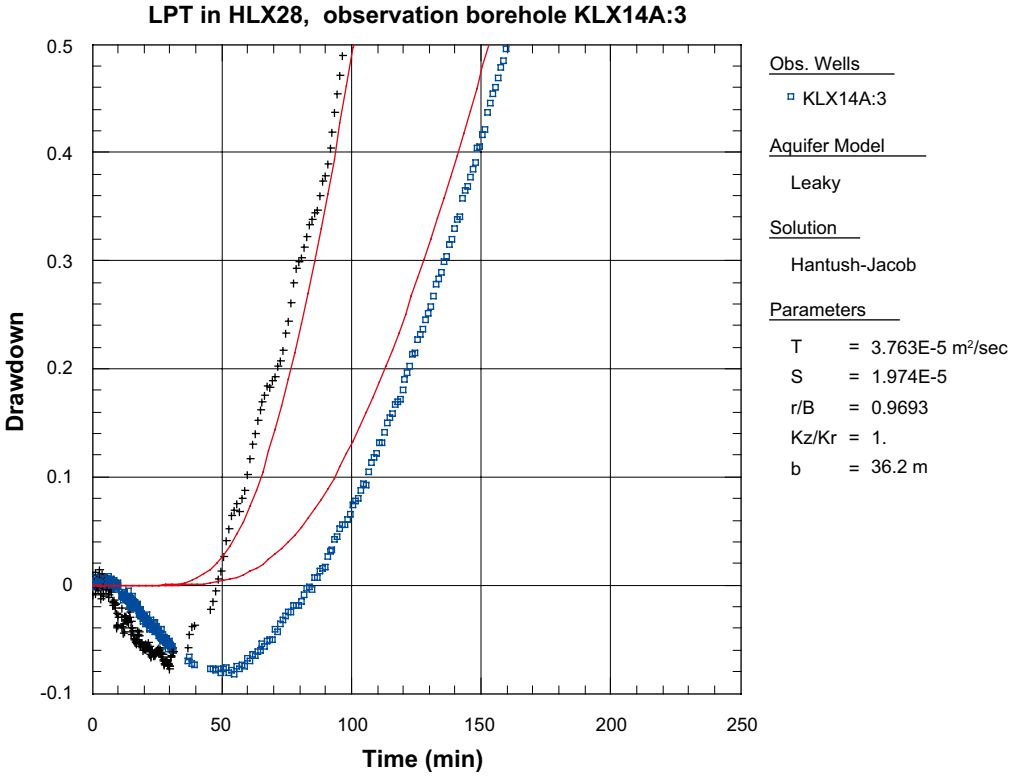

Figure 5-2. *Example of early drawdown behaviour in observation borehole section KLX14A:3 showing slightly increasing head values after start of pumping in HLX28.*

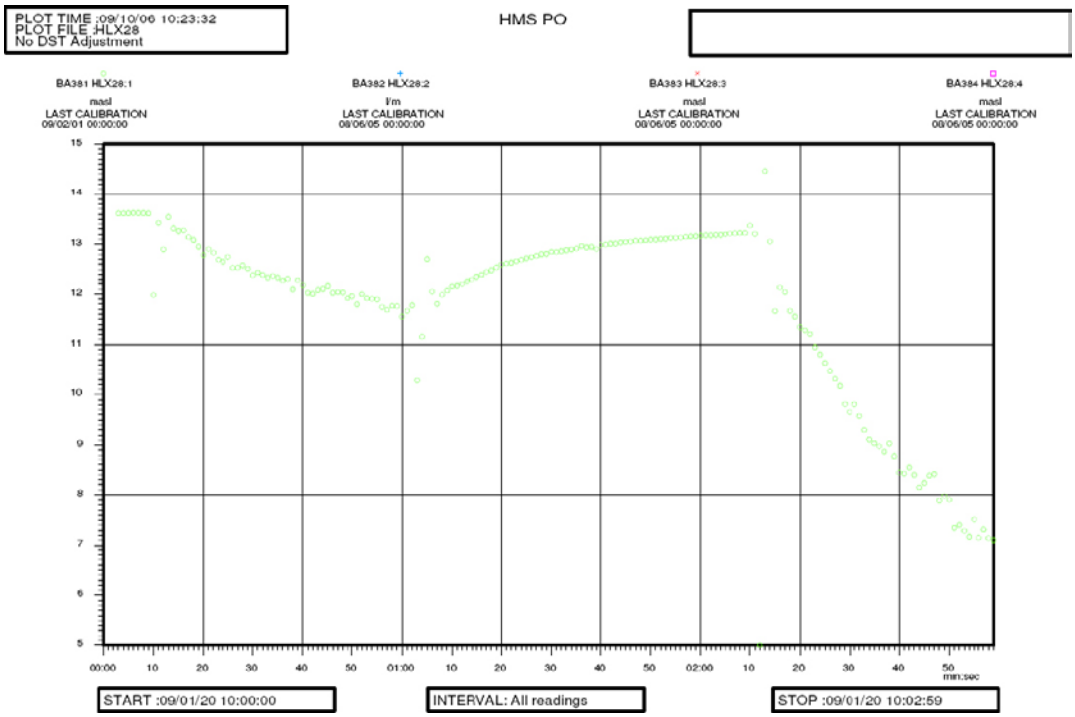

Figure 5-3. *Detail of head response in HLX28 during the first unsuccessful pump start and the real pump start.*

In several of the observation sections, the head showed an oscillating behaviour. This is believed to be caused by so called tidal fluctuations or earth tides in combination with changes in the sea water level. These phenomena have, to some extent, been investigated previously at Forsmark in /Ludvigson et al. 2004/.

In Appendix 1, all observation sections included in the interference test (274) are listed together with a classification of the type of responses and distances to HLX28. Visual inspection of the pressure responses in the observation sections in the linear diagrams indicates that presumed responses were registered in 63 observation borehole sections. Of these, clear responses (Class 1a and 1b) were observed in 53 sections. Transient evaluation could be made in all of these sections except in two (classified as 1b).

In section KLX14A:2, data are missing (see Section 4.7) in the beginning and thus, no transient evaluation could be made for this section. Neither could the response lag time be estimated for this section, which therefore is not included in the response analysis.

In section KLX20A:6, the groundwater level was unstable (slightly rising) before start of pumping (see Appendix 2), which makes the transient evaluation and estimation of the response time for this section somewhat uncertain. In section KLX27A:8, the groundwater level was slightly decreasing just after start of pumping (before the main response) but this trend is probably not related to the pumping in HLX28.

Ten sections showed a weak response (Class 2) to the pumping and the transient evaluation is regarded as uncertain for these sections. Only for one section (KLX16:1), it cannot be confirmed whether the section was affected by the pumping in HLX28 (Class 3) or not. The linear overview plot of head values for this section in Figure A2-15 shows an apparent drawdown during the entire flow period but the drawdown continued a few weeks after stop of pumping. The groundwater head in this section may thus be governed by other factors than the pumping in HLX28. No transient analysis was made for this section. Totally 202 of the observation sections were considered to be unaffected by the pumping in HLX28 (Class 4).

Most of the non-responding sections, i.e. Class 4, are located at a long distance from HLX28. However, some are located closer to HLX28 than other responding sections, see Figure 5-4.

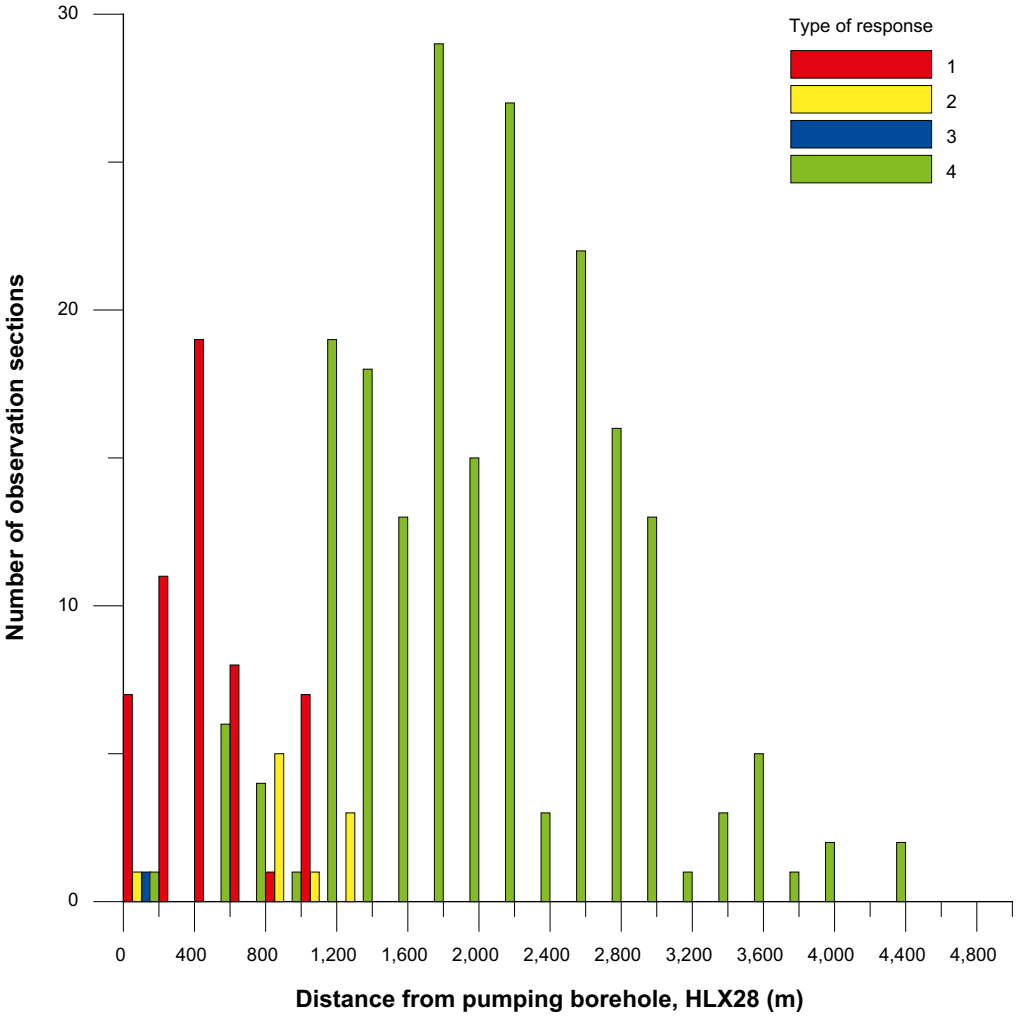

Figure 5-4. *Histogram showing the number of observation sections for each type of response, grouped by distance from the pumping borehole.*

5.3.2 Single-hole evaluation of pumping test in HLX28

A compilation of measured test data from the pumping borehole HLX28 is shown in Table 5-2. In Table 5-3 are calculated hydraulic parameters for the pumping borehole presented.

The response in the pumping borehole HLX28 during the flow period indicates a dual-permeability system with an early short PRF, followed by a transition to a second PRF with lower transmissivity and subsequently to a PSF. After c 25,000 min, the first effects of apparent NFB's occur. After a period with heavy precipitation, a new temporary PSF is developed. By the end of the flow period, strong effects of apparent NFB's show up again.

The estimated transmissivity of the intersecting structure closest to the pumping borehole HLX28 is rather high, $3.0 \cdot 10^{-4}$ m^2/s, see Test Summary Sheet in Table 5-4 and Figure A6-3 in Appendix 6. At later times (i.e. at longer distances from HLX28) the transmissivity decreases to $3.4 \cdot 10^{-5}$ m^2/s, see Figure A6-5. The estimated transmissivities from the observation sections are assumed to be dominated by the transmissivity of the rock or hydraulic structures further away from the pumping borehole.

Table 5-2. Summary of test data from the pumping borehole HLX28 during the interference test in the Laxemar area.

Pumping borehole ID	Section (mbl)	Test Type[1)]	h_i (m)	h_p (m)	h_F (m)	Q_p (m^3/s)	Q_m (m^3/s)	V_p (m^3)
HLX28	6.00–154.20	1B	13.62	–23.18	10.36	4.83E–03	4.97E–03	54108.01

[1)] 1B: Pumping test-submersible pump.
h_i = Head in test section before start of the flow period.
h_p = Head in test section before stop of the flow period.
h_F = Head in test section at end of the recovery period.
Q_p = Flow in test section immediately before stop of flow period.
Q_m = Arithmetical mean flow rate during the flow period.
V_p = Total water volume pumped out during the flow period.

Table 5-3. Summary of calculated hydraulic parameters from the pumping borehole HLX28 during the interference test in the Laxemar area.

Pumping borehole ID	Section (mbl)	Test type	Q/s (m^2/s)	T_M (m^2/s)	T_T (m^2/s)	ζ (-)	C_{WBS} (m^3/Pa)	S* (-)
HLX28	6.00–154.20	1B	$1.3\cdot10^{-4}$	$1.7\cdot10^{-4}$	$3.0\cdot10^{-4}$	–3.3	$2.2\cdot10^{-6}$	$1.2\cdot10^{-5}$

Q/s = specific flow for the pumping borehole (m^2/s).
T_M = steady state transmissivity from Moye´s equation (m^2/s).
T_T = transmissivity from transient evaluation of single-hole test (m^2/s).
S* = assumed/calculated storativity by the estimation of the skin factor (-).
C_{WBS} = wellbore storage coefficient (m^3/Pa).
ζ = skin factor (-).

Table 5-4. Test Summary Sheet for the pumping borehole HLX28 containing borehole data, evaluated parameters and comments to test evaluation.

Test Summary Sheet – Pumping borehole HLX28					
Project:	PLU	Test type:	1B		
Area:	Oskarshamn	Test no:	1		
Borehole ID:	HLX28	Test start:	2009-01-20 10:02:10		
Test section (m):	6.0–154.2	Responsible for test execution:	SKB field crew		
Section diameter, $2 \cdot r_w$ (m):	0.068	Responsible for test evaluation:	GEOSIGMA AB Jan-Erik Ludvigson		
Linear plot Q and p		**Flow period**		**Recovery period**	
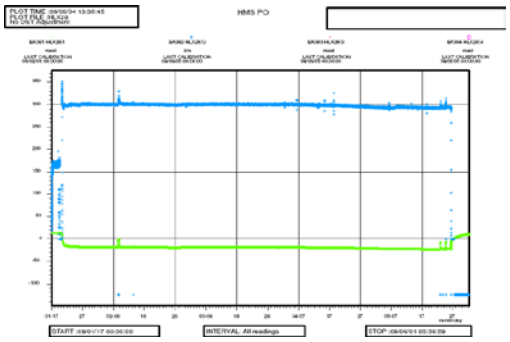		**Indata**		**Indata**	
		p_0 (m)			
		p_i (m)	13.62		
		p_p (m)	–23.18	p_F (kPa)	101.6
		Q_p (m³/s)	$4.83 \cdot 10^{-3}$		
		t_p (min)	181,426	t_F (min)	189,840
		S* (-)	1.21E–5	S* (-)	
		EC_w (mS/m)			
		Te_w(°C)			
		Derivative factor	0.2	Derivative factor	
		r (m)		r (m)	
		Results		**Results**	
		Q/s (m²/s)	$1.3 \cdot 10^{-4}$		
Log-Log plot incl. derivates- flow period		T_M (m²/s)	$1.7 \cdot 10^{-4}$		
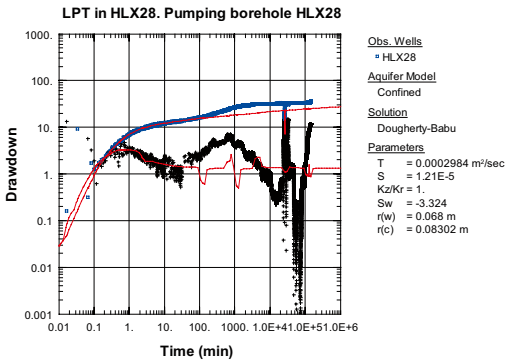		Flow regime:	WBS->PRF1->PRF2->PSF1->NFB->PSF2->NFB	Flow regime:	
		dt_1 (min)	5	dt_1 (min)	
		dt_2 (min)	30	dt_2 (min)	
		T (m²/s)	$3.0 \cdot 10^{-4}$	T (m²/s)	
		S (-)		S (-)	
		K_s (m/s)		K_s (m/s)	
		S_s (1/m)		S_s (1/m)	
		C (m³/Pa)	$2.2 \cdot 10^{-6}$	C (m³/Pa)	
		C_D (-)		C_D (-)	
		ξ (-)	–3.3	ξ (-)	
		T_{GRF} (m²/s)		T_{GRF} (m²/s)	
		S_{GRF} (-)		S_{GRF} (-)	
		D_{GRF} (-)		D_{GRF} (-)	
Log-Log plot incl. derivatives- recovery period		**Selected representative parameters**			
		dt_1 (min)	5	C (m³/Pa)	$2.2 \cdot 10^{-6}$
		dt_2 (min)	30	C_D (-)	
		T_T (m²/s)	$3.0 \cdot 10^{-4}$	ξ (-)	–3.3
		S* (-)	1.2E–5		
		K_s (m/s)			
		S_s (1/m)			
The recovery period was not analysed		Comments: The flow rate was relatively constant during the flow period. The response during the flow period indicates a double-permeability system with an early, short PRF followed by a transition to a second PRF with lower transmissivity and subsequently to a PSF. After c 25,000 min, effects of apparent NFB occur. After a period with heavy precipitation, a new temporary PSF is developed. By the end of the flow period strong effects of apparent NFB again show up. The parameter values estimated from the early phase of the flow period (early PRF between c 5–30 min) are selected as the most representative for the hydraulic conditions in the small scale adjacent to the test section.			

5.3.3 Response analysis and estimation of hydraulic diffusivity

A compilation of measured test data as well as calculated hydraulic parameters for the responding observation sections (denoted "1a", "1b" and "2" in Appendix 1) are presented in Table 5-5. The lag times (dt_L) were derived from the drawdown curves in the observation borehole sections at a drawdown of 0.1 m. The drawdown s_p correspond in this case to the flow rate and drawdown, respectively, at t = 25,000 min during the flow period, i.e. to the maximum time on which the transient test evaluation is based, as discussed in Section 5.3.1.

The numerical values of the response indices as well as the classification, as defined in Section 4.6.2, are shown in Table 5-5**.** Index 1 is directly related to the hydraulic diffusivity (T/S) of the formation and Index 2_new reflects the strength of the response.

Due to the increasing head after start of pumping, as discussed in Section 5.3.1, the estimated time lags in these sections will be slightly higher (delayed) using the standard procedures for defining the initial head at the observation sections and time of pump start, respectively. An alternative procedure would be to redefine the initial head in these sections as the actual head value just before the onset of the real response due to pumping, while maintaining the actual start time for the pumping in HLX28. However, the latter approach has not been applied in this study.

Because of disturbances, e.g. oscillating head or responses to other activities in the area, see for instance Figure A6-34, it was sometimes difficult to determine the exact time lag for a drawdown of 0.1 m. The estimated time lag for some of the responding observation sections must therefore be regarded as rough estimates.

The transmissivity and storativity from the transient evaluation are shown in Figure 5-5 together with the evaluated transmissivity for the two different periods for the pumping borehole HLX28. As seen in Figure 5-5, the estimated transmissivity value for the later period in HLX28 is consistent with the majority of the observation sections. The estimated values for HLX32:3 deviates considerably from the rest and should be regarded as more uncertain.

The hydraulic diffusivity T/S, which is assumed to reflect the hydraulic connection between observation sections and the pumping borehole, of the responding observation sections, was estimated from the response time lag dt_L according to Equation 4-10 in Section 4.6.2. The estimated values of hydraulic diffusivity from the lag times are shown in Table 5-5. For comparison, the ratio of the estimated transmissivity and storativity, T_o/S_o, from the transient evaluation in these sections are also presented. A cross-plot of hydraulic diffusivity estimated from the lag times and the transient test evaluation, respectively, is shown in Figure 5-6.

Table 5-5 and Figure 5-6 show that there is a fair agreement between the estimated hydraulic diffusivity of the sections based on the response time lags and from the transient evaluation, respectively, and this is also the case for observation sections at long distances from the pumping borehole. The estimated hydraulic diffusivity values from the response analysis are consistent with those from the transient evaluation.

A response analysis was made according to the method description for interference tests. All responding sections are included in the response analysis. However, since only one interference test was performed, no response matrix was made.

Figure 5-7 shows a response diagram for the responding observation sections with Index 2_new versus Index 1 at time t = 25,000 min. The basic idea with the response diagram is to group the responses according to their strength and time lag respectively. Observation sections represented by data points towards the upper right corner in the diagram generally indicate better connectivity to the pumping borehole and higher hydraulic diffusivities, whereas sections located towards the bottom left corner in the diagram generally represent sections with weak and delayed responses with presumed low connectivity to the pumping borehole.

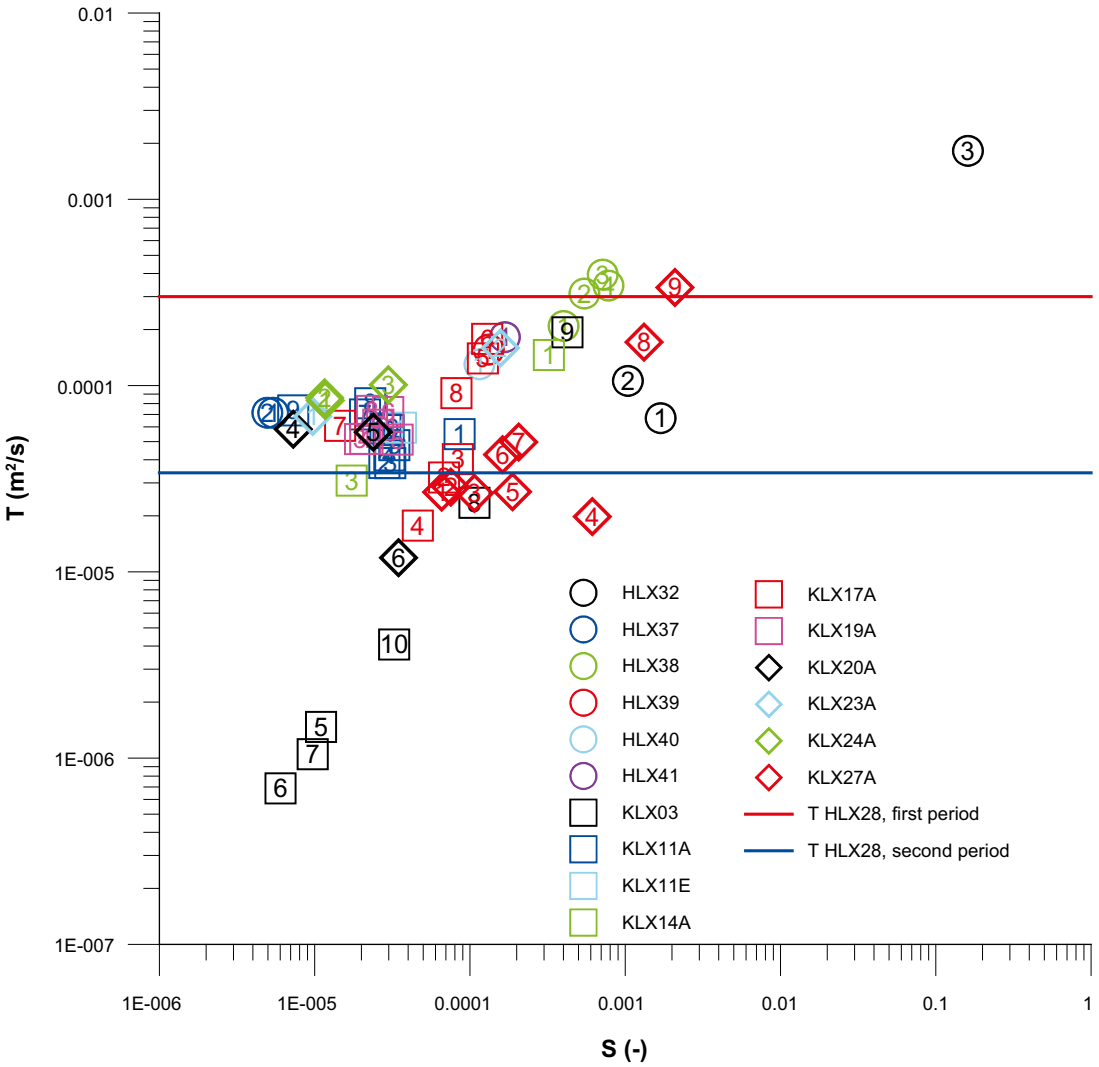

Figure 5-5. *Transmissivity and storativity from the transient evaluation for the responding section during the interference test with pumping in HLX28, as well as evaluated transmissivity for HLX28.*

Figure 5-7 indicates that the most distinct and fastest responses were found in borehole sections HLX37:1-2, KLX11A:2-9, KLX19A:3-8, KLX20A:4 and KLX23A:1. Borehole sections with strong but more delayed responses occurred in borehole KLX27A:1-3 and KLX27A:5-6. Fast but not as strong responses occurred in HLX39:1, KLX11A:1, KLX11E:1, KLX14A:3, KLX17A:5-8, KLX20A:5 and KLX24A:1-3. The response of HLX36:1 was also fast but is not included in Figure 5-7 since no Index 2_new was possible to calculate for that section. The weakest and most delayed responses occurred in sections HLX32:3 and KLX03:5-10. The remaining sections in KLX03 did not respond at all to the pumping in HLX28.

The response in HLX32:3, which represents the groundwater table, is very delayed but shows a certain recovery after stop of pumping, see Figure A2-4 in Appendix 2, indicating some hydraulic connection to HLX28.

It should be noted that sections KLX14A:2 and HLX36:1 are not included in Figure 5-7 due to missing data, see Section 4.7. KLX11E is also mentioned in Section 4.7.

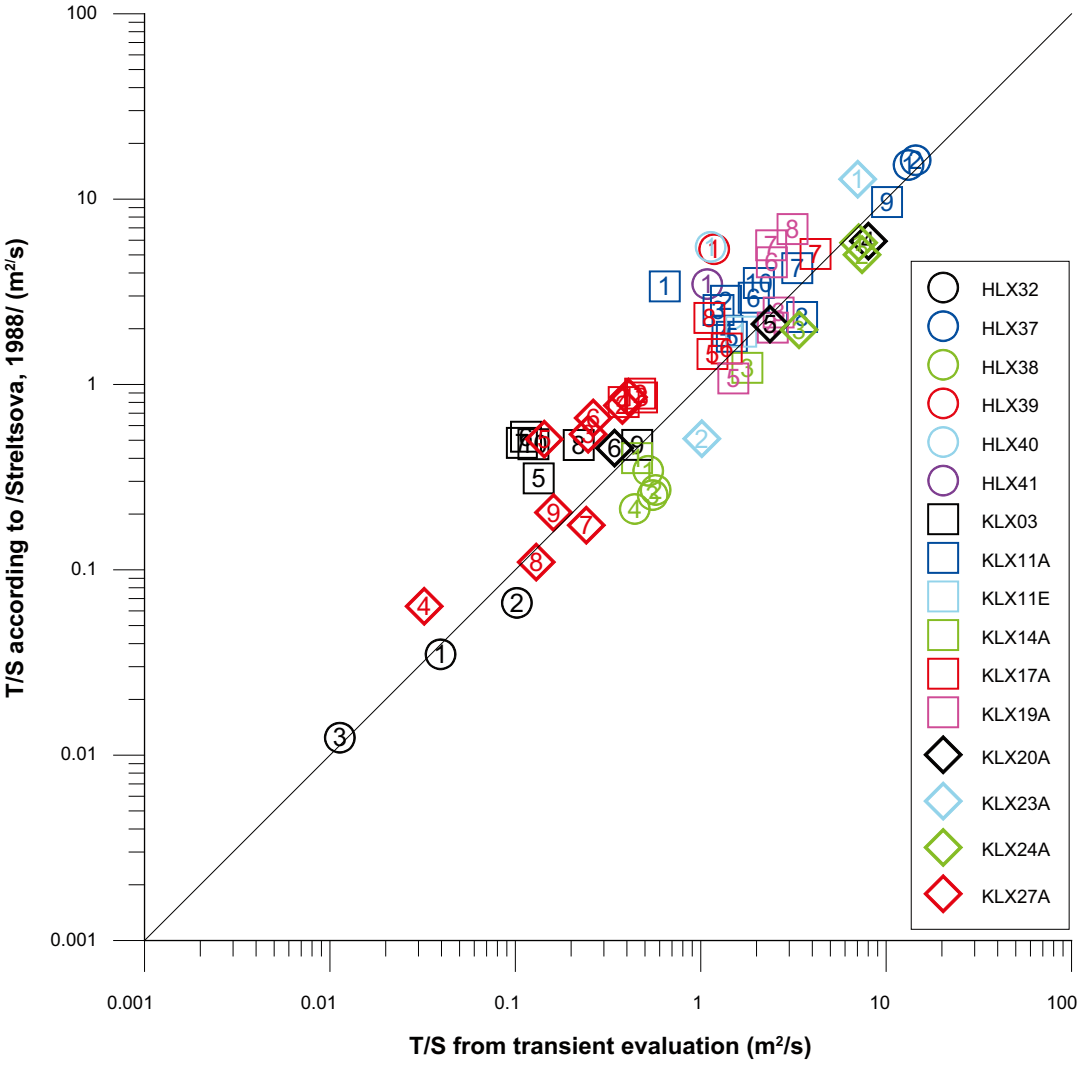

Figure 5-6. *Comparison of estimated hydraulic diffusivity of the responding observation sections from the lag times and test evaluations, respectively, in the interference test in HLX28.*

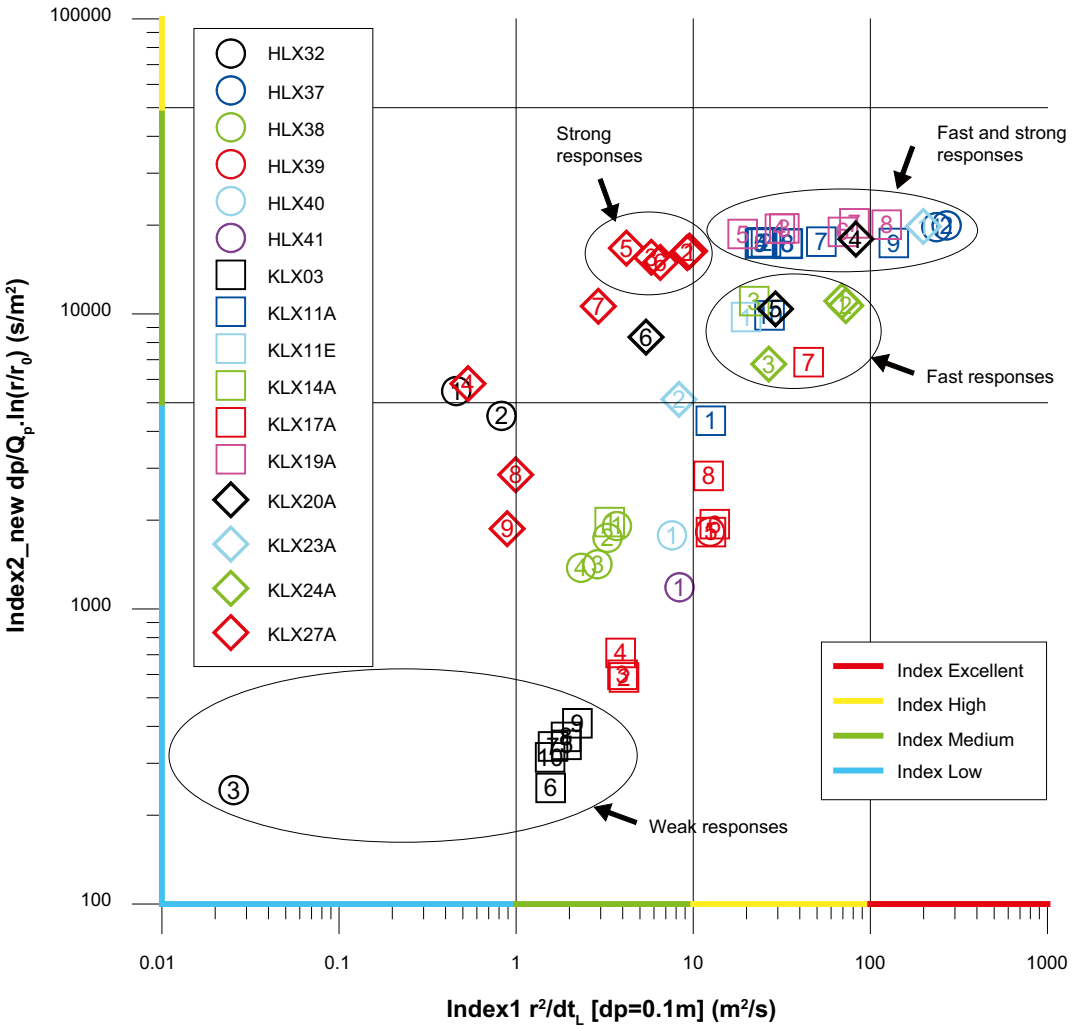

Figure 5-7. Response diagram showing responses in observation sections during the interference test in HLX28. Response Index 2_new is plotted versus Index 1. The classification of the two indices is also shown on the axes of the diagram. Each borehole is colour-coded and the sections are numbered. The lag time is based on a drawdown of 0.1 m. The drawdown sp and flow rate Qp are based on time t=25,000 min.

Table 5-5. Summary of data, response indices and estimated hydraulic parameters from the responding observation boreholes during the interference test in HLX28 in the Laxemar area.

Observation borehole ID: section	Section (mbl)	r_s (m)	dt_L(s) [s=0.1 m]	h_i (m)	h_p (m)	s_p (m)	Index 1: r_s^2/dt_L (m^2/s) [s=0.1 m]	Index 1 class	Index 2_new: $s_p/Q_p \cdot \ln(r_s/r_0)$ (s/m^2)	Index 2_new class	To (m^2/s)	S_o (-)	K'/b' (s^{-1})	T_o/S_o (m^2/s)	T/S (m^2/s)
HLX32:1	31.00–162.60	76.0	12,600	7.96	1.64	6.32	4.6E–01	L	5.5E+03	M	6.7E–05	1.7E–03	8.6E–09	4.0E–02	3.5E–02
HLX32:2	20.00–30.00	122.0	18,000	7.53	2.83	4.70	8.3E–01	L	4.5E+03	L	1.1E–04	1.0E–03	4.1E–09	1.0E–01	6.6E–02
HLX32:3	12.30–19.00	129.5	660,000	7.26	7.01	0.25	2.5E–02	L	2.4E+02	L	1.8E–03	1.6E–01		1.1E–02	1.2E–02
HLX36:1	50.00–199.80	485.0	17,400	14.37	*	*	1.4E+01	H	*	*	*	*	*	*	1.3E+00
HLX37:1	150.00–199.80	486.0	1,002	13.55	–2.35	15.90	2.4E+02	E	2.0E+04	M	7.2E–05	5.4E–06	2.5E–11	1.3E+01	1.5E+01
HLX37:2	111.00–149.00	500.8	930	13.57	–2.49	16.05	2.7E+02	E	2.0E+04	M	7.2E–05	5.0E–06	2.3E–11	1.4E+01	1.6E+01
HLX38:1	81.00–199.50	405.8	44,400	5.91	4.32	1.59	3.7E+00	M	1.9E+03	L	2.1E–04	4.0E–04	1.4E–09	5.2E–01	3.4E–01
HLX38:2	41.00–80.00	360.3	39,600	5.73	4.25	1.48	3.3E+00	M	1.7E+03	L	3.1E–04	5.5E–04	1.6E–09	5.7E–01	2.7E–01
HLX38:3	28.00–40.00	349.1	42,300	5.67	4.46	1.21	2.9E+00	M	1.4E+03	L	3.9E–04	7.2E–04	2.1E–09	5.5E–01	2.5E–01
HLX38:4	15.02–27.00	344.5	51,000	5.74	4.56	1.18	2.3E+00	M	1.4E+03	L	3.4E–04	7.8E–04	2.4E–09	4.4E–01	2.1E–01
HLX39:1	6.02–199.30	1120.7	100,800	17.45	16.15	1.30	1.2E+01	H	1.8E+03	L	1.6E–04	1.3E–04	2.3E–10	1.2E+00	5.4E+00
HLX40:1	6.00–199.50	1148.9	174,000	17.58	16.32	1.26	7.6E+00	M	1.8E+03	L	1.3E–04	1.2E–04	2.3E–10	1.1E+00	5.5E+00
HLX41:1	6.02–199.50	1151.1	158,400	18.24	17.40	0.84	8.4E+00	M	1.2E+03	L	1.8E–04	1.7E–04	3.4E–10	1.1E+00	3.5E+00
KLX03:5	652.50–728.50	1019.0	540,000	10.45	10.20	0.25	1.9E+00	M	3.5E+02	L	1.5E–06	1.1E–05	6.6E–11	1.3E–01	3.1E–01
KLX03:6	465.50–651.50	970.0	600,000	10.03	9.85	0.18	1.6E+00	M	2.5E+02	L	6.9E–07	6.0E–06	4.4E–11	1.1E–01	5.2E–01
KLX03:7	349.50–464.50	933.9	540,000	9.83	9.58	0.25	1.6E+00	M	3.4E+02	L	1.1E–06	9.7E–06	6.1E–11	1.1E–01	4.8E–01
KLX03:8	199.50–348.50	921.7	444,000	10.76	10.49	0.27	1.9E+00	M	3.7E+02	L	2.4E–05	1.1E–04	4.9E–10	2.2E–01	4.7E–01
KLX03:9	193.50–198.50	922.5	384,000	10.88	10.58	0.30	2.2E+00	M	4.1E+02	L	1.9E–04	4.3E–04	1.2E–09	4.5E–01	4.7E–01
KLX03:10	100.05–192.50	926.1	552,000	10.55	10.32	0.23	1.6E+00	M	3.1E+02	L	4.1E–06	3.3E–05	1.8E–10	1.3E–01	4.8E–01
KLX11A:1	703.00–992.29	889.9	63,000	12.73	9.53	3.20	1.3E+01	H	4.3E+03	L	5.5E–05	8.6E–05	1.4E–10	6.4E–01	3.4E+00
KLX11A:2	587.00–702.00	743.9	21,480	14.10	0.89	13.21	2.6E+01	H	1.7E+04	M	3.8E–05	2.8E–05	3.3E–11	1.4E+00	2.8E+00
KLX11A:3	573.00–586.00	702.2	20,400	14.04	0.72	13.32	2.4E+01	H	1.7E+04	M	3.8E–05	3.1E–05	3.7E–11	1.2E+00	2.5E+00
KLX11A:4	495.00–572.00	674.8	18,600	13.99	0.60	13.39	2.4E+01	H	1.7E+04	M	4.2E–05	3.0E–05	3.7E–11	1.4E+00	1.9E+00
KLX11A:5	315.00–494.00	609.3	15,600	13.90	0.40	13.50	2.4E+01	H	1.7E+04	M	4.8E–05	3.3E–05	4.0E–11	1.5E+00	1.8E+00
KLX11A:6	273.00–314.00	570.4	9,600	13.80	0.13	13.67	3.4E+01	H	1.7E+04	M	5.8E–05	3.0E–05	3.5E–11	1.9E+00	2.9E+00
KLX11A:7	256.00–272.00	563.2	6,000	13.37	–0.50	13.87	5.3E+01	H	1.8E+04	M	7.0E–05	2.1E–05	2.7E–11	3.3E+00	4.2E+00
KLX11A:8	180.00–255.00	554.8	9,000	13.80	0.13	13.67	3.4E+01	H	1.7E+04	M	8.0E–05	2.3E–05	1.9E–11	3.5E+00	2.3E+00
KLX11A:9	103.00–179.00	549.0	2,220	14.34	0.55	13.79	1.4E+02	E	1.7E+04	M	7.4E–05	7.3E–06	3.0E–11	1.0E+01	9.6E+00

Observation borehole ID: section	Section (mbl)	r_s (m)	dt_L(s) [s=0.1 m]	h_i (m)	h_p (m)	s_p (m)	Index 1: r_s^2/dt_L (m^2/s) [s=0.1 m]	Index 1 class	Index 2_new: $s_p/Q_p \cdot \ln(r_s/r_0)$ (s/m^2)	Index 2_new class	To (m^2/s)	S_o (-)	K'/b' (s^{-1})	T_o/S_o (m^2/s)	T/S (m^2/s)
KLX11A:10	12.05–102.00	554.3	11,400	16.43	8.61	7.82	2.7E+01	H	9.9E+03	M	5.9E–05	2.9E–05	1.2E–10	2.1E+00	3.5E+00
KLX11E:1	0.00–121.30	545.8	15,000	16.80	9.06	7.74	2.0E+01	H	9.8E+03	M	6.0E–05	3.6E–05	1.3E–10	1.7E+00	1.9E+00
KLX14A:1	123.00–176.27	438.8	57,000	6.25	4.63	1.62	3.4E+00	M	2.0E+03	L	1.5E–04	3.2E–04	1.3E–09	4.5E–01	4.0E–01
KLX14A:2	77.00–122.00	405.9	*	6.00	4.14	1.86	*	*	2.2E+03	L	*	*	*	*	*
KLX14A:3	6.45–76.00	378.5	6,480	11.09	1.78	9.31	2.2E+01	H	1.1E+04	M	3.1E–05	1.7E–05	2.7E–10	1.8E+00	1.2E+00
KLX17A:2	419.00–434.00	1268.5	396,000	16.22	15.81	0.41	4.1E+00	M	5.9E+02	L	3.2E–05	6.8E–05	2.7E–10	4.7E–01	8.9E–01
KLX17A:3	343.00–418.00	1237.6	384,000	16.27	15.85	0.42	4.0E+00	M	6.0E+02	L	4.0E–05	8.4E–05	3.1E–10	4.8E–01	8.5E–01
KLX17A:4	314.00–342.00	1203.4	372,000	16.27	15.77	0.50	3.9E+00	M	7.1E+02	L	1.8E–05	4.6E–05	2.0E–10	3.8E–01	8.0E–01
KLX17A:5	220.00–313.00	1165.6	108,000	17.48	16.19	1.29	1.3E+01	H	1.8E+03	L	1.4E–04	1.2E–04	2.2E–10	1.2E+00	1.5E+00
KLX17A:6	180.00–219.00	1127.5	96,000	17.49	16.11	1.38	1.3E+01	H	1.9E+03	L	1.8E–04	1.3E–04	2.0E–10	1.4E+00	1.6E+00
KLX17A:7	70.00–179.00	1088.5	26,400	17.26	12.35	4.91	4.5E+01	H	6.9E+03	M	6.1E–05	1.5E–05	6.3E–11	4.2E+00	5.1E+00
KLX17A:8	11.95–69.00	1048.5	90,000	17.98	15.95	2.03	1.2E+01	H	2.8E+03	L	9.1E–05	8.2E–05	1.7E–10	1.1E+00	2.3E+00
KLX19A:3	509.00–517.00	420.2	5,400	12.70	–3.44	16.14	3.3E+01	H	1.9E+04	M	5.2E–05	2.0E–05	5.6E–11	2.6E+00	2.4E+00
KLX19A:4	481.50–508.00	408.0	5,400	12.78	–3.39	16.17	3.1E+01	H	1.9E+04	M	5.2E–05	2.1E–05	6.0E–11	2.4E+00	2.0E+00
KLX19A:5	311.00–480.50	316.9	5,280	12.78	–3.42	16.20	1.9E+01	H	1.9E+04	M	5.1E–05	3.4E–05	9.8E–11	1.5E+00	1.1E+00
KLX19A:6	291.00–310.00	242.5	840	12.96	–4.31	17.27	7.0E+01	H	1.9E+04	M	7.2E–05	3.0E–05	7.5E–11	2.4E+00	4.6E+00
KLX19A:7	136.00–290.00	191.3	450	13.36	–5.93	19.29	8.1E+01	H	2.0E+04	M	6.2E–05	2.6E–05	1.2E–10	2.4E+00	5.6E+00
KLX19A:8	98.75–135.00	176.6	252	13.36	–6.03	19.39	1.2E+02	E	2.0E+04	M	7.3E–05	2.3E–05	9.9E–11	3.1E+00	6.9E+00
KLX20A:4	145.00–180.00	606.4	4,440	14.03	0.04	13.99	8.3E+01	H	1.8E+04	M	5.8E–05	7.3E–06	3.3E–11	8.0E+00	5.9E+00
KLX20A:5	103.00–144.00	591.4	12,000	16.43	8.28	8.15	2.9E+01	H	1.0E+04	M	5.6E–05	2.4E–05	1.1E–10	2.4E+00	2.1E+00
KLX20A:6	99.50–102.00	584.0	63,000	16.67	10.12	6.55	5.4E+00	M	8.3E+03	M	1.2E–05	3.5E–05	1.6E–10	3.4E–01	4.5E–01
KLX23A:1	49.00–100.15	327.8	540	13.43	–3.65	17.08	2.0E+02	E	2.0E+04	M	6.8E–05	9.7E–06	5.0E–11	7.0E+00	1.3E+01
KLX23A:2	0.00–48.00	315.6	12,000	15.45	10.99	4.46	8.3E+00	M	5.1E+03	M	1.6E–04	1.6E–04	4.5E–10	1.0E+00	5.1E–01
KLX24A:1	69.00–100.17	600.4	5,220	14.74	6.10	8.64	6.9E+01	H	1.1E+04	M	8.3E–05	1.2E–05	6.6E–11	7.1E+00	5.8E+00
KLX24A:2	41.00–68.00	601.8	4,980	15.85	7.52	8.33	7.3E+01	H	1.1E+04	M	8.6E–05	1.2E–05	6.8E–11	7.4E+00	5.0E+00
KLX24A:3	2.41–40.00	604.7	13,680	17.24	11.96	5.28	2.7E+01	H	6.8E+03	M	1.0E–04	3.0E–05	1.4E–10	3.4E+00	2.0E+00
KLX27A:1	640.00–650.56	518.5	28,200	13.04	–0.02	13.06	9.5E+00	M	1.6E+04	M	2.7E–05	6.6E–05	8.8E–11	4.1E–01	8.5E–01
KLX27A:2	580.00–639.00	485.5	25,500	13.11	0.07	13.04	9.2E+00	M	1.6E+04	M	2.9E–05	7.5E–05	9.7E–11	3.8E–01	7.7E–01
KLX27A:3	490.00–579.00	417.2	30,000	13.09	0.20	12.89	5.8E+00	M	1.6E+04	M	2.6E–05	1.1E–04	1.4E–10	2.5E–01	5.4E–01
KLX27A:4	380.00–489.00	330.2	204,000	12.65	7.65	5.00	5.3E–01	L	5.8E+03	M	2.0E–05	6.1E–04	5.1E–10	3.2E–02	6.4E–02

Observation borehole ID: section	Section (mbl)	r_s (m)	dt_L(s) [s=0.1 m]	h_i (m)	h_p (m)	s_p (m)	Index 1: r_s^2/dt_L (m^2/s) [s=0.1 m]	Index 1 class	Index 2_new: $s_p/Q_p \cdot \ln(r_s/r_0)$ (s/m^2)	Index 2_new class	To (m^2/s)	S_o (-)	K'/b' (s^{-1})	T_o/S_o (m^2/s)	T/S (m^2/s)
KLX27A:5	260.00–379.00	224.2	12,000	12.30	–3.14	15.44	4.2E+00	M	1.7E+04	M	2.7E–05	1.9E–04	3.9E–10	1.4E–01	5.1E–01
KLX27A:6	220.00–259.00	197.8	6,000	12.25	–1.88	14.13	6.5E+00	M	1.5E+04	M	4.3E–05	1.6E–04	4.2E–10	2.6E–01	6.6E–01
KLX27A:7	115.00–219.00	179.7	11,100	9.87	–0.36	10.23	2.9E+00	M	1.1E+04	M	5.0E–05	2.1E–04	8.3E–10	2.4E–01	1.7E–01
KLX27A:8	80.00–114.00	188.6	35,760	10.16	7.44	2.72	9.9E–01	L	2.9E+03	L	1.7E–04	1.3E–03	3.1E–09	1.3E–01	1.1E–01
KLX27A:9	14.76–79.00	209.3	49,200	10.24	8.49	1.75	8.9E–01	L	1.9E+03	L	3.4E–04	2.1E–03	3.2E–09	1.6E–01	2.0E–01

* No value available due to missing data.
r_s = Distance from HLX28.
h_i = Water level above reference level in test section before start of flow period.
h_p = Water level above reference level in test section at t=25,000 minutes.
s_p = Draw down in test section at t=25,000 minutes.
T_o = Transmissivity from transient evaluation of observation section.
S_o = Storativity from transient evaluation of observation section.
K'/b' = Leakage coefficient from transient evaluation.
T_o/S_o = Hydraulic diffusivity from transient evaluation.
T/S = Hydraulic diffusivity based on time lag according to /Streltsova 1988/.

5.4 Tracer test

5.4.1 General

Samples from the pumping borehole were sent for analysis in several batches during the tracer test in order to monitor tracer breakthrough and for decision-making during the course of the experiment.

In order to reduce uncertainty of the tracer analysis, samples from the pumping borehole, covering the entire tracer test period, were sent for analysis after the completion of the pumping in HLX28. This last batch of samples is the only batch reported to Sicada and used for further evaluation in the present report.

5.4.2 Tracer breakthrough

The tracer concentrations in the samples from the pumping borehole are shown in Figure 5-8 to Figure 5-13. Circles represent all analyzed samples from the last batch. Filled circles represent outliers (cyan) and background (purple), respectively. The selection of outliers and background samples was performed manually. Hence, a certain degree of subjectivity can not be avoided in this selection. However, in most cases it was relatively clear whether a sample would be regarded as an outlier or a background value. The outliers were removed from the data set and not used in further evaluation. The background level was calculated as the mean of the background samples.

Clearly visible tracer breakthrough was obtained from injections in HLX32:2, HLX37:1 and HLX38:3. No increased levels of tracers from KLX11A:3 and KLX20A:5 could be detected prior to the pump stop.

In the case of KLX27A:6, it was rather difficult to firmly establish whether a tracer breakthrough had occurred or not. Except for some obvious outliers, the concentration was initially relatively stable around $1.5 \cdot 10^{-11}$ g/g. After c 500 h, the data becomes more scattered and also shows slightly larger values. This could indicate a weak tracer breakthrough but it could also be an effect of increased analysis uncertainty, possibly due to interference with other tracers. Since tracer breakthrough from KLX27A:6 could not be firmly established, transport parameters evaluated in this report are regarded as too uncertain for reporting to Sicada.

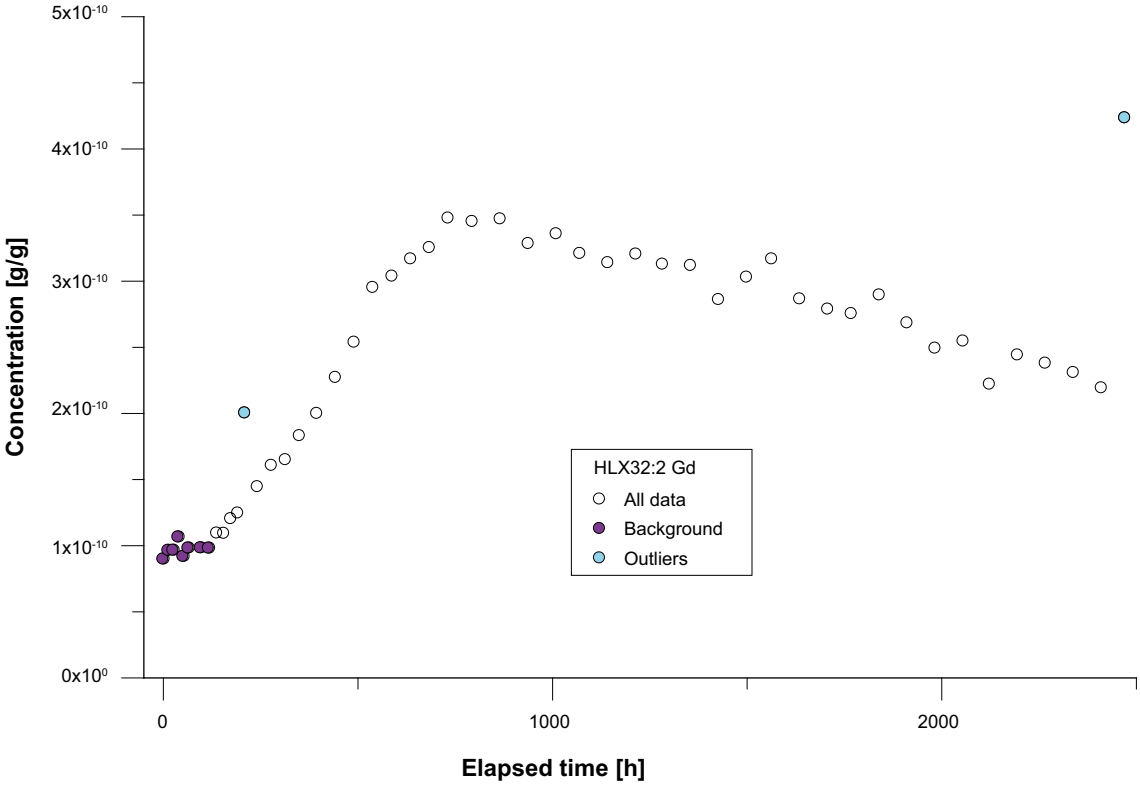

Figure 5-8. *Concentration of Gd in HLX28 from the injection in HLX32:2.*

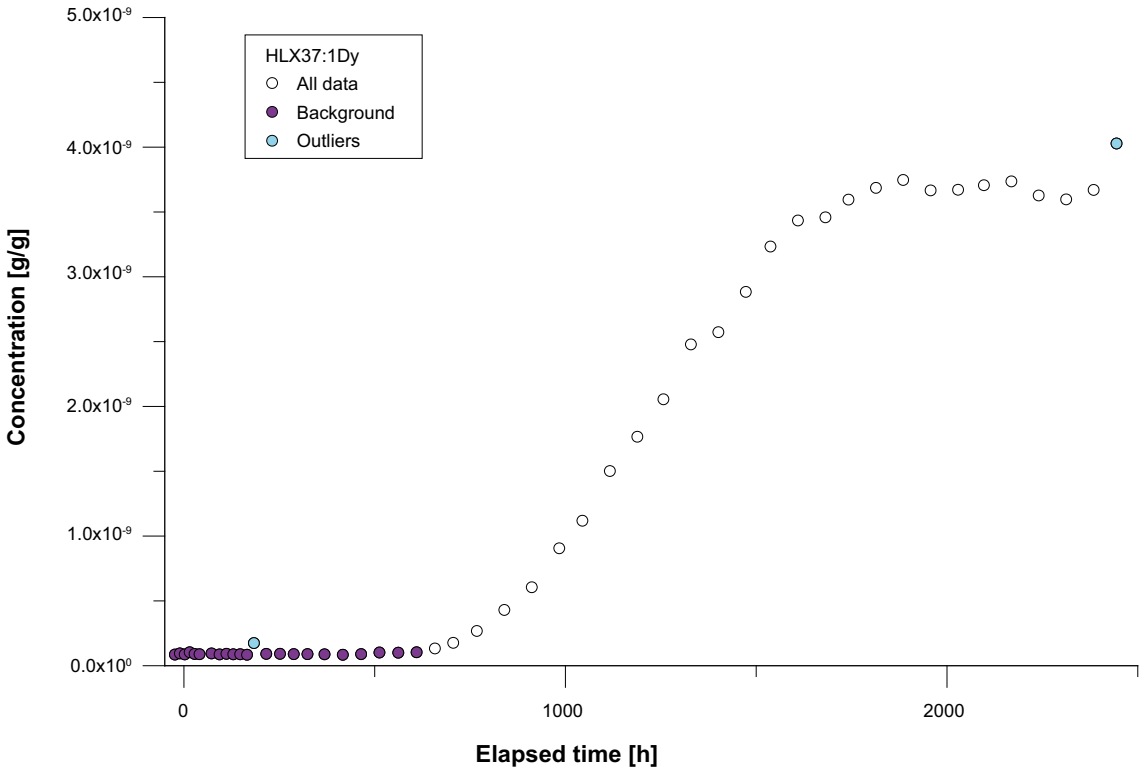

Figure 5-9. *Concentration of Dy in HLX28 from the injection in HLX37:1.*

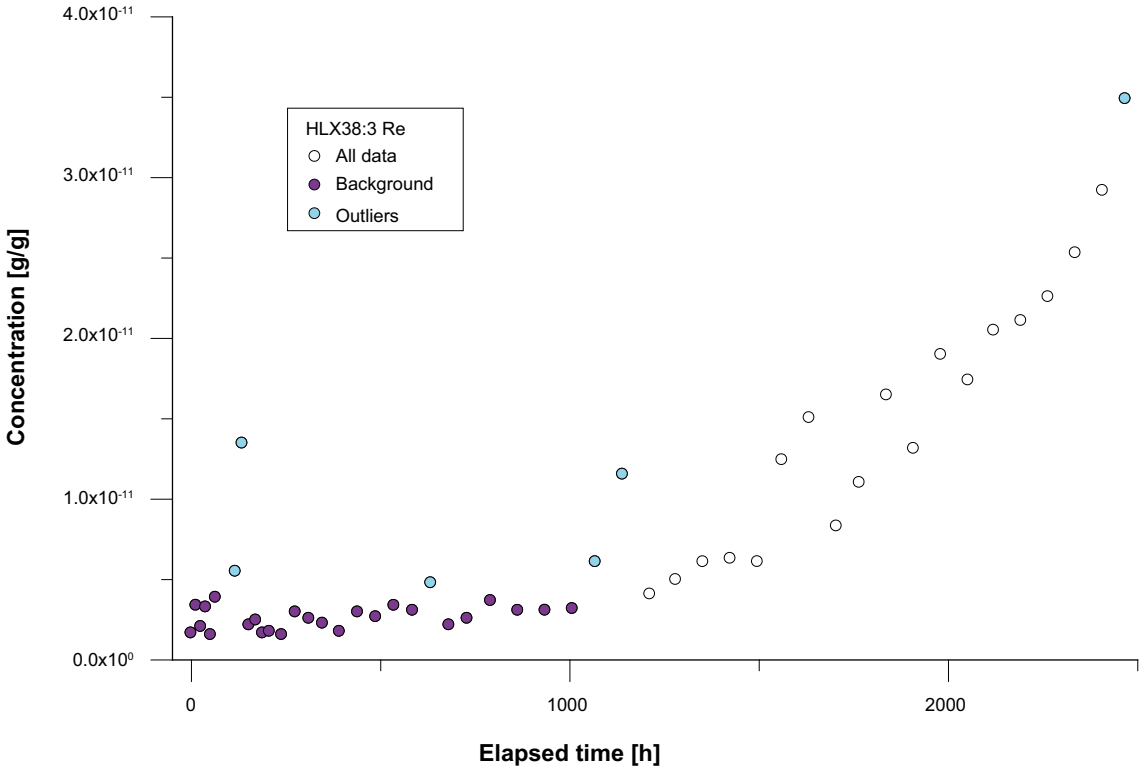

Figure 5-10. *Concentration of Re in HLX28 from the injection in HLX38:3.*

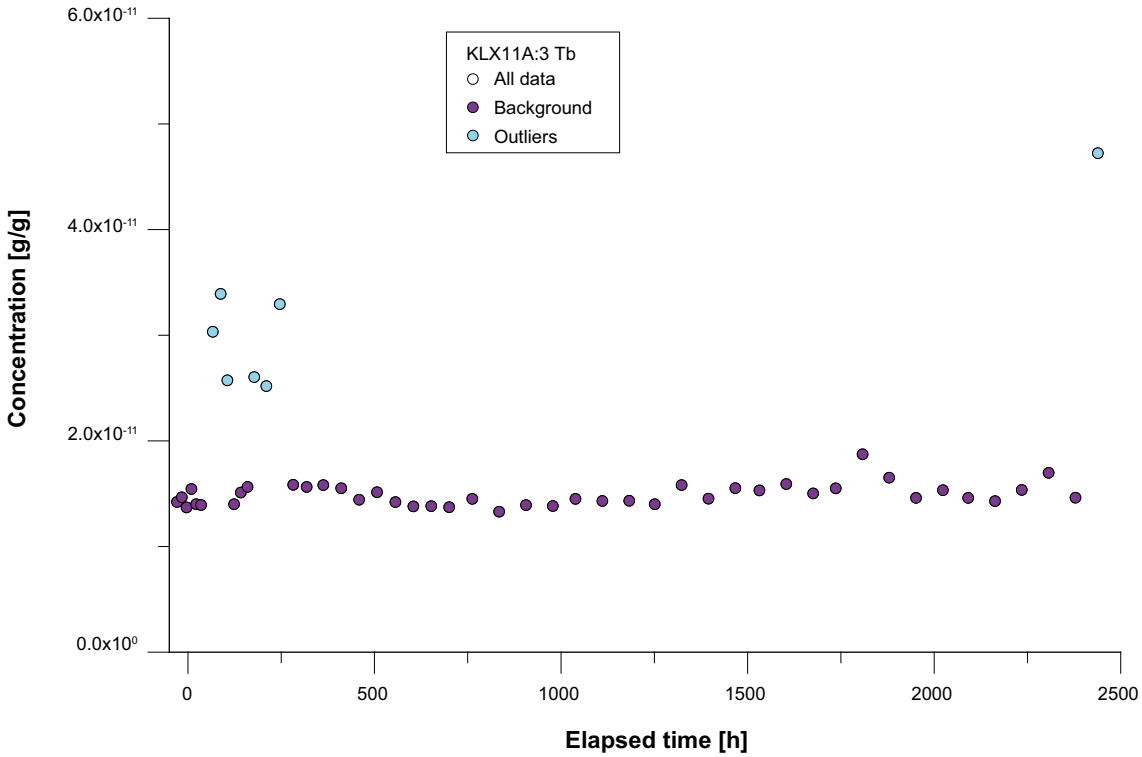

Figure 5-11. *Concentration of Tb in HLX28 from the injection in KLX11A:3.*

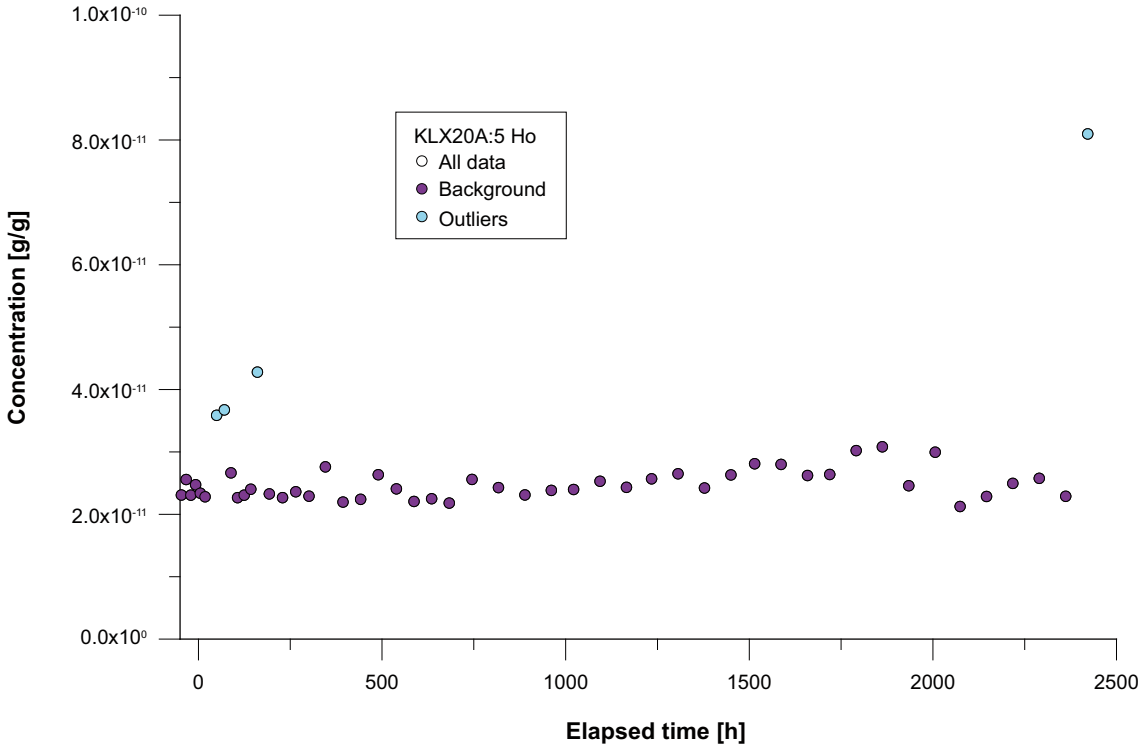

Figure 5-12. *Concentration of Ho in HLX28 from the injection in KLX20A:5.*

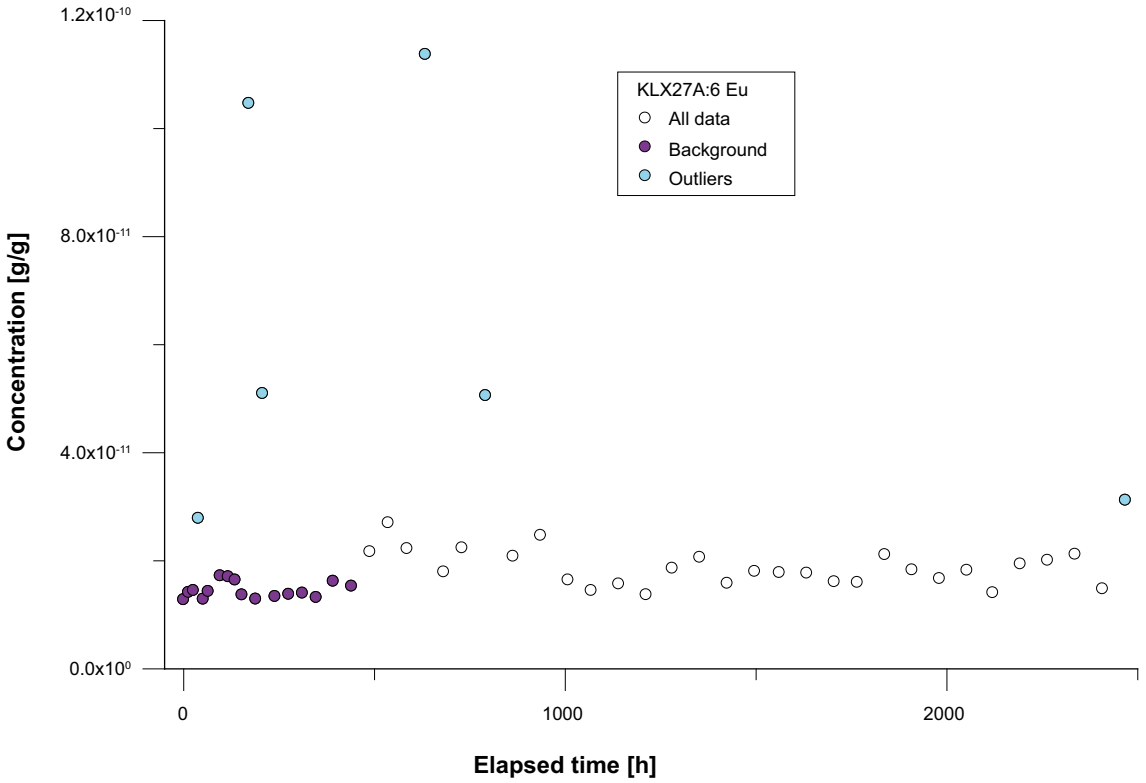

Figure 5-13. *Concentration of Eu in HLX28 from the injection in KLX27A:6.*

In order to compare breakthrough of the various tracers in HLX28, Figure 5-14 shows the data in terms of normalized mass flux (h^{-1}). In Figure 5-14, it is obvious that the possible breakthrough from KLX27A:6 is very limited compared with HLX32:2, HLX37:1 and HLX38:3.

The time to first arrival for each tracer was determined, by manual inspection, as the first value clearly above background concentration. Hence, a certain degree of subjectivity is unavoidable in this process. The tracer recovery to the time of the last analyzed sample was calculated by integration of the data shown in Figure 5-14. The time to first arrival and the tracer recovery are shown in Table 5-6. The values for KLX27:6 are regarded as uncertain and therefore in parentheses.

5.4.3 Model results and evaluated parameters

The input functions for the modelling was calculated according to Section 4.6.3, except for HLX37:1 due to the deviating injection procedure in this section, see Section 4.7. Instead, the injection function for HLX37:1 was approximated with a step function with the same duration as the injection.

The modelling approach for the various tracers varied somewhat depending on the degree of tracer breakthrough in HLX28. For tracer breakthrough from the injections in HLX32:2 and HLX37:1, the modelling was rather straightforward since the tracer recovery was large enough to enable a quite robust solution with the AD-1 model and all fitting parameters (t_m, Pe and pf) free. The evaluation of tracer breakthrough in HLX28 from the injections in HLX32:2 and HLX37:1 is presented in Figure 5-15 and Figure 5-16. As seen in the figures, the AD-1 model fits the data very well.

Table 5-6. Tracer recovery in HLX28 to the time of the last analyzed sample and first arrival.

Borehole:section	Recovery (%)	First arrival (h)
HLX32:2	46.7%	140
HLX37:1	27.0%	660
HLX38:3	2.6%	1,210
KLX27A:6	(0.4%)	(490)

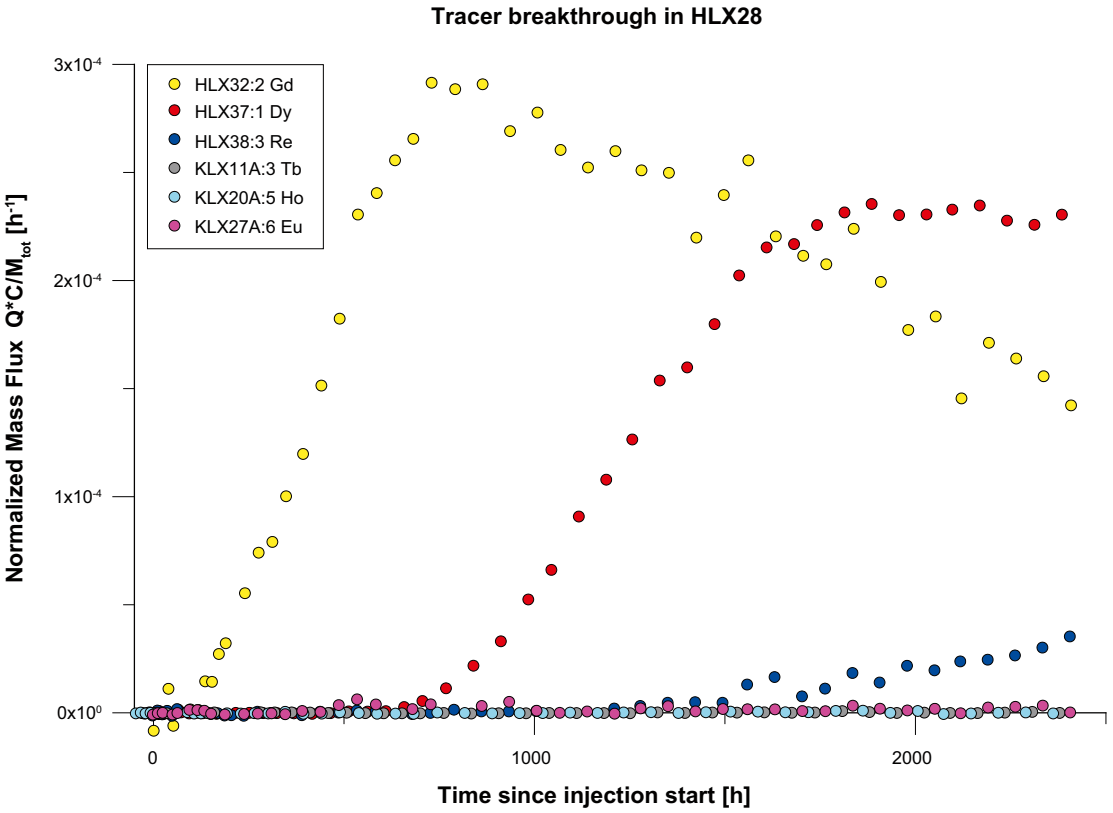

Figure 5-14. *Linear plot of tracer breakthrough in HLX28 in terms of normalized mass flux (h^{-1}).*

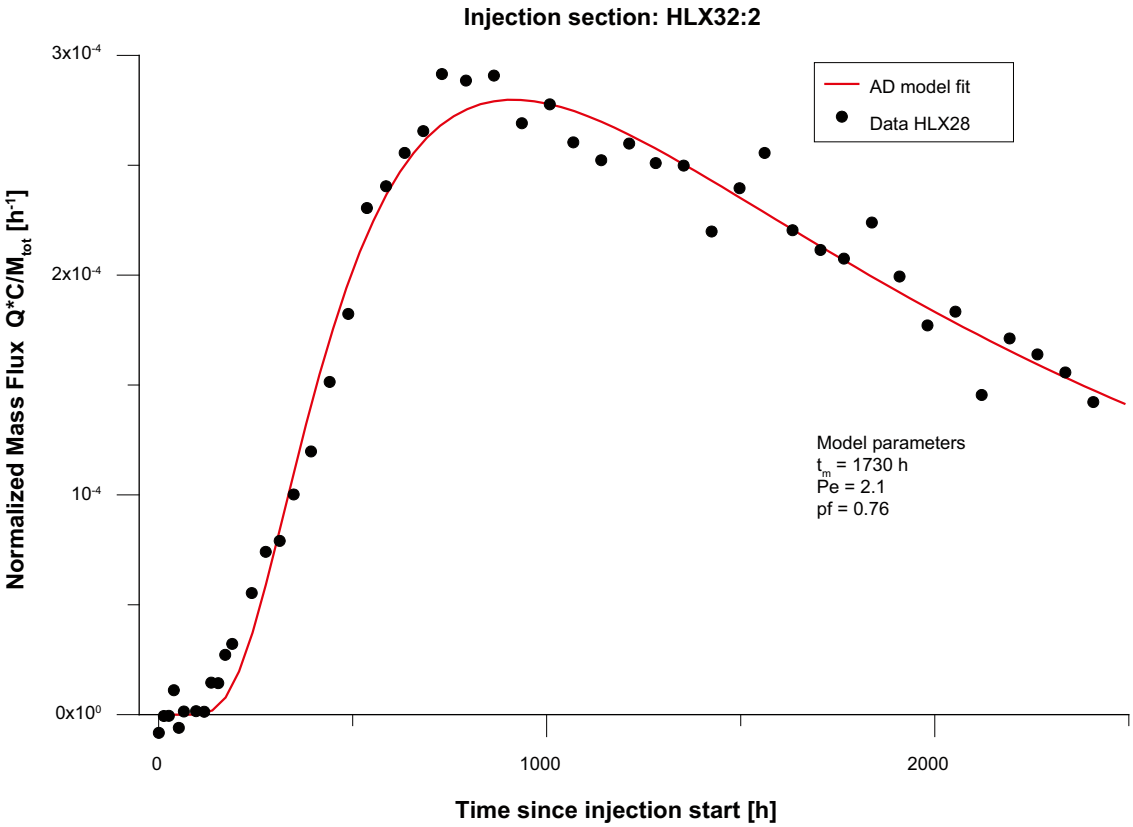

Figure 5-15. *Linear plot of model fit using the AD-1 model to experimental data for Gd in HLX28 from the injection in HLX32:2.*

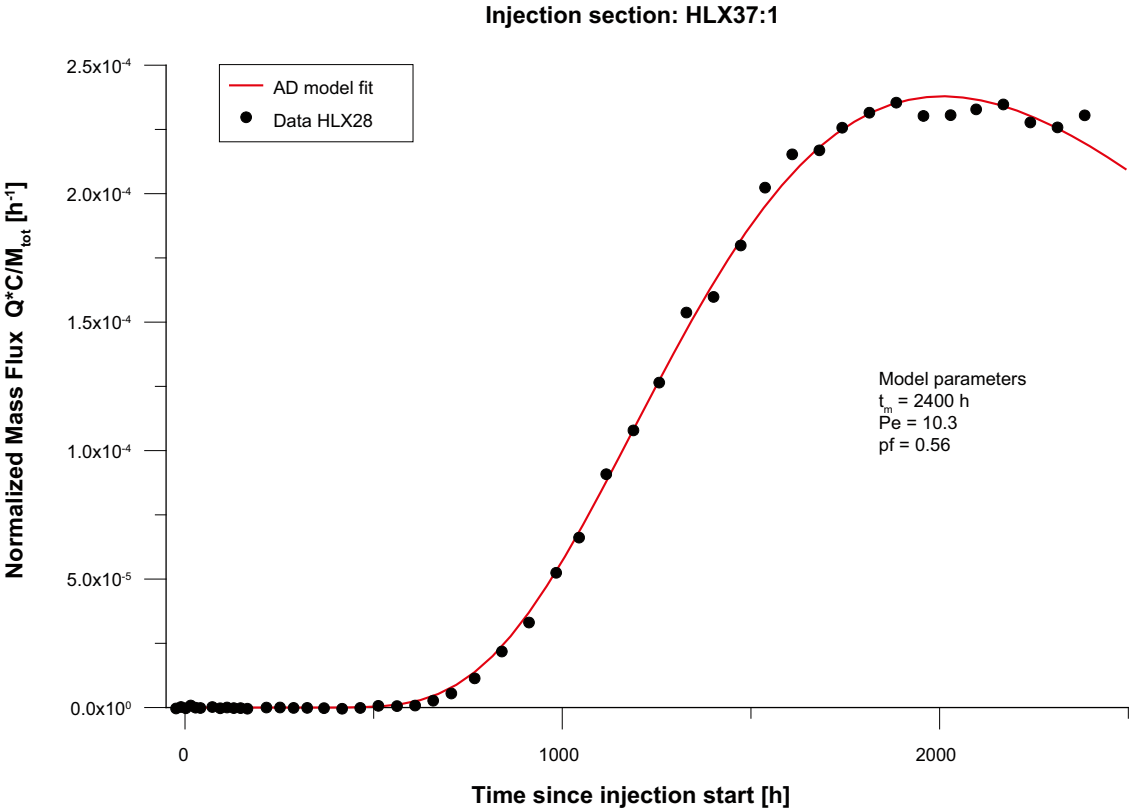

Figure 5-16. *Linear plot of model fit using the AD-1 model to experimental data for Dy in HLX28 from the injection in HLX37:1.*

For HLX38:3, in which only the beginning of a breakthrough curve is indicated, it was not possible to get an unambiguous fit with the AD-1 model with three fitting parameters. The approach in this case was instead to vary fixed values of pf and let t_m and Pe be fitting parameters, thus covering a range of possible tracer recovery values.

The data regarding HLX38:3 are still, despite removal of some outliers as explained in Section 5.4.2, rather scattered, especially between 1,500 and 2,000 h. One may argue that some of these data should be regarded as outliers and consequently removed from the data set used for modelling. All outliers previously identified showed higher values than the rest of the data. Hence, an alternative data set used for modelling was created by removing four high values between 1,500 and 2,000 h.

The evaluation of HLX38:3 with the basic data set is displayed in Figure 5-17 while the evaluation with the alternative data set is shown in Figure 5-18. The two figures indicate that pf should be between 0.1 and 1.0 (i.e. recovery between 10 and 100 percent) in order to get a reasonable good fit to the data.

Figure 5-19 shows the resulting t_m (red) and Pe (blue) for the different fits displayed in Figure 5-17 and Figure 5-18. The solid lines and circles indicate the fitting parameters for the basic data set while the dashed lines and crosses indicate the fitting parameters for the alternative data set. The fits to the alternative data set results in slightly higher Pe and lower t_m compared with the fits to the basic data set. Assuming that pf is between 0.1 and 1.0 (as discussed above) and taking both of the data sets into account, then Pe should be between 3 and 16 while t_m should be between 3,000 h and 9,000 h.

No automatic fitting was carried out for the tracers injected in KLX11A:3, KLX20A:5 and KLX27A:6 because no or only very limited tracer breakthrough could be detected in HLX28. Instead, Pe and pf where set to some reasonable values and the minimum value of t_m was estimated by trial and error. The parameter pf was set to the range of 0.1 to 1.0 while Pe values varied between 2.0 and 15, which may be considered a typical range based on numerous previous evaluations of tracer tests /Hjerne et al. in prep/.

In Figure 5-20 to Figure 5-22 a number of simulations with the AD-1 model are shown. The data for KLX11A:3 and KLX20A:5 are very similar and also results in the same estimated range for minimum values of t_m: 7,000–30,000 h. The data for KLX27A:6 is, as discussed above, somewhat more scattered. The estimate range of minimum values of t_m for KLX27A:6 was 5,000–20,000 h.

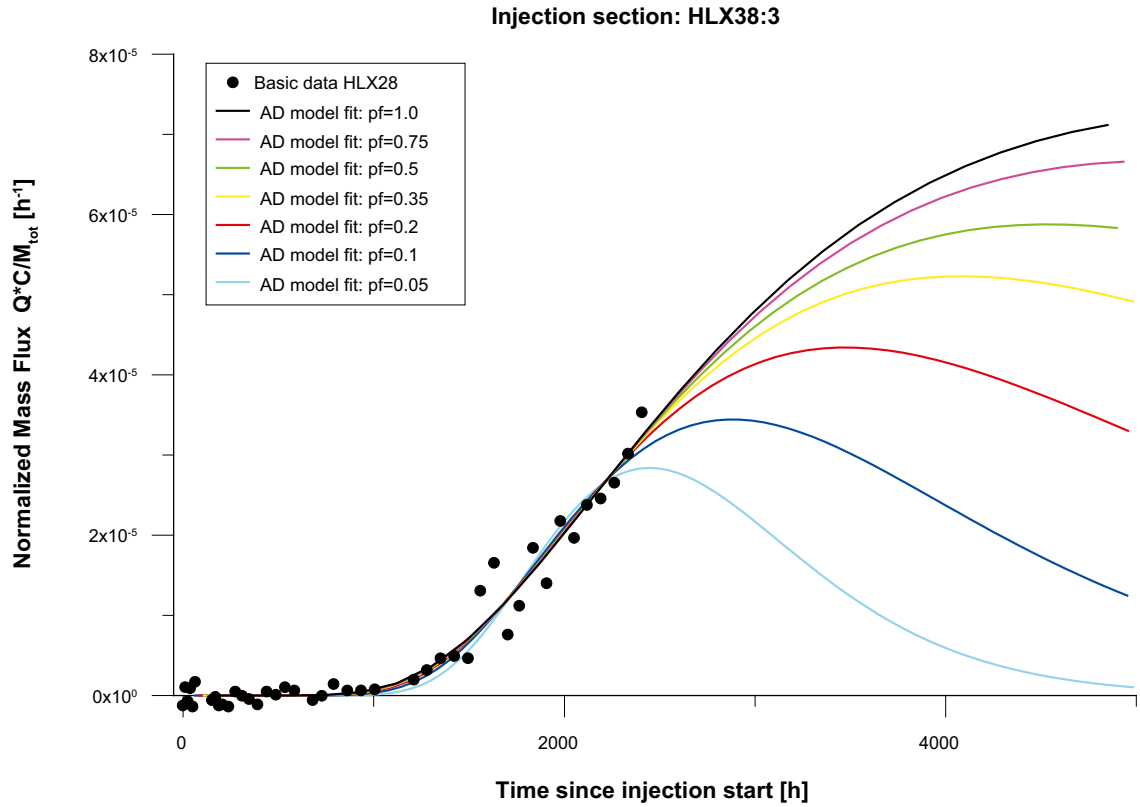

Figure 5-17. *Linear plot of model fits using the AD-1 model to the basic data set for Re in HLX28 from the injection in HLX38:3 for different assumptions of pf.*

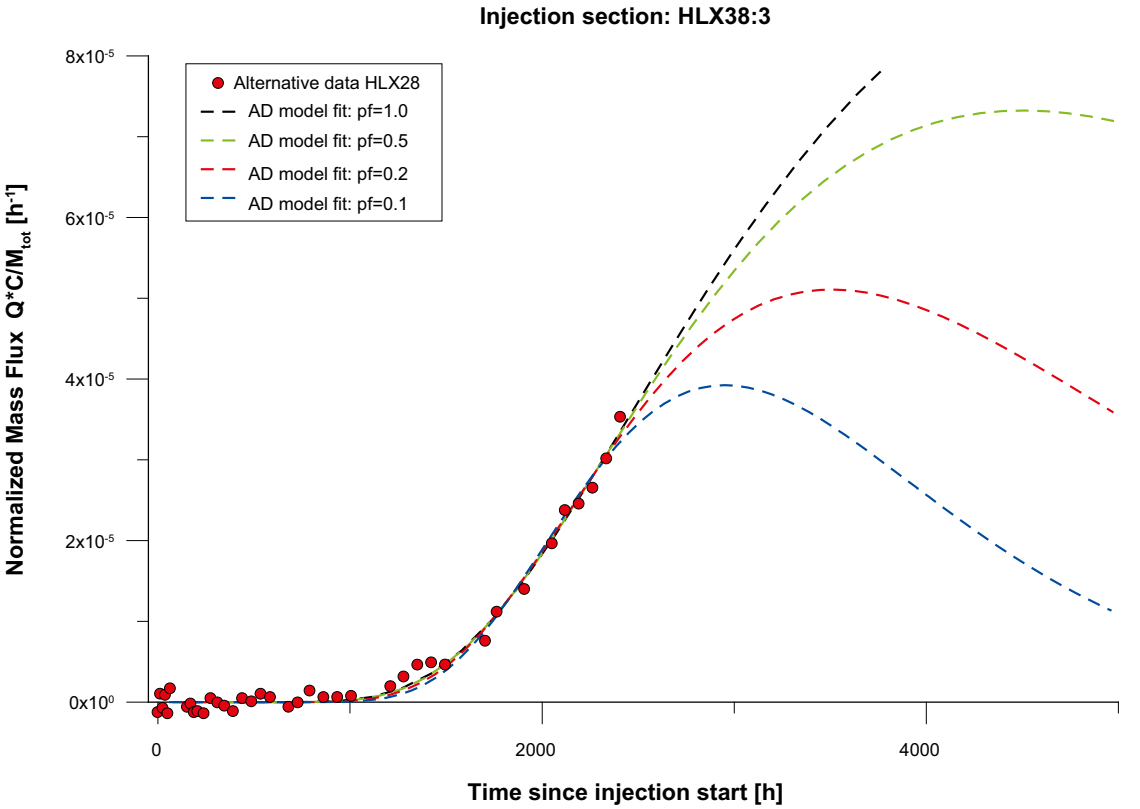

Figure 5-18. *Linear plot of model fits using the AD-1 model to the alternative data set for Re in HLX28 from the injection in HLX38:3 for different assumptions of pf.*

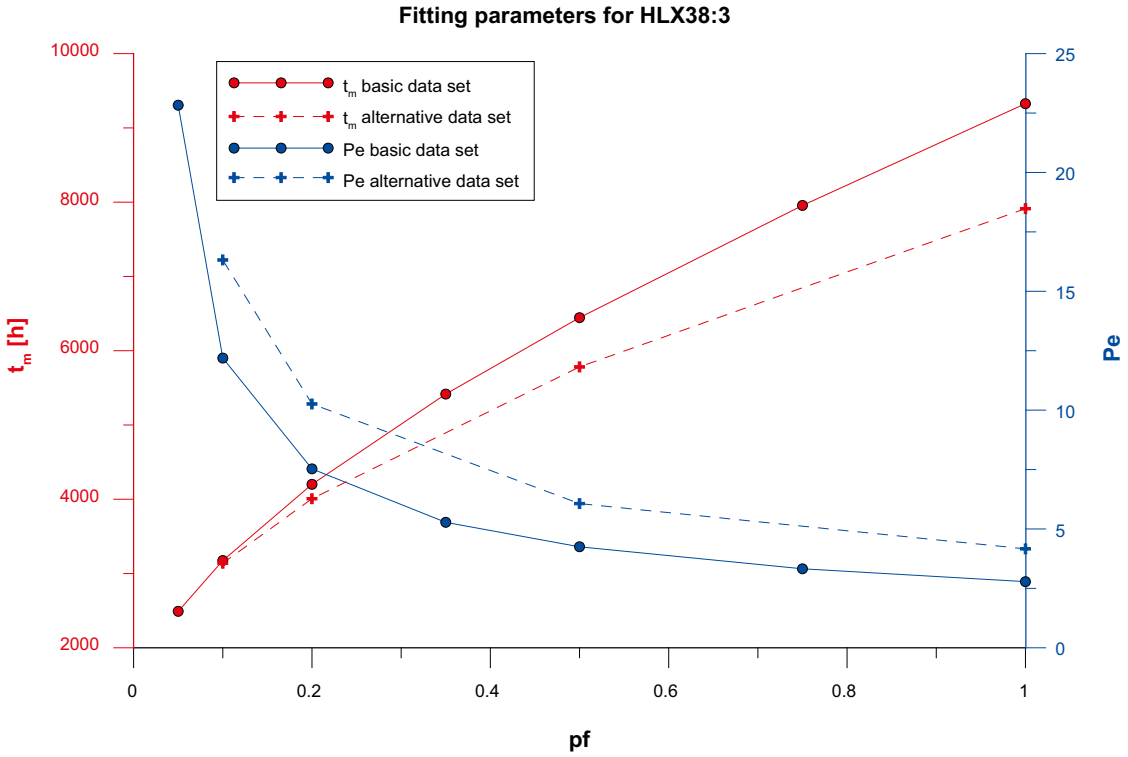

Figure 5-19. *Fitting parameters (t_m and Pe) for different fixed values of pf.*

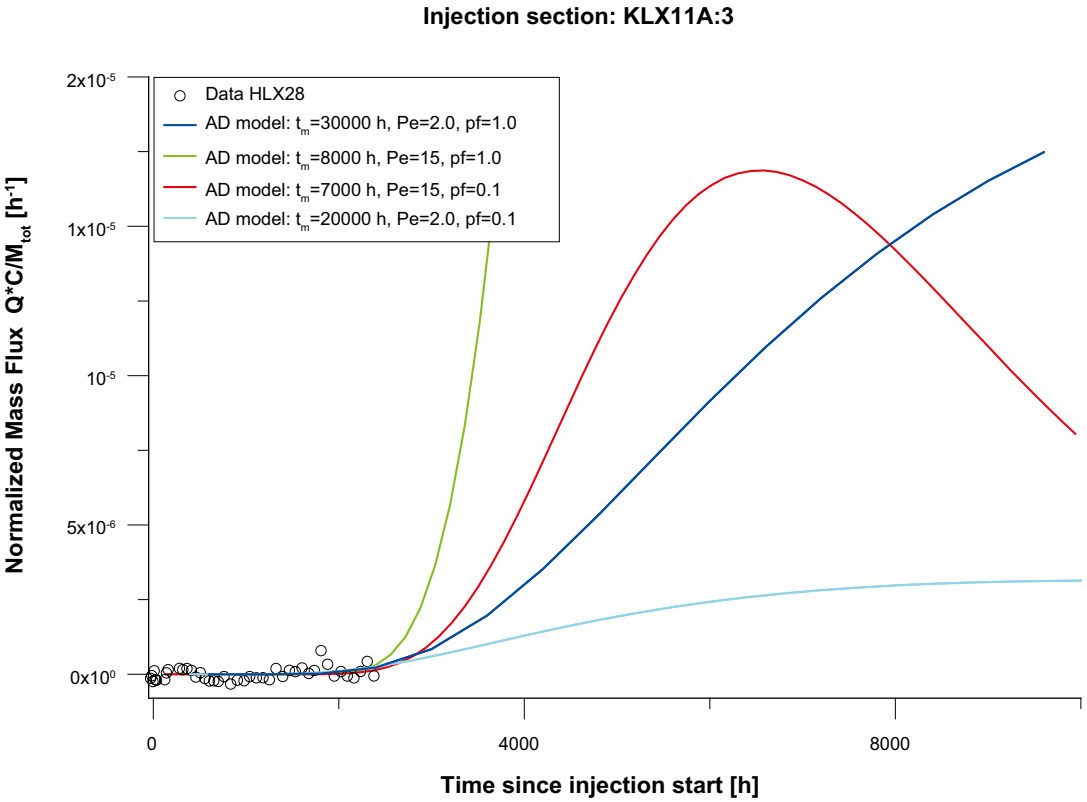

Figure 5-20. *Linear plot of simulations using the AD-1 model and experimental data for Tb in HLX28 from the injection in KLX11A:3.*

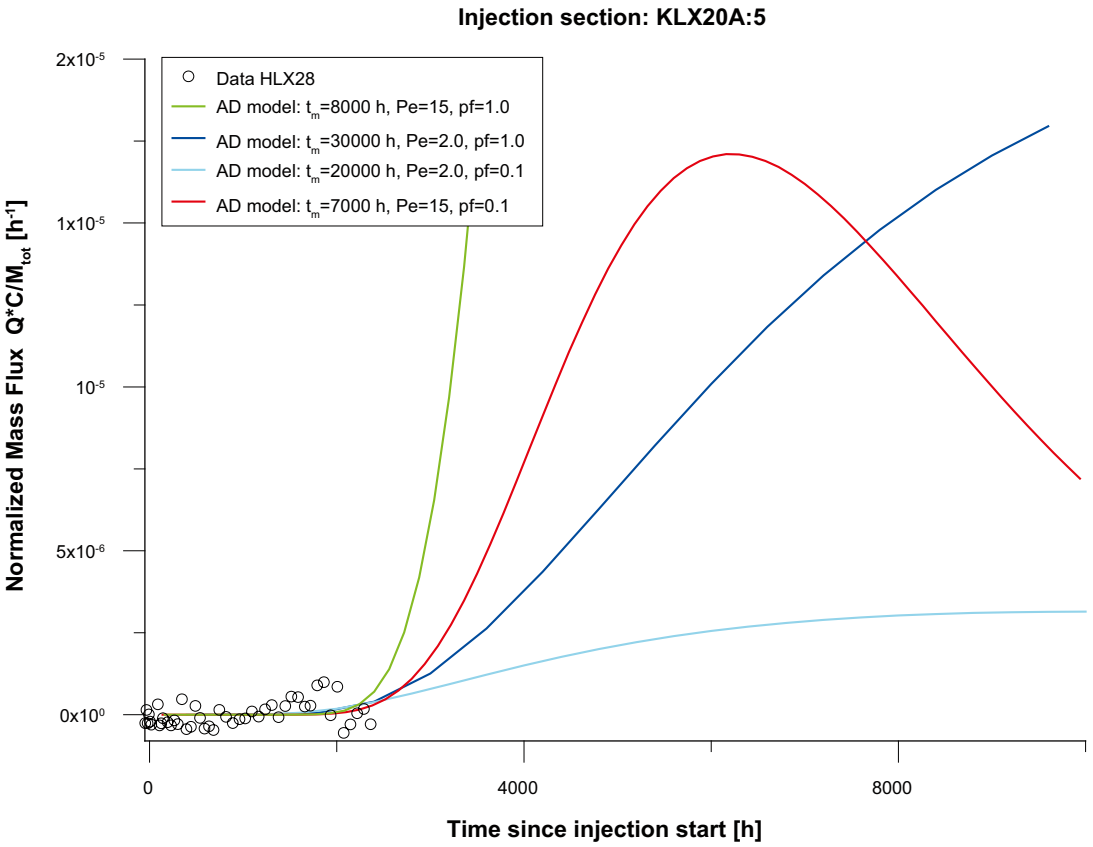

Figure 5-21. *Linear plot of simulations using the AD-1 model and experimental data for Ho in HLX28 from the injection in KLX20A:5.*

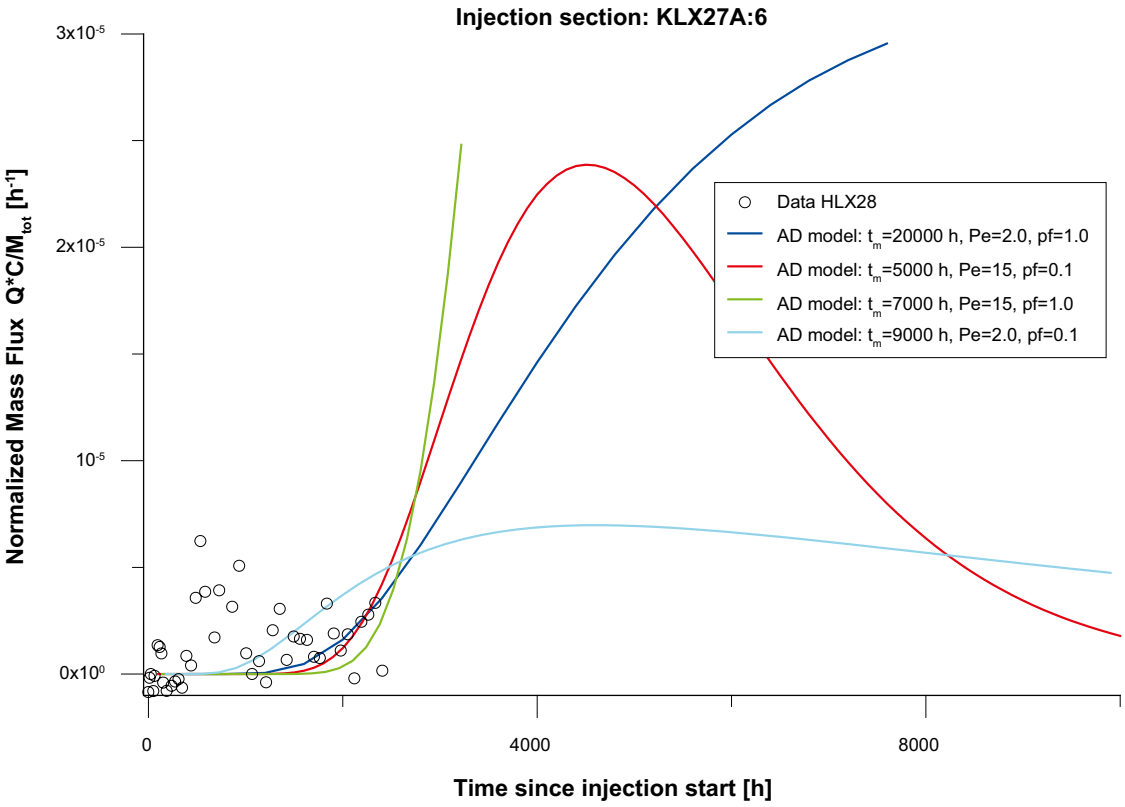

Figure 5-22. *Linear plot of simulations using the AD-1 model and experimental data for Eu in HLX28 from the injection in KLX27A:6.*

As discussed in Section 4.6.4, possible alternative modelling approaches include an AD model with several pathways and/or an AD-MD model for the evaluation of the tracer breakthrough. However, this was not performed. The basis for this decision is further discussed in Section 6.4.2. Table 5-8 shows the calculated transport parameters according to the equations in Section 4.6.6. Note that the values presented for HLX38:3 represents an interval of possible values. For KXL11A:7, KLX20A:5 and KLX27A:6, the values only represent a range of possible minimum values. The values for K_{fr} and ε_f were calculated based on pressure registrations at 25,000 min in consistency with the evaluation of the pumping and interference test.

5.5 Water sampling for chemical analysis

The results from the water sampling performed in order to monitor the chemical conditions during the pumping period are presented in Table 5-9. For scoping calculations and planning the background values from 2008-06-11 were used. Several constituents showed an increasing trend during the continuous pumping in HLX28 from January until May 2009, indicating that the origin of the sampled groundwater in HLX28 changes during the pumping test.

Table 5-7. Results from the evaluation using the AD-1 model.

Borehole:section	t_m (h)	Pe	pf
HLX32:2	1,730	2.1	0.76
HLX37:1	2,400	10.3	0.56
HLX38:3	3,000–9,000	3–16	0.1–1.0
KLX11A:3	> 7,000–30,000	Assumed 2–15	Assumed 0.1–1.0
KLX20A:5	> 7,000–30,000	Assumed 2–15	Assumed 0.1–1.0
KLX27A:6	> 5,000–20,000	Assumed 2–15	Assumed 0.1–1.0

Table 5-8. Calculated transport parameters.

Borehole:section	δ_m (m)	K_{fr} (m/s)	ε_f
HLX32:2	6.7E–01	3.7E–04	3.2E–03
HLX37:1	5.8E–02	6.7E–03	1.8E–04
HLX38:3	1.4E–01–4.2E–01	1.9E–03–6.3E–04	6.4E–04–1.9E–03
KLX11A:3	> 8.1E–02–3.5E–01	> 4.2E–03–9.9E–04	> 2.8E–04–1.2E–03
KLX20A:5	> 1.1E–01–4.9E–01	> 2.1E–03–5.0E–04	> 5.6E–04–2.4E–03
KLX27A:6	> 7.3E–01–2.9E+00	> 4.6E–04–1.2E–04	> 2.6E–03–1.0E–02

Table 5-9. Water sampling.

Sample nr Date		15595 2008-06-11	15822 2009-01-20	15854 2009-03-11	15944 2009-05-26
Ca	mg/L	14	14.6	21.3	28.6
Fe	mg/L	0.0814	0.105	0.146	0.218
K	mg/L	3.18	3.4	3.96	4.62
Mg	mg/L	4.36	4.78	6.68	8.53
Na	mg/L	126	139	151	159
S	mg/L	20.9	22.2	26.1	23.5
Si	mg/L	6.39	7.4	7.59	7.62
Li	µg/L	11.3	12.2	13.6	14.6
Mn	µg/L	74.9	76.2	139	207
Sr	µg/L	185	204	294	394
Dy	µg/L	0.0681			
Eu	µg/L	0.0147			
Gd	µg/L	0.0703			
Ho	µg/L	0.0179			
Re	µg/L	<0.001			
Tb	µg/L	0.0098			
HCO_3	mg/L	232	231	224	216
Cl	mg/L	73.4	71.0	97.0	155
SO_4	mg/L	59.9	61.1	75.6	63.3
Br	mg/L	<0.5	<0.5	0.5	0.6
F	mg/L	4.4	4.3	3.4	3.3
pH	pH unit	8.16	8.18	8.04	8.01
Conductivity	mS/m	76	91	84	98
Uranine	%	0.3	0.3	0.1	0.1

6 Summary and discussions

6.1 Equipment and procedures

In general, equipment, methods and experimental performance worked as planned. Some interruptions in the pumping of HLX28 occurred during the tests, see Section 4.7. However, the interruptions were relatively short and thus not considered to significantly affect the performed tests.

The accuracy of the tracer analyses performed by ALS Scandinavia early within the activity, especially regarding Gd, was not as good as expected, see Section 4.7. In order to reduce uncertainty, only samples from a single batch covering the entire tracer test period were used for reporting. Still, obvious outliers had to be deleted from the analysis. The overall assessment is that the data presented as results in this report and used for modelling are considered reliable. For further discussion about sources of uncertainty regarding tracer analysis, see /Lindquist et al. 2008b/.

6.2 Groundwater flow measurements

Ten borehole sections were, prior to the tracer test, selected as candidates for tracer injection. These sections were used for groundwater flow measurements using the dilution method, both during natural conditions and during pumping in HLX28. All ten sections were tested at two occasions during natural conditions. Five of the sections were also tested at two occasions during pumping. The other five were only tested once during pumping in HLX28.

For seven of the sections, the groundwater flow rate during the two measurement periods with natural conditions varied by less than a factor of 3. The largest change between the two periods was found in KLX20A:2, which displayed a change in groundwater flow by a factor of 8.

Only in four sections the groundwater flow rate changed with more than a factor of 2 at the time of pump start, indicating relatively weak responses to the pumping in HLX28 in general. For a couple of sections, the flow rate even decreased slightly. No clear correlation between the flow response due to pumping and the distance from HLX28 was possible to find, which might indicate a heterogeneous system. It should also be noted that groundwater flow is a vectorial entity which means that even a decrease in flow rate could imply a flow response where groundwater flow changes direction.

During the pumping in HLX28 the groundwater flow rates also varied, especially in HXL32:2, where the highest flow rate was found at the end of the measurement period. Also for HLX38:3, the flow rate, although relatively low, seemed to increase with time. For KLX11A:3 and KLX20A:5, the flow rate instead decreased with time. Such changes with time may indicate changes in hydraulic conditions in general during the interference test.

The late flow response in HLX32:2, and to some degree also HLX38:3, is consistent with the relatively late pressure response indicated by the hydraulic response analysis in Section 5.3.3. It is also notable that KLX20A:2, which displays a very small or non-existing flow response due to the pumping in HLX28, is judged to be non-responding in the evaluation of the hydraulic interference test.

6.3 Geohydraulic conditions

The response in the pumping borehole HLX28 during the flow period indicates a dual-permeability system with an early short PRF (pseudo-radial flow), followed by a transition to a second PRF with lower transmissivity and subsequently to a PSF (pseudo-spherical flow). By the end of the flow period, the test display strong effects of an apparent NFB (no-flow boundary), possibly in combination with a decreasing natural trend of the groundwater levels.

The estimated transmissivity of the intersecting structure closest to the pumping borehole HLX28 is rather high, $3 \cdot 10^{-4}$ m^2/s. At later times (i.e. at longer distances from HLX28) the transmissivity decreases about one order of magnitude. The estimated transmissivities from the observation sections are dominated by the transmissivity of the rock or hydraulic structures further away from the pumping borehole. The transmissivity values estimated from the observation boreholes are consistent with those estimated from the pumping borehole at later times.

The pressure was monitored in a total 274 observation sections during the interference test in HLX28. Visual inspection of the pressure responses in the observation sections in linear diagrams indicates that presumed responses were registered in 63 observation borehole sections. Clear responses (Class 1a and 1b) were observed in 53 sections. Ten sections showed a weak response (Class 2) to the pumping. For one section (KLX16:1), it cannot be confirmed whether the section was affected or not by the pumping in HLX28 (Class 3). A total of 202 of the observation sections were considered to be virtually unaffected by the pumping in HLX28 (Class 4). Most of the non-responding sections are located at long distances from HLX28. However, some are located closer to HLX28 than other responding sections.

Among the responding borehole sections (Class 1 and 2), the most distinct and fastest responses were found in HLX37, KLX11A, KLX19A, KLX20A and KLX23A. Borehole sections with strong but more delayed responses include KLX27A. Fast but not as strong responses occurred in HLX39, KLX11A, KLX11E, KLX14A, KLX17A, KLX20A and KLX24A. Some of these sections may represent more or less direct responses along potential fracture zones or other hydraulic structures between borehole HLX28 and some of the observations sections. Alternatively, some of the sections may also be hydraulically connected via interconnecting fractures in the upper part of the bedrock. The weakest and most delayed responses occurred in HLX32 and KLX03.

6.4 Tracer test

6.4.1 Tracer breakthrough

Clear tracer breakthrough was obtained from the injections in HLX32:2, HLX37:1 and HLX38:3. A possible but very uncertain tracer breakthrough could also be detected from the injection in KLX27A:6. These borehole sections are situated closer to the pumping section than the two sections in KLX11A:3 and KLX20A:5 from which no tracer breakthrough could be detected.

Groundwater flow measurements, as discussed above, indicated flow responses due to pumping in HLX28 in all of the tracer injection sections, although there are some differences among them that may be important for interpretation of the tracer test. For KLX11A:3 and KLX20A:5, the flow rate during the pumping seems to have decreased with time, while the flow rate for HLX32:3 and HLX38:3 increased with time. The decreasing flow rates during pumping in KLX11A:3 and KLX20A:5 may partly explain the absence of tracer breakthrough in HLX28 from these sections, as the flow response due to pumping in HLX28 may have been a temporary effect and/or weaker during the tracer test.

As shown in Figure 6-1, which basically is the same hydraulic response diagram as in Figure 5-7, it is evident that the hydraulic responses in HLX32:2 and HLX38:3 were considerably weaker and slower than in the rest of the tracer injection sections (relative their distance to HLX28). The fact that tracer breakthrough from these sections occurred may be a result of their relative closeness to HLX28, 122 m and 349 m, respectively. Section HLX37:1 shows one of the fastest and strongest responses, which may explain the clear breakthrough, despite the long distance (486 m) from HLX28. Despite the relative strong and fast hydraulic responses in KLX11A:3, KLX20A:5 and KLX27A:6, no or very limited tracer breakthrough was observed in HLX28 from these sections. For KLX11A:3 and KLX20A:5, this may be explained by their relative long distance to HLX28, 702 m and 591 m, respectively. For KLX27A:6, which is only 198 m from HLX28, the distance in itself may not explain the absence of a tracer breakthrough.

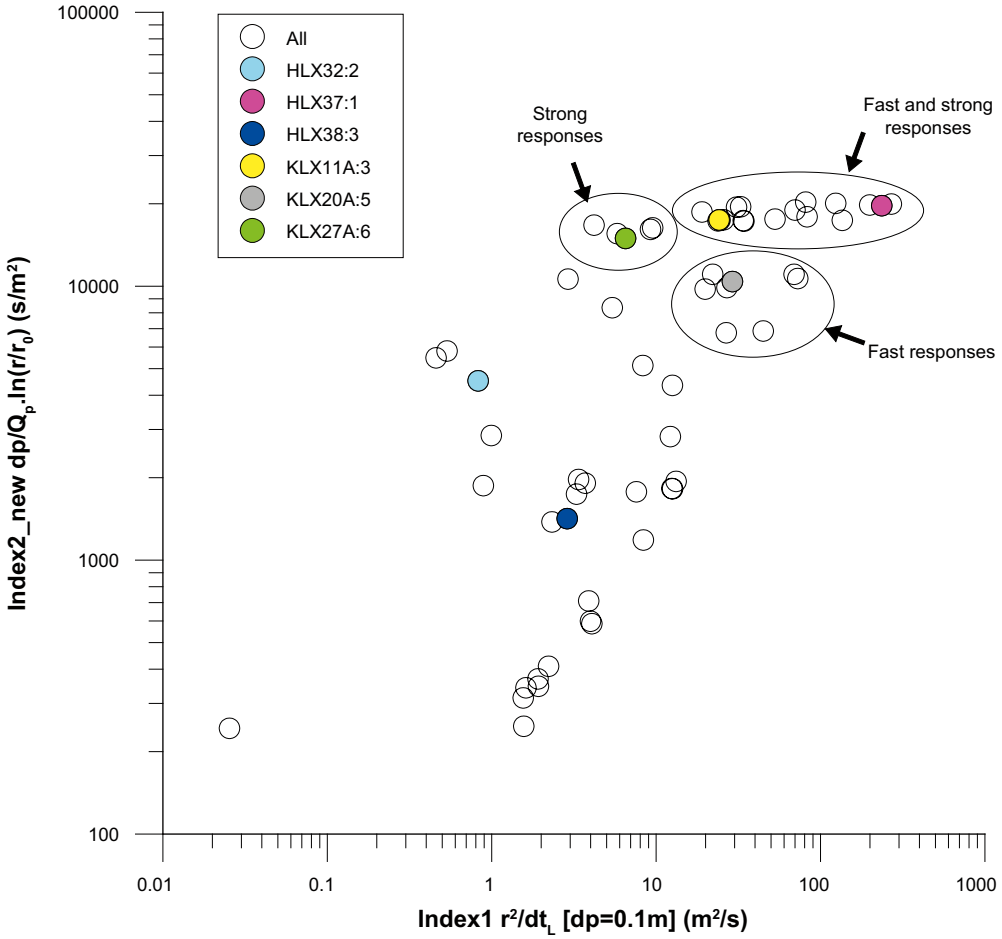

Figure 6-1. *Hydraulic response diagram showing presumed responses in observation sections during the interference test in HLX28 with indication of the sections used for tracer injection.*

6.4.2 Model simulation and evaluated parameters

The tracer breakthrough results led to a somewhat modified modelling approach because of the varying degree of tracer breakthrough. From two of the tracer injections, Gd in HLX32:2 and Dy in HLX37:1, tracer breakthrough in the pumping section was considered sufficient for an evaluation with the AD-1 model. The AD-1 model gave a very good fit to the breakthrough of Gd and Dy. However, most of the descending parts of the breakthrough curves had not been obtained at the time of pump stop. Because of the incomplete breakthrough curves and the fact that the simplest model resulted in good fits, more complicated models (with more fitting parameters) were not applied.

For the injection in HLX38:3 with Re, the concentration was still increasing in HLX28 at the time of pump stop. That is, only the beginning of the ascending part of the breakthrough curve is available for interpretation, which further restricts the number of parameters that may be estimated. In this case, a range of fixed values of were assumed resulting in a range of estimated values of the two other parameters.

Regarding the remaining three tracer injections, in KLX11A:3, KLX20A:5 and KLX27A:6, from which no or possibly a very limited tracer breakthrough were detected, the model simulations was performed by assuming values of pf and Pe while minimum values of t_m were estimated. The lack of tracer breakthrough from these three borehole section does not seem to be caused by excess dilution since the model simulations show that even such unfavourable parameters for tracer detection as pf=0.1 and Pe=2 would result in detectable tracer breakthrough. Instead, it is likely that the mean residence time from these borehole sections is too large, or that the tracer transport is not directed towards the pumping section during the test.

6.4.3 Comparison with scoping calculations and prevoius tracer tests

It is clear that the evaluated mean residence times, t_m, from the tracer test, as presented in Table 5-7, are considerably higher than t_m according to the scoping calculations made prior to the test as presented in Table 4-1. The assumptions in the scoping calculations were made based on the results of previous tracer tests presented in /Hjerne et al. in prep/.

This difference between the results in the present report and previous tracer tests is illustrated in Figure 6-2, where mass balance aperture (δ_m) is plotted against transmissivity for the previous test (empty circles) as presented in /Hjerne et al. in prep/. The results for HLX32:2 and HLX37:1 are shown as filled circles, while the others are shown as intervals for δ_m due to evaluation uncertainty. The values of T in Figure 6-2 come from the evaluation of the interference test in this report and may therefore differ from the values used in the scoping calculations.

It is clear that the estimated values of mass balance aperture, for a given value of transmissivity, from the evaluation in this report are large in comparison with the majority of values from previous tracer tests, as the filled circles and lines are plotted above the best-fit line in Figure 6-2. However, this should not necessarily be interpreted as a very different relationship (compared with other areas) between δ_m and T for single hydraulic features. Instead, this might be due to differences in the test geometry as the absolute majority of the previous tracer tests were carried out within what was interpreted as a single hydraulic feature. For a system where the injection is carried out in a different hydraulic feature than the pumping, it may be reasonable to expect that the actual travel distances are longer than the distance used for calculation of δ_m, thereby resulting in over-estimation of δ_m compared with a system with a single planar hydraulic feature.

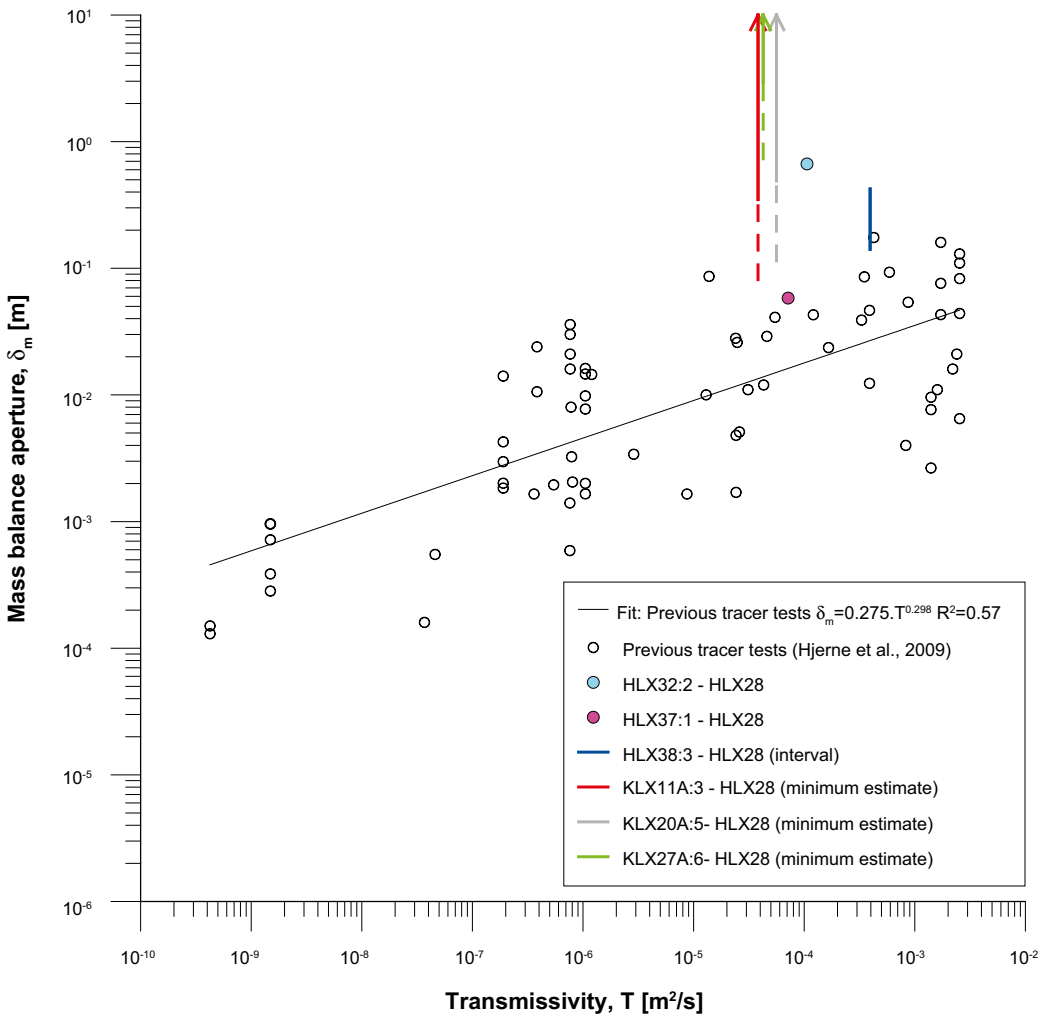

Figure 6-2. *Mass balance aperture versus transmissivity for previous tracer tests compared with results in the present report.*

Figure 6-2 shows that the estimated mass balance aperture, δ_m, for HLX37:1 is closer to interpreted values from previous tracer tests compared with HLX32:2, and the same can to some degree also be said about HLX38:3. The relatively small value of δ_m for HLX37:1 may indicate that the flow path from HLX37:1 to HLX28 is more direct and less complex than the flow paths from HLX32:2 and HLX38:3 to HLX28. This is supported by the interpretation of the hydraulic interference test above, where the fast and strong hydraulic response in HLX37:2 may represent more or less direct responses along potential fracture zones, or other hydraulic structures, to HLX28. Further, the rather weak and slow responses in HLX32:2 and HLX38:3 is interpreted to represent a system of poor connectivity and/or a complex connected fracture system with relatively long flow paths compared with the straight-line distances between the injection sections and HLX28.

An inspection of the relationship between δ_m and storativity, S, gives a somewhat different impression than the relationship between δ_m and T. In Figure 6-3, δ_m are plotted against S for previous tests (empty circles) and the present test (filled circles and lines). It is clear that the injection sections in HLX32:2 and HLX38:3 show higher values of S than previous tracer tests. However, they seem to be approximately consistent with the relationship from the previous tracer but with larger δ_m and S. Section HLX37:1 display a relationship rather similar to the previous test as well, but with a more intermediate value of S. One interpretation of this may be that use of S could provide a better estimate of δ_m in scoping calculations than T, at least when the tested flow paths are more complex than usual for tracer tests.

The same pattern as S versus δ_m can also be seen for the mean residence time, t_m, versus the pressure response time, dt, in Figure 6-4. This indicates that pressure response time, if available, may be useful for scoping calculations. Data from previous tests are also in this case taken from /Hjerne et al. in prep/.

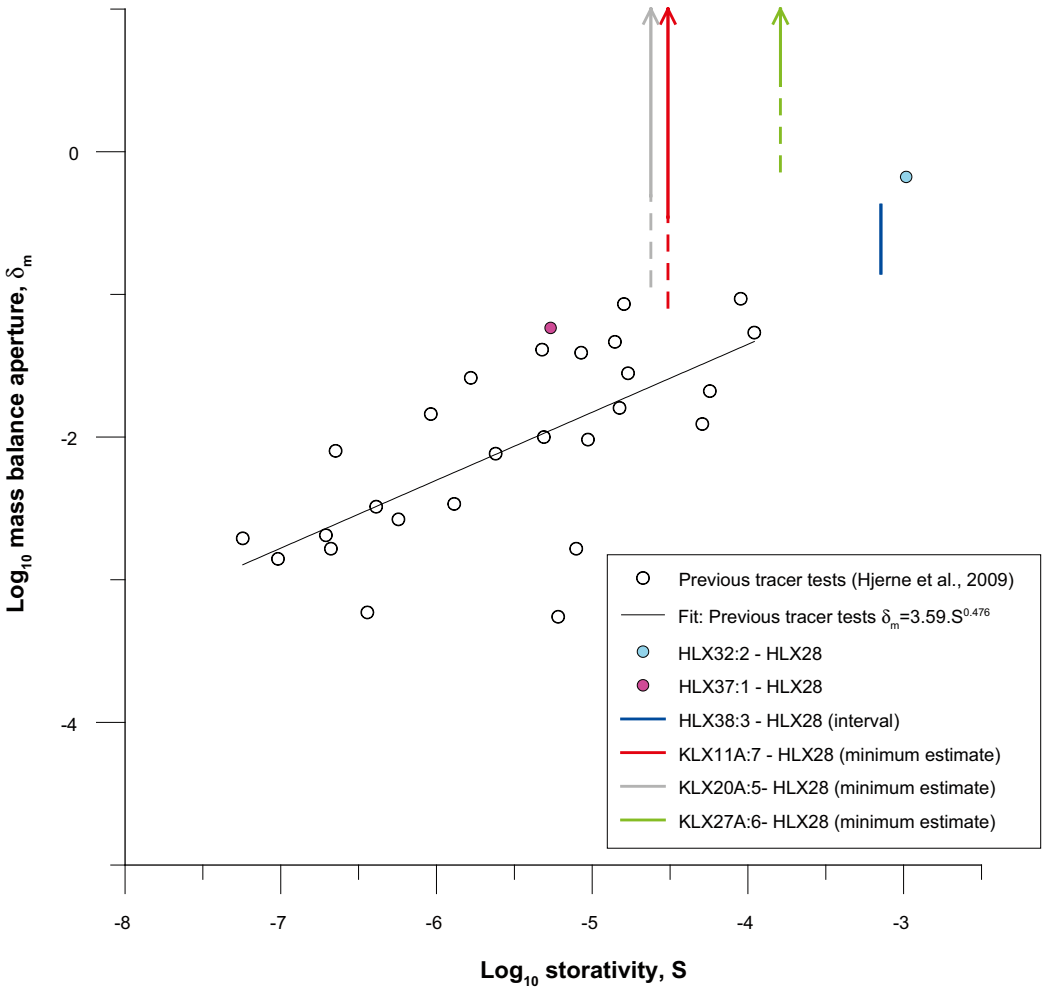

Figure 6-3. *Mass balance aperture versus storativity for previous tracer tests compared with results in the present report.*

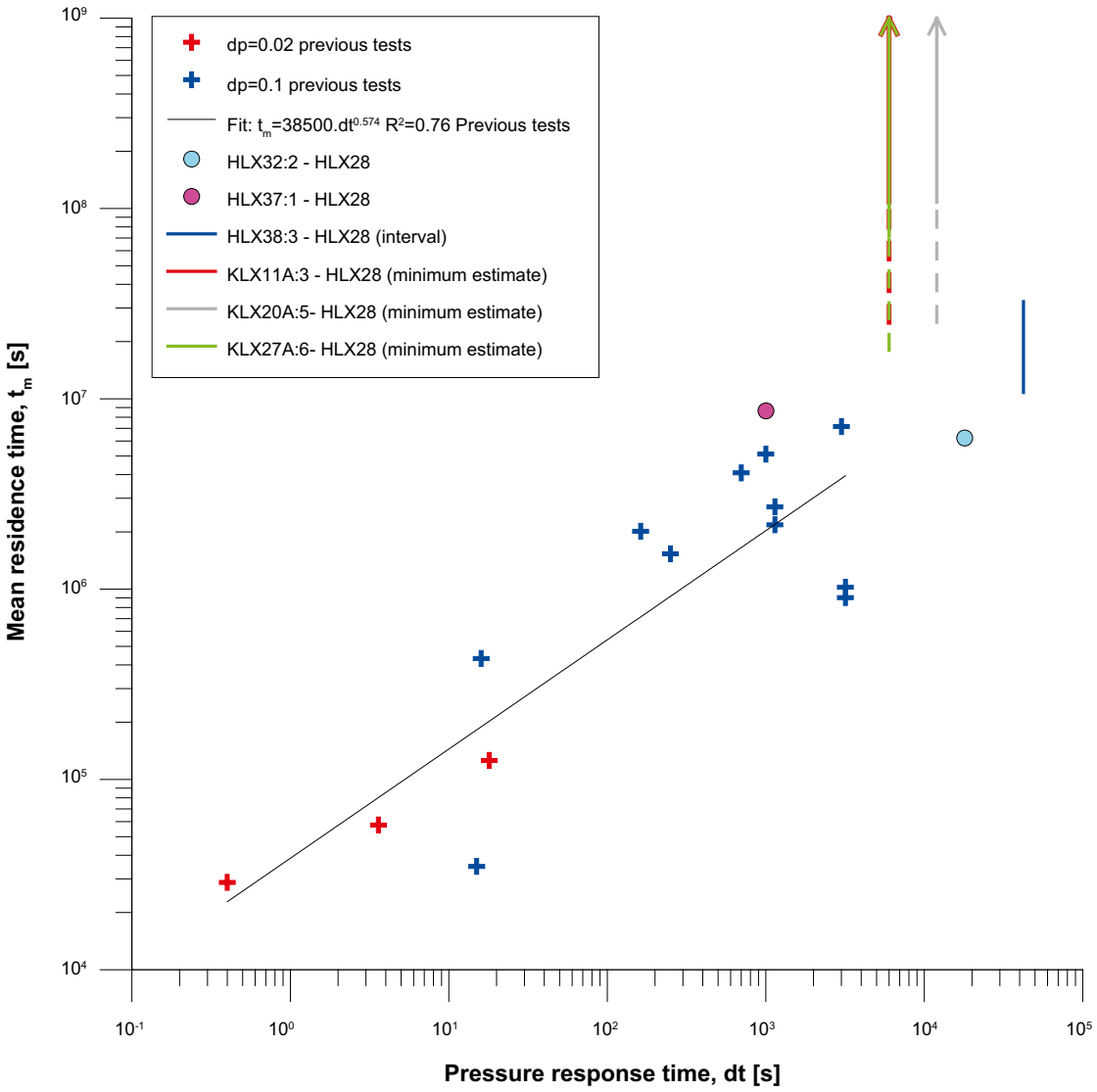

Figure 6-4. *Mean residence time, t_m, versus pressure response time (dp=0.1 m) for previous tracer tests compared with results in the present report. Note that the red and green lines coincide.*

6.5 The hydrogeological model

The results of the hydraulic interference test and tracer test were compared with the hydrogeological model for the Laxemar area.

An analysis of the response classes, described in Appendix 1, reveal that boreholes with all sections situated more than 1,400 m from HLX28, and all soil monitoring wells, only display response class 4, i.e. no response. Hence, the boreholes included in the comparison with the hydrogeological model are all percussion- or core-drilled boreholes with at least one section within 1,400 m of HLX28. These borehole sections are listed together with distances to HLX28, responses and interpreted deformation zones within the borehole section in Table 6-1. The information about the deformation zones is obtained from Table 5-5 in /Wahlgren et al. 2008/ and Appendix 3 and 4 in /Rhén et al. 2009/. The responses in the vicinity of HLX28 are visualized in Figure 6-5. Each symbol in the figure represents an observation section during the interference and the shape of each symbol represents the response class (1 to 4). For response class 1 and 2, the colour represents Index 1 (normalised distance with respect to the response time) and the size of the symbol represents Index 2_new (normalised drawdown with respect to the pumping rate) according to the legend in Figure 6-5. The position of the symbols represents the relative order of sections in the borehole, although the length scale is not accurate.

Figure 6-5 shows that the most clearly responding sections are found north of HLX28 while many sections to the east and a few to the west and south show no response. However, it should also be noted that there are no observation boreholes at larger distances to the west and south. In particular, the zone ZSMNS001C seems to act as a hydraulic barrier since no responses were observed in sections in HLX37 and KLX20A, located to the west of the zone which confirms earlier results /Enachescu et al. 2007, Walger et al. 2007/. Whether ZSMNS059A also acts as a hydraulic barrier is less supported by test data since sections in HLX38 responded in similar ways on both sides of the zone. In addition, weak responses were observed in KLX03, which is located to the east of ZSMNS059A.

The borehole sections corresponding to ZSMNW042A in HLX32, KLX19A and KLX27A showed responses but less clear than in other borehole sections. However, in the borehole sections HLX32:3, KLX19A:1-2 and KLX27A:8-9, all located south of ZSMNW042A, the responses were relatively weak, indicating that the zone acts as a barrier. This observation also confirms results from earlier interference test in KLX19A showing weak responses in HLX28 and HLX32 /Walger et al. 2007/.

The zone HLX28_DZ1 is interpreted to be present in HLX28, HLX32:2 and KLX11A:9. The response in HLX32:2 was not particularly good considering the proximity to HLX28. The response in KLX11A:9, on the other hand, was one of the sections with the highest values of response index 1 and 2_new, as seen in Figure 5-7.

As discussed above, the results of the tracer test in combination with the interference test indicates a relatively direct flow path with good connectivity from HLX37:1 to HLX28. No zone is interpreted for HLX37:1 although it is situated close to, and to the east of ZSMNS001C, for which it is reasonable to assume that it is involved in the tracer transport. Borehole section KLX20A:5, in which no tracer breakthrough was detected, includes ZSMNS001C. The lack of tracer breakthrough in this section may however, as discussed above, be a result of the relatively long distance from KLX20A:5 to HLX28, rather than a true characteristic of ZSMNS001C.

In comparison with the results regarding HLX37:1, the flow paths from HLX32:2 and HLX38:3, respectively, to HLX28 suggests a more poorly connected system and/or a more complex connected fracture system with relatively long flow paths. Section HLX38:3 is interpreted to contain the zone ZSMNS059A. For KLX27A:6, from which no or very little tracer breakthrough occurred, and HLX32:2, are in the model suggested to be intersected by the zone ZSMNW042A. This indicates that neither of ZSMNS059A and ZSMNW042A is well connected to HLX28_DZ1 in HLX28 and/or that these zones have other characteristics making them less favourable for tracer transport.

No major zone is suggested to intercept the tracer injection borehole section KLX11A:3 and no tracer breakthrough was detected in HLX28 from this section.

Table 6-1. Hydraulic response and interpreted deformation zones. Response type: 1a = clear response (transient evaluation), 1b = clear response (no unambiguous transient evaluation can be made due to missing data), 2 = weak response (uncertain transient evaluation), 3 = uncertain response (no transient evaluation, response cannot be separated from background pressure variations), 4 = no response. Index1 and Index 2_new: E = excellent, H = high, M = medium, L = low.

Borehole	Section	Distance from HLX28 (m)	Reponse Type	Index1	Index2_new	Model
HLX28		Pumping borehole				HLX28_DZ1
HLX13	1	1,384	4			ZSMEW007A
HLX25	1	1,361	4			ZSMEW007A
HLX25	2	1,361	4			ZSMEW007A
HLX27	1	1,094	4			
HLX27	2	1,087	4			
HLX32	1	76	1a	L	M	ZSMNW042A HLX28_DZ1
HLX32	2	122	1a	L	L	ZSMNW042A
HLX32	3	130	2	L	L	
HLX36	1	485	1b	H	–	ZSMNS001C
HLX36	2	447	4			
HLX37	1	486	1a	E	M	
HLX37	2	501	1a	E	M	ZSMNS001C
HLX37	3	511	4			
HLX37	4	530	4			
HLX38	1	406	1a	M	L	
HLX38	2	360	1a	M	L	ZSMNS059A
HLX38	3	349	1a	M	L	ZSMNS059A
HLX38	4	345	1a	M	L	
HLX39	1	1,121	1a	H	L	ZSMEW900A ZSMEW900B
HLX40	1	1,149	1a	M	L	ZSMEW900A ZSMEW900B
HLX41	1	1,151	1a	M	L	ZSMEW900B
HLX42	1	1,128	4			ZSMNS947A
HLX42	2	1,170	4			
KLX03	1	1,159	4			DZ8
KLX03	2	1,119	4			
KLX03	3	1,064	4			KLX03_DZ1b KLX03_DZ1c
KLX03	4	1,041	4			ZSMEW946A
KLX03	5	1,019	2	M	L	DZ4
KLX03	6	970	2	M	L	
KLX03	7	934	2	M	L	DZ3
KLX03	8	922	2	M	L	
KLX03	9	923	2	M	L	
KLX03	10	926	2	M	L	
KLX11A	1	890	1a	H	L	DZ16
KLX11A	2	744	1a	H	M	DZ14
KLX11A	3	702	1a	H	M	DZ13
KLX11A	4	675	1a	H	M	KLX11_DZ11 DZ12
KLX11A	5	609	1a	H	M	KLX11_DZ11 DZ8
KLX11A	6	570	1a	H	M	DZ6
KLX11A	7	563	1a	H	M	
KLX11A	8	555	1a	H	M	DZ4
KLX11A	9	549	1a	E	M	HLX28_DZ1 DZ1–DZ3
KLX11A	10	554	1a	H	M	
KLX11E	1	546	1a	H	M	DZ1–DZ4
KLX14A	1	439	1a	M	L	ZSMNS059A DZ5–DZ6
KLX14A	2	406	1b	–	L	ZSMNS059A
KLX14A	3	379	1a	H	M	ZSMNS059A DZ2–DZ3
KLX15A	1	1,436	4			ZSMNW042A
KLX15A	2	1,353	4			ZSMNE107A

Borehole	Section	Distance from HLX28 (m)	Reponse Type	Index1	Index2_new	Model
KLX15A	3	1,289	4			DZ12
KLX15A	4	1,258	4			DZ10
KLX15A	5	1,207	4			DZ8
KLX15A	6	1,188	4			DZ4
KLX15A	7	1,184	4			DZ2
KLX15A	8	1,181	4			DZ1
KLX15A	9	1,185	4			
KLX16A	1	1,167	3			ZSMNE107A
KLX16A	2	1,207	4			ZSMNE107A DZ3–DZ4 DZ7 MDZ
KLX16A	3	1,264	4			DZ1
KLX17A	1	1,372	4			DZ10
KLX17A	2	1,269	2	M	L	DZ5–DZ6
KLX17A	3	1,238	2	M	L	
KLX17A	4	1,203	2	M	L	
KLX17A	5	1,166	1a	H	L	ZSMEW900B
KLX17A	6	1,128	1a	H	L	ZSMEW900B
KLX17A	7	1,089	1a	H	M	ZSMEW900A
KLX17A	8	1,049	1a	H	L	
KLX18A	1	1,311	4			ZSMEW946A
KLX18A	2	1,297	4			
KLX18A	3	1,288	4			KLX18A_DZ9KLX18_DZ9
KLX18A	4	1,276	4			DZ4–DZ8
KLX18A	5	1,270	4			ZSMNE944A
KLX18A	6	1,276	4			DZ1–DZ2
KLX18A	7	1,286	4			
KLX19A	1	625	4			
KLX19A	2	491	4			
KLX19A	3	420	1a	H	M	MDZ
KLX19A	4	408	1a	H	M	MDZ
KLX19A	5	317	1a	H	M	ZSMNE942A MDZ DZ3
KLX19A	6	243	1a	H	M	MDZ
KLX19A	7	191	1a	H	M	
KLX19A	8	177	1a	E	M	DZ1
KLX20A	1	727	4			
KLX20A	2	663	4			
KLX20A	3	633	4			ZSMNS001C
KLX20A	4	606	1a	H	M	ZSMNS001C
KLX20A	5	591	1a	H	M	ZSMNS001C
KLX20A	6	584	1a	M	M	
KLX23A	1	328	1a	E	M	
KLX23A	2	316	1a	M	M	
KLX24A	1	600	1a	H	M	DZ4
KLX24A	2	602	1a	H	M	DZ2–DZ3
KLX24A	3	605	1a	H	M	DZ1
KLX27A	1	519	1a	M	M	
KLX27A	2	486	1a	M	M	
KLX27A	3	417	1a	M	M	
KLX27A	4	330	1a	L	M	
KLX27A	5	224	1a	M	M	
KLX27A	6	198	1a	M	M	ZSMNW042A
KLX27A	7	180	1a	M	M	ZSMNW042A
KLX27A	8	189	1a	L	L	
KLX27A	9	209	1a	L	L	

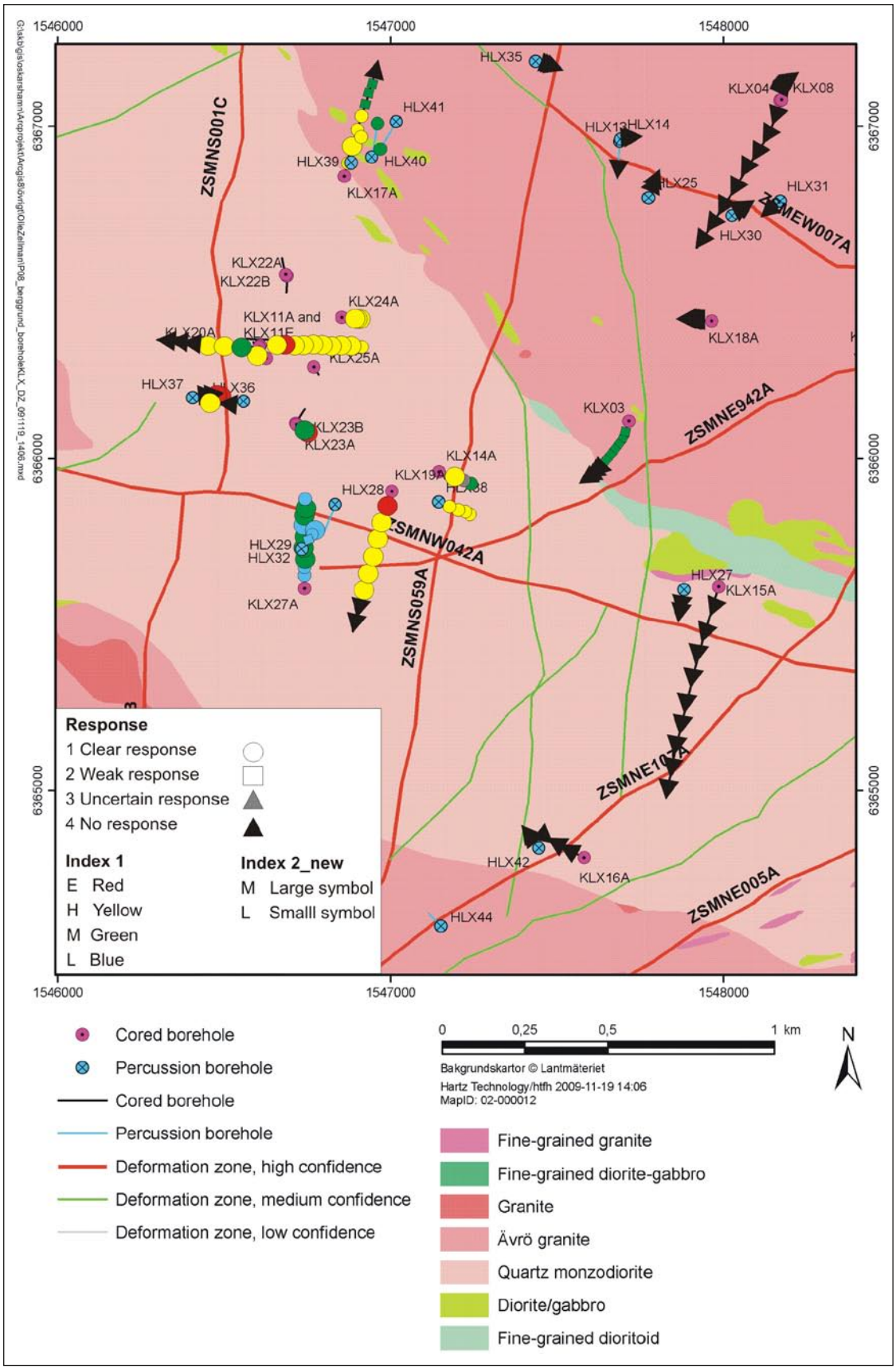

Figure 6-5. *Illustration of the hydraulic responses of the pumping in HLX28 (in the centre of the map). The shape, size and colour of each symbol indicate the hydraulic response according to Appendix 1. Each symbol represents a borehole section response.*

7 References

Cooley R L, 1979. A method of estimating parameters and assessing reliability for models of steady ground water flow. 2. Applications of statistical analyses. Water Resources Research, 15:318-324.

Enachescu C, Roh S, Wolf P, 2007. Hydraulic interference test, pumping borehole KLX20A Subarea Laxemar. Oskarshamn site investigation. SKB P-07-39, Svensk Kärnbränslehantering AB.

Gustafsson E, 2002. Bestämning av grundvattenglödet med utspädningsteknik – Modifiering av utrustning och kompletterande mätningar. SKB R-02-31, Svensk Kärnbränslehantering AB.

Harrström J, Walger E, Ludvigson J-E, Morosini M, 2008. Hydraulic interference tests of HLX27, HLX28, HLX32 and single hole pumping test of KLX27A. Subarea Laxemar. Oskarshamn site investigation. SKB P-07-186, Svensk Kärnbränslehantering AB.

Hjerne C, Nordqvist R, Harrström J, in prep 2009. Compilation and analyses of results from cross-hole tracer tests with conservative tracers. SKB R-09-28, Svensk Kärnbränslehantering AB.

Javandel I, Doughty C, Tsang C F, 1984. Groundwater transport: Handbook of mathematical models. American Geophysical Union, Washington, D.C.

Kristiansson S, 2007. Different flow logging of borehole KLX20A. Subarea Laxemar, Oskarshamn site investigation. SKB P-06-183, Svensk Kärnbränslehantering AB.

Kruseman G P, de Ridder N A, 1990. Analysis and Evaluation of Pumping Test Data. ILRI publication 47, The Netherlands, Int. Inst. For Land Reclamation and Improvement.

Kyllönen H, Leppänen H, Kristiansson S, 2007. Different flow logging of borehole KLX19A. Subarea Laxemar, Oskarshamn site investigation. SKB P-07-20, Svensk Kärnbränslehantering AB.

Lindquist A, Hjerne C, Nordquist R, Wass E, 2008a. Large-scale confirmatory multiple-hole tracer test. Forsmark site investigation. SKB P-08-59, Svensk Kärnbränslehantering AB.

Lindquist A, Hjerne C, Nordquist R, Ludvigson J-E, Harrström Johan, Carlsten S, 2008b. Confirmatory hydraulic interference test and tracer test in Laxemar. Oskarshamn site investigation. SKB P-08-96, Svensk Kärnbränslehantering AB.

Ludvigson J-E, Jönsson S, Levén J, 2004. Hydraulic evaluation of pumping activities prior to hydro-geochemical sampling in borehole KFM03A – Comparison with results from difference flow logging. Forsmark site investigation. SKB P-04-96, Svensk Kärnbränslehantering AB.

Moye D G, 1967. Diamond drilling for foundation exploration. Civ. Eng. Trans. 7th.Inst. Eng. Australia.

Pöllänen J, Pekkanen J, Väisäsvaara J, 2008. Different flow logging in borehole KLX27A. Subarea Laxemar, Oskarshamn site investigation. SKB P-08-22, Svensk Kärnbränslehantering AB.

Rhén I, Forsmark T, Hartley L, Jackson P, Roberts D, Swan D, Gylling B, 2009. Hydrogeological conceptualisation and parameterisation. Site Descriptive modelling SDM-Site Laxemar. SKB R-08-78, Svensk Kärnbränslehantering AB.

Rohs S, 2006. Flow logging in boreholes HLX21, HLX35 and HLX38. Subarea Laxemar. Oskarshamn site investigation. SKB P-06-147, Svensk Kärnbränslehantering AB.

Rohs S, van der Wall R, Wolf P, 2007. Flow logging in boreholes HLX14, HLX20, HLX27, HLX28, HLX32, HLX33, HLX37, HLX39 and HLX43 Subarea Laxemar. Oskarshamn site investigation. SKB P-06-319, Svensk Kärnbränslehantering AB.

SKB, 2006. Preliminary site description. Laxemar subarea – version 1.2. SKB R-06-10, Svensk Kärnbränslehantering AB.

Streltsova T D, 1988. Well testing in heterogeneous formations. Exxon Monograph. John Wiley and sons.

Väisäsvaara J, Kristiansson S, Sokolnicki M, 2007. Different flow logging of borehole KLX11A. Subarea Laxemar, Oskarshamn site investigation. SKB P-07-24, Svensk Kärnbränslehantering AB.

Wahlgren C-H, Curtis P, Hermanson J, Forssberg O, Öhman J, Fox A, La Pointe P, Drake H, Triumf C-A, Mattsson H, Thunehed H, Juhlin C, 2008. Geology Laxemar. Site descriptive modelling. SDM-Site Laxemar. SKB R-08-54, Svensk Kärnbränslehantering AB.

Walger E, Ludvigson J-E, Svensson T, Thur P, Harrström J, Morosini M, 2007. Hydraulic interference tests in boreholes KLX06, KLX14A, KLX15A, KLX16A, KLX17A, KLX18A, KLX19A, KLX21A, KLX22A, KLX22B, KLX23A, KLX23B, KLX26A and KLX26B. Subarea Laxemar. Oskarshamn site investigation. SKB P-07-183, Svensk Kärnbränslehantering AB.

Appendix 1

Response classification and radial distance to observation borehole sections

Response classification denotation:

1a. Clear response (transient evaluation).

1b. Clear response (transient evaluation cannot be made due to missing data).

2. Weak response (uncertain transient evaluation).

3. Uncertain response (no transient evaluation, response cannot be separated from background pressure variations).

4. No response.

Borehole	Section	Secup (mbl)	Seclow (mbl)	Distance from HLX28 (m)	Type of response
HLX01	1	16.00	100.00	3,137.5	4
HLX01	2	0.00	15.00	3,149.0	no data
HLX02	1	0.00	132.00	3,867.8	4
HLX03	1	0.00	100.00	3,678.4	no data
HLX04	1	0.00	125.00	3,500.6	no data
HLX05	1	0.00	100.00	3,587.8	no data
HLX06	1	0.00	100.00	3,243.8	4
HLX07	1	16.00	100.00	3,487.8	4
HLX07	2	0.00	15.00	3,466.0	4
HLX08	1	0.00	40.00	3,856.9	4
HLX09	1	17.00	151.00	4,224.8	4
HLX09	2	0.00	16.00	4,231.1	4
HLX11	1	14.00	70.00	2,413.0	4
HLX11	2	0.00	13.00	2,404.9	4
HLX13	1	0.00	200.20	1,384.0	4
HLX14	1	96.00	115.90	1,462.3	4
HLX14	2	0.00	95.00	1,448.5	4
HLX15	1	0.00	0.00	1,903.6	4
HLX18	1	90.00	181.20	3,299.2	4
HLX18	2	0.00	89.00	3,266.7	4
HLX20	1	81.00	202.20	2,774.1	4
HLX20	2	70.00	80.00	2,746.8	4
HLX20	3	0.00	69.00	2,730.8	4
HLX21	1	73.00	150.30	2,892.2	4
HLX21	2	0.00	72.00	2,906.0	4
HLX22	1	0.00	163.20	2,940.8	4
HLX23	1	61.00	160.20	2,181.2	4
HLX23	2	0.00	60.00	2,198.8	4
HLX25	1	61.00	202.50	1,417.0	4
HLX25	2	0	60.00	1,374.0	4
HLX26	1	11.00	151.20	1,857.1	4
HLX26	2	0.00	10.00	1,864.3	4
HLX27	1	153.00	164.70	1,093.5	4
HLX27	2	0.00	152.00	1,087.1	4
HLX30	1	101.00	163.40	1,573.0	4
HLX30	2	0.00	100.00	1,536.5	4
HLX31	1	0.00	133.20	1,623.3	4

Borehole	Section	Secup (mbl)	Seclow (mbl)	Distance from HLX28 (m)	Type of response
HLX32	1	31.00	162.60	76.0	1a
HLX32	2	20.00	30.00	122.0	1a
HLX32	3	12.30	19.00	129.5	2
HLX33	1	50.00	202.10	1,960.1	4
HLX33	2	0.00	49.00	1,871.6	4
HLX34	1	0.00	151.80	1,680.7	4
HLX35	1	136.00	151.80	1,518.9	4
HLX35	2	120.00	135.00	1,517.0	4
HLX35	3	0.00	119.00	1,511.3	4
HLX36	1	50.00	199.80	485.0	1b
HLX36	2	0.00	49.00	447.1	4
HLX37	1	150.00	199.80	486.0	1a
HLX37	2	111.00	149.00	500.8	1a
HLX37	3	94.00	110.00	510.9	4
HLX37	4	13.25	93.00	529.5	4
HLX38	1	81.00	199.50	405.8	1a
HLX38	2	41.00	80.00	360.3	1a
HLX38	3	28.00	40.00	349.1	1a
HLX38	4	15.02	27.00	344.5	1a
HLX39	1	6.02	199.30	1,120.7	1a
HLX40	1	6.00	199.50	1,148.9	1a
HLX40	2	0.00	39.00	1,104.2	no data
HLX41	1	6.02	199.50	1,151.1	1a
HLX42	1	30.00	152.60	1,127.9	4
HLX42	2	0.00	29.00	1,170.3	4
HLX43	1	135.00	147.00	1,719.3	4
HLX43	2	75.00	134.00	1,715.1	4
HLX43	3	30.00	74.00	1,710.4	4
HLX43	4	0.00	29.00	1,708.6	4
KLX01	1	705.00	1,077.99	3,634.3	4
KLX01	2	191.00	704.00	3,551.9	4
KLX01	3	171.00	190.00	3,528.7	4
KLX01	4	0.00	170.00	3,525.0	4
KLX02	1	1,165.00	1,700.00	2,979.1	4
KLX02	2	1,145.00	1,164.00	2,848.2	4
KLX02	3	718.00	1,144.00	2,760.6	4
KLX02	4	495.00	717.00	2,662.5	4
KLX02	5	452.00	494.00	2,633.2	4
KLX02	6	348.00	451.00	2,620.0	4
KLX02	7	208.00	347.00	2,603.3	4
KLX02	8	0.00	207.00	2,589.8	4
KLX03	1	965.50	971.50	1,159.0	4
KLX03	2	830.50	964.50	1,118.8	4
KLX03	3	752.50	829.50	1,064.1	4
KLX03	4	729.50	751.50	1,040.6	4
KLX03	5	652.50	728.50	1,019.0	2
KLX03	6	465.50	651.50	970.0	2
KLX03	7	349.50	464.50	933.9	2
KLX03	8	199.50	348.50	921.7	2
KLX03	9	193.50	198.50	922.5	2
KLX03	10	100.05	192.50	926.1	2
KLX04	1	898.00	993.49	2,118.6	4
KLX04	2	870.00	897.00	2,087.3	4

Borehole	Section	Secup (mbl)	Seclow (mbl)	Distance from HLX28 (m)	Type of response
KLX04	3	686.00	869.00	2,037.7	4
KLX04	4	531.00	685.00	1,969.2	4
KLX04	5	507.00	530.00	1,939.2	4
KLX04	6	231.00	506.00	1,897.8	4
KLX04	7	163.00	230.00	1,865.3	4
KLX04	8	0.00	162.00	1,852.4	4
KLX05	1	721.00	1,000.00	2,101.7	4
KLX05	2	634.00	720.00	2,093.4	4
KLX05	3	625.00	633.00	2,091.6	4
KLX05	4	501.00	624.00	2,090.7	4
KLX05	5	361.00	500.00	2,093.1	4
KLX05	6	256.00	360.00	2,094.9	4
KLX05	7	241.00	255.00	2,095.5	4
KLX05	8	220.00	240.00	2,095.6	4
KLX05	9	128.00	219.00	2,095.5	4
KLX05	10	0.00	127.00	2,097.5	4
KLX06	1	761.00	994.49	2,999.6	4
KLX06	2	571.00	760.00	2,862.1	4
KLX06	3	554.00	570.00	2,805.7	4
KLX06	4	411.00	553.00	2,767.0	4
KLX06	5	276.00	410.00	2,714.1	4
KLX06	6	256.00	275.00	2,692.5	4
KLX06	7	146.00	255.00	2,678.5	4
KLX06	8	0.00	145.00	2,655.8	4
KLX07A	1	781.00	844.73	2,535.3	4
KLX07A	2	753.00	780.00	2,529.6	4
KLX07A	3	612.00	752.00	2,521.4	4
KLX07A	4	457.00	611.00	2,513.9	4
KLX07A	5	333.00	456.00	2,523.8	4
KLX07A	6	204.00	332.00	2,536.3	4
KLX07A	7	104.00	203.00	2,546.9	4
KLX07A	8	0.00	103.00	2,557.4	4
KLX07B	1	95.00	200.00	2,561.7	4
KLX07B	2	0.00	94.00	2,563.3	4
KLX08	1	840.00	1,000.41	1,579.8	4
KLX08	2	684.00	839.00	1,597.3	4
KLX08	3	626.00	683.00	1,616.5	4
KLX08	4	594.00	625.00	1,626.6	4
KLX08	5	497.00	593.00	1,643.0	4
KLX08	6	355.00	496.00	1,679.2	4
KLX08	7	243.00	354.00	1,725.5	4
KLX08	8	160.00	242.00	1,764.1	4
KLX08	9	102.00	159.00	1,782.0	4
KLX08	10	0.00	101.00	1,829.6	4
KLX09	1	564.00	880.38	2,547.8	4
KLX09	2	470.00	563.00	2,524.5	4
KLX09	3	199.00	469.00	2,517.9	4
KLX09	4	104.00	198.00	2,525.2	4
KLX09	5	0.00	103.00	2,534.1	4
KLX09F	1	0.00	152.30	2,527.1	4
KLX09G	1	0.00	100.10	2,596.7	4
KLX10	1	711.00	1,001.00	1,842.2	4
KLX10	2	689.00	710.00	1,798.5	4

Borehole	Section	Secup (mbl)	Seclow (mbl)	Distance from HLX28 (m)	Type of response
KLX10	3	465.00	688.00	1,773.0	4
KLX10	4	369.00	464.00	1,752.5	4
KLX10	5	351.00	368.00	1,748.7	4
KLX10	6	291.00	350.00	1,747.2	4
KLX10	7	131.00	290.00	1,747.8	4
KLX10	8	0.00	130.00	1,762.4	4
KLX10C	1	66.00	146.25	1,790.3	4
KLX10C	2	32.00	65.00	1,780.7	4
KLX10C	3	0.00	31.00	1,780.5	4
KLX11A	1	703.00	992.29	889.9	1a
KLX11A	2	587.00	702.00	743.9	1a
KLX11A	3	573.00	586.00	702.2	1a
KLX11A	4	495.00	572.00	674.8	1a
KLX11A	5	315.00	494.00	609.3	1a
KLX11A	6	273.00	314.00	570.4	1a
KLX11A	7	256.00	272.00	563.2	1a
KLX11A	8	180.00	255.00	554.8	1a
KLX11A	9	103.00	179.00	549.0	1a
KLX11A	10	12.05	102.00	554.3	1a
KLX11E	1	0.00	121.30	545.8	1a
KLX12A	1	546.00	602.29	2,026.4	4
KLX12A	2	535.00	545.00	2,025.6	4
KLX12A	3	426.00	534.00	2,025.6	4
KLX12A	4	386.00	425.00	2,028.2	4
KLX12A	5	291.00	385.00	2,033.1	4
KLX12A	6	160.00	290.00	2,049.7	4
KLX12A	7	142.00	159.00	2,063.6	4
KLX12A	8	104.00	141.00	2,069.5	4
KLX12A	9	0.00	103.00	2,085.4	4
KLX13A	1	508.00	595.85	1,748.3	4
KLX13A	2	490.00	507.00	1,738.8	4
KLX13A	3	341.00	489.00	1,727.1	4
KLX13A	4	244.00	340.00	1,716.6	4
KLX13A	5	131.00	243.00	1,714.5	4
KLX13A	6	0.00	130.00	1,720.5	4
KLX14A	1	123.00	176.27	438.8	1a
KLX14A	2	77.00	122.00	405.9	1b
KLX14A	3	6.45	76.00	378.5	1a
KLX15A	1	902.00	1,000.43	1,435.5	4
KLX15A	2	641.00	901.00	1,352.9	4
KLX15A	3	623.00	640.00	1,288.8	4
KLX15A	4	481.00	622.00	1,257.5	4
KLX15A	5	273.00	480.00	1,206.7	4
KLX15A	6	260.00	272.00	1,188.3	4
KLX15A	7	191.00	259.00	1,184.3	4
KLX15A	8	79.00	190.00	1,180.8	4
KLX15A	9	0.00	78.00	1,185.4	4
KLX16A	1	327.00	433.55	1,166.5	3
KLX16A	2	86.00	326.00	1,206.5	4
KLX16A	3	0.00	85.00	1,263.5	4
KLX17A	1	435.00	701.08	1,371.6	4
KLX17A	2	419.00	434.00	1,268.5	2
KLX17A	3	343.00	418.00	1,237.6	2

Borehole	Section	Secup (mbl)	Seclow (mbl)	Distance from HLX28 (m)	Type of response
KLX17A	4	314.00	342.00	1,203.4	2
KLX17A	5	220.00	313.00	1,165.6	1a
KLX17A	6	180.00	219.00	1,127.5	1a
KLX17A	7	70.00	179.00	1,088.5	1a
KLX17A	8	11.95	69.00	1,048.5	1a
KLX18A	1	571.00	611.28	1,310.9	4
KLX18A	2	490.00	570.00	1,296.9	4
KLX18A	3	472.00	489.00	1,287.7	4
KLX18A	4	315.00	471.00	1,276.0	4
KLX18A	5	155.00	314.00	1,270.0	4
KLX18A	6	104.00	154.00	1,276.4	4
KLX18A	7	0.00	103.00	1,286.2	4
KLX19A	1	661.00	800.07	625.4	4
KLX19A	2	518.00	660.00	490.6	4
KLX19A	3	509.00	517.00	420.2	1a
KLX19A	4	481.50	508.00	408.0	1a
KLX19A	5	311.00	480.50	316.9	1a
KLX19A	6	291.00	310.00	242.5	1a
KLX19A	7	136.00	290.00	191.3	1a
KLX19A	8	98.75	135.00	176.6	1a
KLX20A	1	294.00	457.92	726.7	4
KLX20A	2	260.00	293.00	663.2	4
KLX20A	3	181.00	259.00	633.2	4
KLX20A	4	145.00	180.00	606.4	1a
KLX20A	5	103.00	144.00	591.4	1a
KLX20A	6	99.50	102.00	584.0	1a
KLX21B	1	720.00	858.78	2,780.1	4
KLX21B	2	573.00	719.00	2,789.8	4
KLX21B	3	558.00	572.00	2,798.0	4
KLX21B	4	441.00	557.00	2,806.5	4
KLX21B	5	281.00	440.00	2,829.7	4
KLX21B	6	171.00	280.00	2,859.0	4
KLX21B	7	102.50	170.00	2,881.5	4
KLX21B	8	0.00	101.50	2,904.4	4
KLX23A	1	49.00	100.15	327.8	1a
KLX23A	2	0.00	48.00	315.6	1a
KLX24A	1	69.00	100.17	600.4	1a
KLX24A	2	41.00	68.00	601.8	1a
KLX24A	3	2.41	40.00	604.7	1a
KLX26A	1	48.00	101.14	2,265.5	4
KLX26A	2	22.00	47.00	2,246.7	4
KLX26A	3	0.00	21.00	2,235.3	4
KLX26B	1	21.00	50.37	2,238.3	no data
KLX26B	2	0.00	20.00	2,229.2	no data
KLX27A	1	640.00	650.56	518.5	1a
KLX27A	2	580.00	639.00	485.5	1a
KLX27A	3	490.00	579.00	417.2	1a
KLX27A	4	380.00	489.00	330.2	1a
KLX27A	5	260.00	379.00	224.2	1a
KLX27A	6	220.00	259.00	197.8	1a
KLX27A	7	115.00	219.00	179.7	1a
KLX27A	8	80.00	114.00	188.6	1a
KLX27A	9	14.76	79.00	209.3	1a

Borehole	Section	Secup (mbl)	Seclow (mbl)	Distance from HLX28 (m)	Type of response
KLX28A	1	0.00	80.23	2,517.9	4
KLX29A	1	0.00	60.25	2,518.5	4
SSM11				1,775.9	4
SSM17				908.1	4
SSM19				1,011.5	4
SSM21				1,393.2	4
SSM41				1,902.4	4
SSM213				2,068.3	4
SSM215				1,083.4	4
SSM220				1,811.9	4
SSM221				1,863.6	4
SSM222				1,527.2	4
SSM223				1,520.5	4
SSM228				2,020.5	4
SSM229				2,014.1	4
SSM236				447.9	4
SSM237				413	4
SSM250				1,320.1	4
SSM252				1,163.7	4
SSM253				1,153	4
SSM255				126.4	4
SSM268				1,142.1	4
SSM269				1,170.3	4
SSM270				1,171.3	no data
SSM271				1,248.9	4

Summary

Type of response:	Number of sections
1a	51
1b	2
2	10
3	1
4	202
no data	8
Total	**274**

Appendix 2

Linear plots of hydraulic head versus time for responding sections together with precipitation, barometric pressure and sea level data

Comments to presented plots
Peaks in the head curves are seen in several of the plots at the 7th of February and the 22nd and 24th of May. This is caused by pump failure in the pumping borehole HLX28A due to power supply outages.

Mini-packers in the standpipes were released in connection to manual levelling and when injection pumps were disconnected. This resulted in pressure peaks seen in several of the plots on the 2nd of March, 11th of May and 22nd and 23rd of April.

In HLX32:2 a distinct shift in hydraulic head of c 0.75 m occurred in connection to tracer test activities (i.e. on-going circulation of the water in the borehole section). This is normally not seen in borehole sections used for tracer injection and no explanation to this phenomenon has been found.

In HLX36:1 and KLX11E the water level decreased below the position of the pressure transmitter. Hence pressure data is not representative for parts of the test period.

Borehole HLX39 served as back-up fresh water supply to households nearby in case of tracer contamination of existing private wells. Hence, only the ground water surface level was monitored (i.e. open borehole) up until packers were installed in early May.

Sections HLX39:3 and KLX17A:8 show very similar behaviour in early May. The similar behaviour of the uppermost sections (i.e. the ground water table) in the two boreholes is explained by their proximity to each other. No external factor has been identified as the reason for the similarity. Local rainfall and installation of packers in HLX39 might contribute to the abrupt head changes observed.

Data is missing for borehole section KLX14A:2 in conjunction with start of the pumping in HLX28. Data has been deleted due to a defect pressure transmitter.

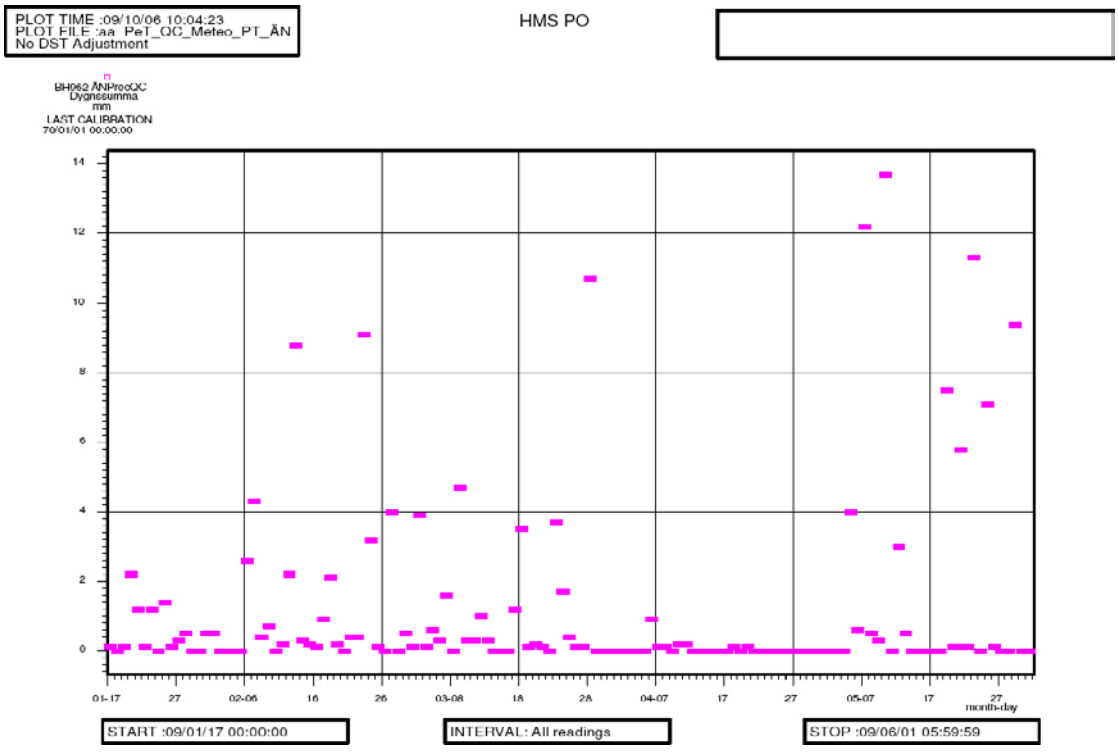

Figure A2-1. *Precipitation data registered at meteorological station at Äspö during pumping in HLX28. Each point is representing 24 hours.*

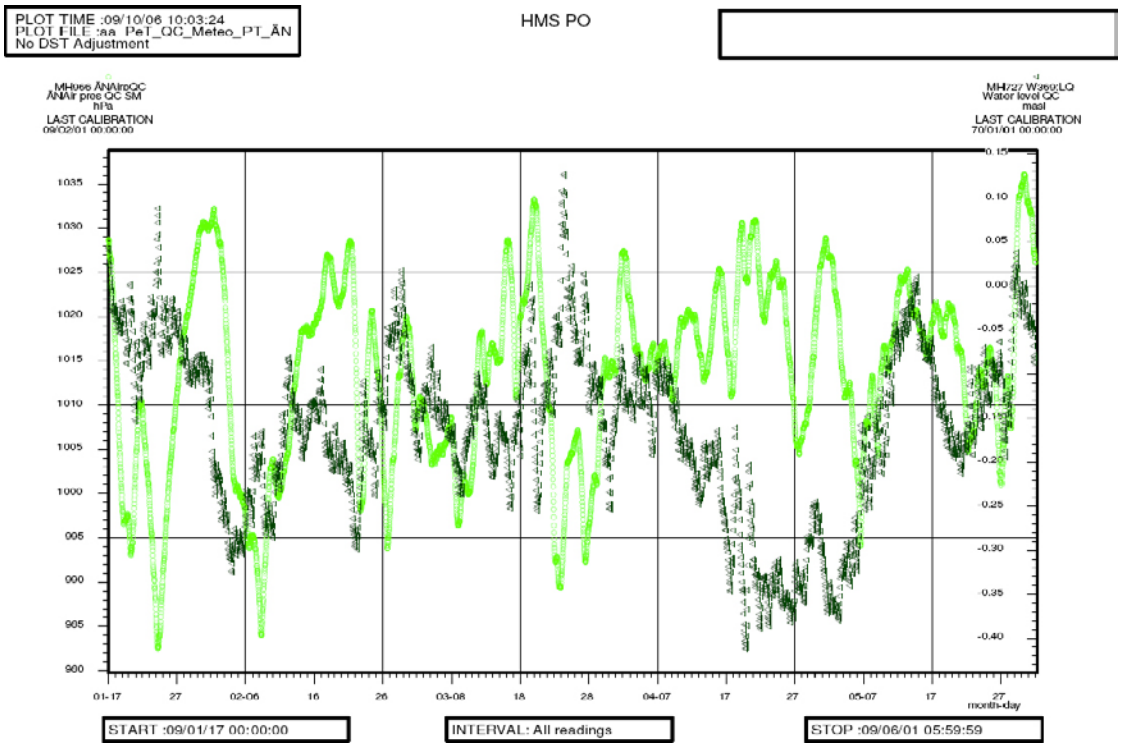

Figure A2-2. *Barometric pressure registered at meteorological station at Äspö together with sea water level registered at Southern Äspö during pumping in HLX28.*

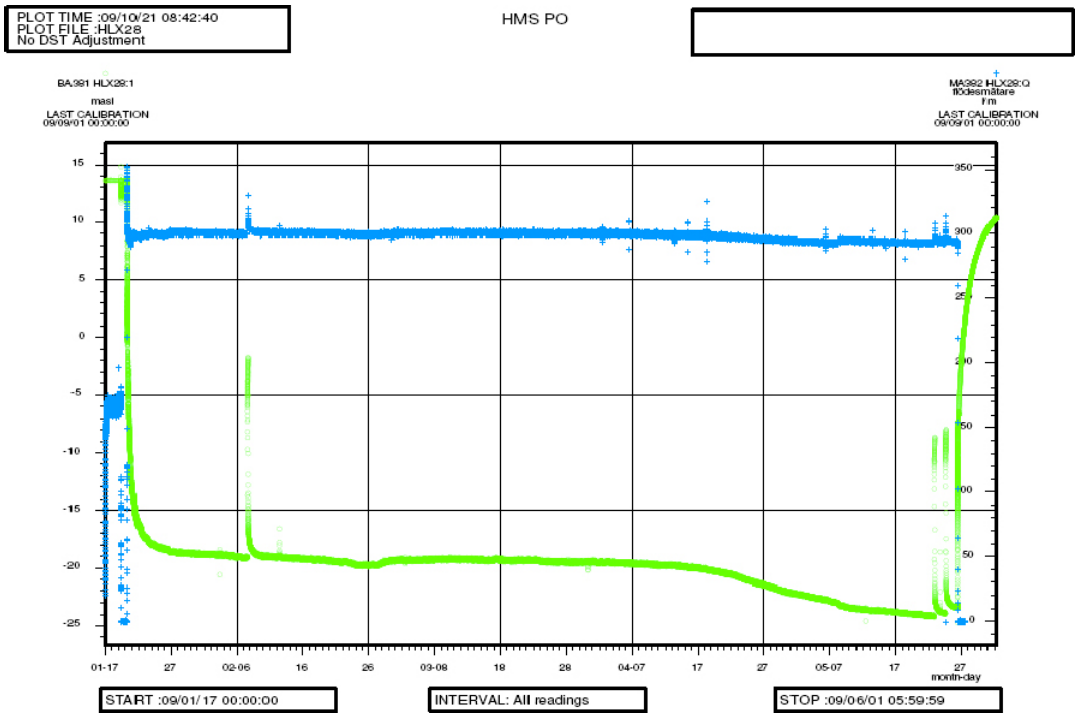

Figure A2-3. *Linear plot of observed head versus time in the pumping borehole HLX28.Figure A2-4. Linear plot of observed head versus time in observation borehole HLX32 during pumping in HLX28.*

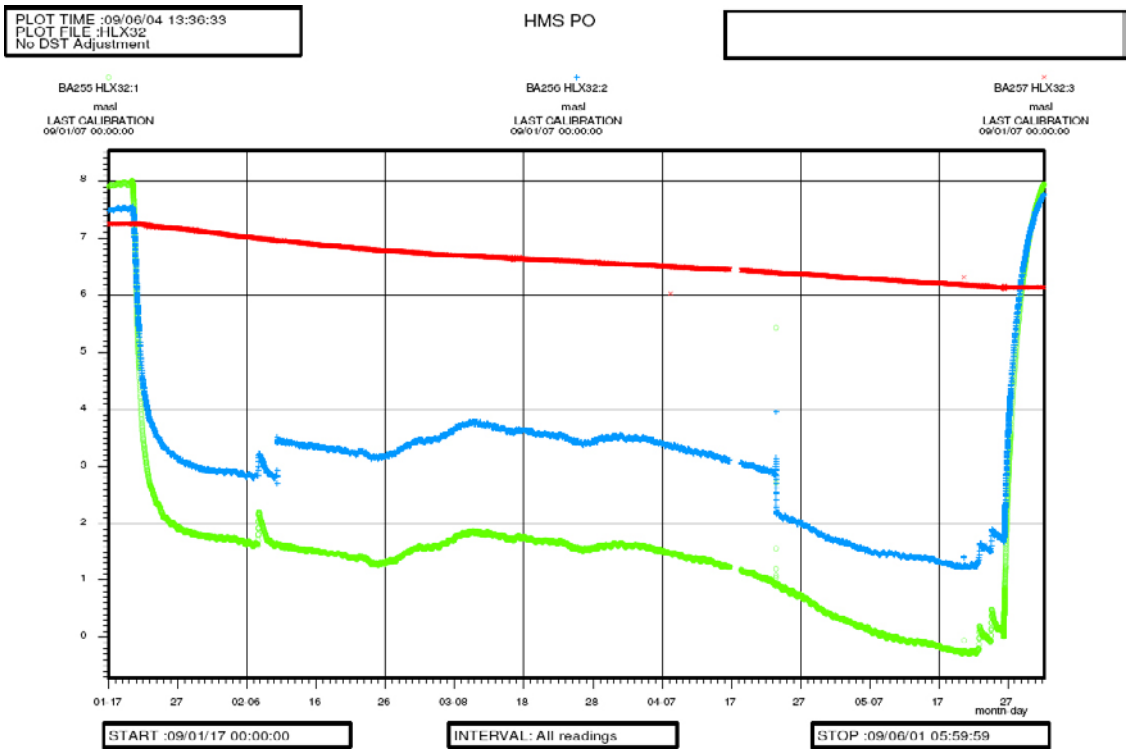

Figure A2-4. *Linear plot of observed head versus time in observation borehole HLX32 during pumping in HLX28.*

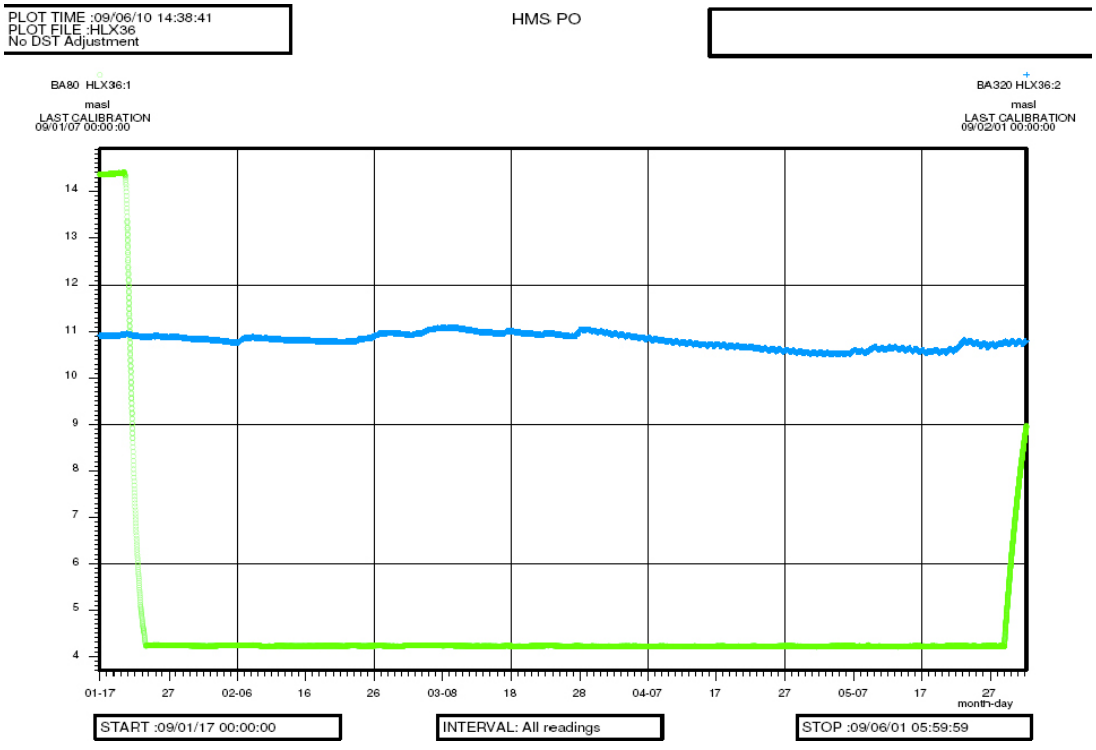

Figure A2-5. *Linear plot of observed head versus time in observation borehole HLX36 during pumping in HLX28.*

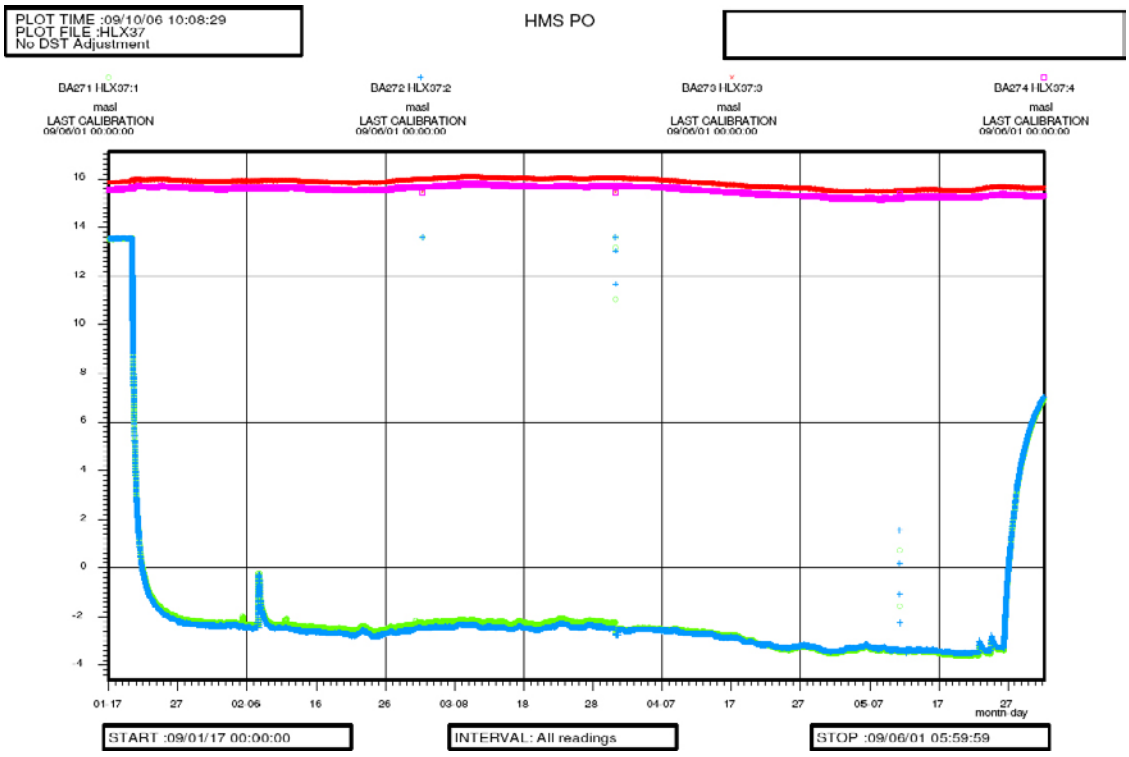

Figure A2-6. *Linear plot of observed head versus time in observation borehole HLX37 during pumping in HLX28.*

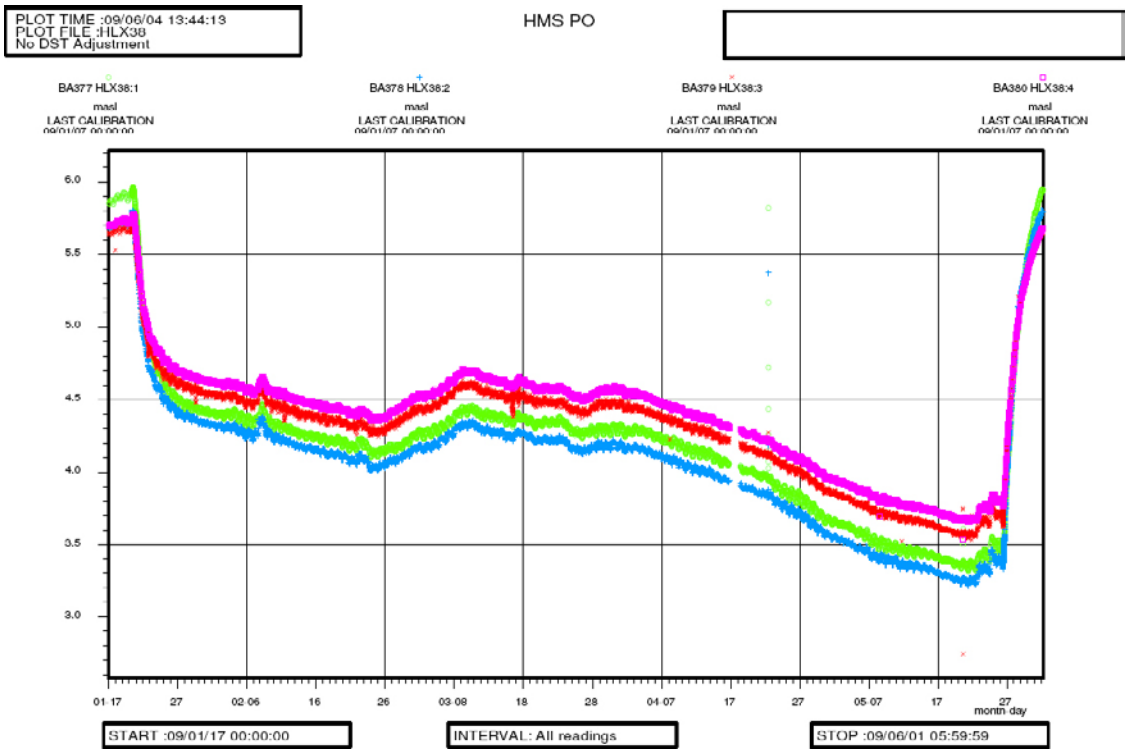

Figure A2-7. *Linear plot of observed head versus time in observation borehole HLX38 during pumping in HLX28.*

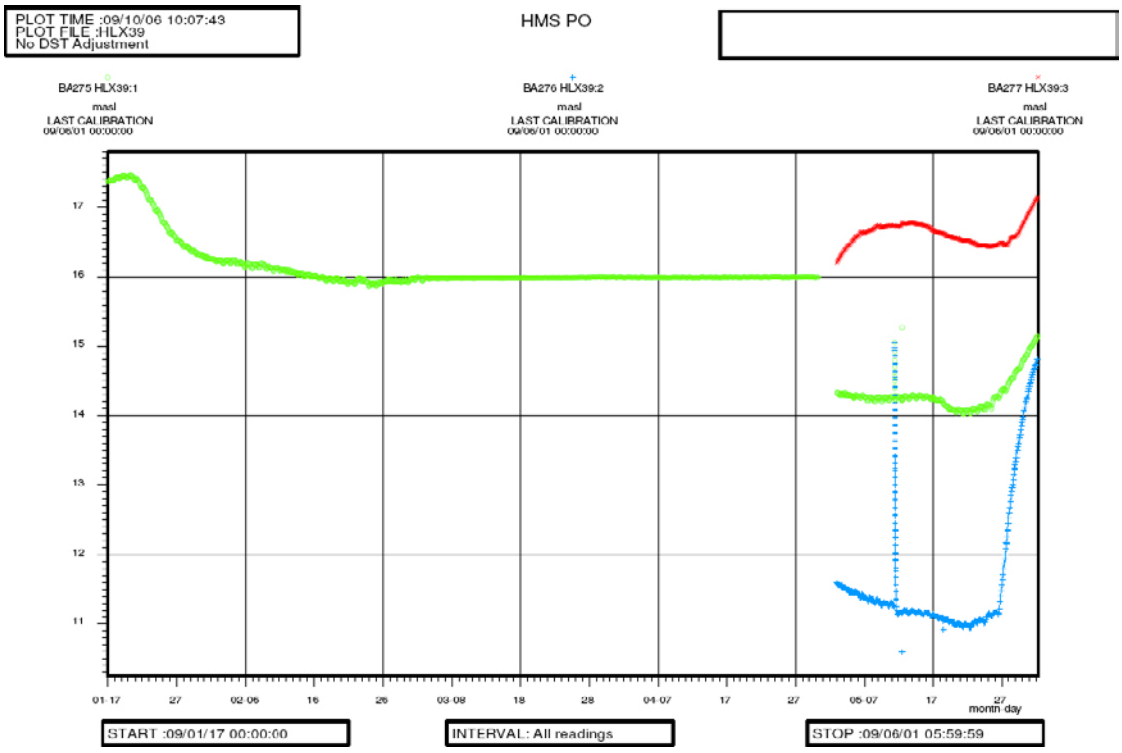

Figure A2-8. *Linear plot of observed head versus time in observation borehole HLX39 during pumping in HLX28.*

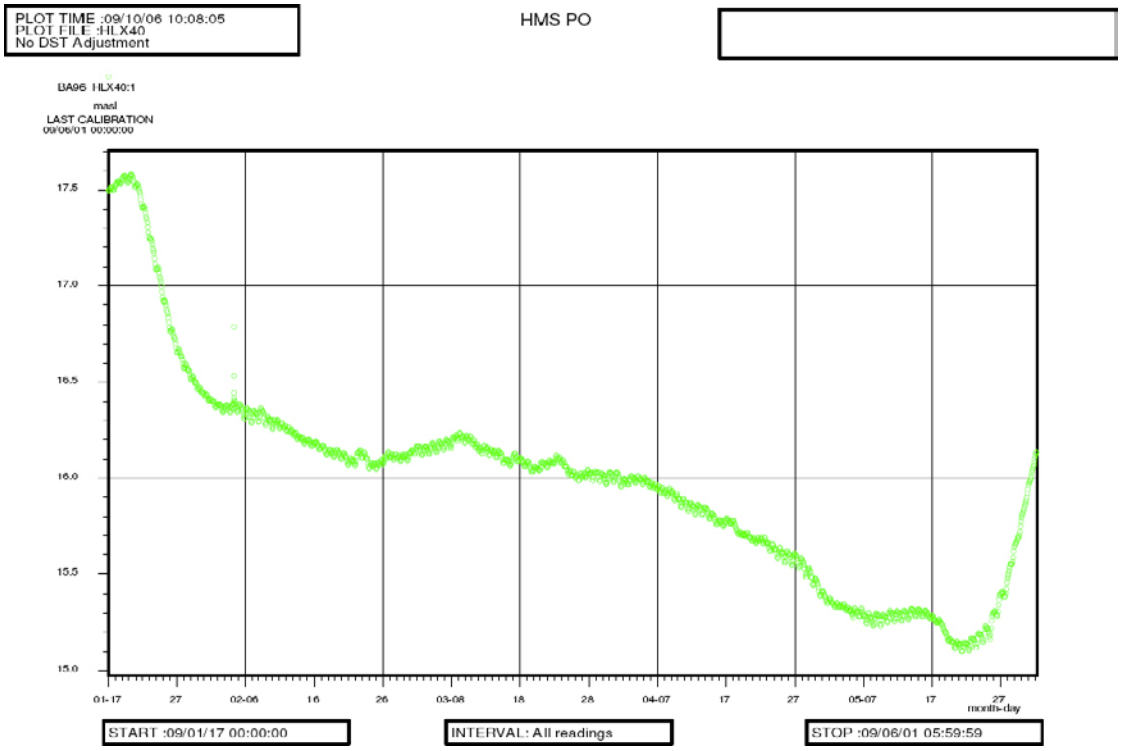

Figure A2-9. *Linear plot of observed head versus time in observation borehole HLX40 during pumping in HLX28.*

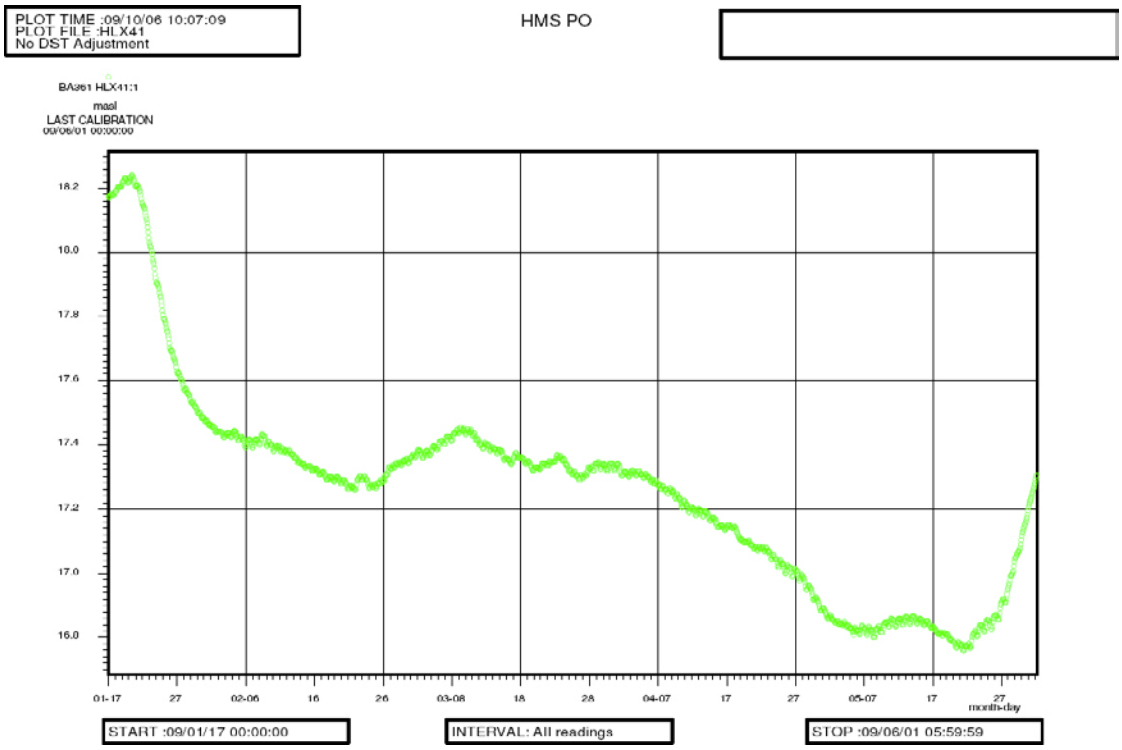

Figure A2-10. *Linear plot of observed head versus time in observation borehole HLX41 during pumping in HLX28.*

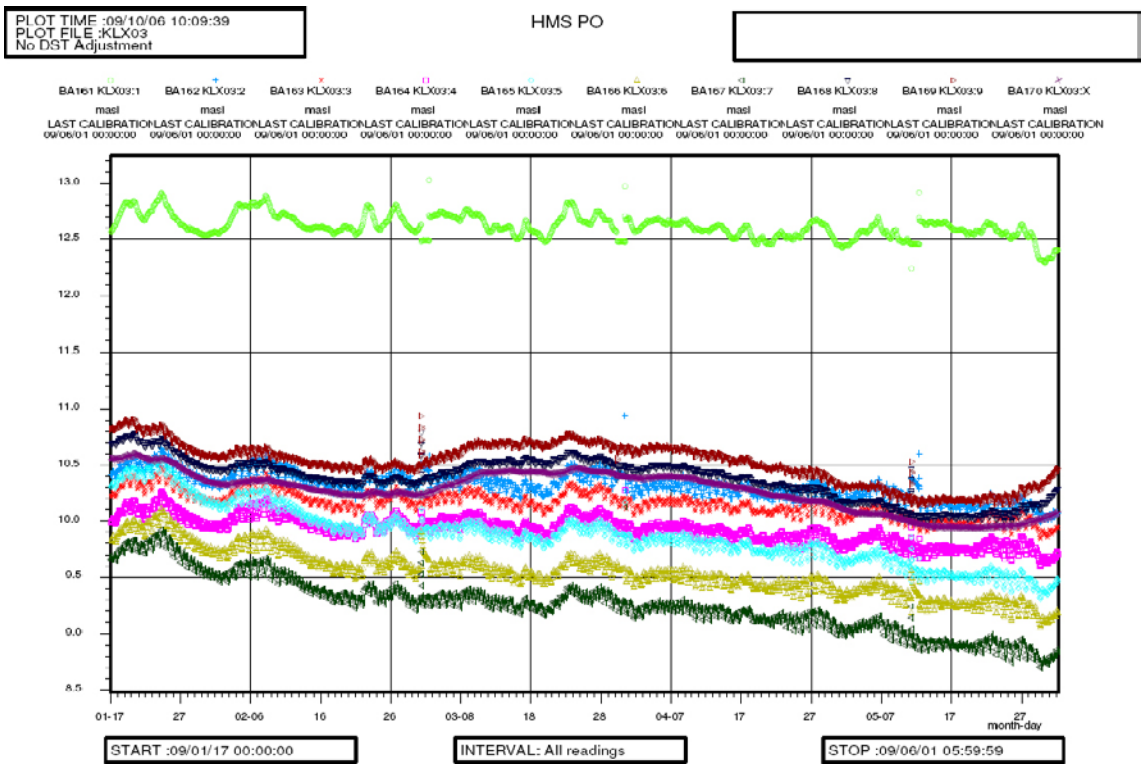

Figure A2-11. *Linear plot of observed head versus time in observation borehole KLX03 during pumping in HLX28.*

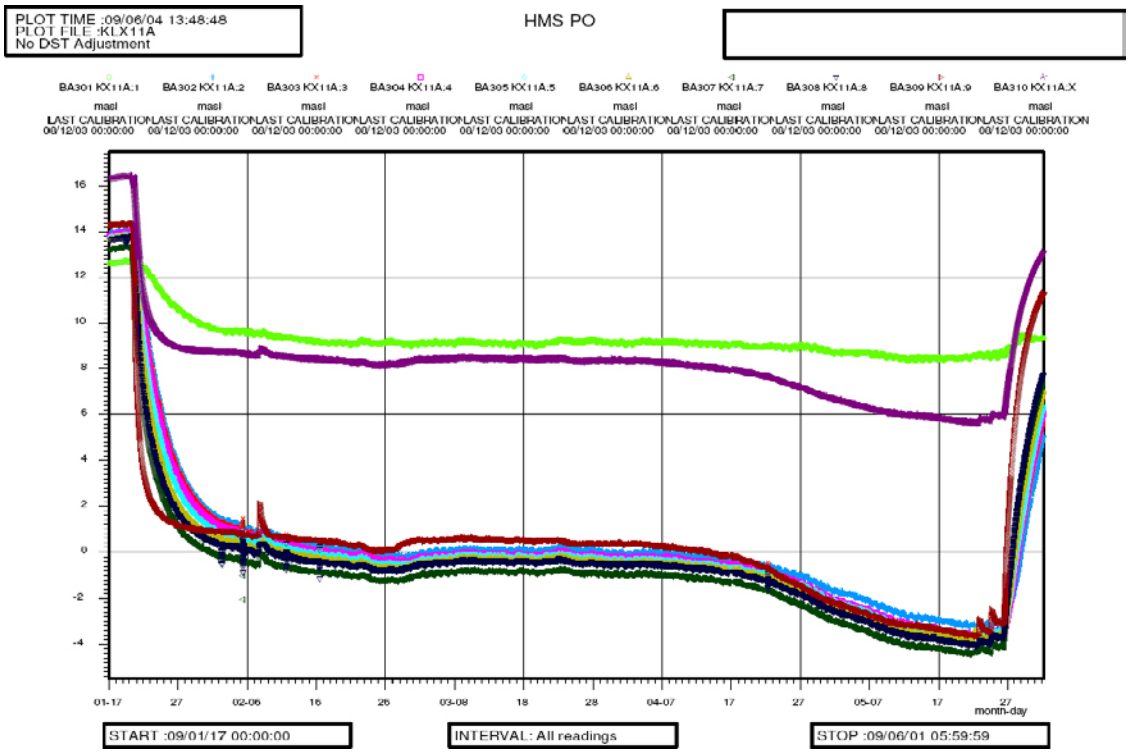

Figure A2-12. *Linear plot of observed head versus time in observation borehole KLX11A during pumping in HLX28.*

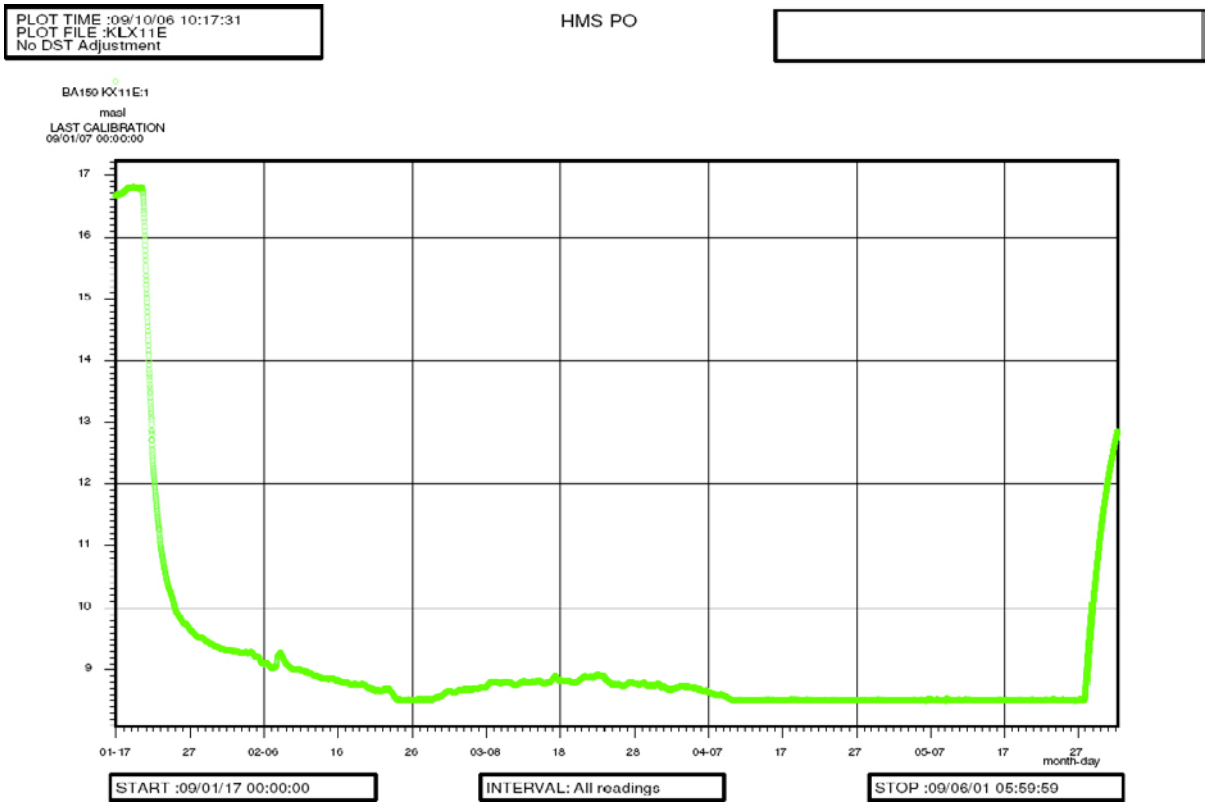

Figure A2-13. *Linear plot of observed head versus time in observation borehole KLX11E during pumping in HLX28.*

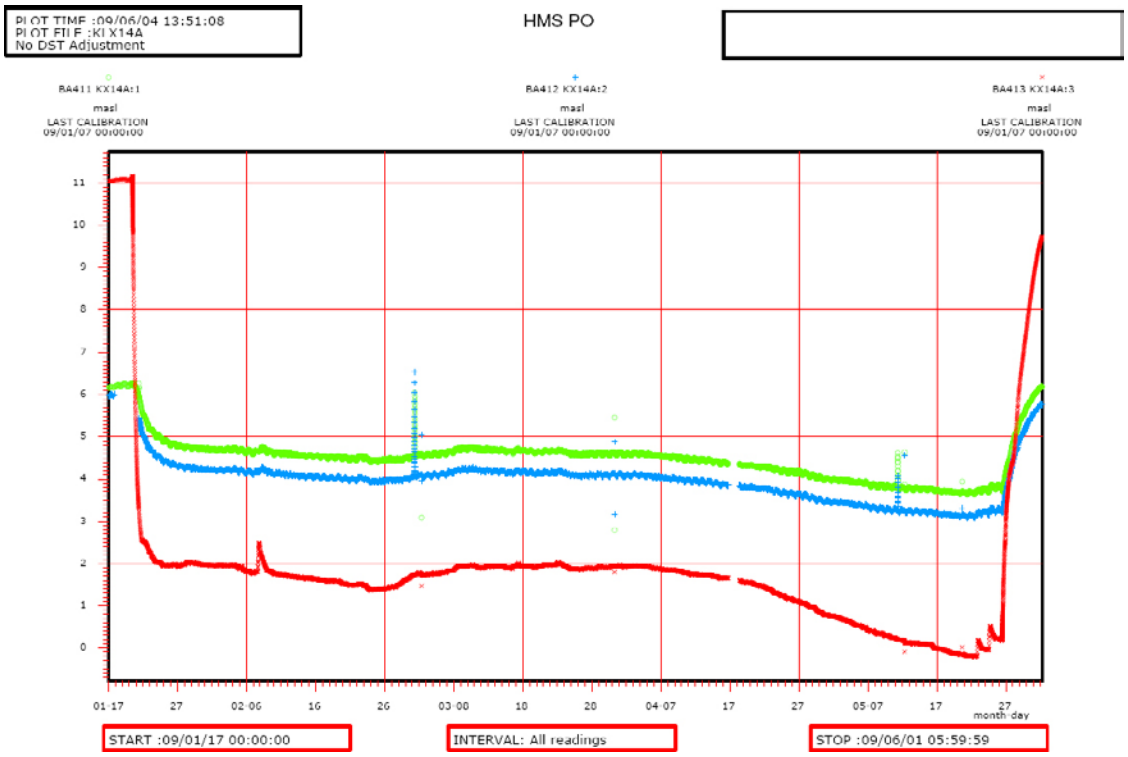

Figure A2-14. *Linear plot of observed head versus time in observation borehole KLX14A during pumping in HLX28.*

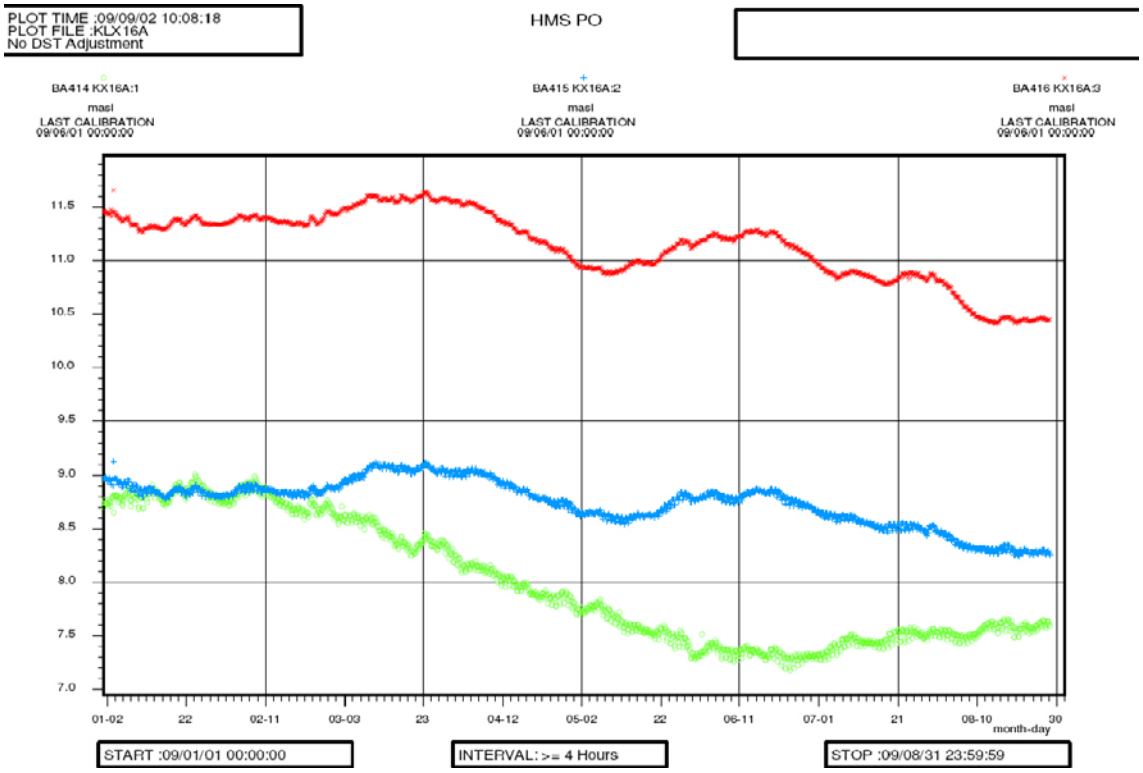

Figure A2-15. *Linear plot of observed head versus time in observation borehole KLX16A during pumping in HLX28.*

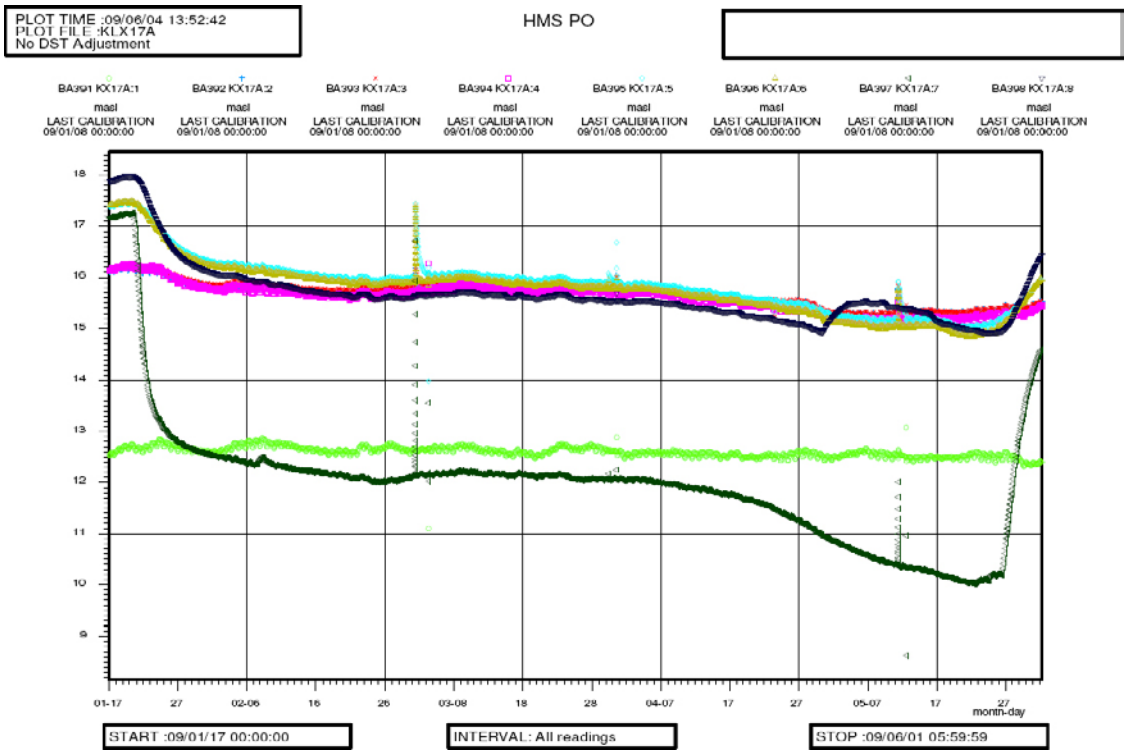

Figure A2-16. *Linear plot of observed head versus time in observation borehole KLX17A during pumping in HLX28.*

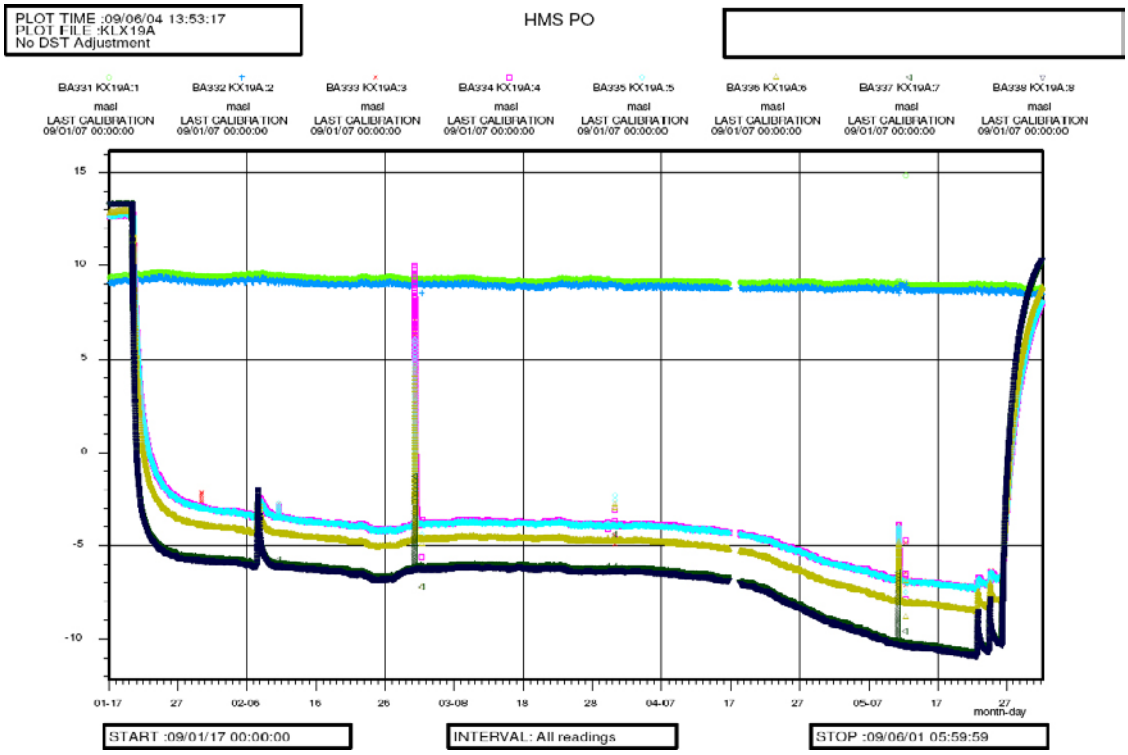

Figure A2-17. *Linear plot of observed head versus time in observation borehole KLX19A during pumping in HLX28.*

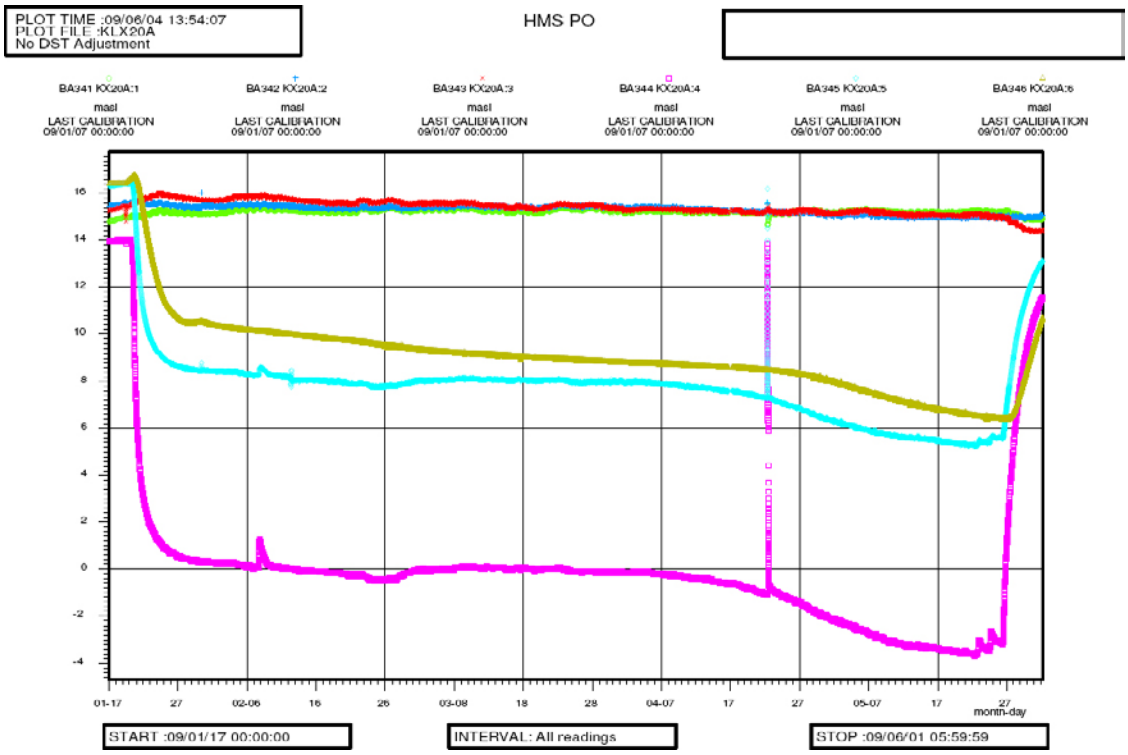

Figure A2-18. *Linear plot of observed head versus time in observation borehole KLX20A during pumping in HLX28.*

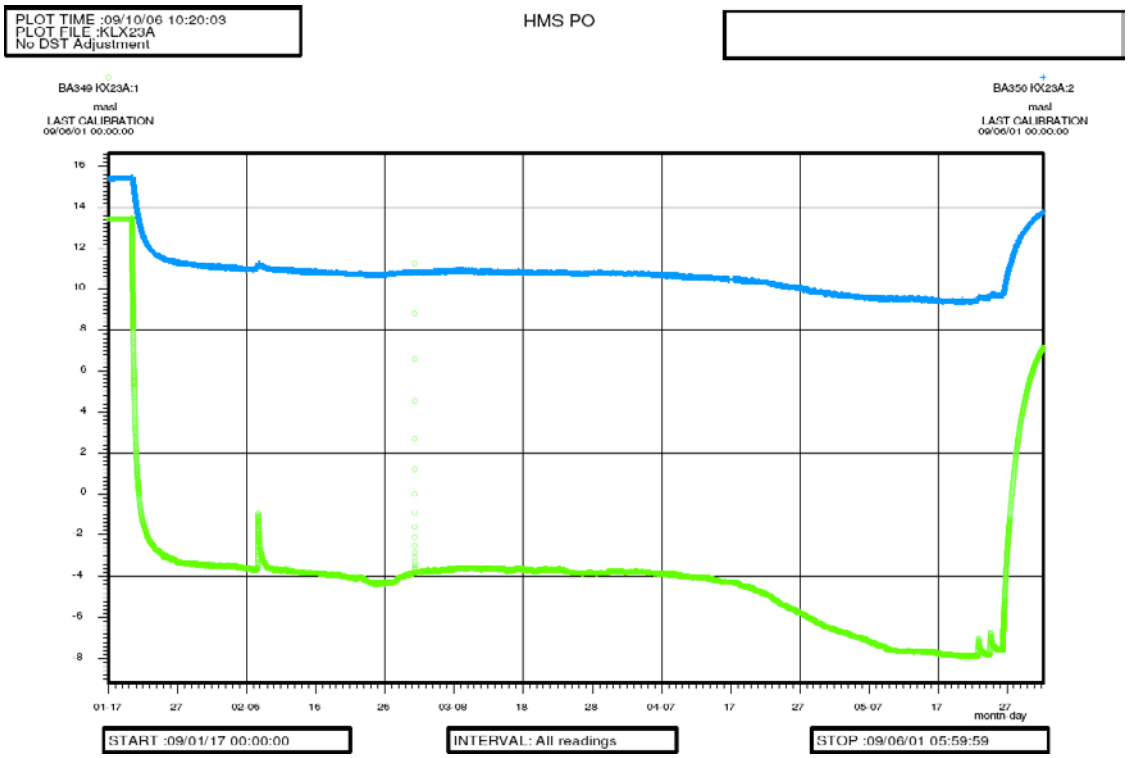

Figure A2-19. *Linear plot of observed head versus time in observation borehole KLX23A during pumping in HLX28.*

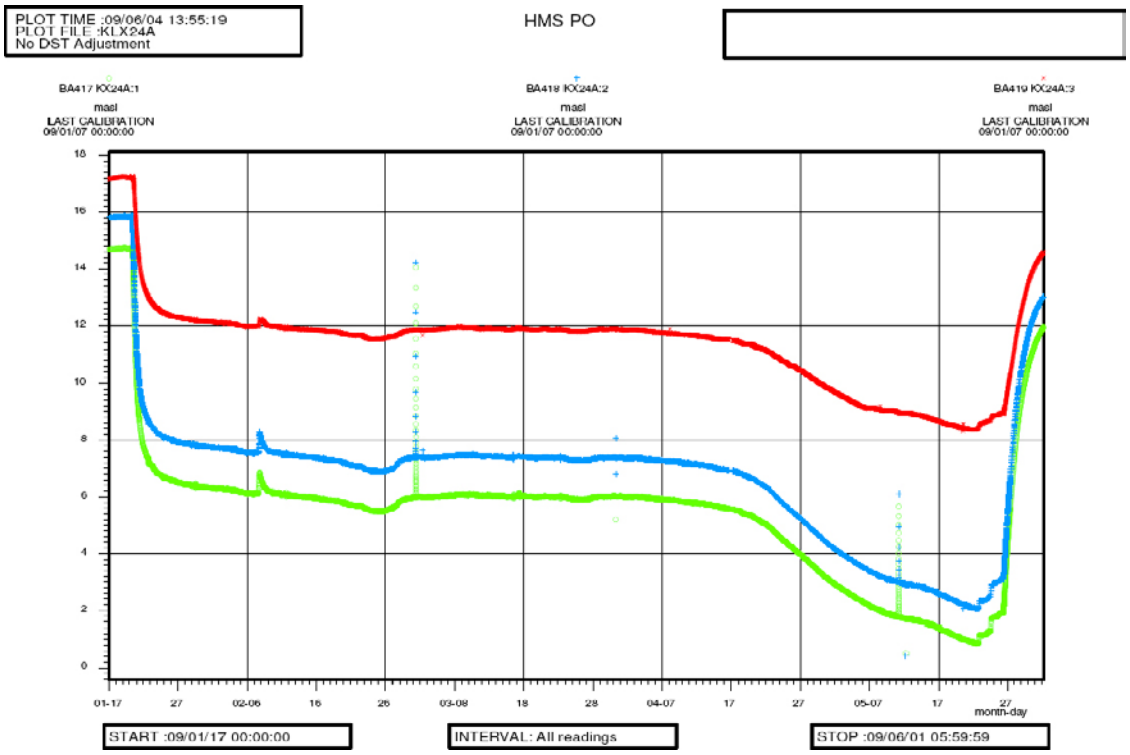

Figure A2-20. *Linear plot of observed head versus time in observation borehole KLX24A during pumping in HLX28.*

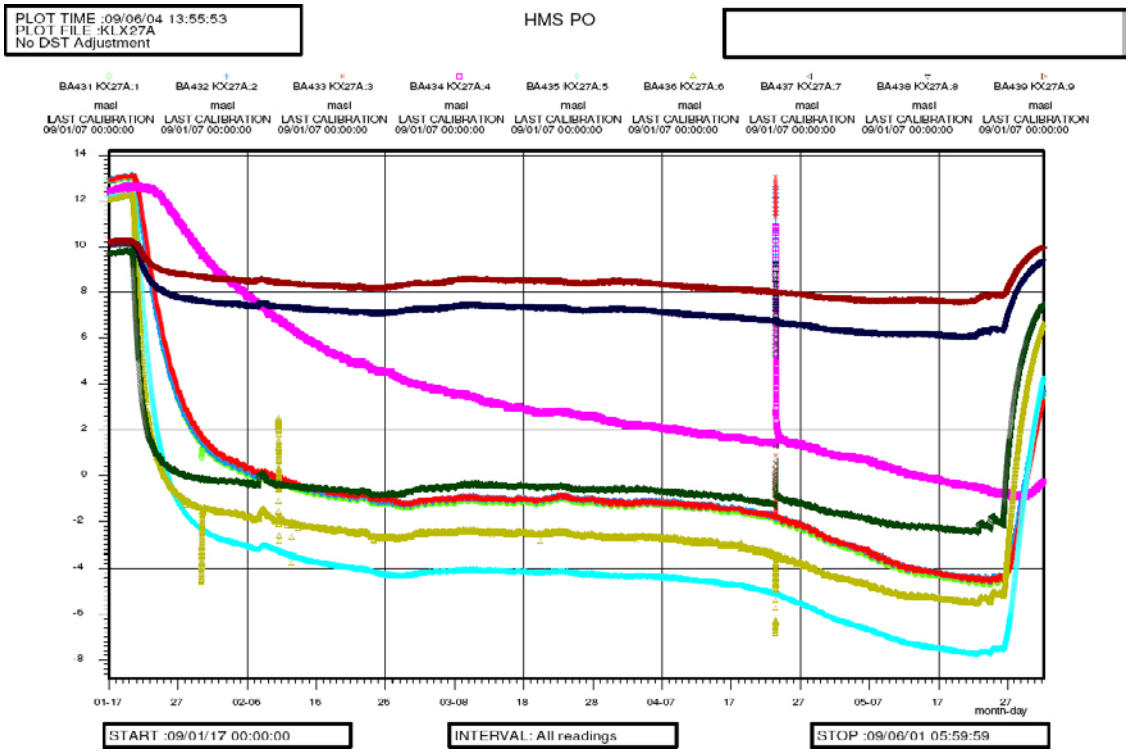

Figure A2-21. *Linear plot of observed head versus time in observation borehole KLX27A during pumping in HLX28.*

Amino-G dilution graphs

First campaign

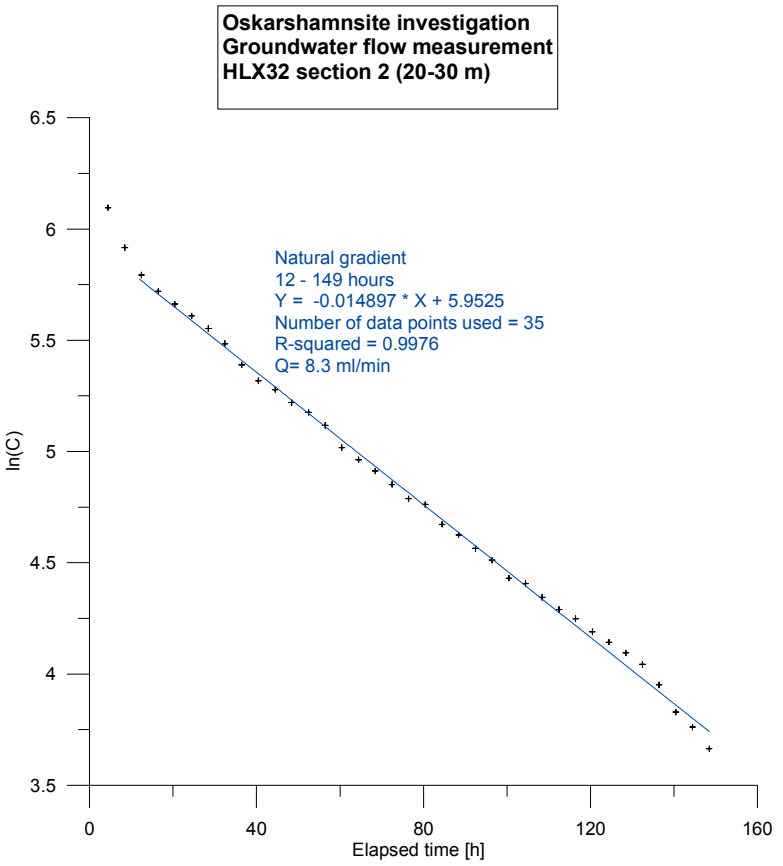

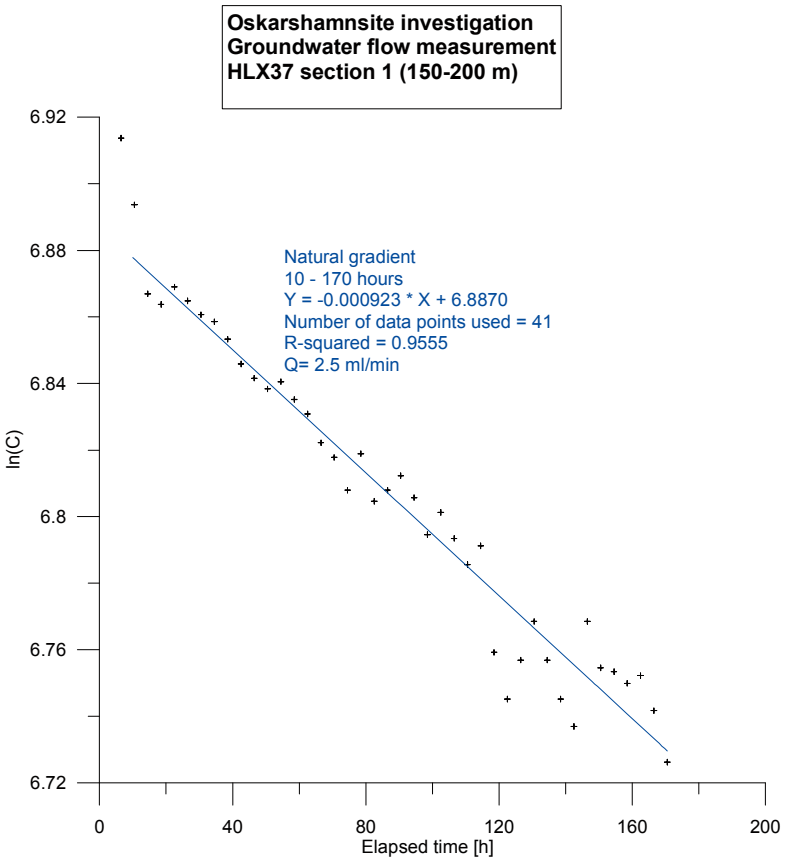

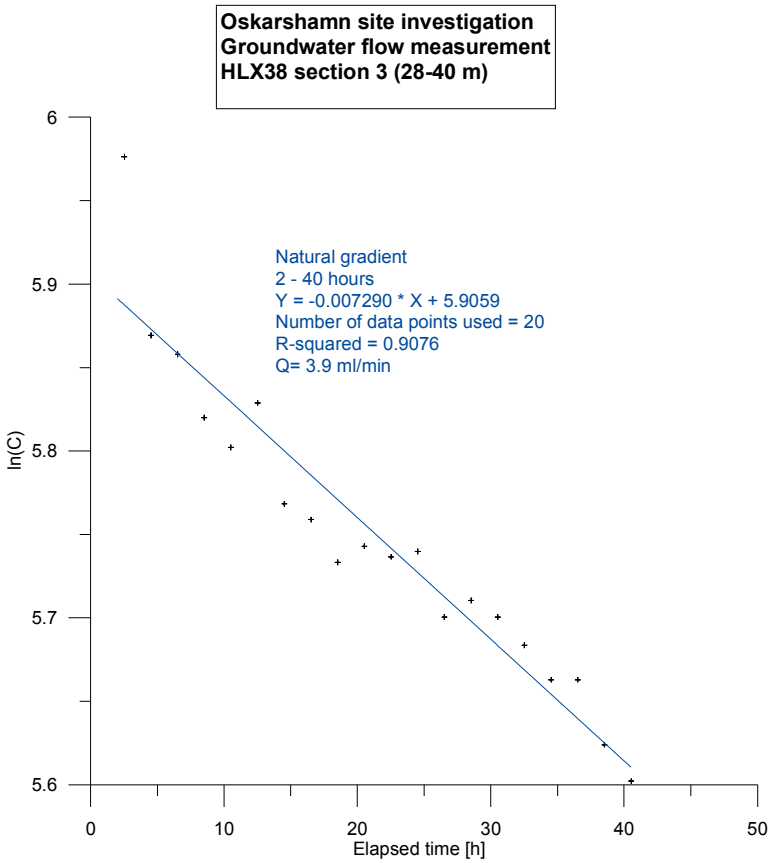
Oskarshamn site investigation
Groundwater flow measurement
HLX38 section 3 (28-40 m)
Natural gradient
2 - 40 hours
Y = -0.007290 * X + 5.9059
Number of data points used = 20
R-squared = 0.9076
Q= 3.9 ml/min
ln(C)
Elapsed time [h]
6
5.9
5.8
5.7
5.6
0
10
20
30
40
50

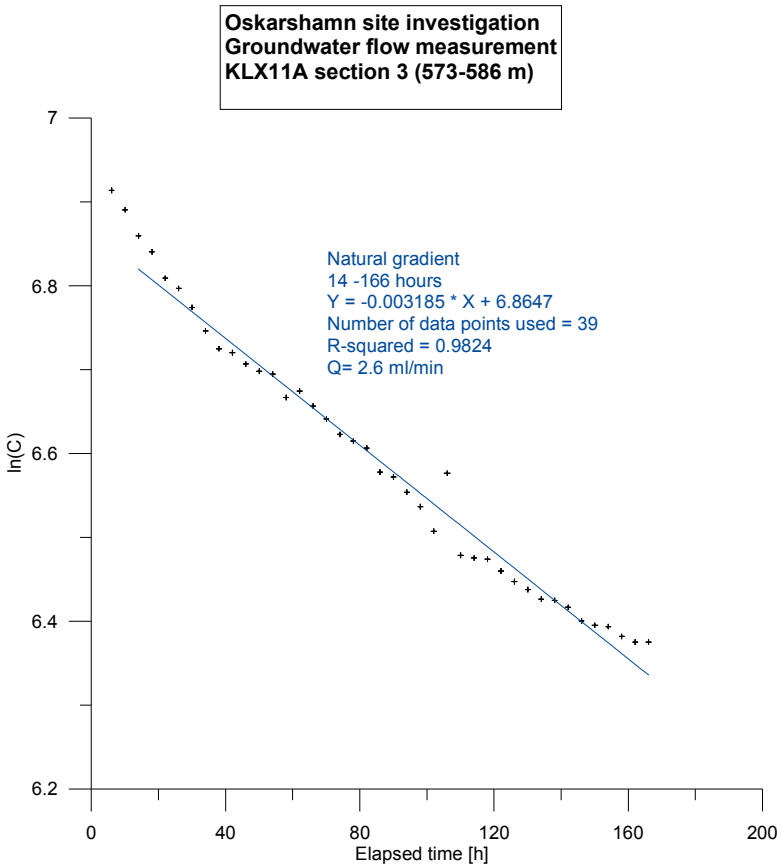
Oskarshamn site investigation
Groundwater flow measurement
KLX11A section 3 (573-586 m)
Natural gradient
14 -166 hours
Y = -0.003185 * X + 6.8647
Number of data points used = 39
R-squared = 0.9824
Q= 2.6 ml/min
ln(C)
Elapsed time [h]
7
6.8
6.6
6.4
6.2
0
40
80
120
160
200

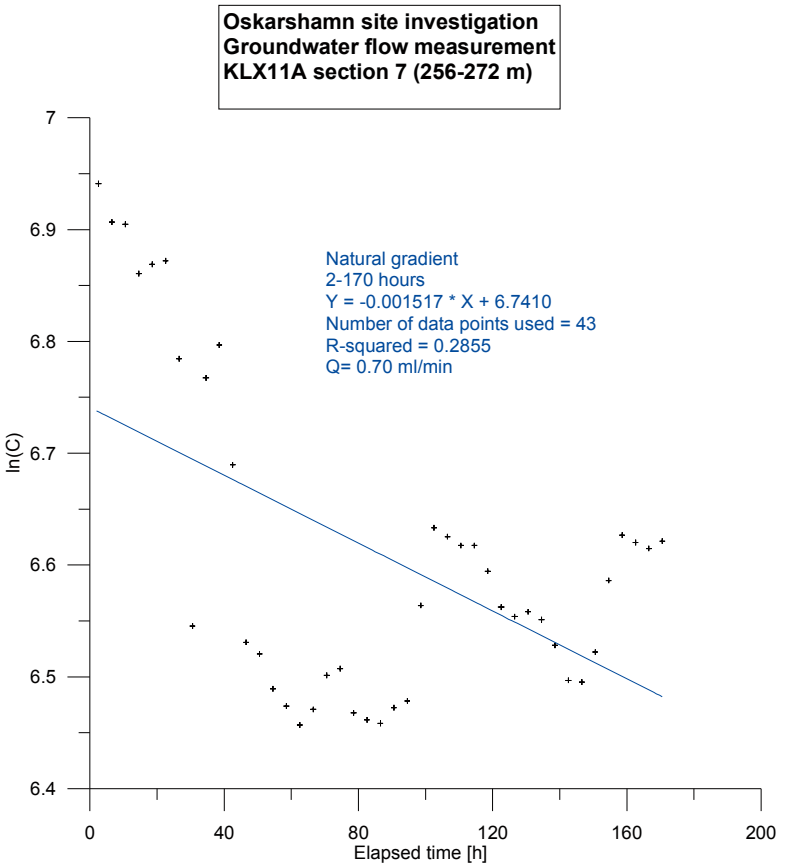
Oskarshamn site investigation
Groundwater flow measurement
KLX11A section 7 (256-272 m)
Natural gradient
2-170 hours
Y = -0.001517 * X + 6.7410
Number of data points used = 43
R-squared = 0.2855
Q= 0.70 ml/min
ln(C)
Elapsed time [h]
7
6.9
6.8
6.7
6.6
6.5
6.4
0
40
80
120
160
200

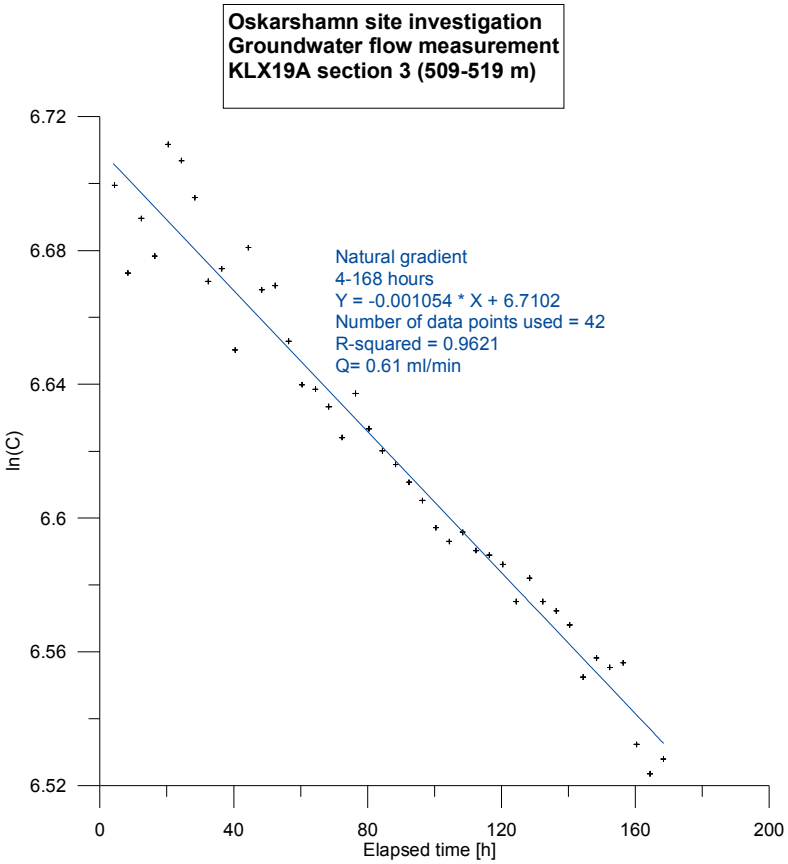
Oskarshamn site investigation
Groundwater flow measurement
KLX19A section 3 (509-519 m)
Natural gradient
4-168 hours
Y = -0.001054 * X + 6.7102
Number of data points used = 42
R-squared = 0.9621
Q= 0.61 ml/min
ln(C)
Elapsed time [h]
6.72
6.68
6.64
6.6
6.56
6.52
0
40
80
120
160
200

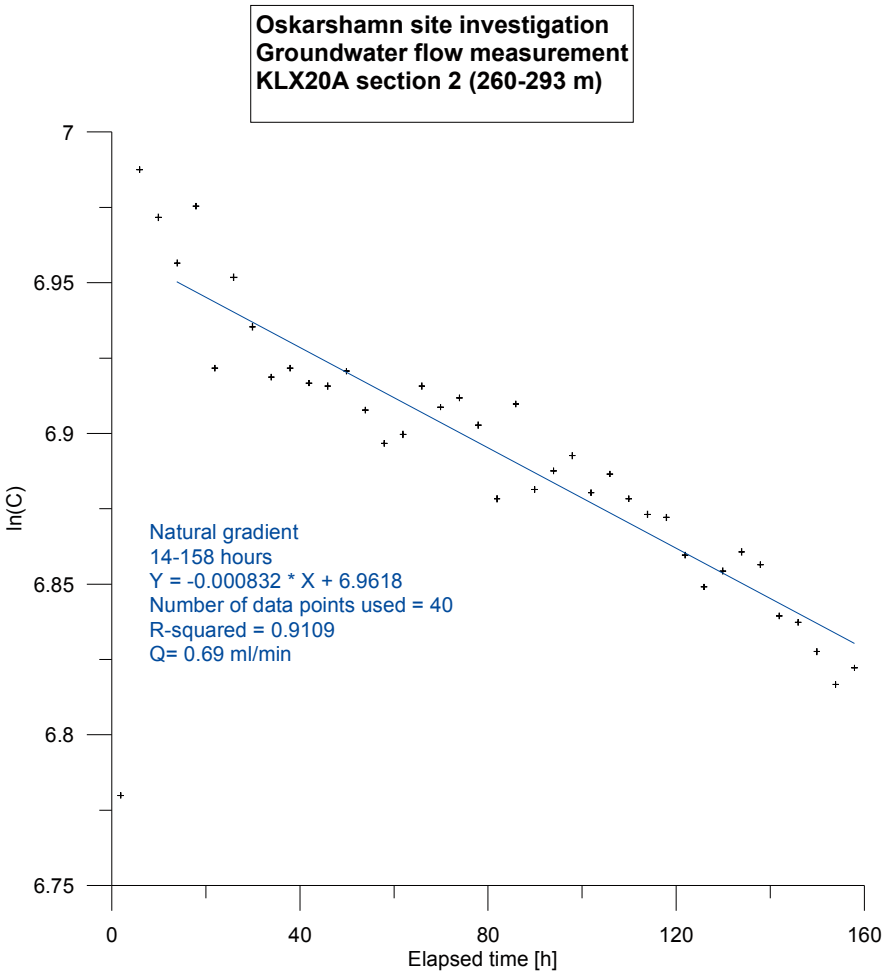
Oskarshamn site investigation
Groundwater flow measurement
KLX20A section 2 (260-293 m)
Natural gradient
14-158 hours
Y = -0.000832 * X + 6.9618
Number of data points used = 40
R-squared = 0.9109
Q= 0.69 ml/min
ln(C)
Elapsed time [h]
7
6.95
6.9
6.85
6.8
6.75
0
40
80
120
160

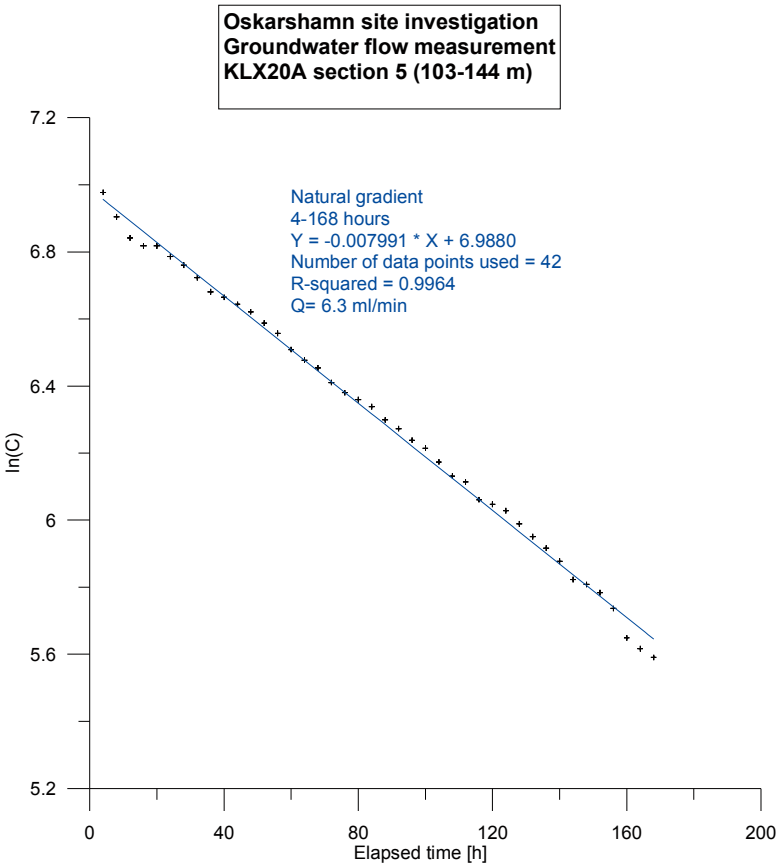
Oskarshamn site investigation
Groundwater flow measurement
KLX20A section 5 (103-144 m)
Natural gradient
4-168 hours
Y = -0.007991 * X + 6.9880
Number of data points used = 42
R-squared = 0.9964
Q= 6.3 ml/min
ln(C)
Elapsed time [h]
7.2
6.8
6.4
6
5.6
5.2
0
40
80
120
160
200

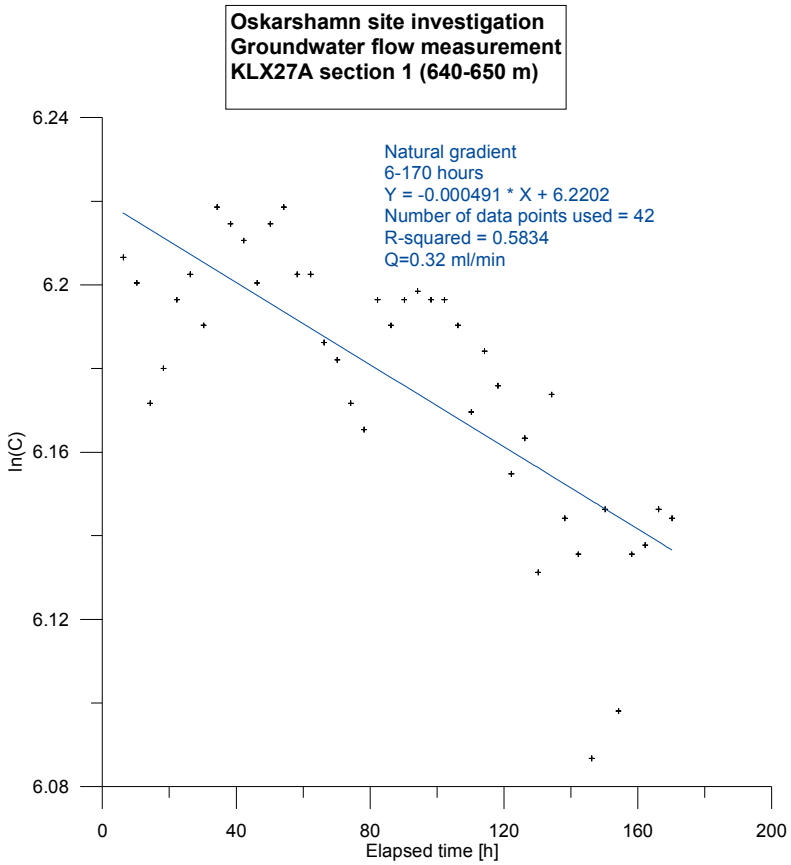
Oskarshamn site investigation
Groundwater flow measurement
KLX27A section 1 (640-650 m)
Natural gradient
6-170 hours
Y = -0.000491 * X + 6.2202
Number of data points used = 42
R-squared = 0.5834
Q=0.32 ml/min
ln(C)
Elapsed time [h]

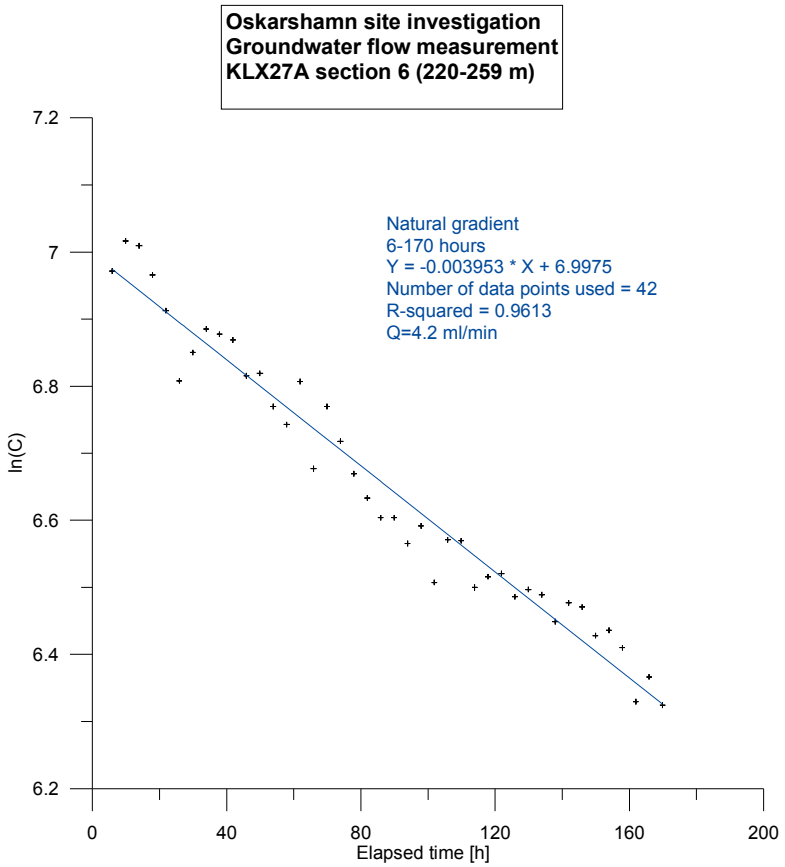
Oskarshamn site investigation
Groundwater flow measurement
KLX27A section 6 (220-259 m)
Natural gradient
6-170 hours
Y = -0.003953 * X + 6.9975
Number of data points used = 42
R-squared = 0.9613
Q=4.2 ml/min
ln(C)
Elapsed time [h]

Amino-G dilution graphs

Second campaign

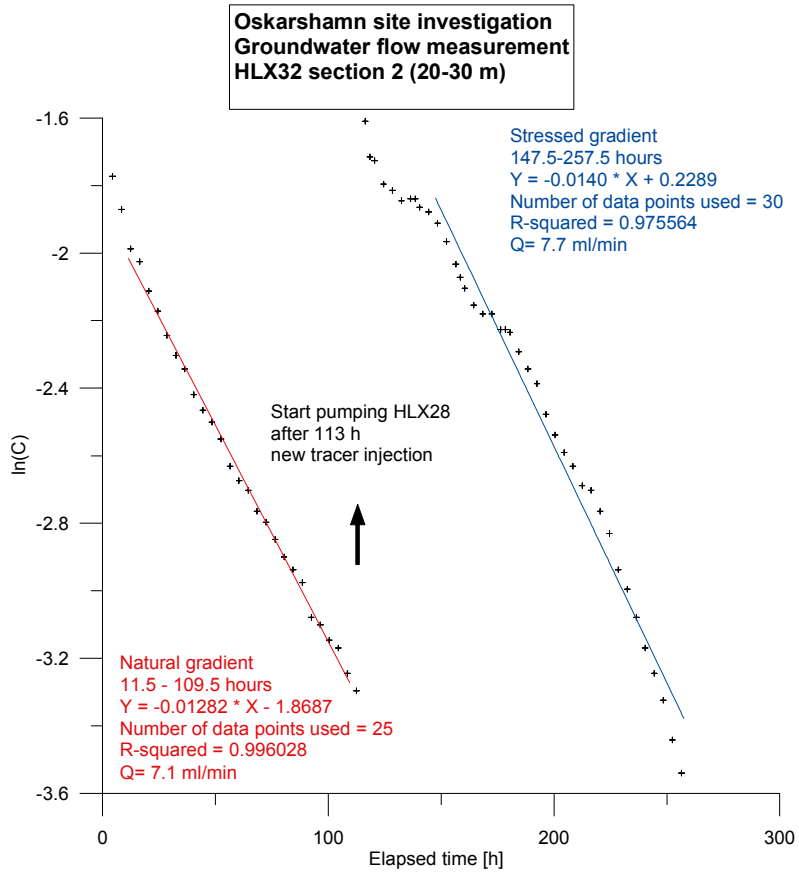

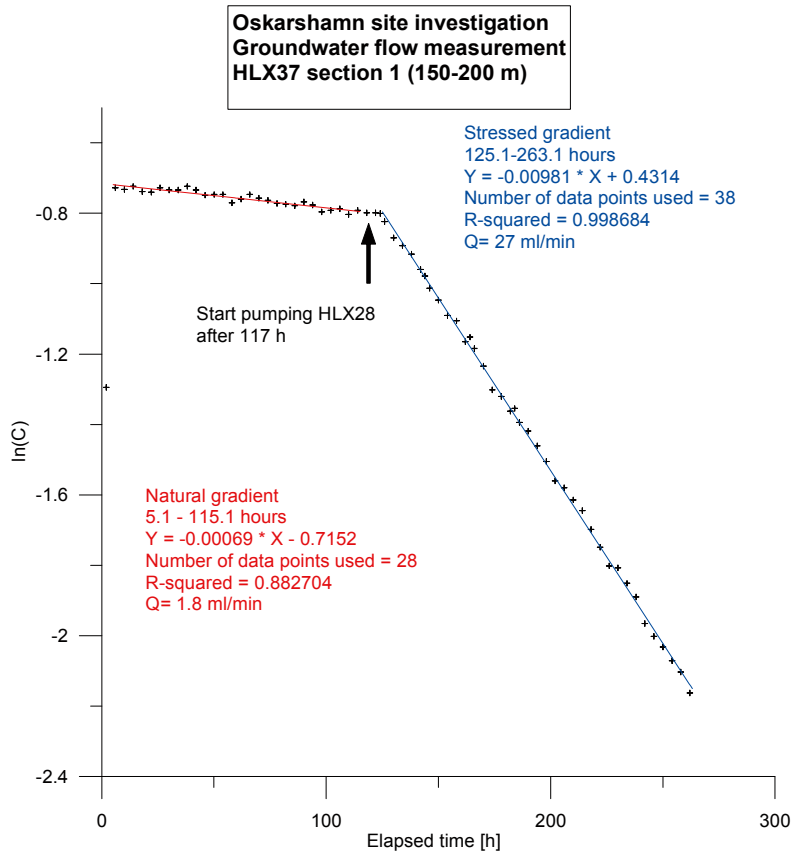

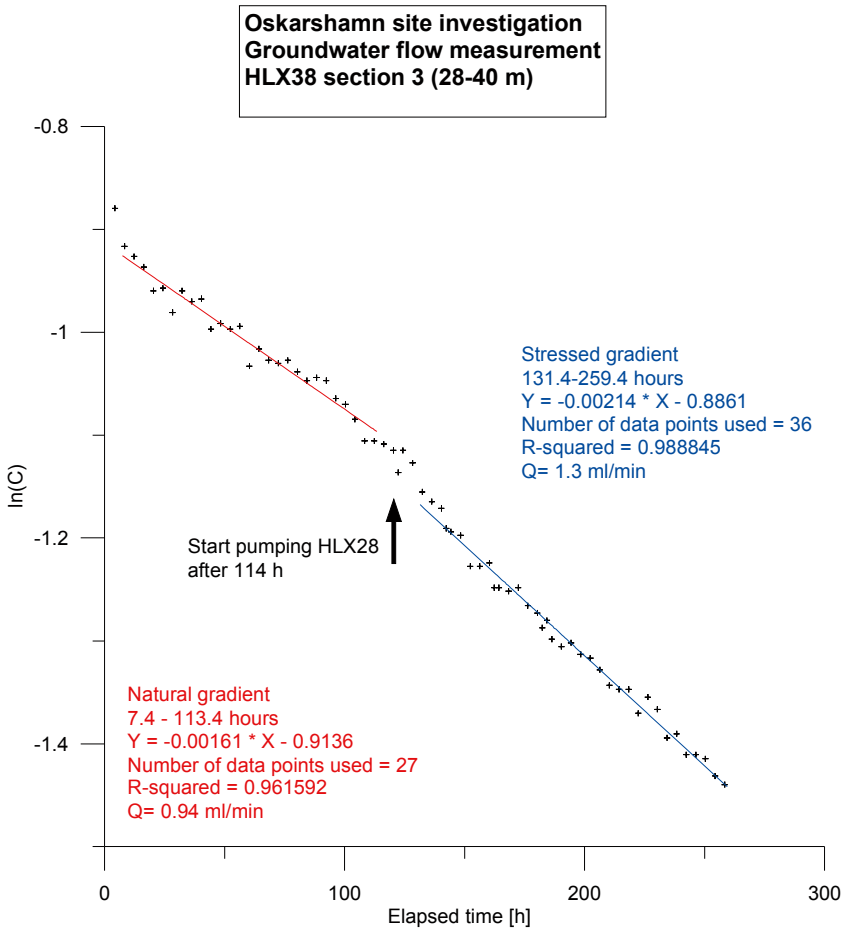
Oskarshamn site investigation
Groundwater flow measurement
HLX38 section 3 (28-40 m)
-0.8
-1
-1.2
-1.4
ln(C)
0
100
200
300
Elapsed time [h]
Stressed gradient
131.4-259.4 hours
Y = -0.00214 * X - 0.8861
Number of data points used = 36
R-squared = 0.988845
Q= 1.3 ml/min
Start pumping HLX28
after 114 h
Natural gradient
7.4 - 113.4 hours
Y = -0.00161 * X - 0.9136
Number of data points used = 27
R-squared = 0.961592
Q= 0.94 ml/min

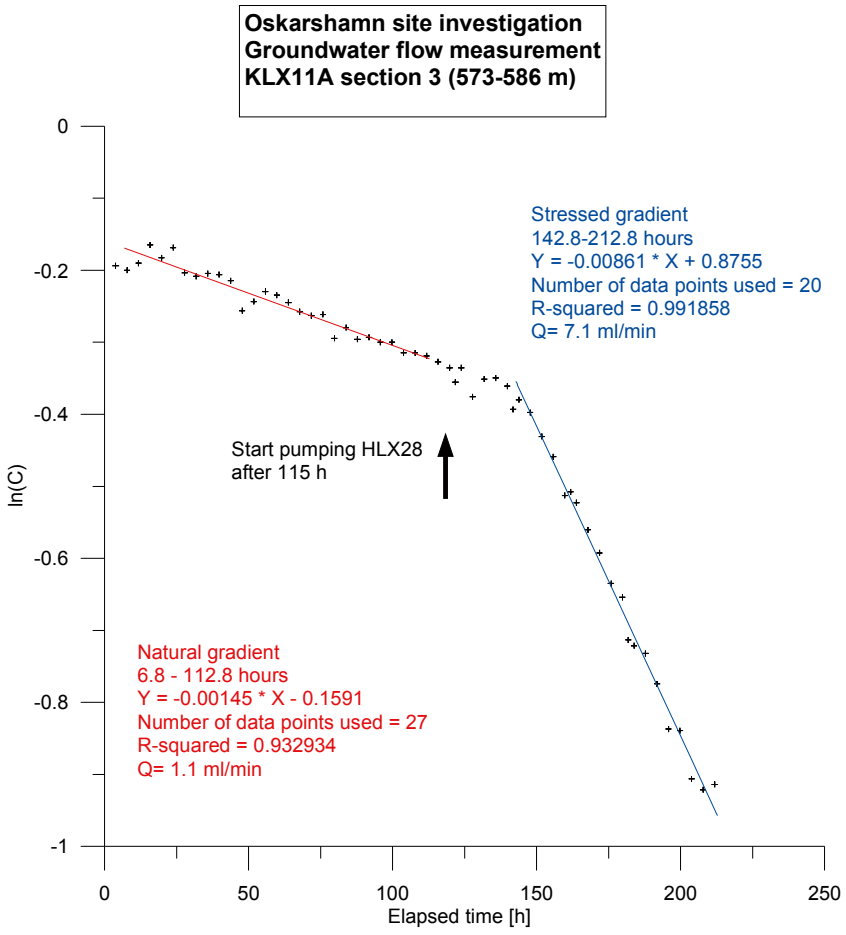
Oskarshamn site investigation
Groundwater flow measurement
KLX11A section 3 (573-586 m)
0
-0.2
-0.4
-0.6
-0.8
-1
ln(C)
0
50
100
150
200
250
Elapsed time [h]
Stressed gradient
142.8-212.8 hours
Y = -0.00861 * X + 0.8755
Number of data points used = 20
R-squared = 0.991858
Q= 7.1 ml/min
Start pumping HLX28
after 115 h
Natural gradient
6.8 - 112.8 hours
Y = -0.00145 * X - 0.1591
Number of data points used = 27
R-squared = 0.932934
Q= 1.1 ml/min

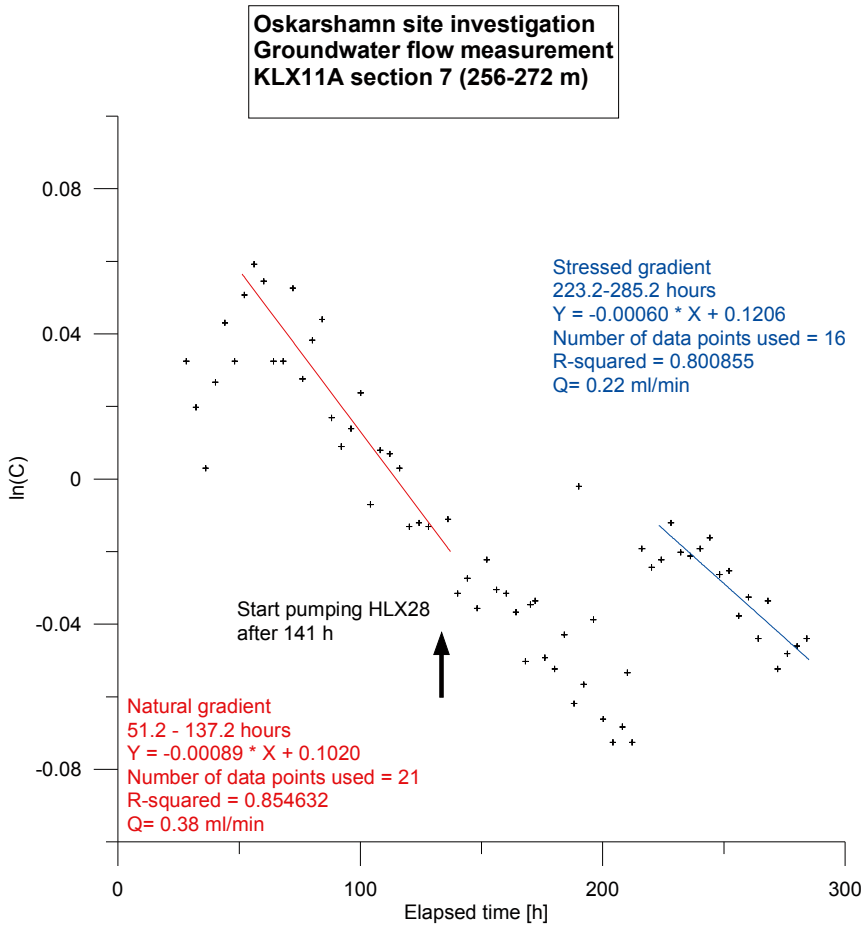
Oskarshamn site investigation
Groundwater flow measurement
KLX11A section 7 (256-272 m)
0.08
0.04
0
-0.04
-0.08
ln(C)
Stressed gradient
223.2-285.2 hours
Y = -0.00060 * X + 0.1206
Number of data points used = 16
R-squared = 0.800855
Q= 0.22 ml/min
Start pumping HLX28
after 141 h
Natural gradient
51.2 - 137.2 hours
Y = -0.00089 * X + 0.1020
Number of data points used = 21
R-squared = 0.854632
Q= 0.38 ml/min
0
100
200
300
Elapsed time [h]

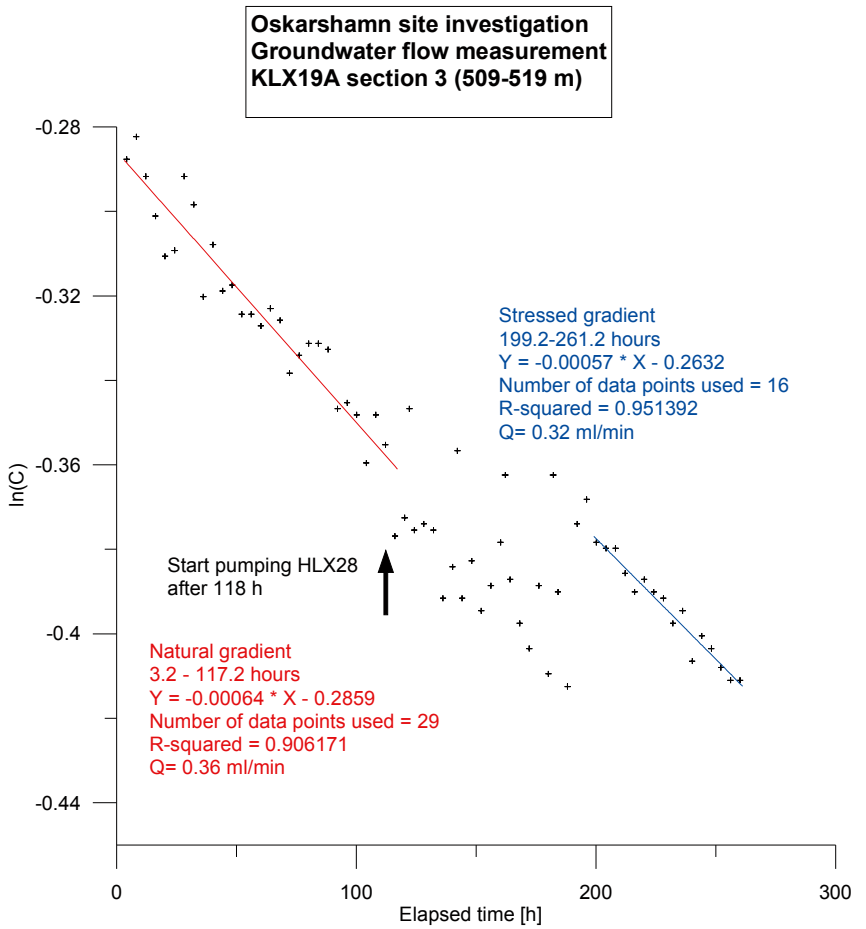
Oskarshamn site investigation
Groundwater flow measurement
KLX19A section 3 (509-519 m)
-0.28
-0.32
-0.36
-0.4
-0.44
ln(C)
Stressed gradient
199.2-261.2 hours
Y = -0.00057 * X - 0.2632
Number of data points used = 16
R-squared = 0.951392
Q= 0.32 ml/min
Start pumping HLX28
after 118 h
Natural gradient
3.2 - 117.2 hours
Y = -0.00064 * X - 0.2859
Number of data points used = 29
R-squared = 0.906171
Q= 0.36 ml/min
0
100
200
300
Elapsed time [h]

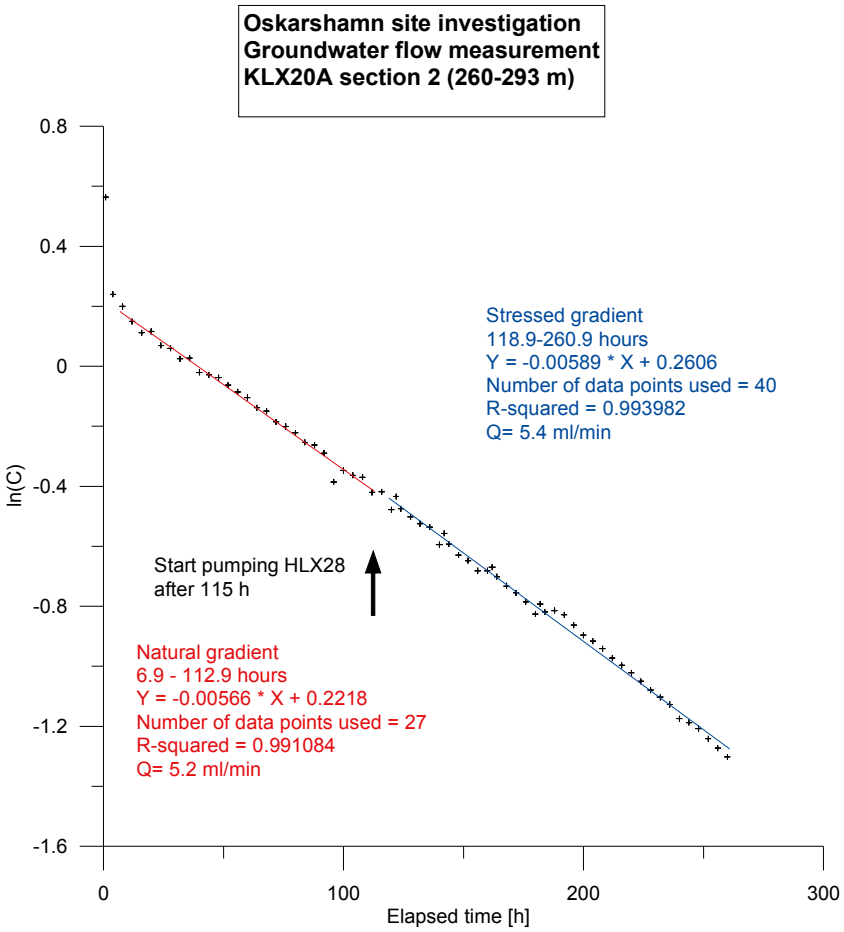
Oskarshamn site investigation
Groundwater flow measurement
KLX20A section 2 (260-293 m)
Stressed gradient
118.9-260.9 hours
Y = -0.00589 * X + 0.2606
Number of data points used = 40
R-squared = 0.993982
Q= 5.4 ml/min
Start pumping HLX28
after 115 h
Natural gradient
6.9 - 112.9 hours
Y = -0.00566 * X + 0.2218
Number of data points used = 27
R-squared = 0.991084
Q= 5.2 ml/min
ln(C)
Elapsed time [h]

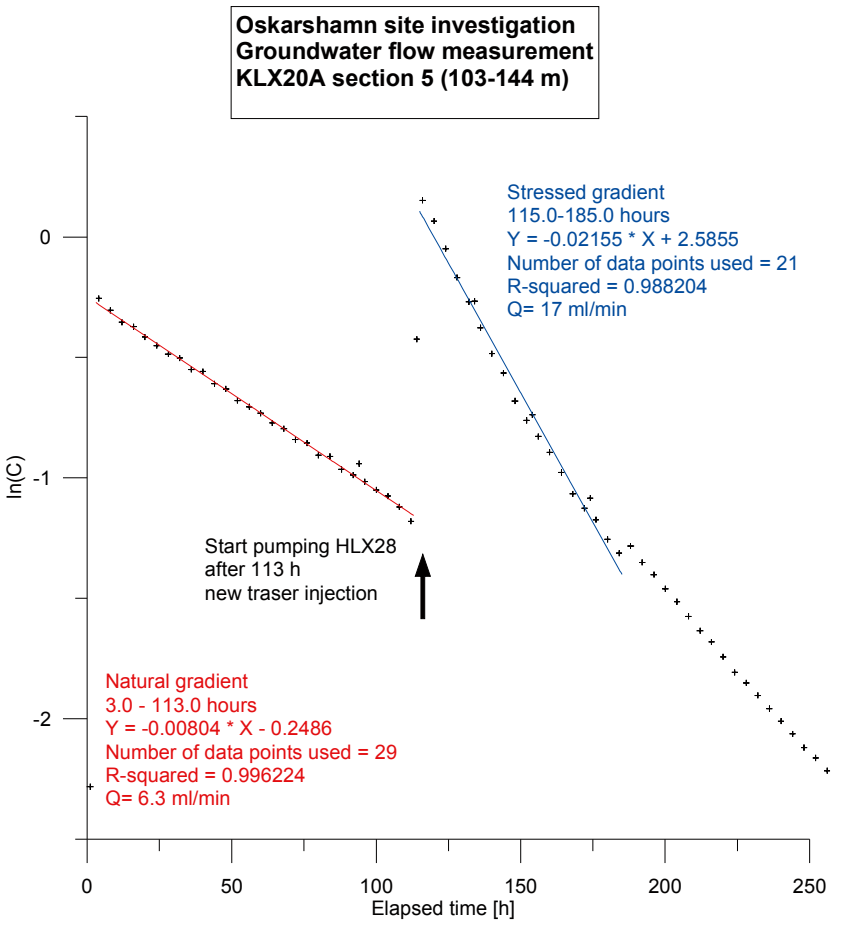
Oskarshamn site investigation
Groundwater flow measurement
KLX20A section 5 (103-144 m)
Stressed gradient
115.0-185.0 hours
Y = -0.02155 * X + 2.5855
Number of data points used = 21
R-squared = 0.988204
Q= 17 ml/min
Start pumping HLX28
after 113 h
new traser injection
Natural gradient
3.0 - 113.0 hours
Y = -0.00804 * X - 0.2486
Number of data points used = 29
R-squared = 0.996224
Q= 6.3 ml/min
ln(C)
Elapsed time [h]

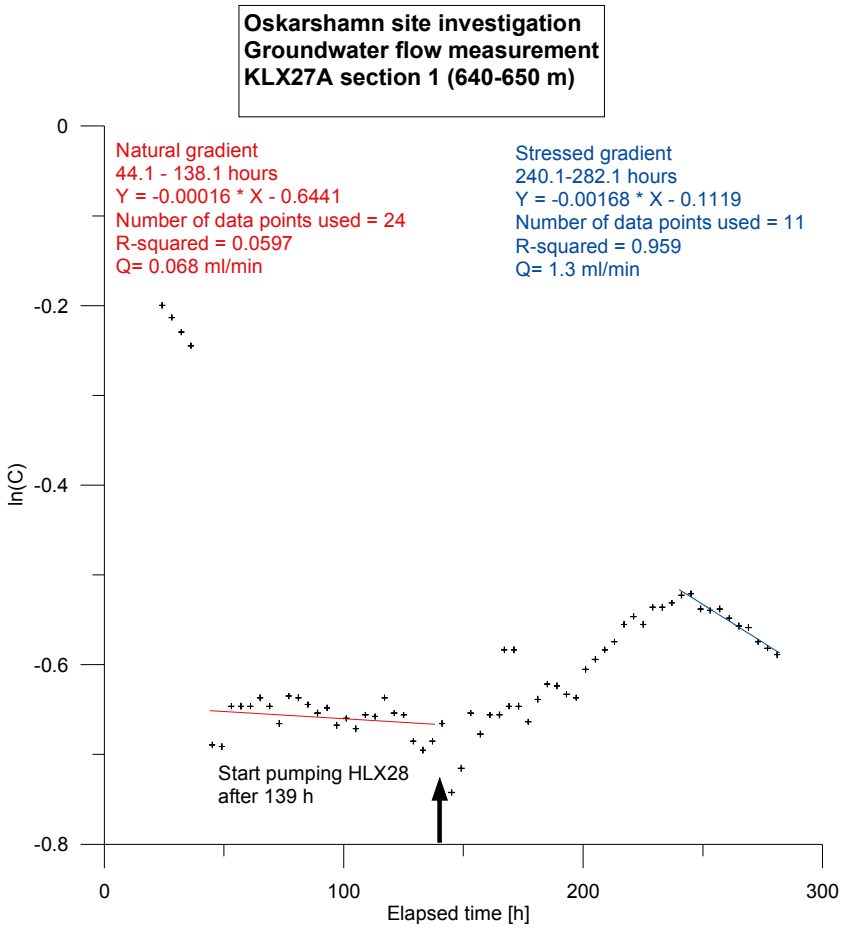
Oskarshamn site investigation
Groundwater flow measurement
KLX27A section 1 (640-650 m)
Natural gradient
44.1 - 138.1 hours
Y = -0.00016 * X - 0.6441
Number of data points used = 24
R-squared = 0.0597
Q= 0.068 ml/min
Stressed gradient
240.1-282.1 hours
Y = -0.00168 * X - 0.1119
Number of data points used = 11
R-squared = 0.959
Q= 1.3 ml/min
Start pumping HLX28
after 139 h
ln(C)
Elapsed time [h]

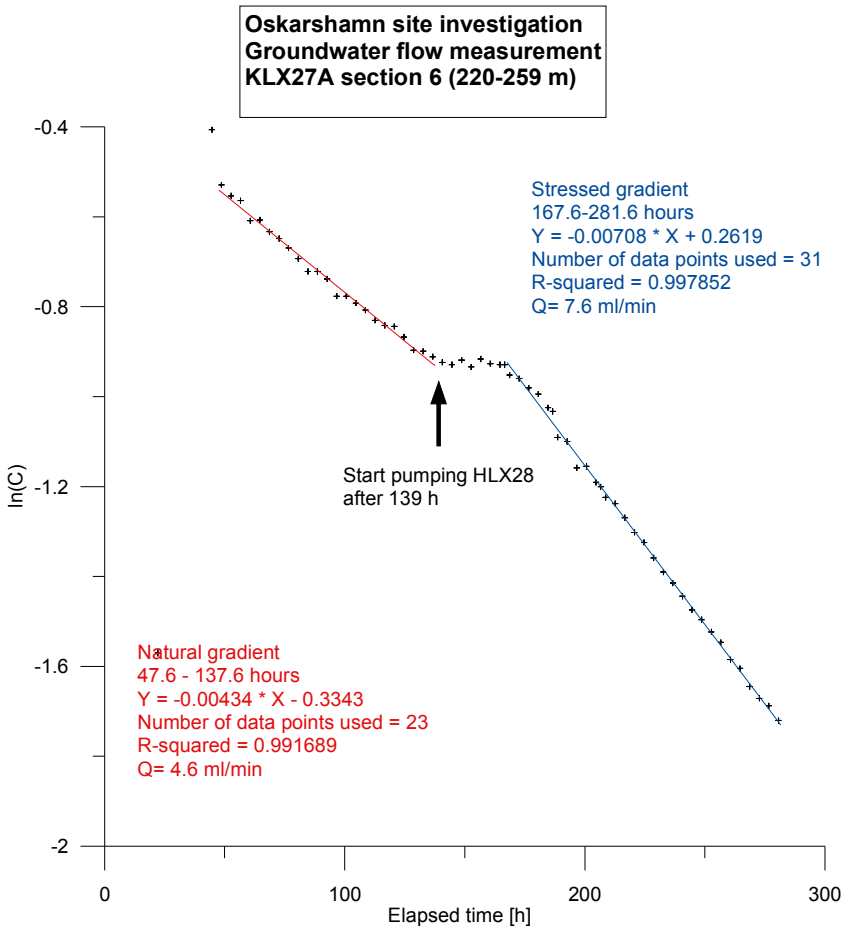
Oskarshamn site investigation
Groundwater flow measurement
KLX27A section 6 (220-259 m)
Stressed gradient
167.6-281.6 hours
Y = -0.00708 * X + 0.2619
Number of data points used = 31
R-squared = 0.997852
Q= 7.6 ml/min
Start pumping HLX28
after 139 h
Natural gradient
47.6 - 137.6 hours
Y = -0.00434 * X - 0.3343
Number of data points used = 23
R-squared = 0.991689
Q= 4.6 ml/min
ln(C)
Elapsed time [h]

Dilution graphs from the tracer test

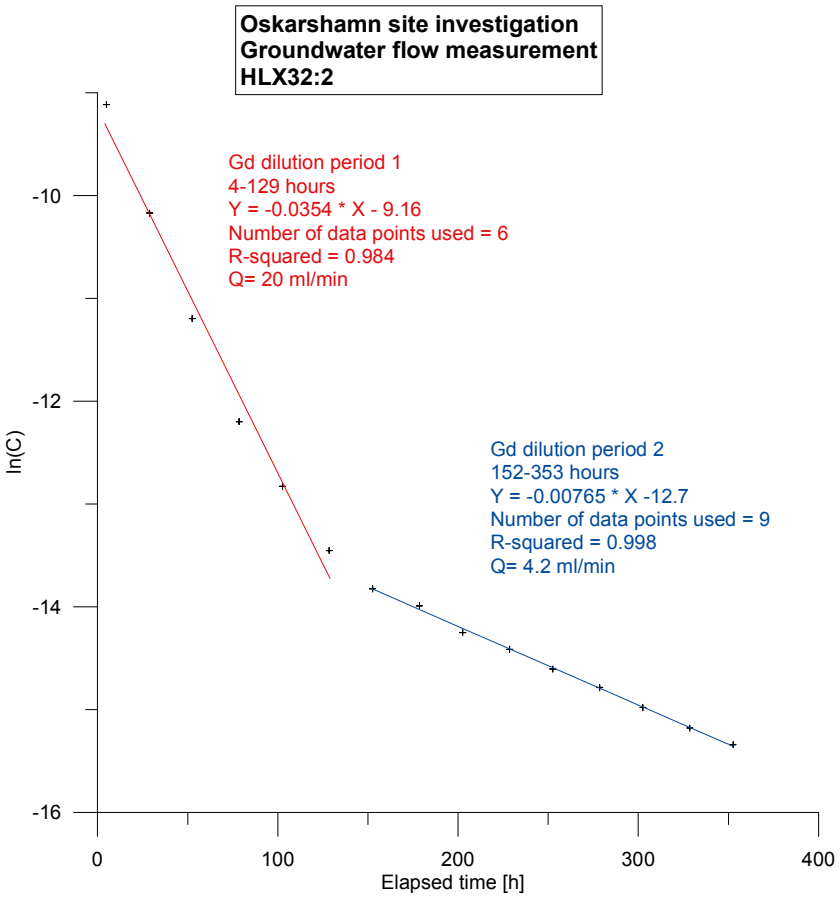

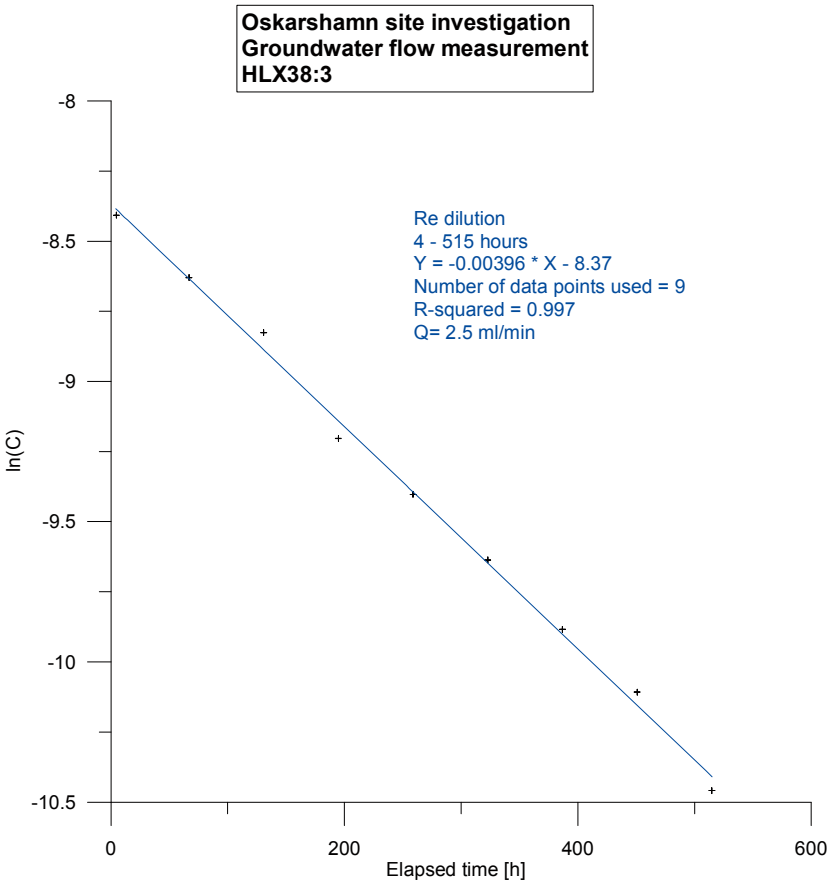

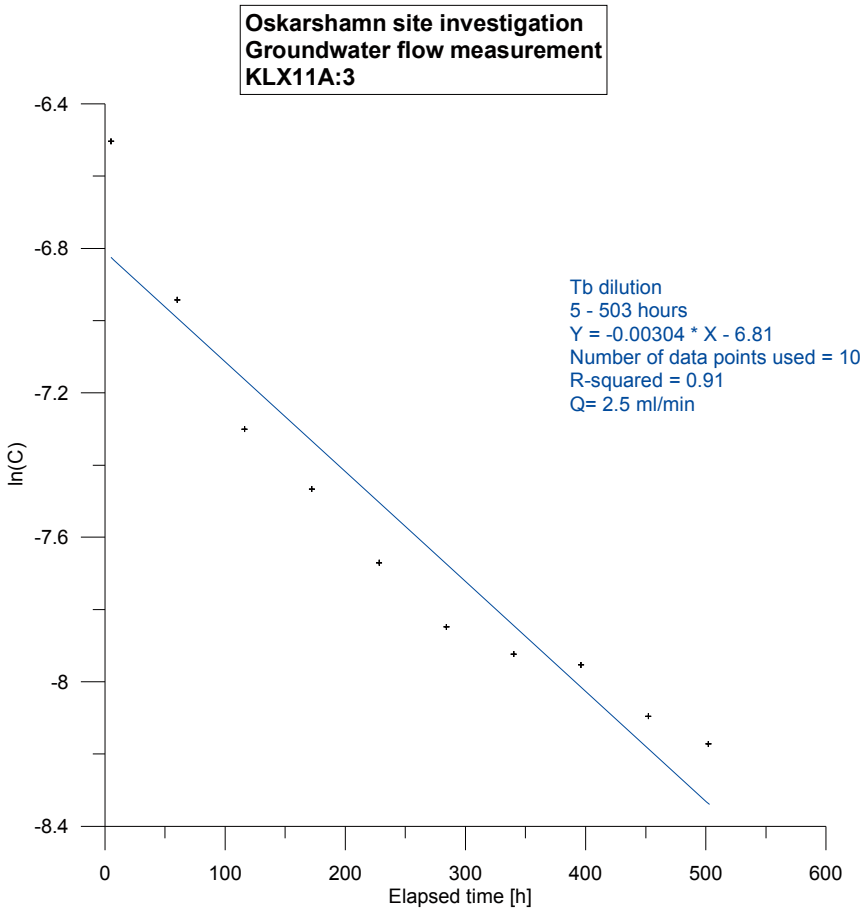
Oskarshamn site investigation
Groundwater flow measurement
KLX11A:3
Tb dilution
5 - 503 hours
Y = -0.00304 * X - 6.81
Number of data points used = 10
R-squared = 0.91
Q= 2.5 ml/min
ln(C)
Elapsed time [h]

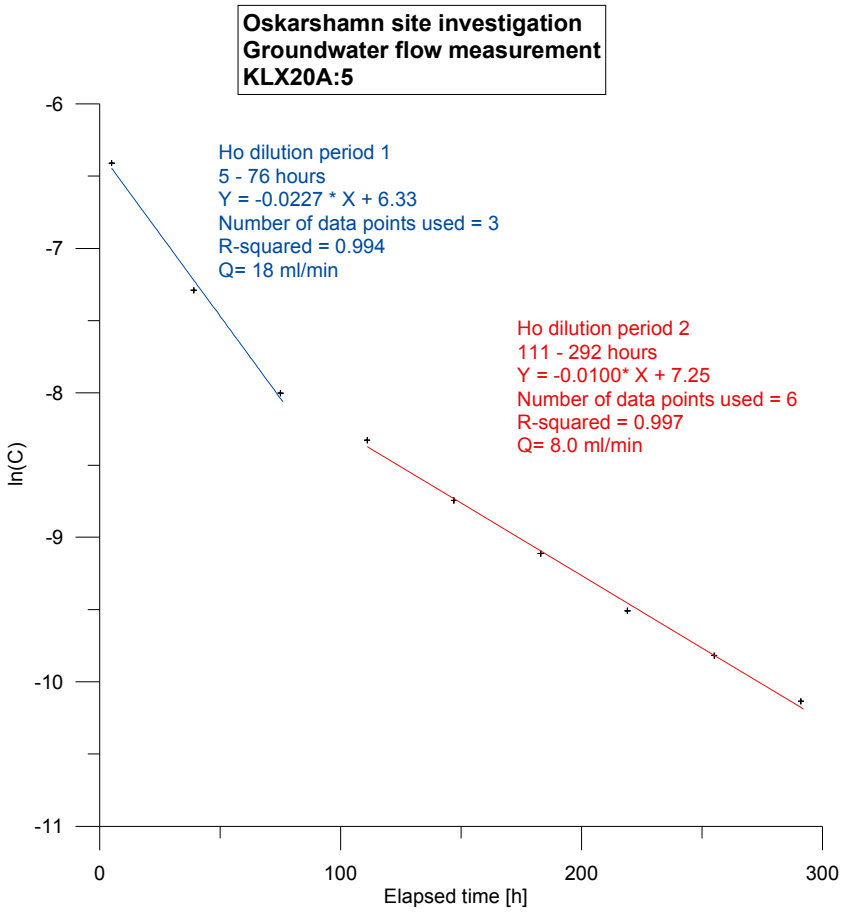
Oskarshamn site investigation
Groundwater flow measurement
KLX20A:5
Ho dilution period 1
5 - 76 hours
Y = -0.0227 * X + 6.33
Number of data points used = 3
R-squared = 0.994
Q= 18 ml/min
Ho dilution period 2
111 - 292 hours
Y = -0.0100* X + 7.25
Number of data points used = 6
R-squared = 0.997
Q= 8.0 ml/min
ln(C)
Elapsed time [h]

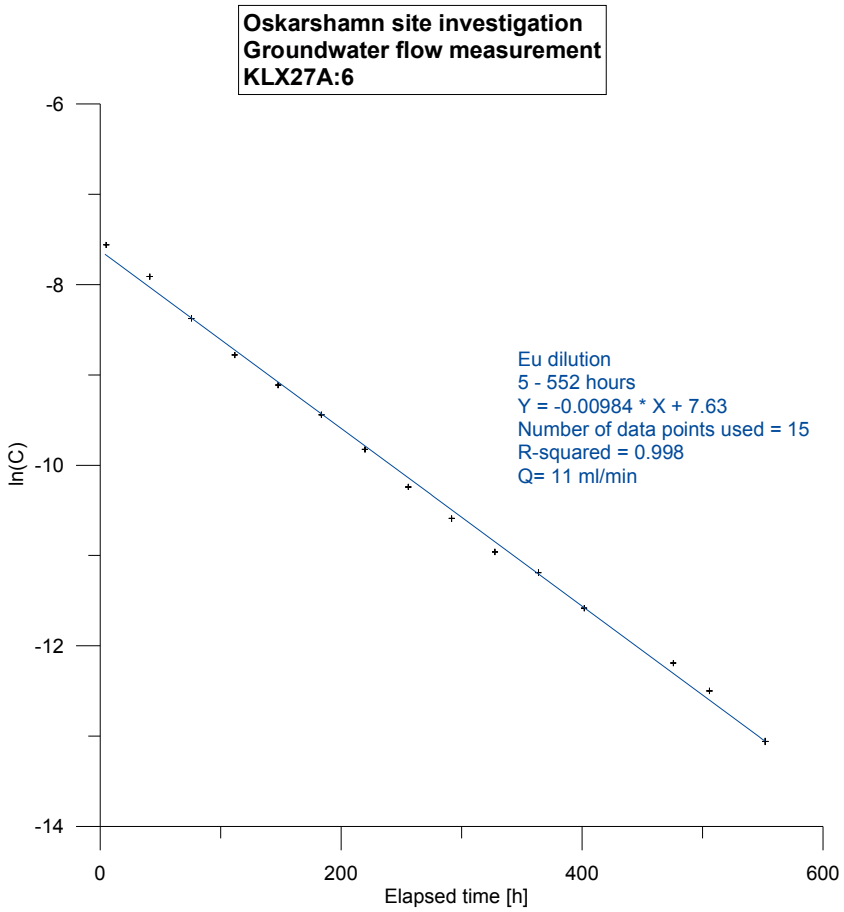
Oskarshamn site investigation
Groundwater flow measurement
KLX27A:6
-6
-8
-10
-12
-14
ln(C)
0
200
400
600
Elapsed time [h]
Eu dilution
5 - 552 hours
Y = -0.00984 * X + 7.63
Number of data points used = 15
R-squared = 0.998
Q= 11 ml/min

Appendix 6

Test diagrams

Nomenclature:

T = Transmissivity (m^2/s).

S = Storativity (-).

K_Z/K_r = Ratio of hydraulic conductivities in the vertical and radial direction (set to 1).

Sw = Skin factor.

r(w) = Borehole radius (m).

r(c) = Effective casing radius (m).

r/B = Leakage coefficient (s^{-1}).

b = Thickness of formation (m).

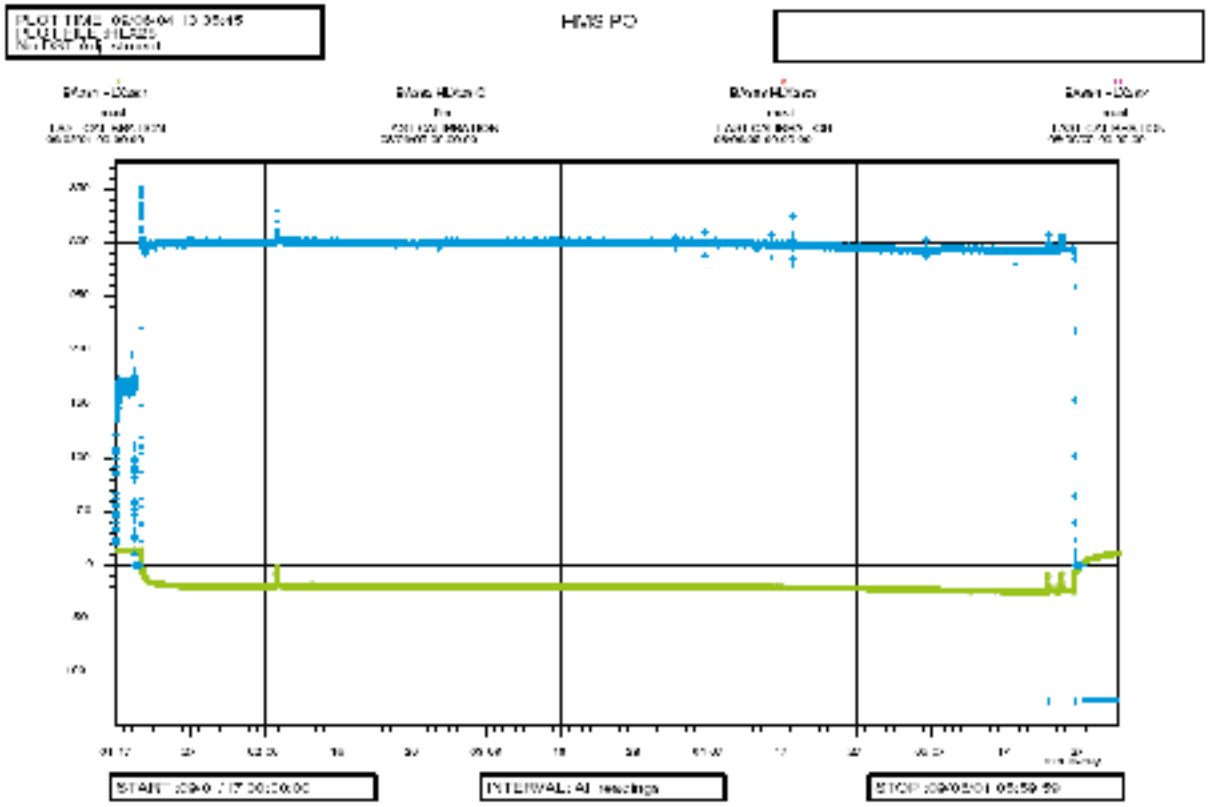

Figure A6-1. Linear plot of measured pressure (+) and flow rate (o) versus time in the pumping borehole HLX28, 6.00–154.20 m during the interference test in HLX28.

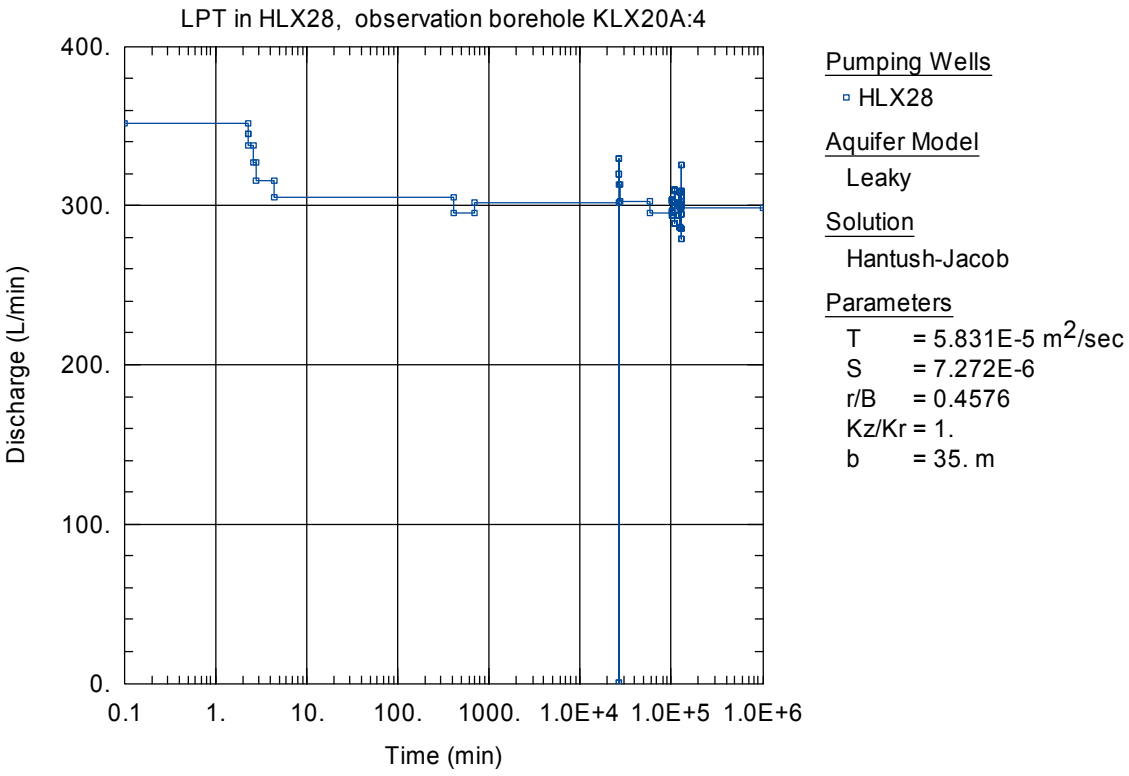

Figure A6-2. Lin-log plot of flow rate (▫) versus time in the pumping borehole HLX28 during the interference test in HLX28.

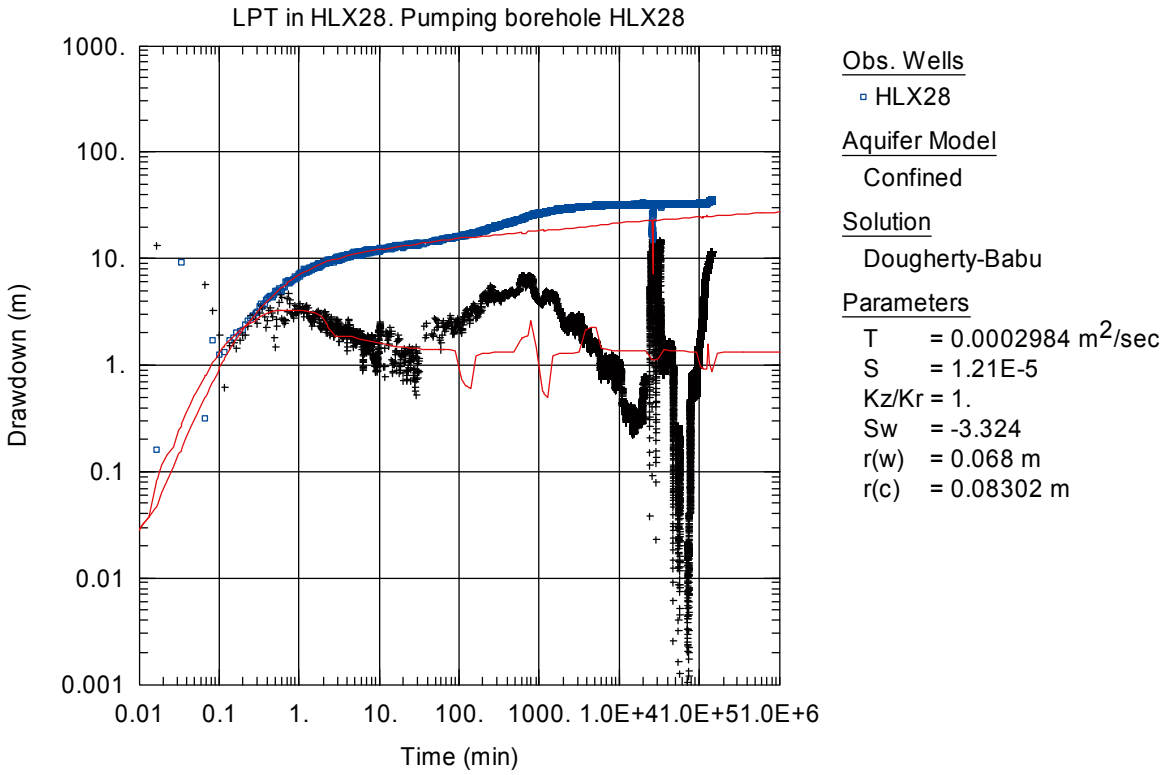

Figure A6-3. *Log-log plot of drawdown (▫) and drawdown derivative, ds/d(ln t) (+), versus time in the pumping borehole HLX28 during the interference test in HLX28. Transient evaluation is based on the early part of the flow period.*

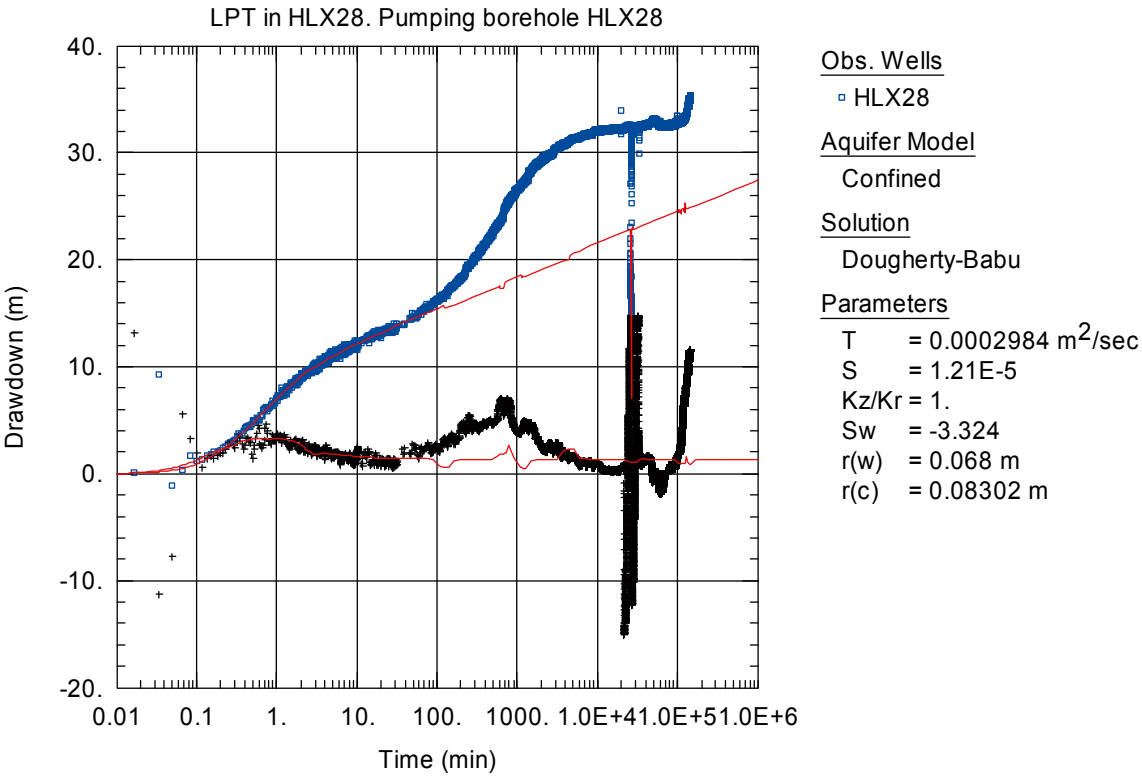

Figure A6-4. *Lin-log plot of drawdown (▫) and drawdown derivative, ds/d(ln t) (+), versus time in the pumping borehole HLX28 during the interference test in HLX28. Transient evaluation is based on the early part of the flow period.*

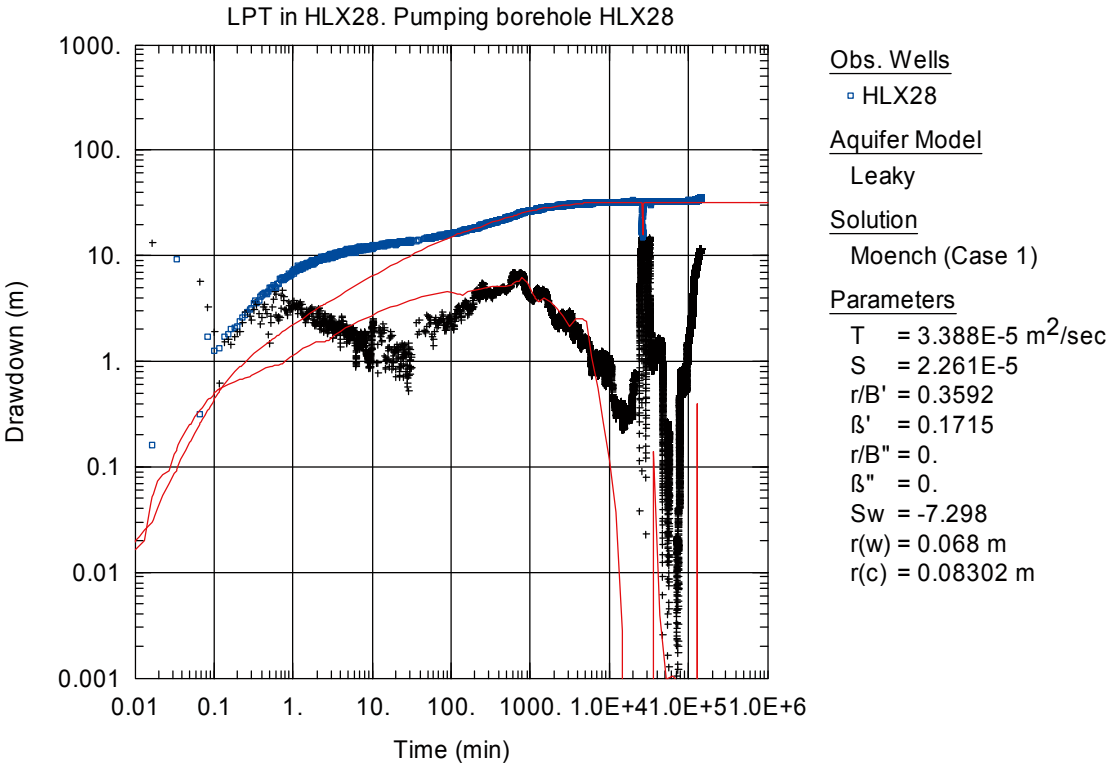

Figure A6-5. *Log-log plot of drawdown (▫) and drawdown derivative, ds/d(ln t) (+), versus time in HLX28 during the interference test in HLX28. Transient evaluation is based on the intermediate part of the flow period.*

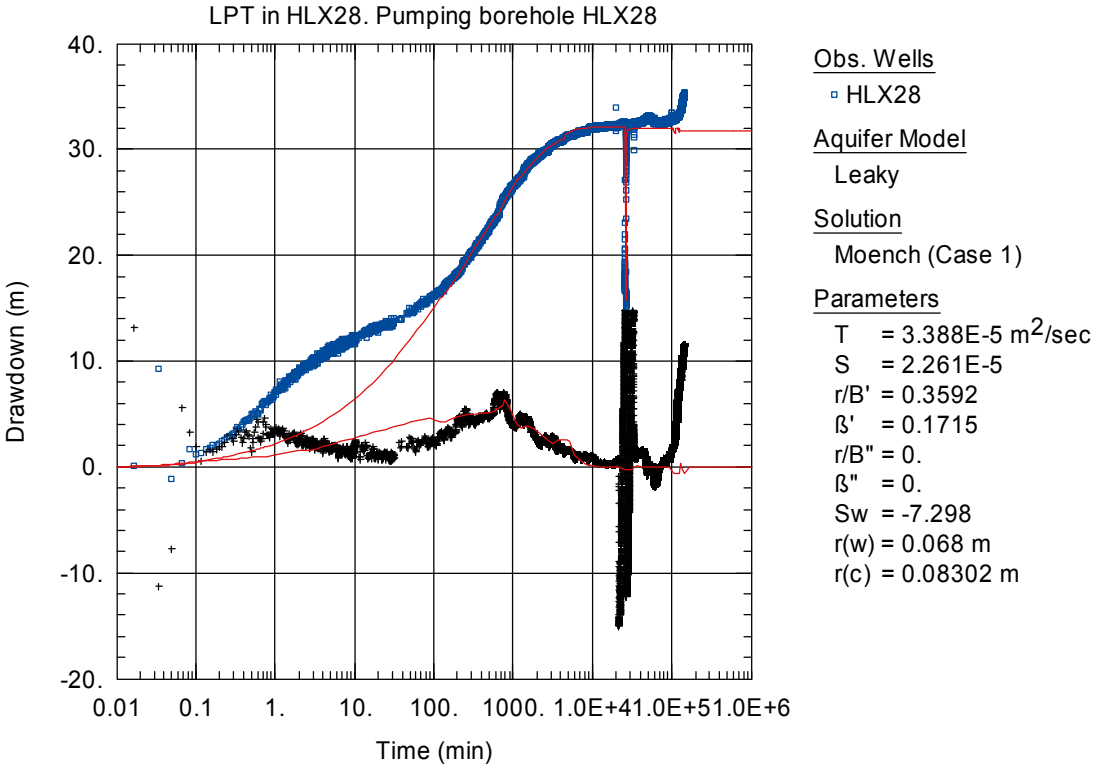

Figure A6-6. *Lin-log plot of drawdown (▫) and drawdown derivative, ds/d(ln t) (+), versus time in HLX28 during the interference test in HLX28. Transient evaluation is based on the intermediate part of the flow period.*

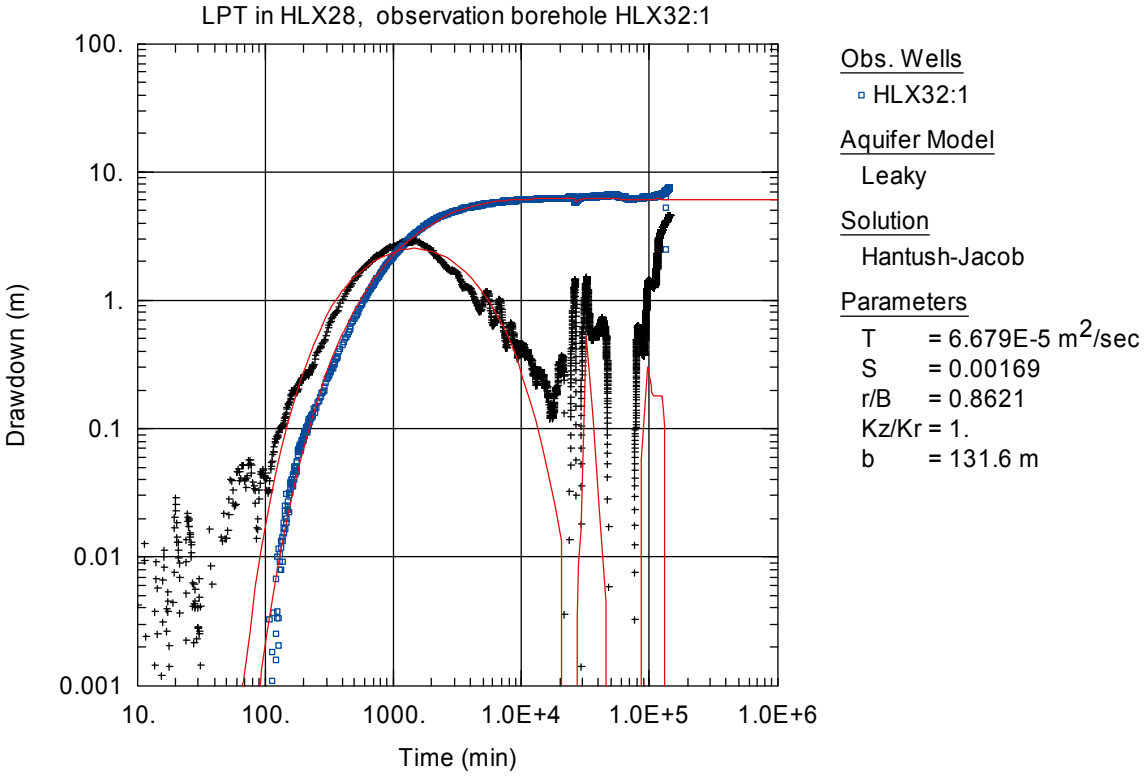

Figure A6-7. *Log-log plot of drawdown (▫) and drawdown derivative, ds/d(ln t) (+), versus time in HLX32:1 during the interference test in HLX28. Transient evaluation is based on the first part of the drawdown period.*

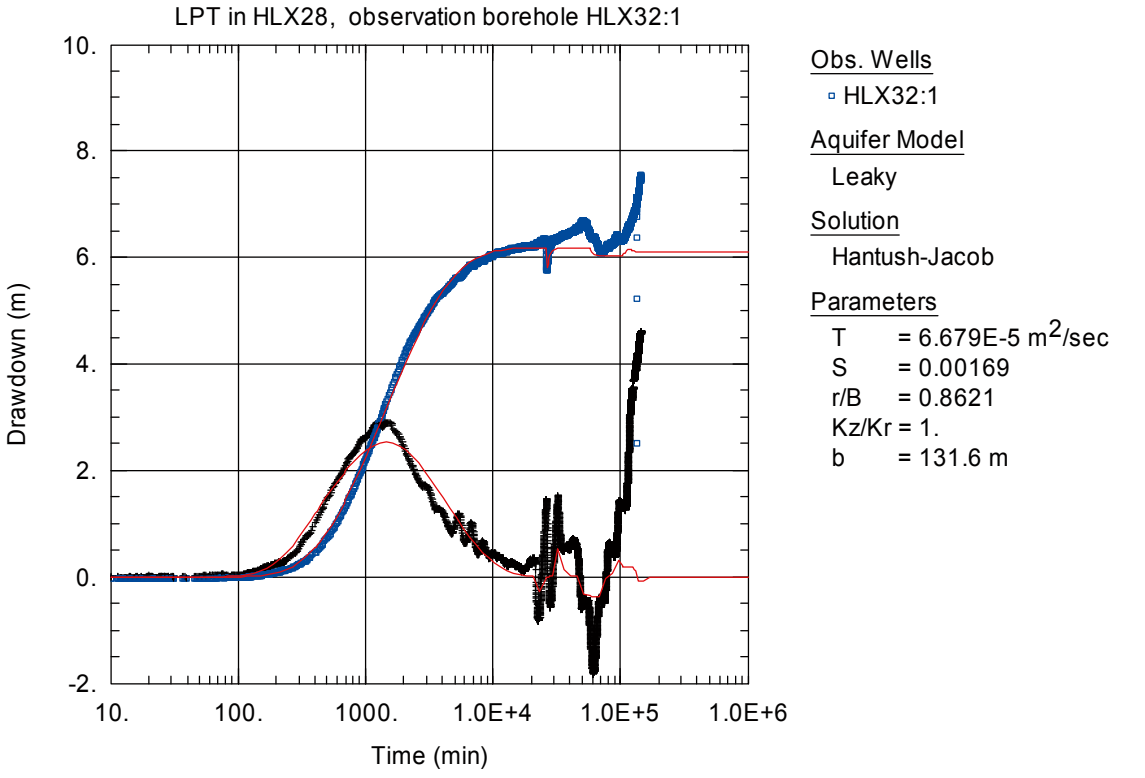

Figure A6-8. *Lin-log plot of drawdown (▫) and drawdown derivative, ds/d(ln t) (+), versus time in HLX32:1 during the interference test in HLX28. Transient evaluation is based on the first part of the drawdown period.*

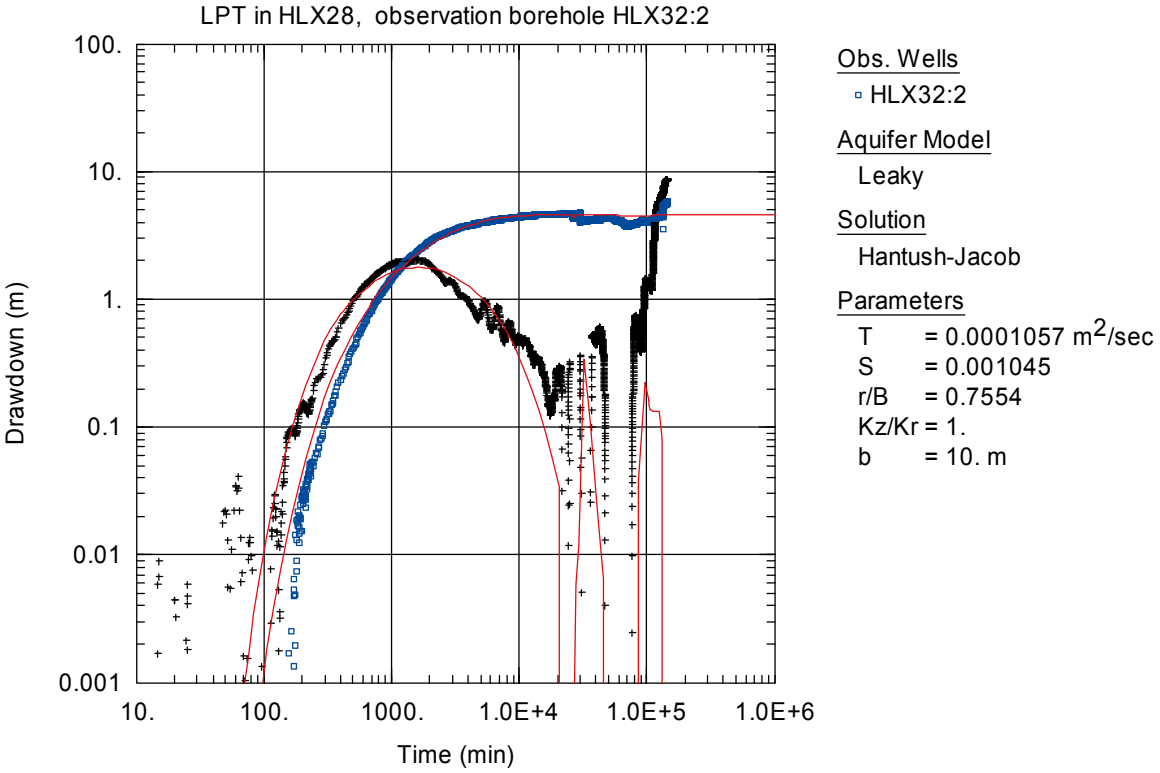

Figure A6-9. *Log-log plot of drawdown (▫) and drawdown derivative, ds/d(ln t) (+), versus time in HLX32:2 during the interference test in HLX28. Transient evaluation is based on the first part of the drawdown period. The section was used for tracer injection.*

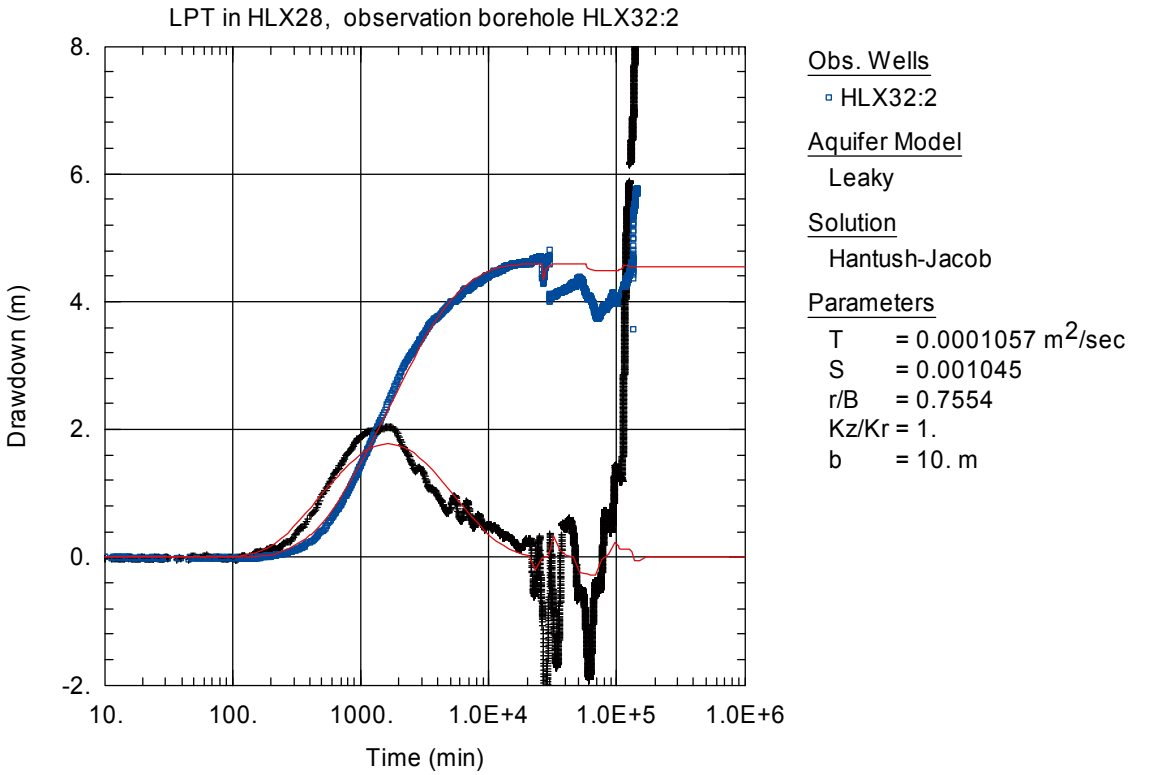

Figure A6-10. *Lin-log plot of drawdown (▫) and drawdown derivative, ds/d(ln t) (+), versus time in HLX32:2 during the interference test in HLX28. Transient evaluation is based on the first part of the drawdown period. The section was used for tracer injection.*

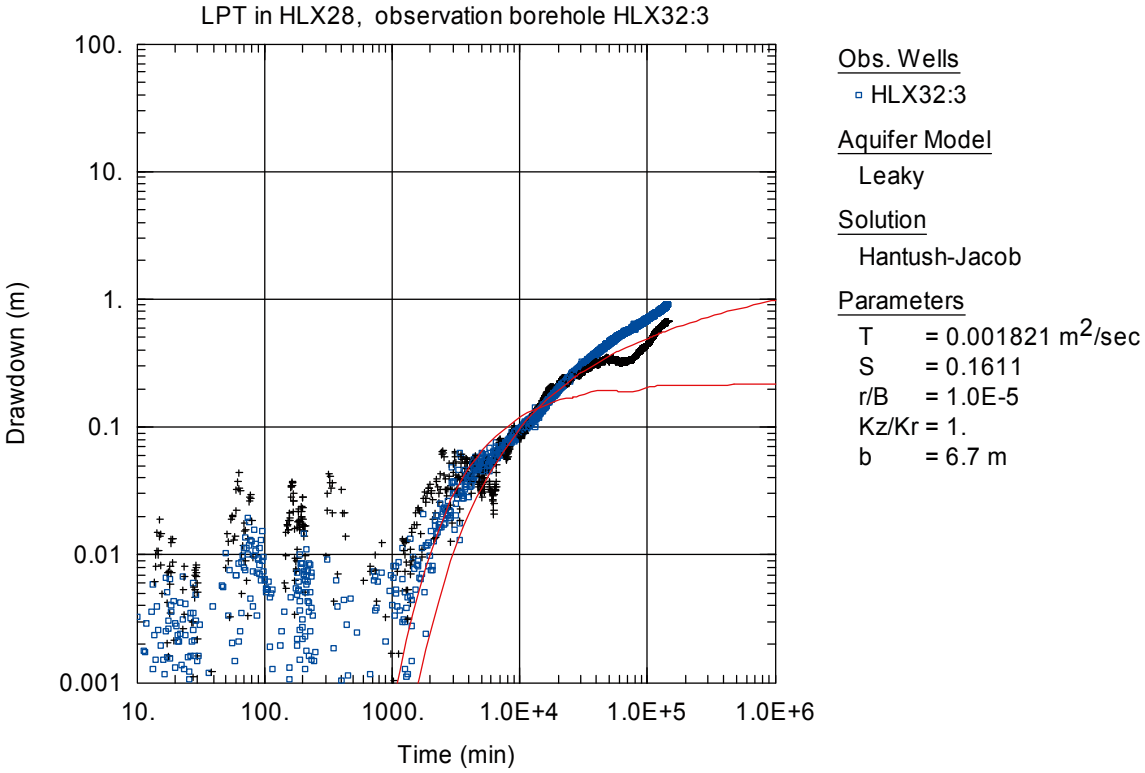

Figure A6-11. *Log-log plot of drawdown (▫) and drawdown derivative, ds/d(ln t) (+), versus time in HLX32:3 during the interference test in HLX28. Transient evaluation is based on the first part of the drawdown period.*

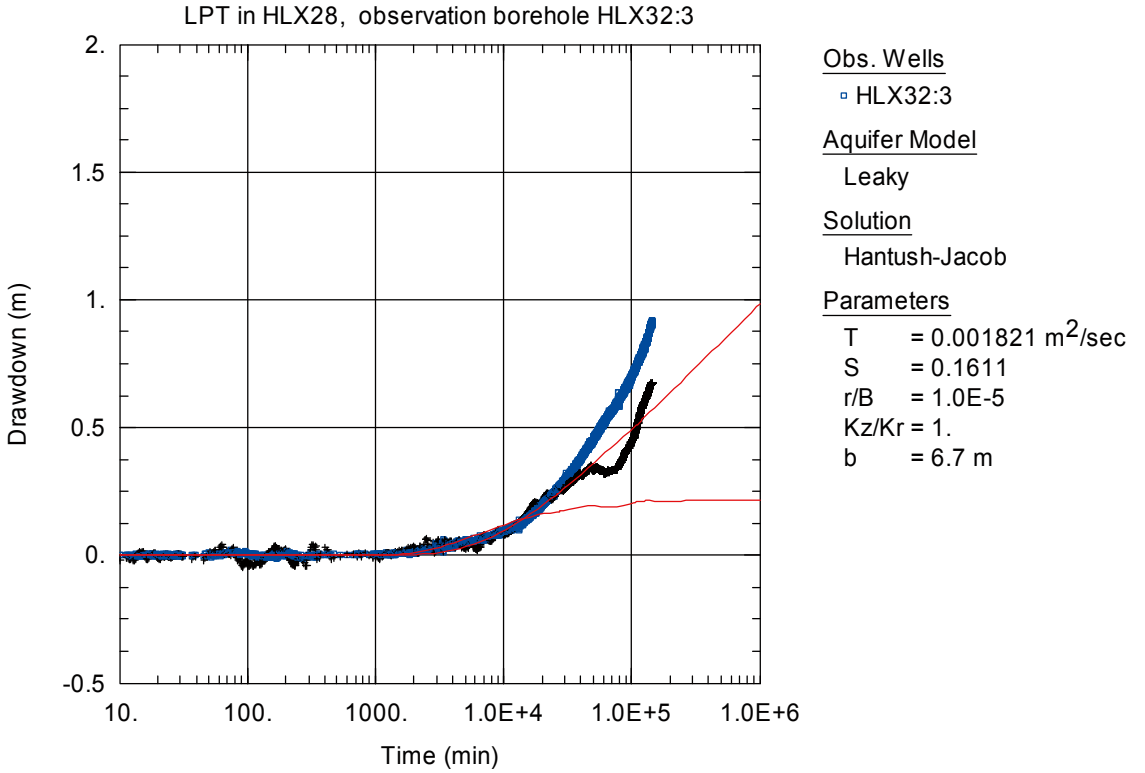

Figure A6-12. *Lin-log plot of drawdown (▫) and drawdown derivative, ds/d(ln t) (+), versus time in HLX32:3 during the interference test in HLX28. Transient evaluation is based on the first part of the drawdown period.*

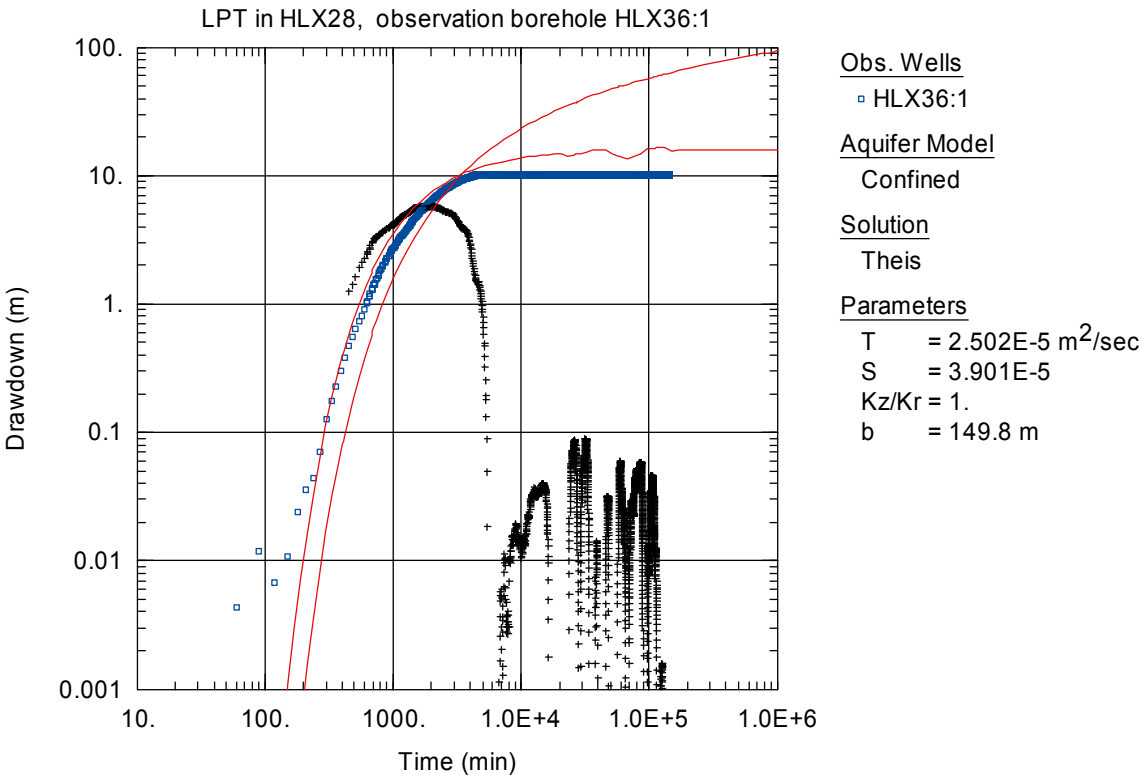

Figure A6-13. *Log-log plot of drawdown (▫) and drawdown derivative, ds/d(ln t) (+), versus time in HLX36:1 during the interference test in HLX28. No unambiguous transient evaluation can be made for this section since the groundwater level is below the pressure sensor by the end of the flow period. The presented evaluation is only an example.*

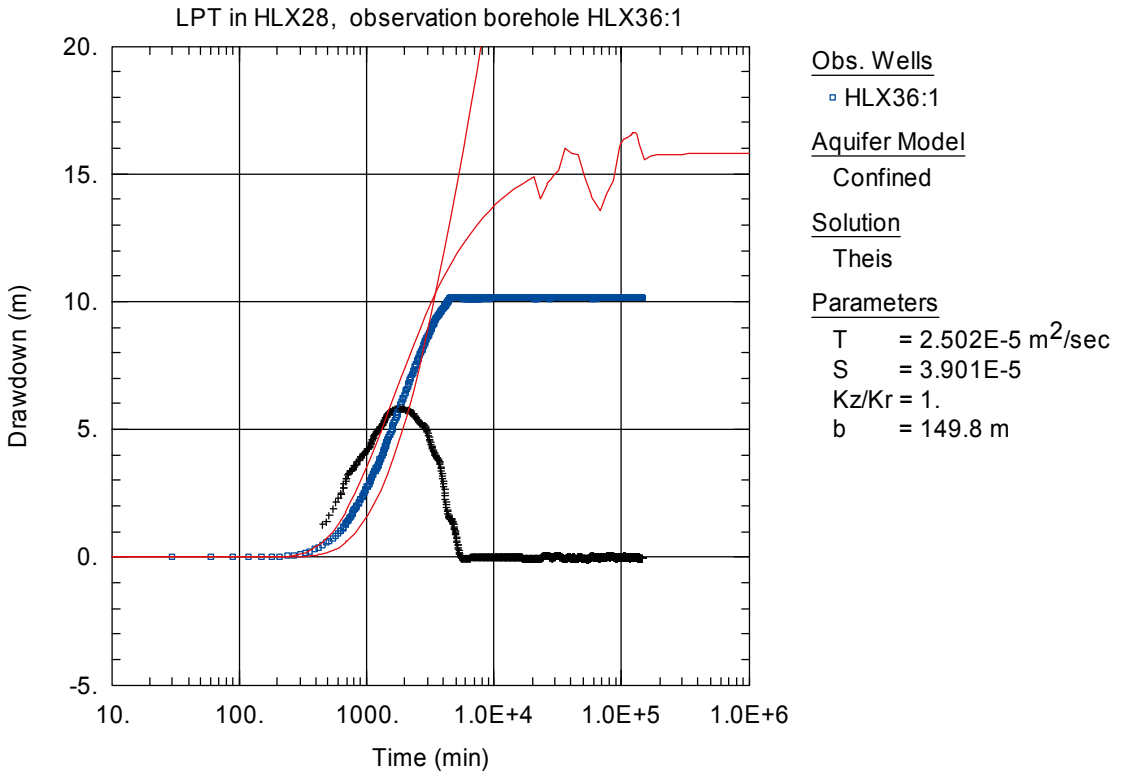

Figure A6-14. *Lin-log plot of drawdown (▫) and drawdown derivative, ds/d(ln t) (+), versus time in HLX36:1 during the interference test in HLX28, see explanation above.*

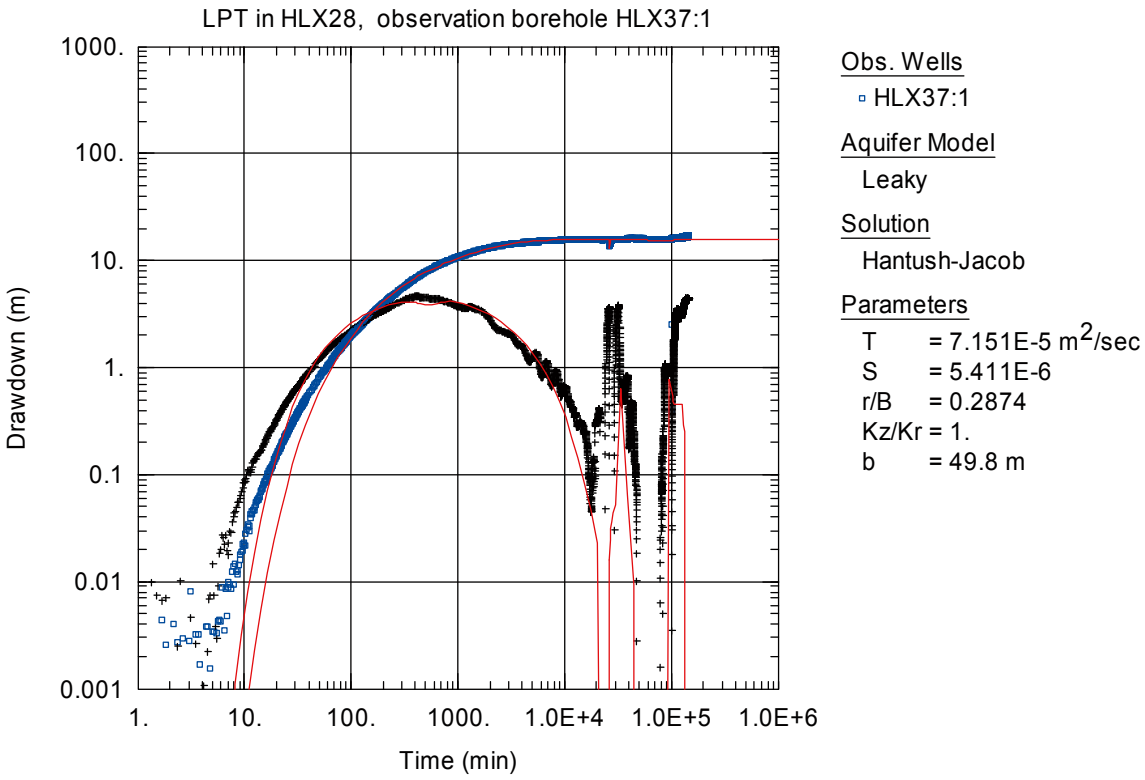

Figure A6-15. *Log-log plot of drawdown (▫) and drawdown derivative, ds/d(ln t) (+), versus time in HLX37:1 during the interference test in HLX28. The transient evaluation is based on the first part of the drawdown period. The section was used for tracer injection.*

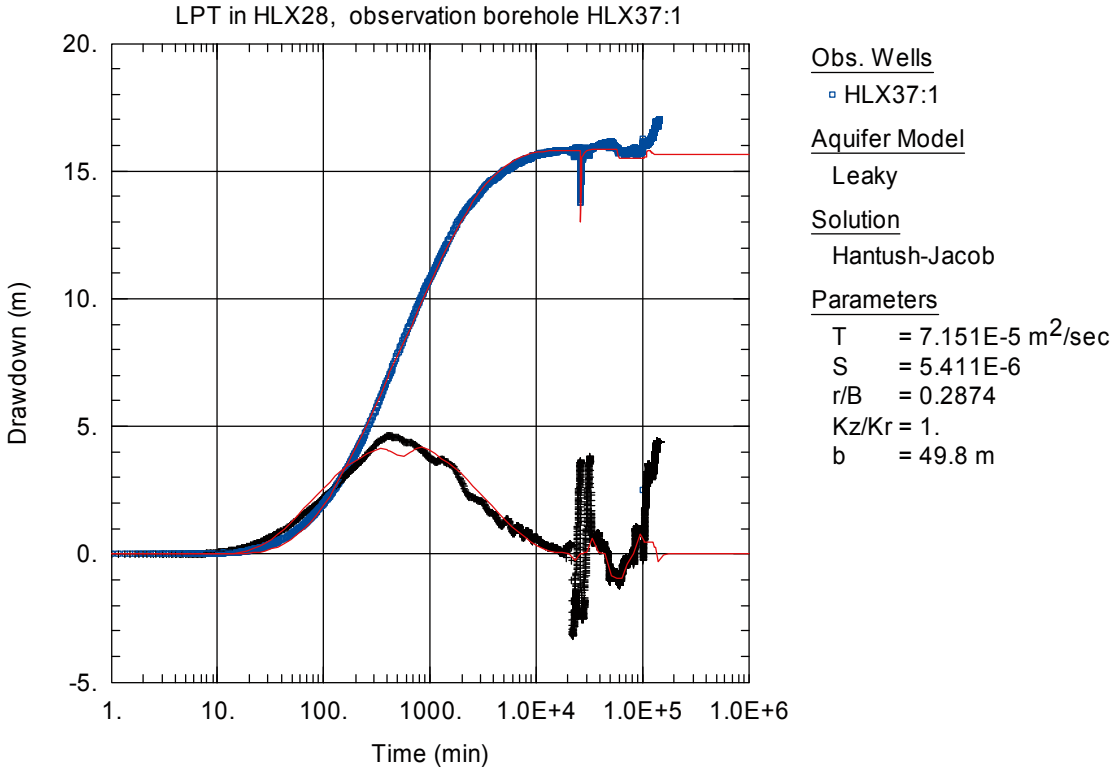

Figure A6-16. *Lin-log plot of drawdown (▫) and drawdown derivative, ds/d(ln t) (+), versus time in HLX37:1 during the interference test in HLX28. The transient evaluation is based on the first part of the flow period. The section was used for tracer injection.*

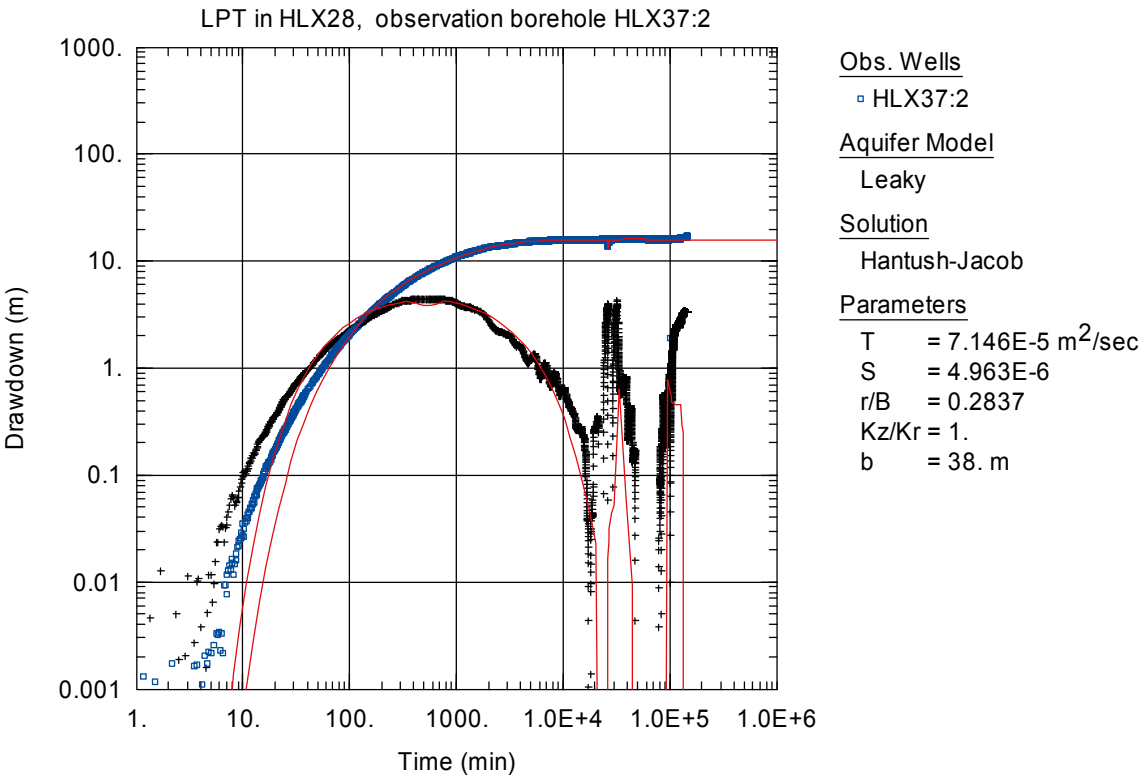

Figure A6-17. *Log-log plot of drawdown (▫) and drawdown derivative, ds/d(ln t) (+), versus time in HLX37:2 during the interference test in HLX28. The transient evaluation is based on the first part of the flow period.*

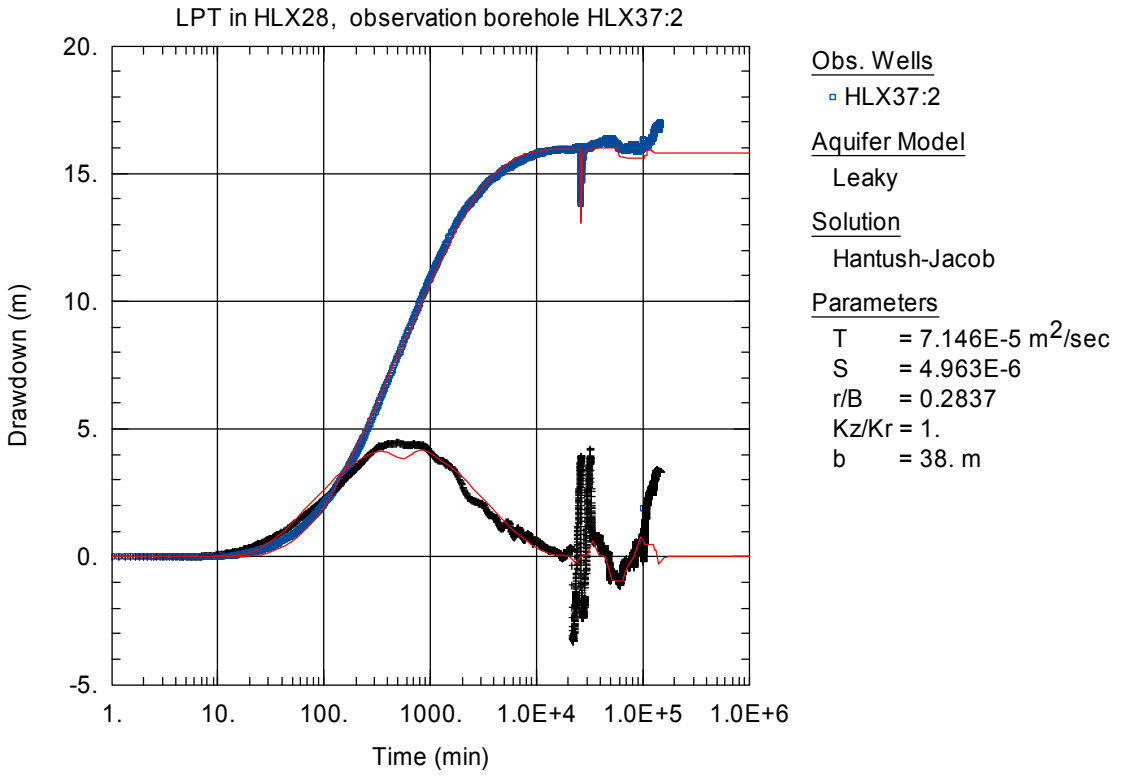

Figure A6-18. *Lin-log plot of drawdown (▫) and drawdown derivative, ds/d(ln t) (+), versus time in HLX37:2 during the interference test in HLX28. The transient evaluation is based on the first part of the flow period.*

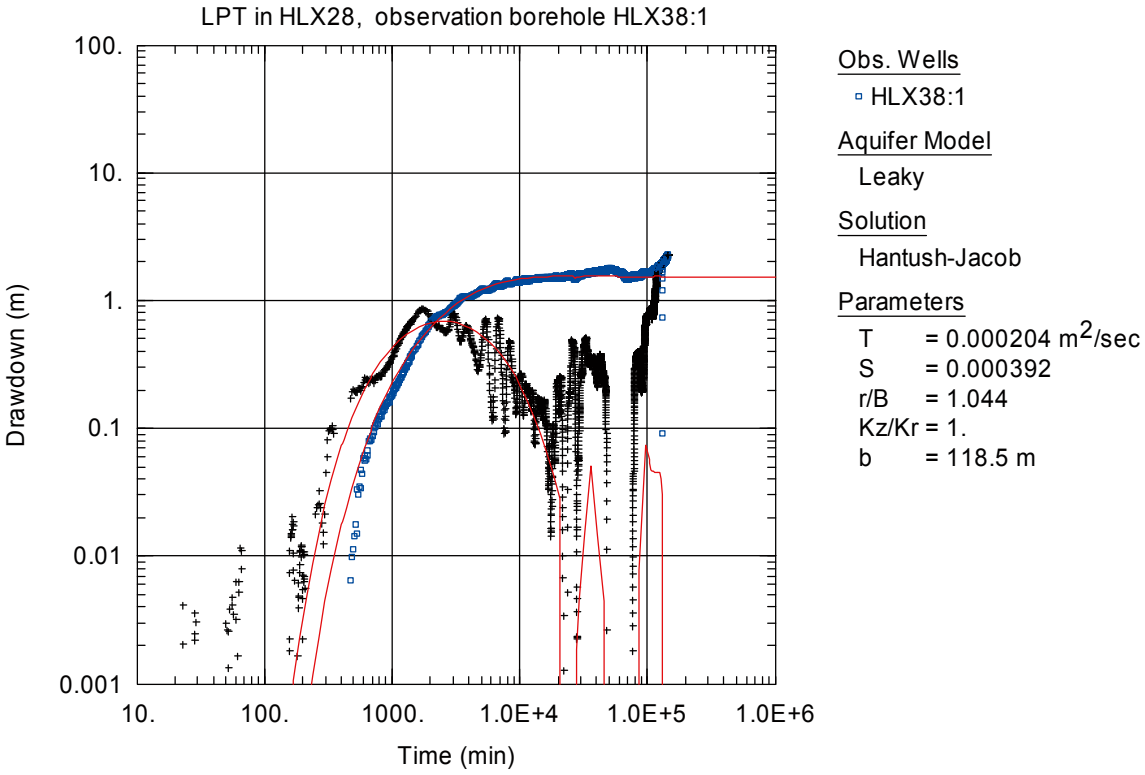

Figure A6-19. *Log-log plot of drawdown (▫) and drawdown derivative, ds/d(ln t) (+), versus time in HLX38:1 during the interference test in HLX28. The transient evaluation is based on the first part of the flow period.*

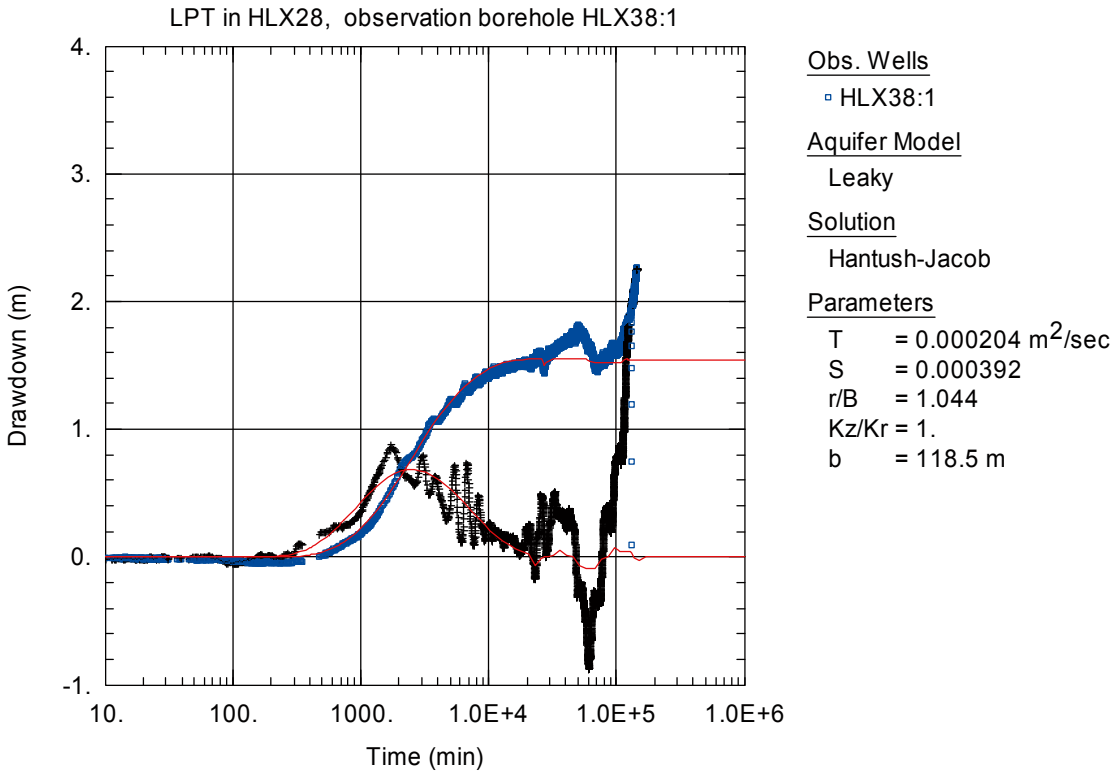

Figure A6-20. *Lin-log plot of drawdown (▫) and drawdown derivative, ds/d(ln t) (+), versus time in HLX38:1 during the interference test in HLX28. The transient evaluation is based on the first part of the flow period.*

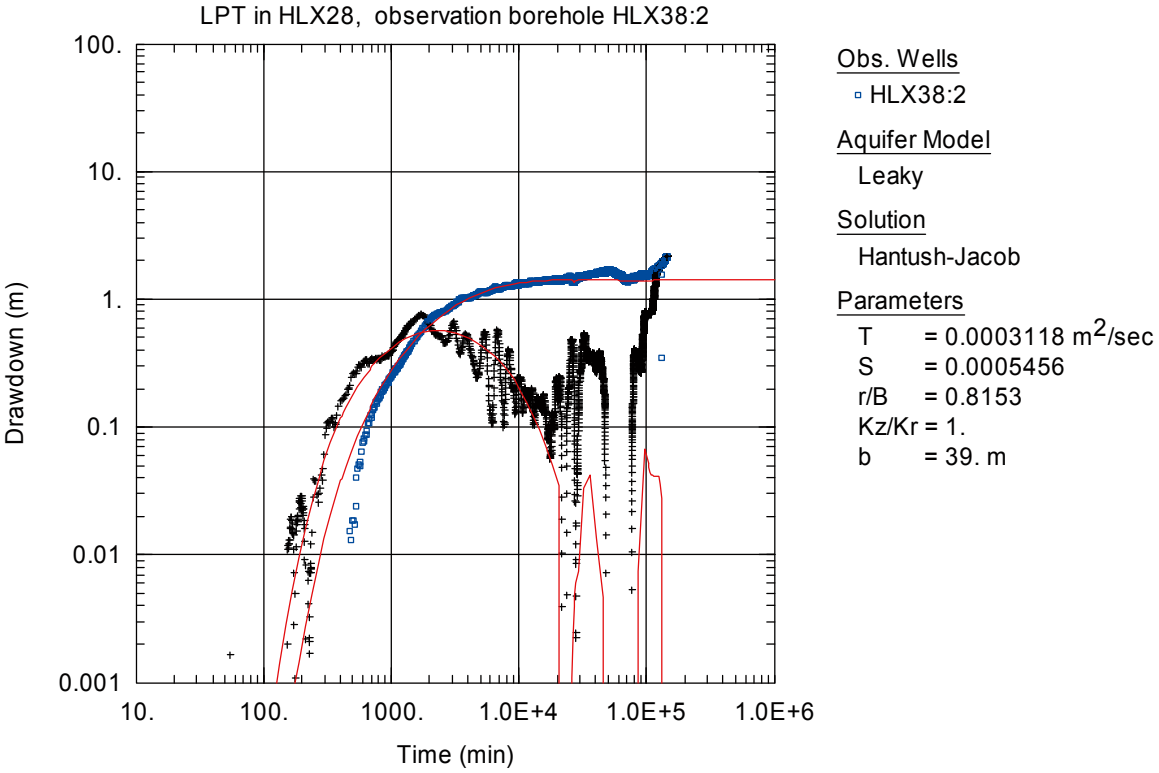

Figure A6-21. *Log-log plot of drawdown (▫) and drawdown derivative, ds/d(ln t) (+), versus time in HLX38:2 during the interference test in HLX28. The transient evaluation is based on the first part of the flow period.*

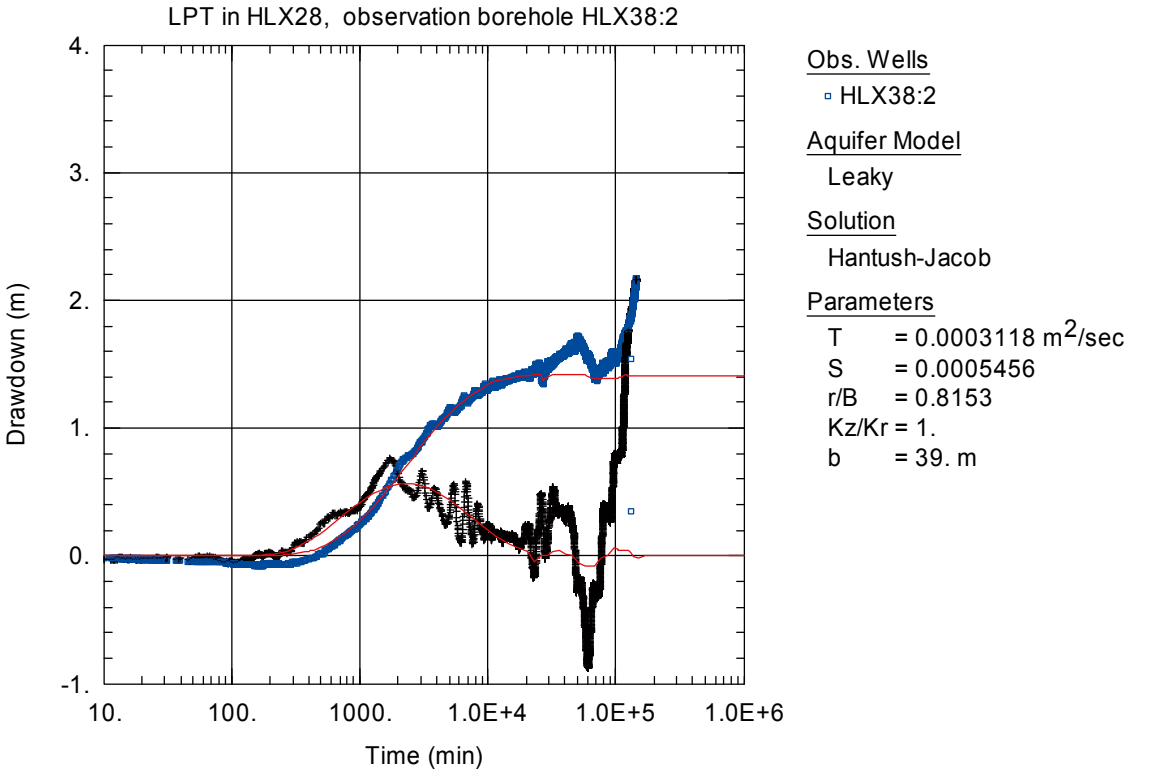

Figure A6-22. *Lin-log plot of drawdown (▫) and drawdown derivative, ds/d(ln t) (+), versus time in HLX38:2 during the interference test in HLX28. The transient evaluation is based on the first part of the flow period.*

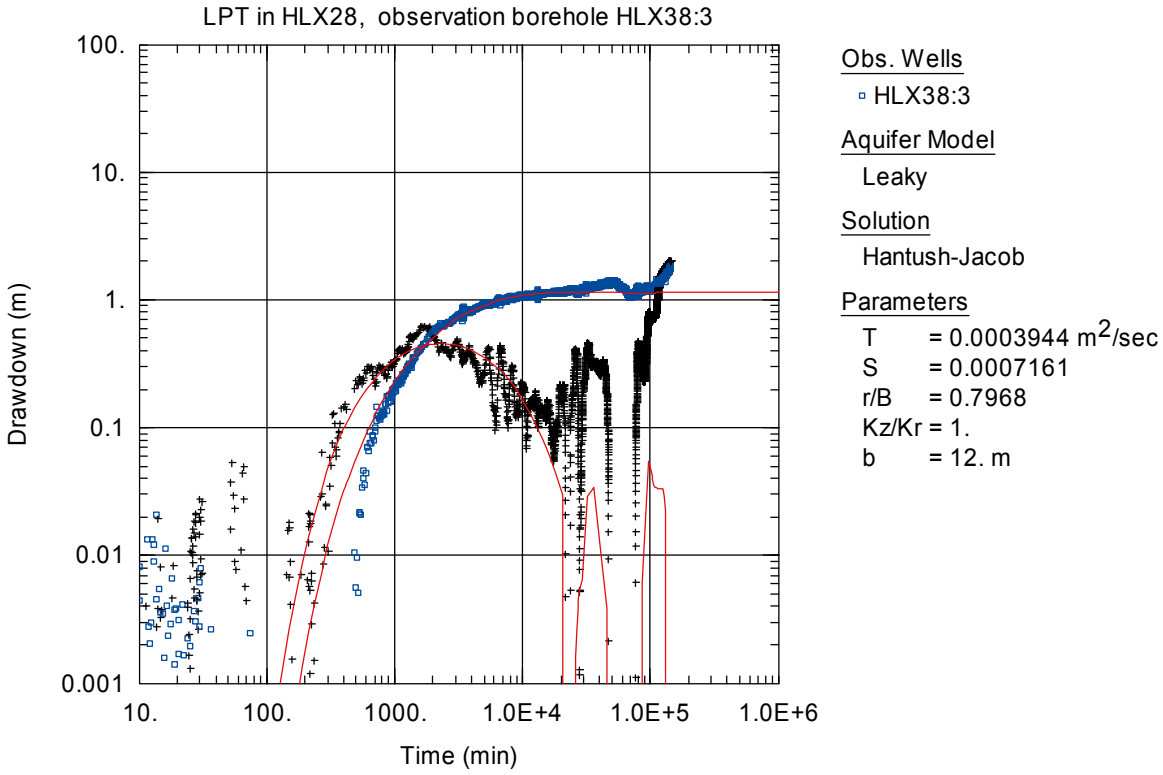

Figure A6-23. *Log-log plot of drawdown (▫) and drawdown derivative, ds/d(ln t) (+), versus time in HLX38:3 during the interference test in HLX28. The transient evaluation is based on the first part of the flow period. The section was used for tracer injection.*

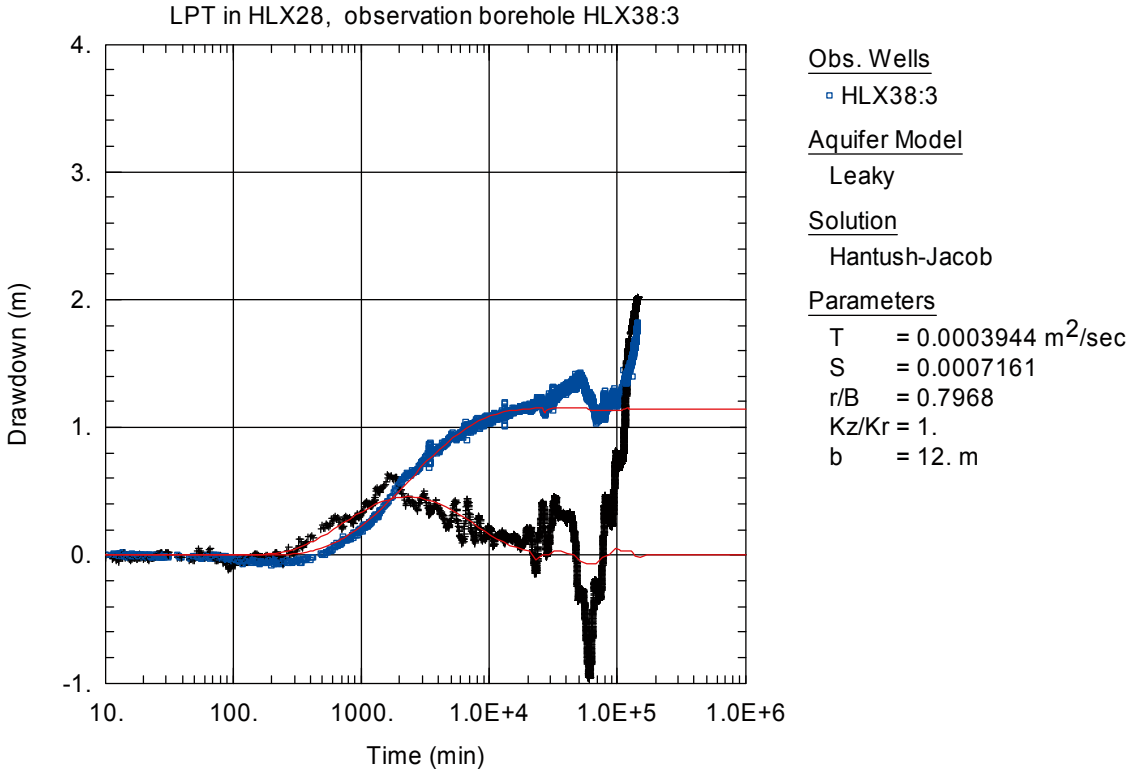

Figure A6-24. *Lin-log plot of drawdown (▫) and drawdown derivative, ds/d(ln t) (+), versus time in HLX38:3 during the interference test in HLX28. The transient evaluation is based on the first part of the flow period. The section was used for tracer injection.*

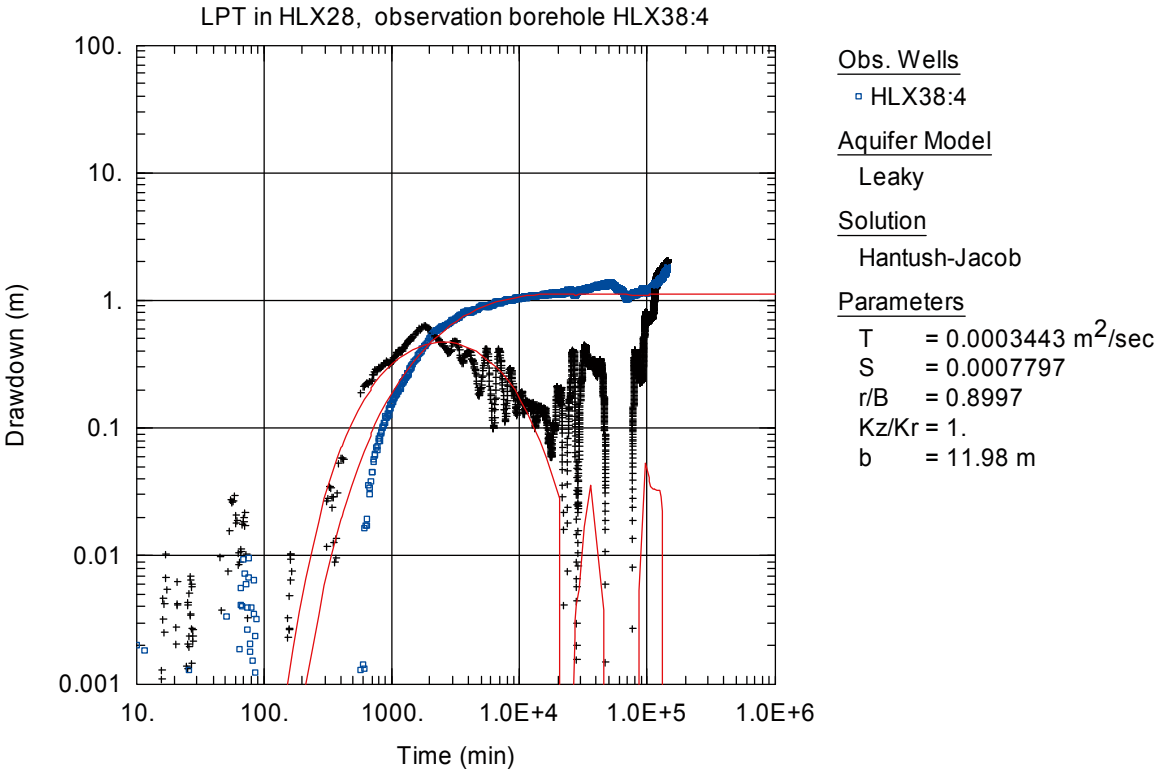

Figure A6-25. *Log-log plot of drawdown (▫) and drawdown derivative, ds/d(ln t) (+), versus time in HLX38:4 during the interference test in HLX28. The transient evaluation is based on the first part of the flow period.*

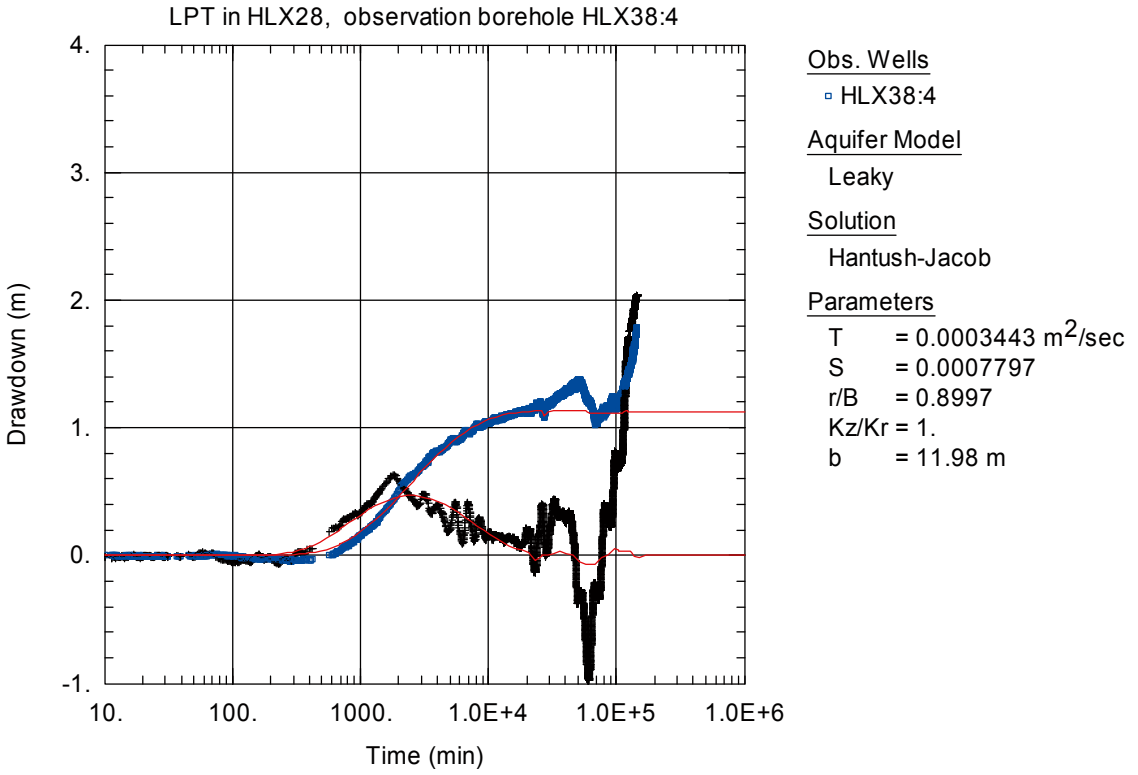

Figure A6-26. *Lin-log plot of drawdown (▫) and drawdown derivative, ds/d(ln t) (+), versus time in HLX38:4 during the interference test in HLX28. The transient evaluation is based on the first part of the flow period.*

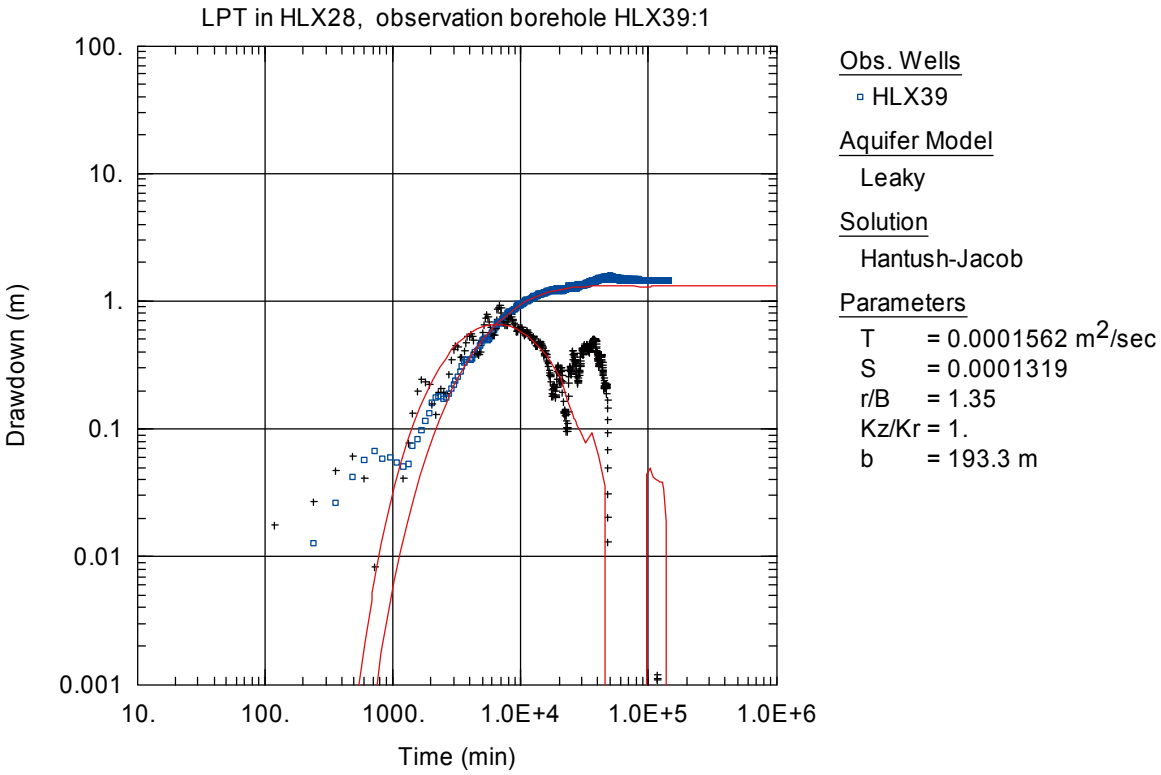

Figure A6-27. *Log-log plot of drawdown (▫) and drawdown derivative, ds/d(ln t) (+), versus time in HLX39 during the interference test in HLX28. Transient evaluation is based on the first part of the drawdown period.*

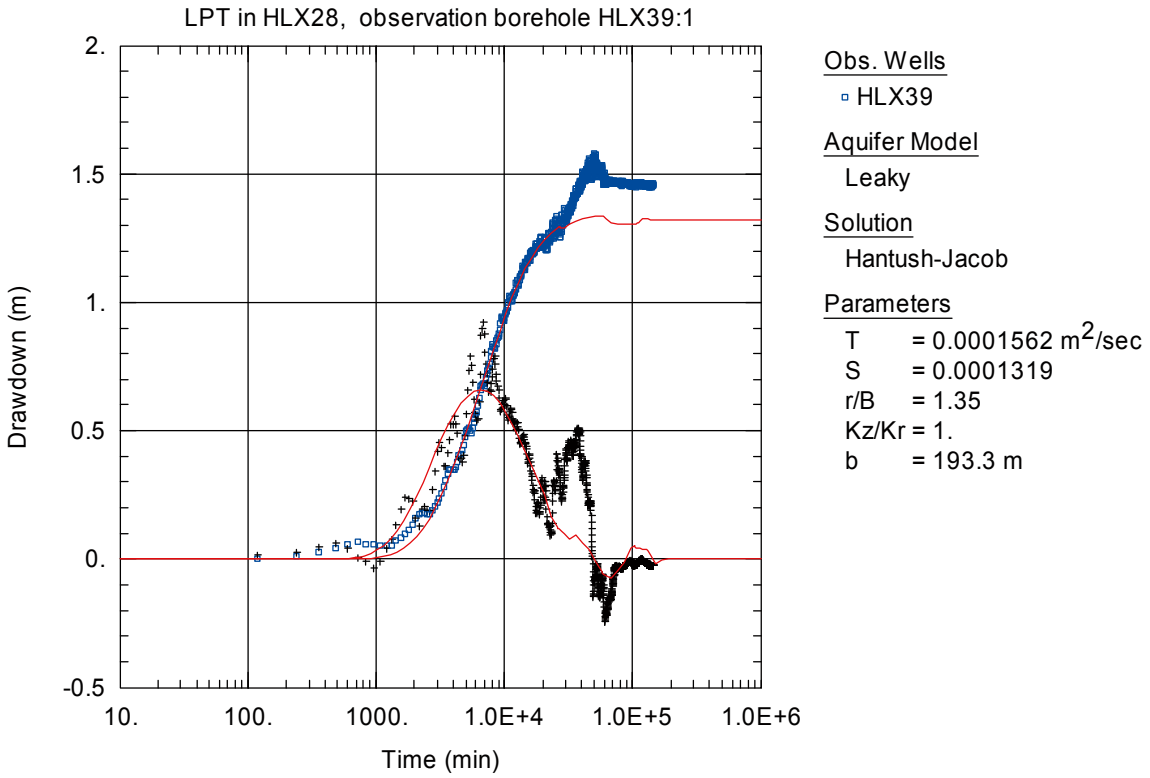

Figure A6-28. *Lin-log plot of drawdown (▫) and drawdown derivative, ds/d(ln t) (+), versus time in HLX39 during the interference test in HLX28. Transient evaluation is based on the first part of the drawdown period.*

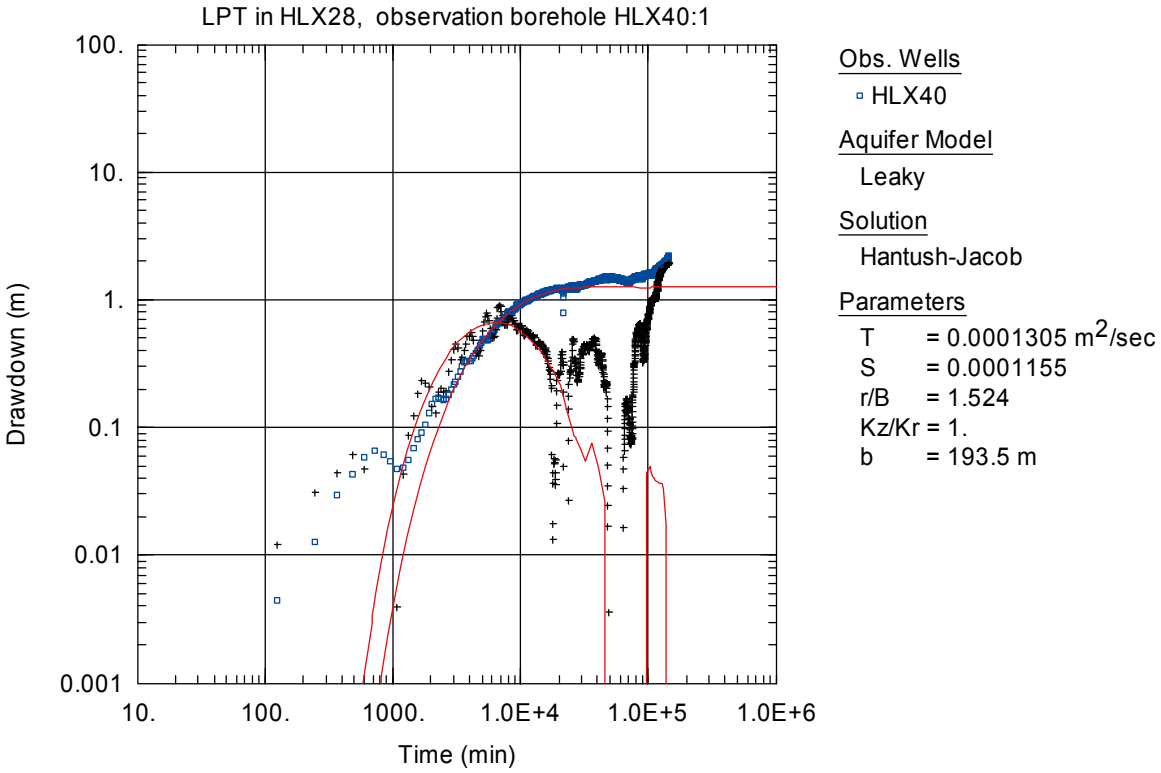

Figure A6-29. *Log-log plot of drawdown (▫) and drawdown derivative, ds/d(ln t) (+), versus time in HLX40 during the interference test in HLX28. Transient evaluation is based on the first part of the drawdown period.*

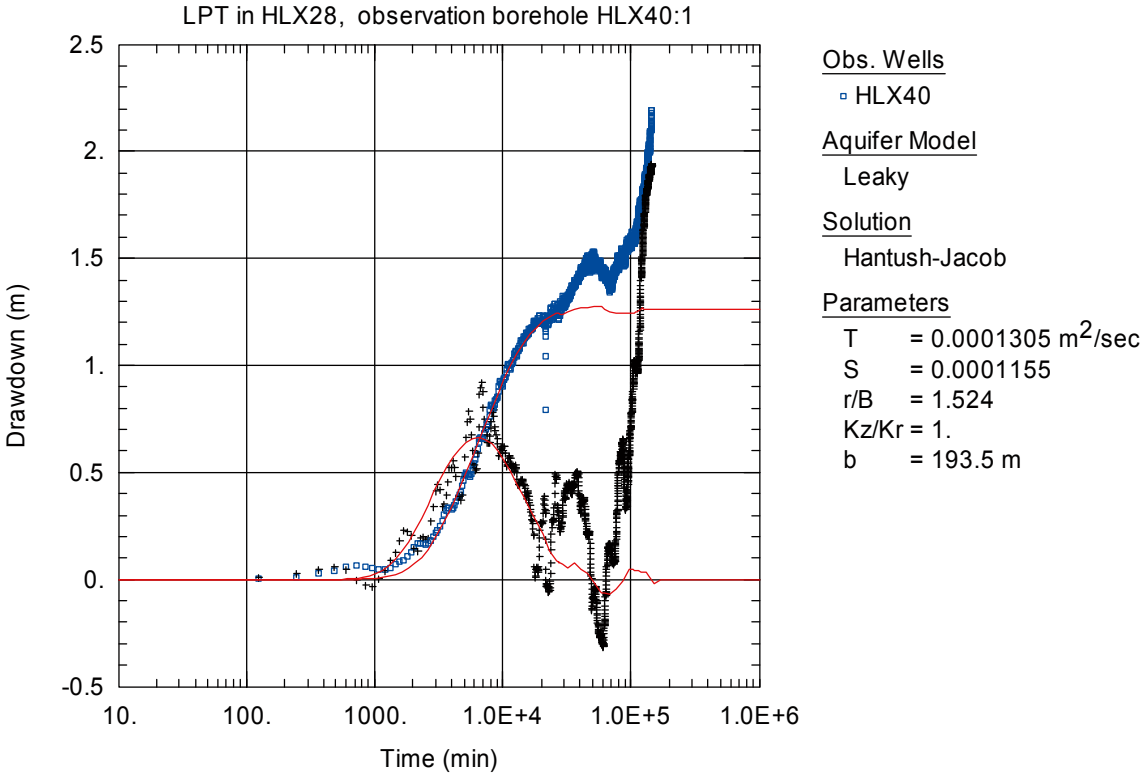

Figure A6-30. *Lin-log plot of drawdown (▫) and drawdown derivative, ds/d(ln t) (+), versus time in HLX40 during the interference test in HLX28. Transient evaluation is based on the first part of the drawdown period.*

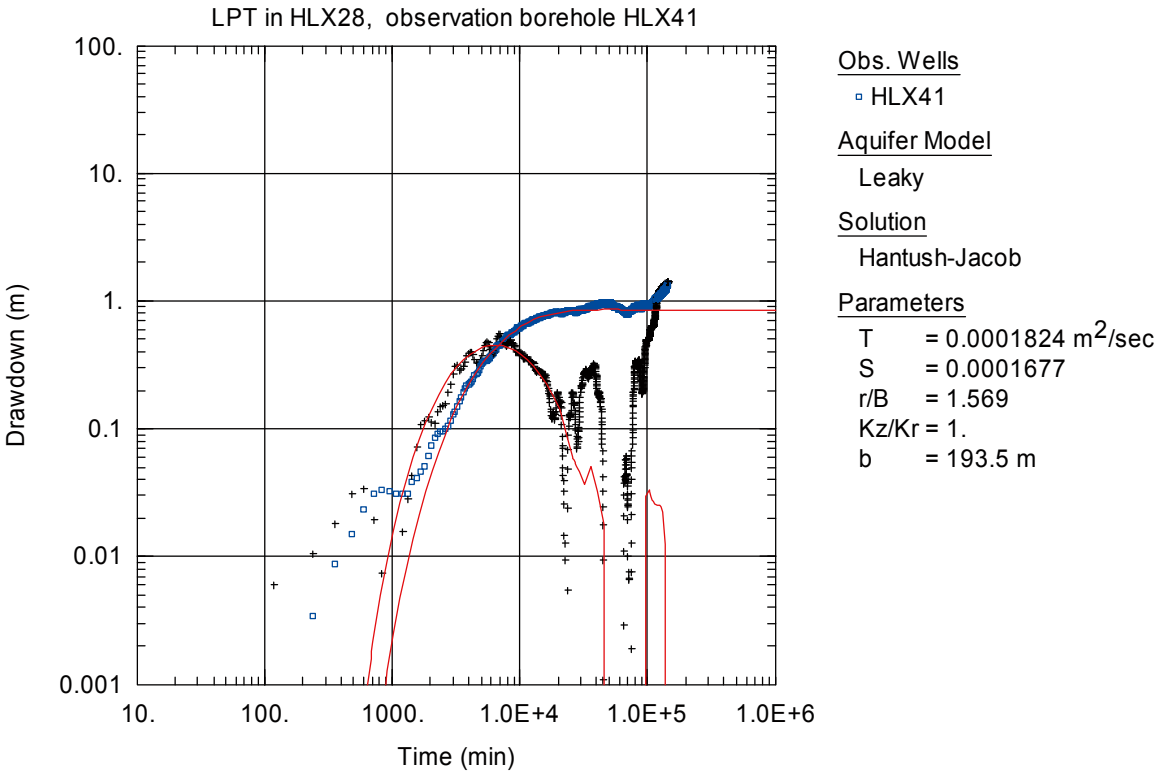

Figure A6-31. *Log-log plot of drawdown (▫) and drawdown derivative, ds/d(ln t) (+), versus time in HLX41 during the interference test in HLX28. Transient evaluation is based on the first part of the drawdown period.*

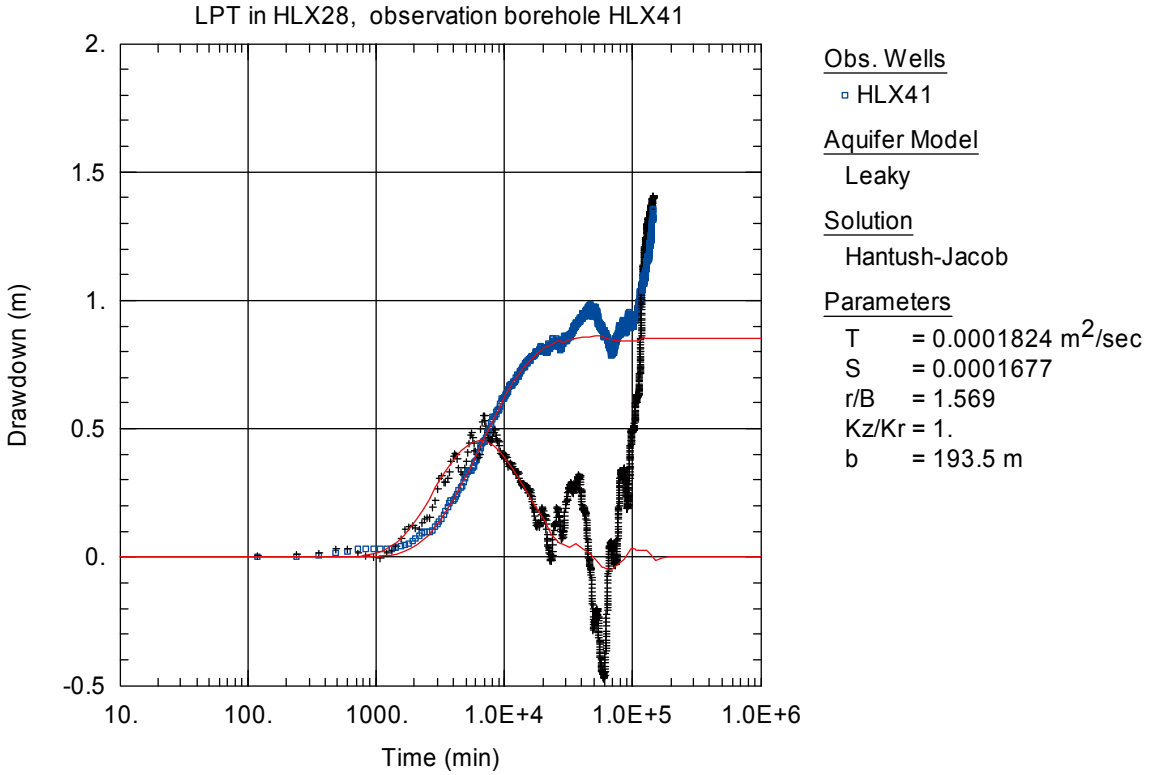

Figure A6-32. *Lin-log plot of drawdown (▫) and drawdown derivative, ds/d(ln t) (+), versus time in HLX41 during the interference test in HLX28. Transient evaluation is based on the first part of the drawdown period.*

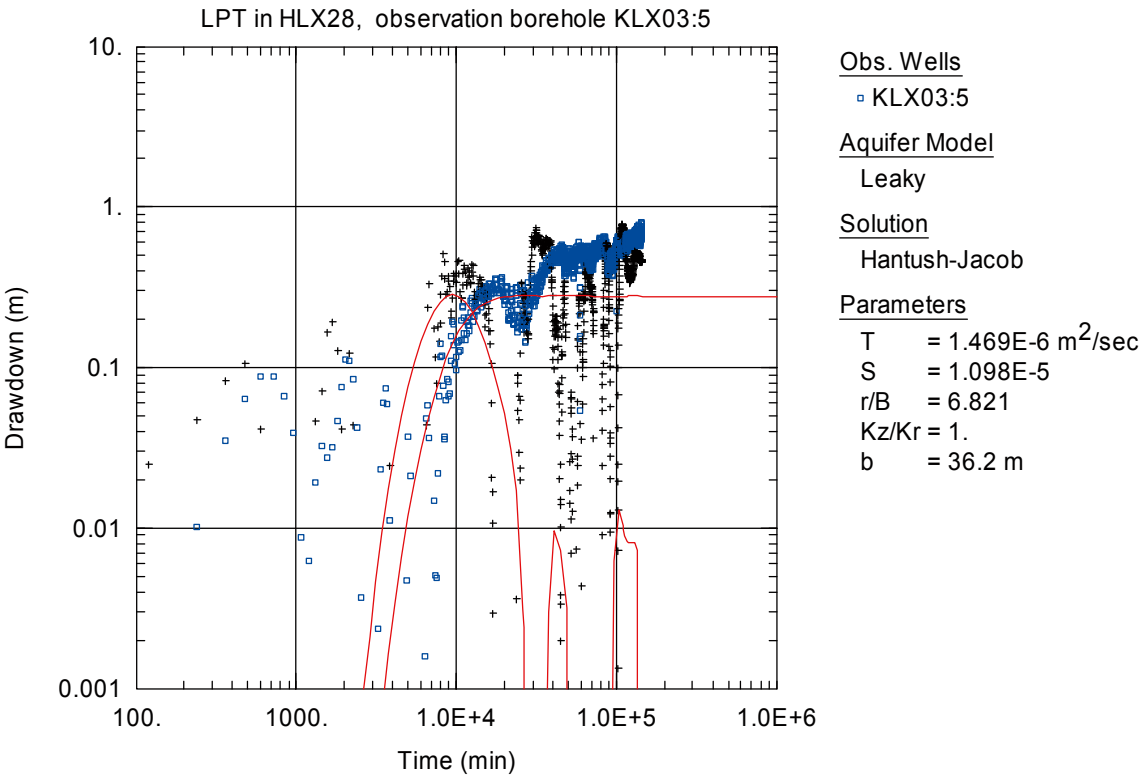

Figure A6-33. *Log-log plot of drawdown (▫) and drawdown derivative, ds/d(ln t) (+), versus time in KLX03:5 during the interference test in HLX28. Transient evaluation is based on the later part of the drawdown period.*

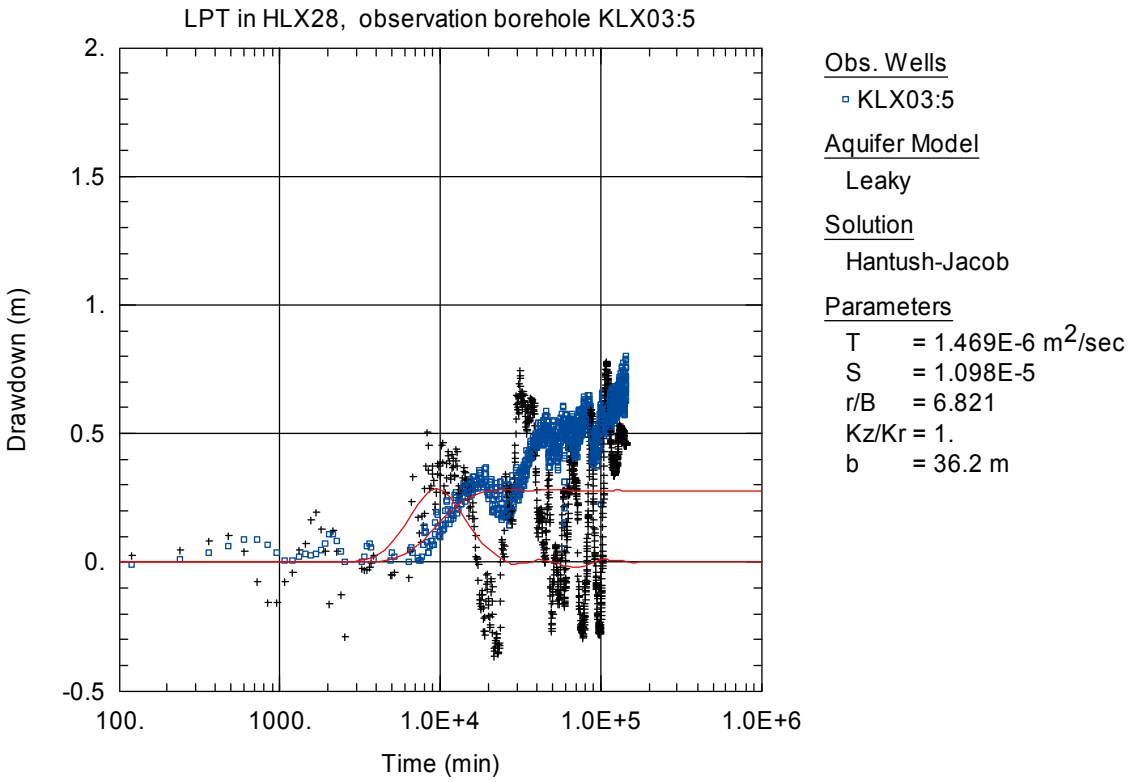

Figure A6-34. *Lin-log plot of drawdown (▫) and drawdown derivative, ds/d(ln t) (+), versus time in KLX03:5 during the interference test in HLX28. Transient evaluation is based on the later part of the drawdown period.*

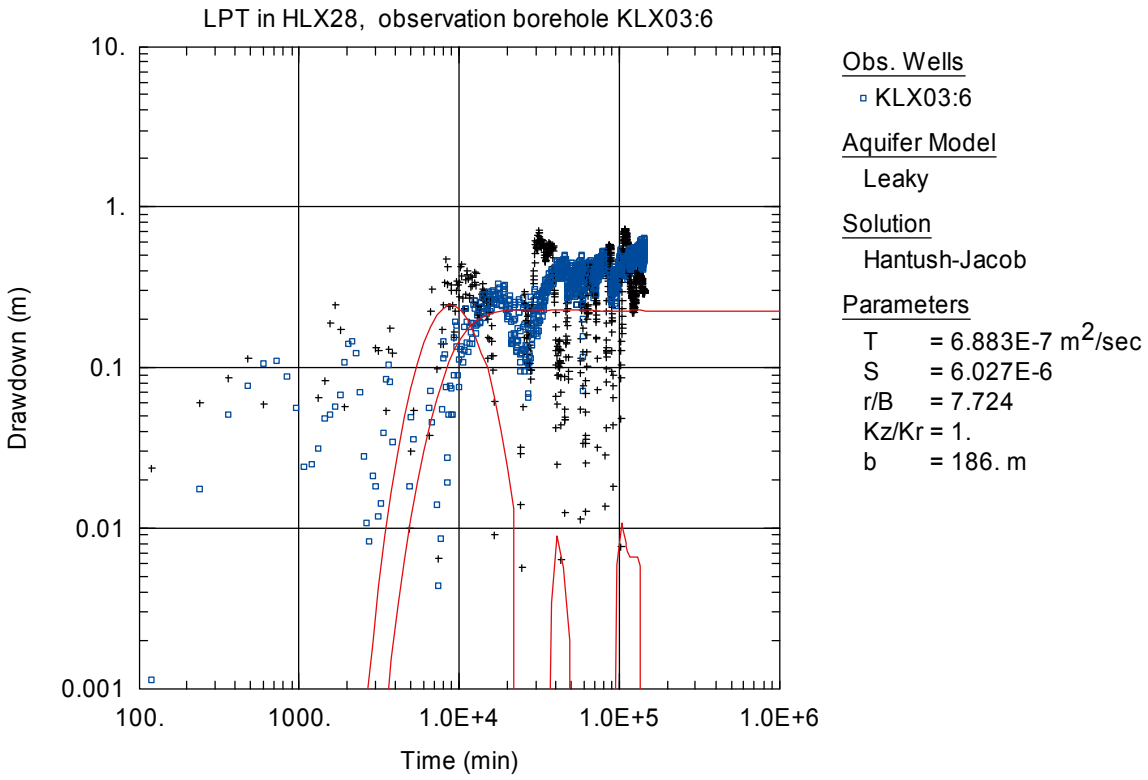

Figure A6-35. *Log-log plot of drawdown (▫) and drawdown derivative, ds/d(ln t) (+), versus time in KLX03:6 during the interference test in HLX28. Transient evaluation is based on the first part of the drawdown period.*

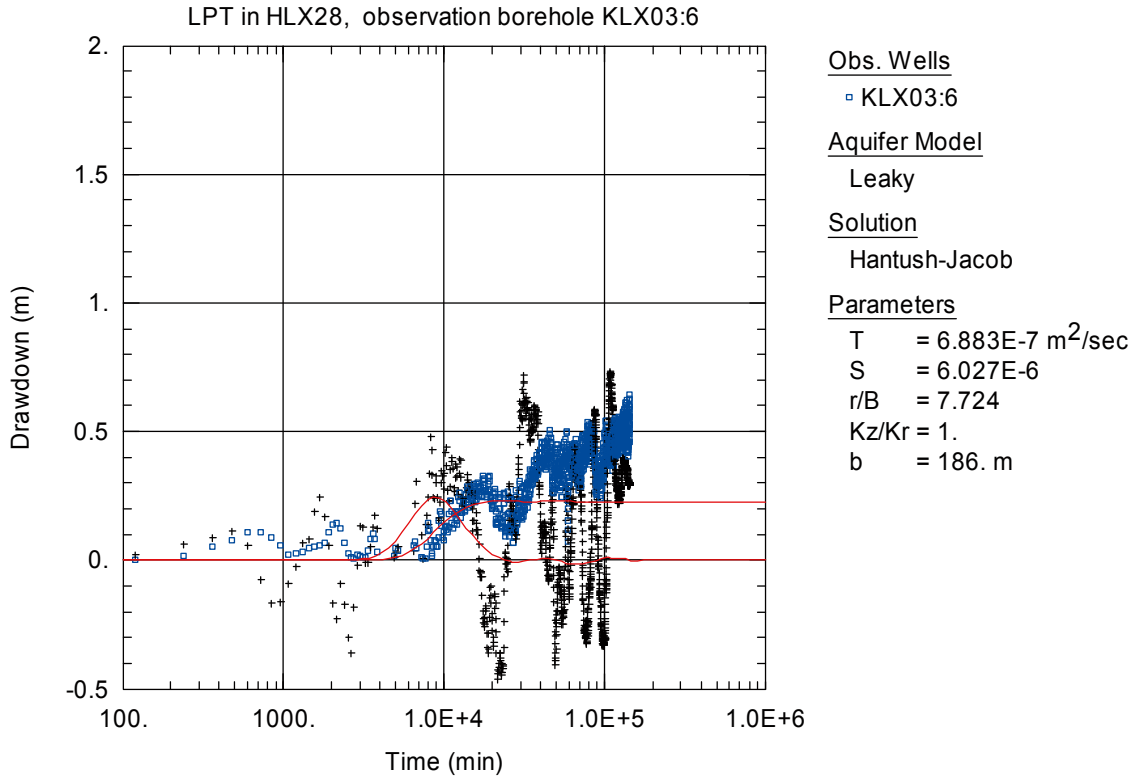

Figure A6-36. *Lin-log plot of drawdown (▫) and drawdown derivative, ds/d(ln t) (+), versus time in KLX03:6 during the interference test in HLX28. Transient evaluation is based on the first part of the drawdown period.*

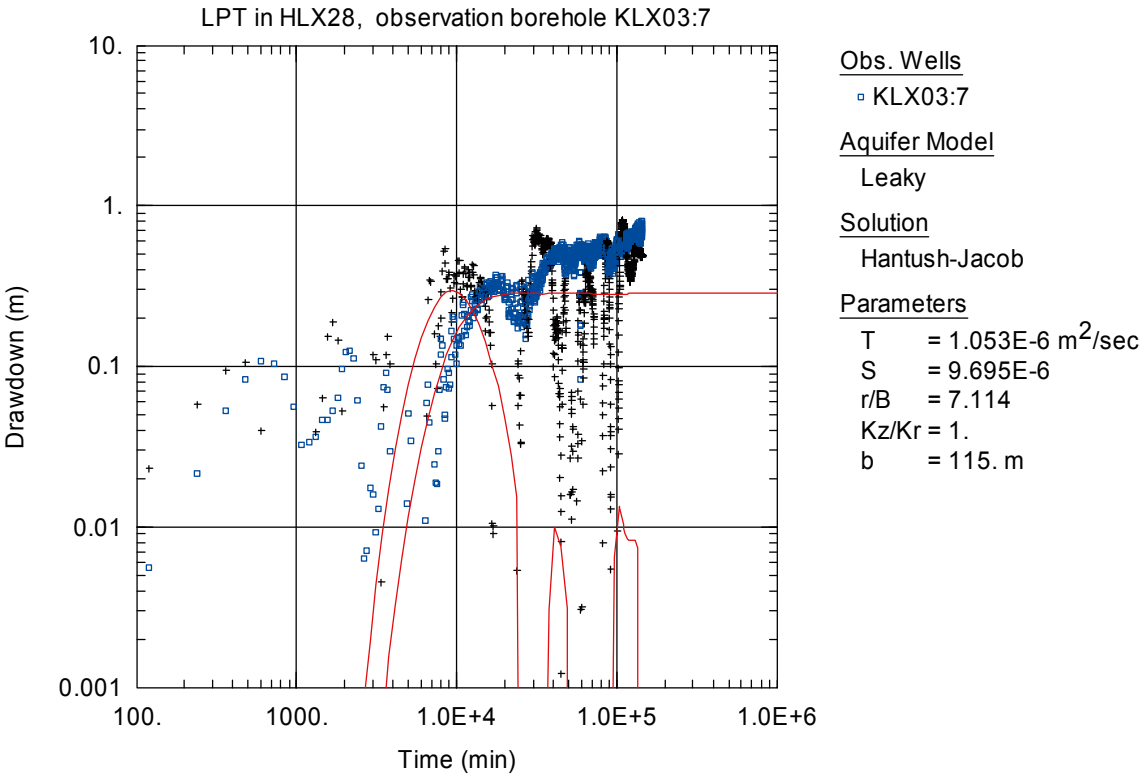

Figure A6-37. *Log-log plot of drawdown (▫) and drawdown derivative, ds/d(ln t) (+), versus time in KLX03:7 during the interference test in HLX28. Transient evaluation is based on the first part of the drawdown period.*

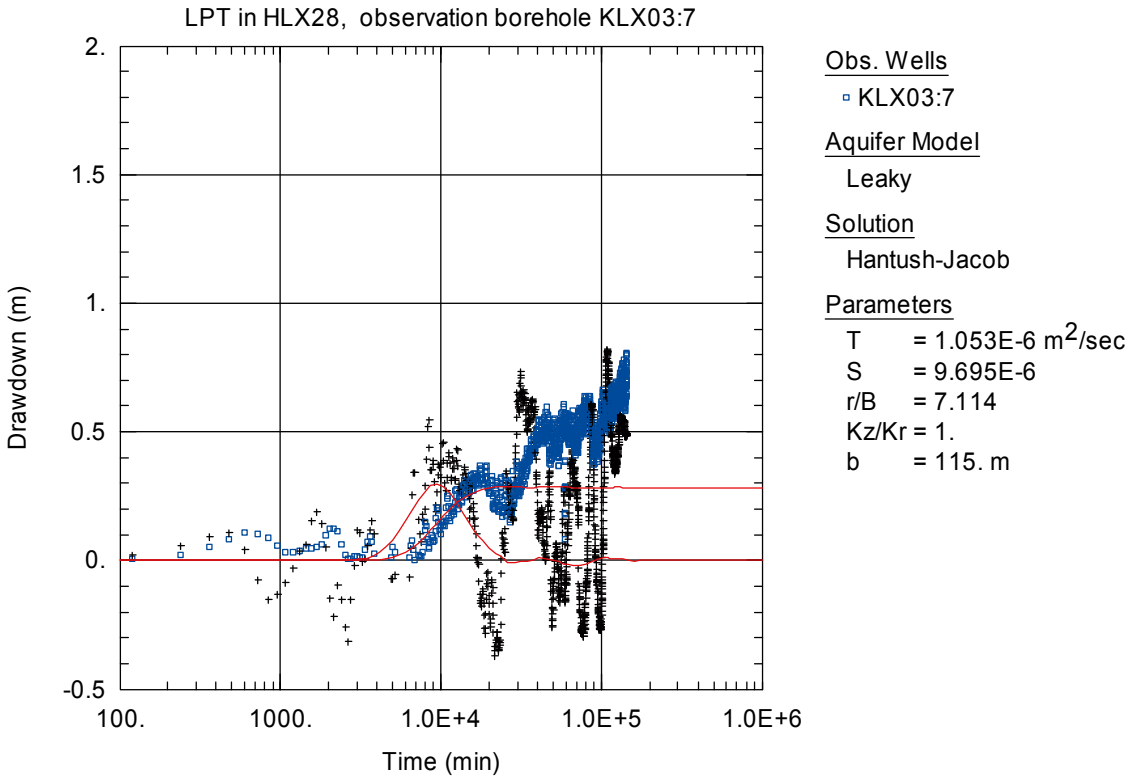

Figure A6-38. *Lin-log plot of drawdown (▫) and drawdown derivative, ds/d(ln t) (+), versus time in KLX03:7 during the interference test in HLX28. Transient evaluation is based on the first part of the drawdown period.*

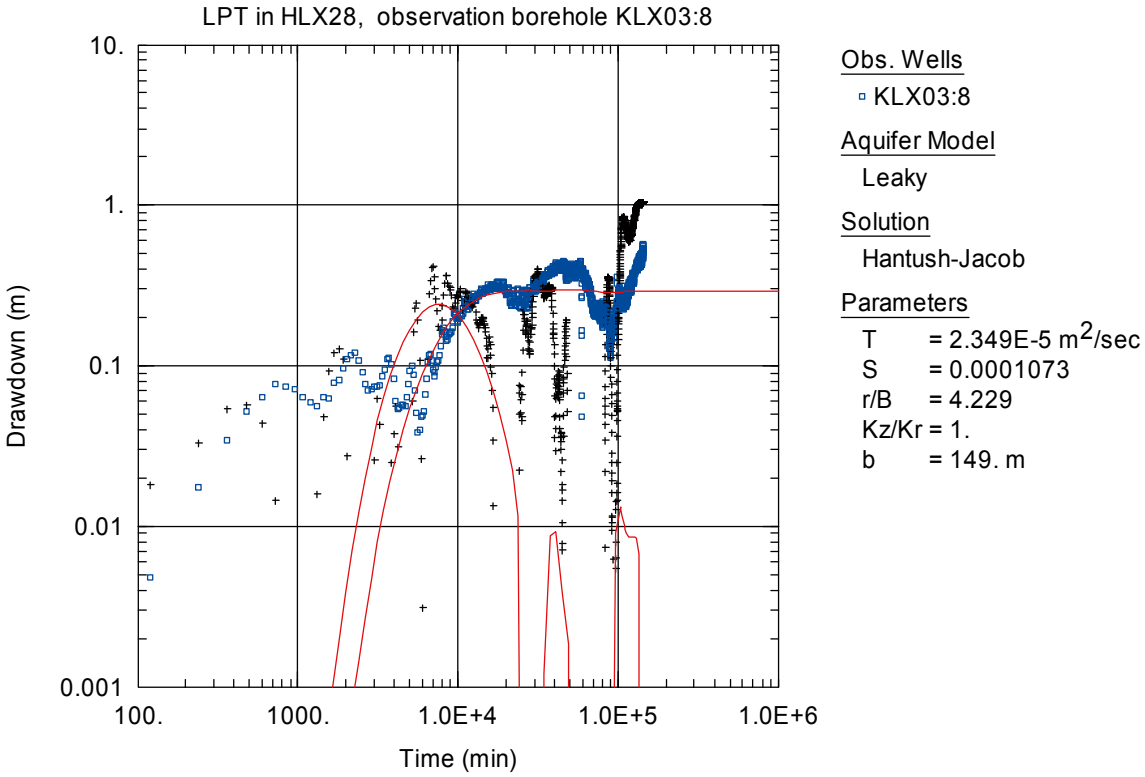

Figure A6-39. *Log-log plot of drawdown (▫) and drawdown derivative, ds/d(ln t) (+), versus time in KLX03:8 during the interference test in HLX28. Transient evaluation is based on the first part of the drawdown period.*

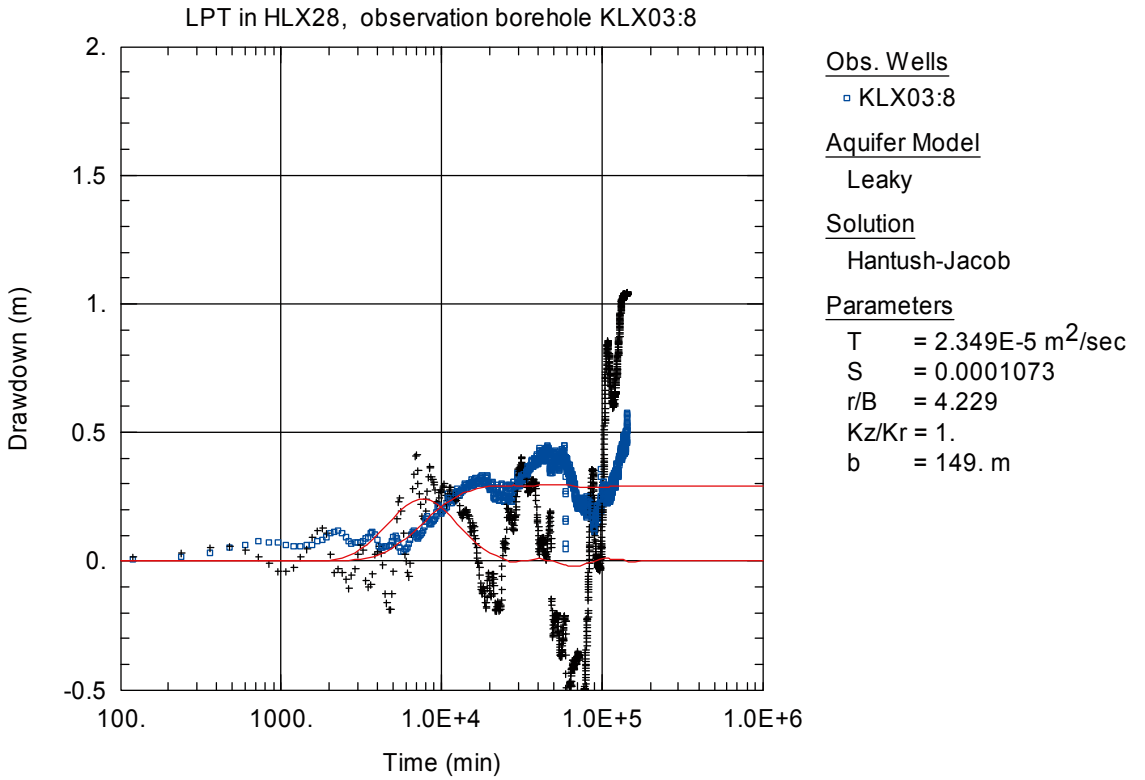

Figure A6-40. *Lin-log plot of drawdown (▫) and drawdown derivative, ds/d(ln t) (+), versus time in KLX03:8 during the interference test in HLX28. Transient evaluation is based on the first part of the drawdown period.*

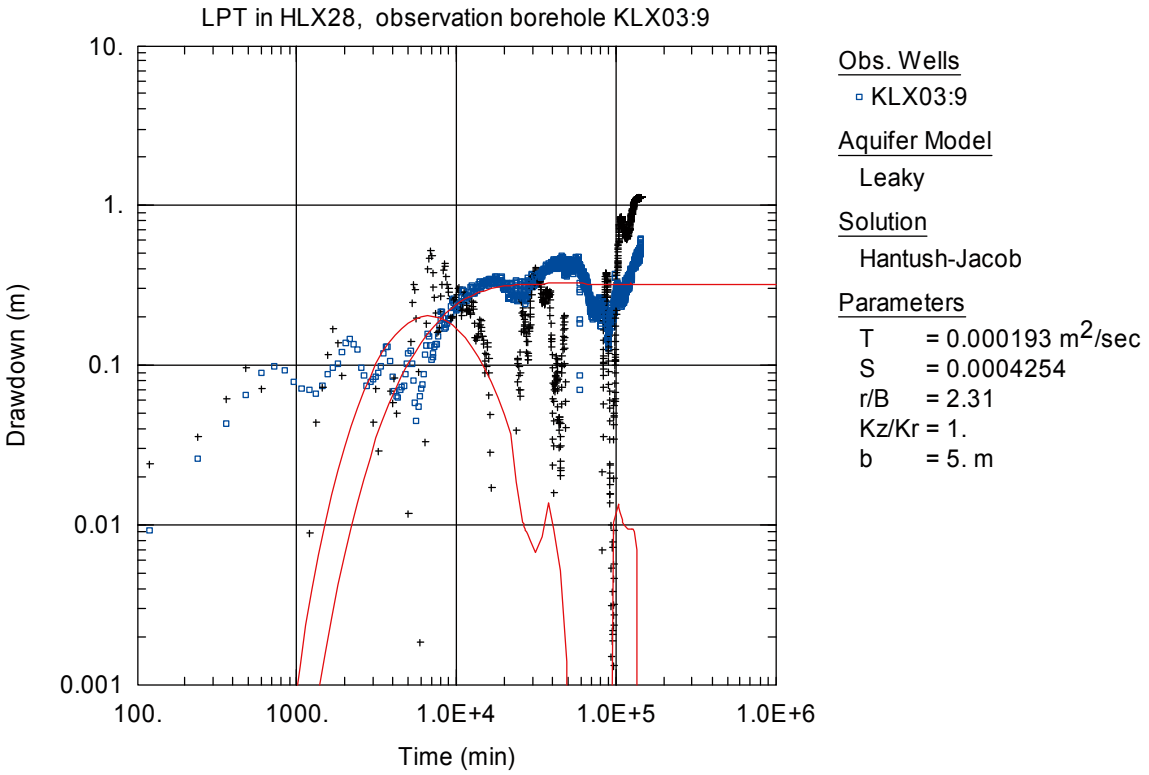

Figure A6-41. *Log-log plot of drawdown (▫) and drawdown derivative, ds/d(ln t) (+), versus time in KLX03:9 during the interference test in HLX28. Transient evaluation is based on the first part of the drawdown period.*

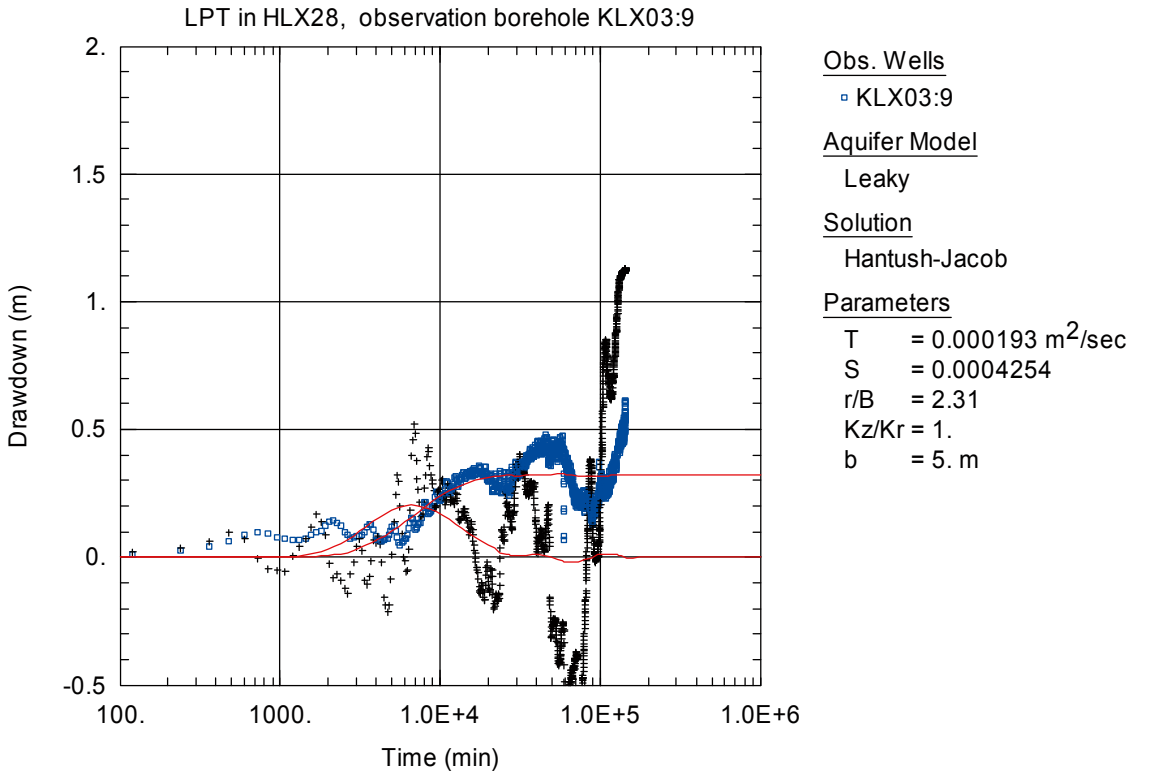

Figure A6-42. *Lin-log plot of drawdown (▫) and drawdown derivative, ds/d(ln t) (+), versus time in KLX03:9 during the interference test in HLX28. Transient evaluation is based on the first part of the drawdown period.*

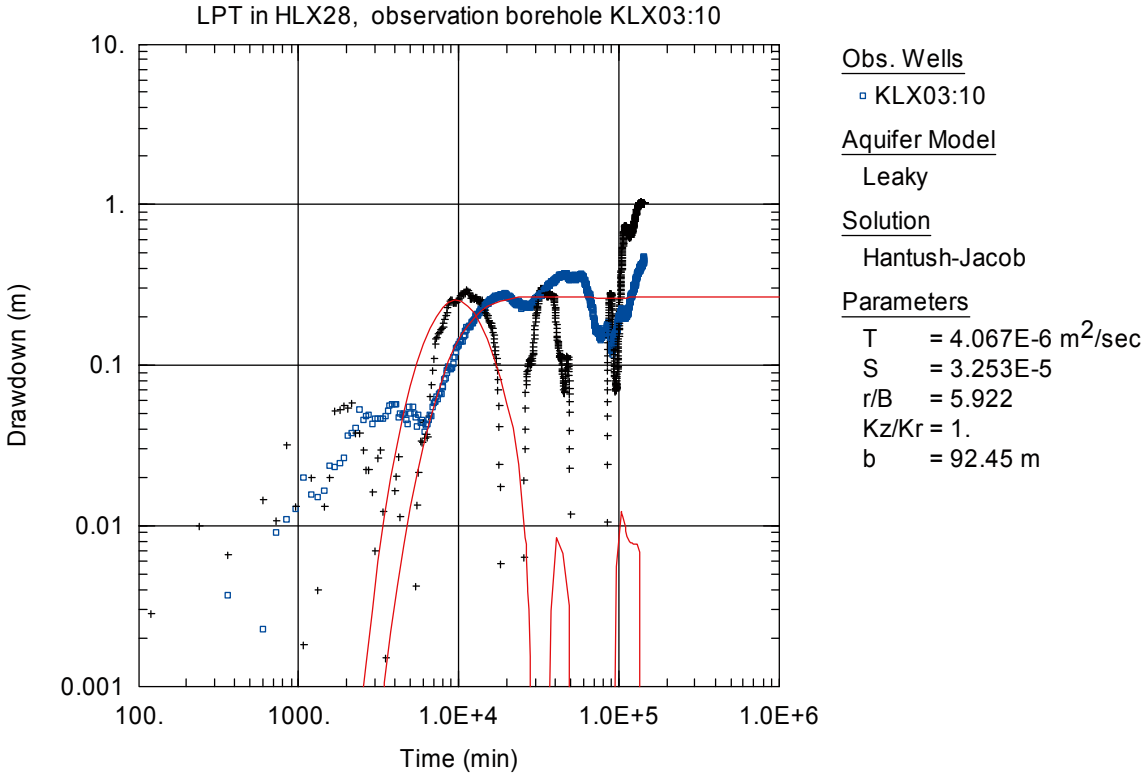

Figure A6-43. *Log-log plot of drawdown (▫) and drawdown derivative, ds/d(ln t) (+), versus time in KLX03:10 during the interference test in HLX28. Transient evaluation is based on the first part of the drawdown period.*

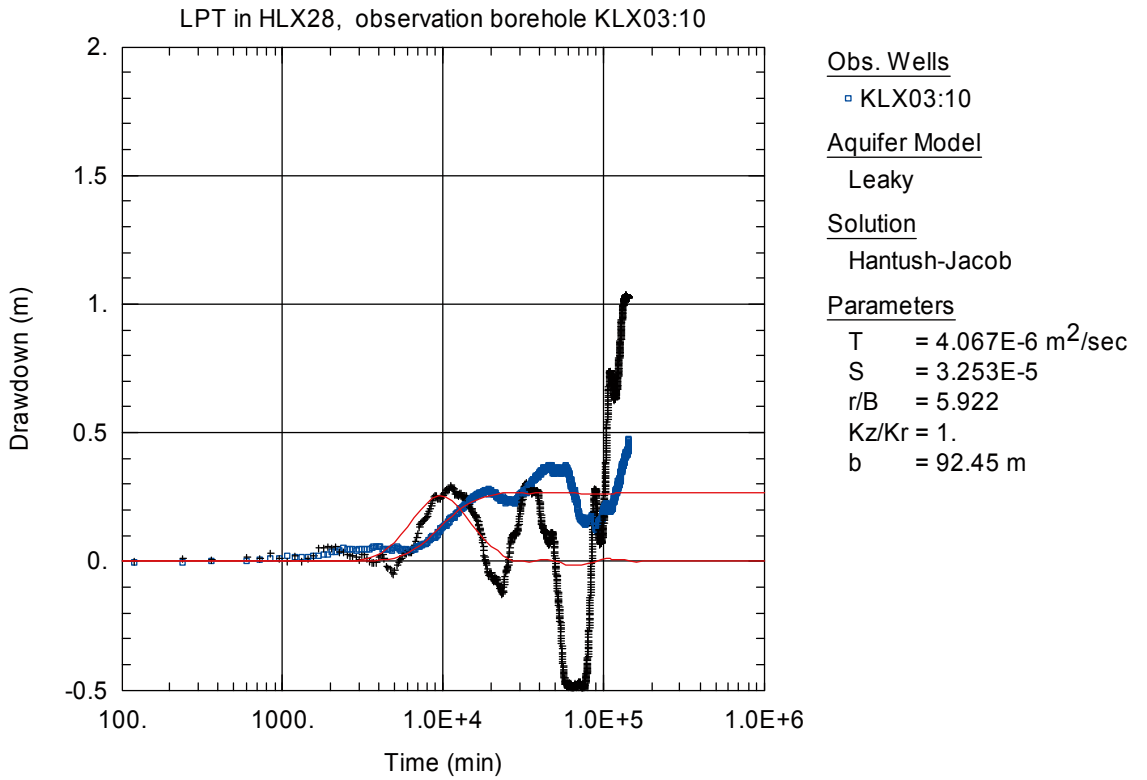

Figure A6-44. *Lin-log plot of drawdown (▫) and drawdown derivative, ds/d(ln t) (+), versus time in KLX03:10 during the interference test in HLX28. Transient evaluation is based on the first part of the drawdown period.*

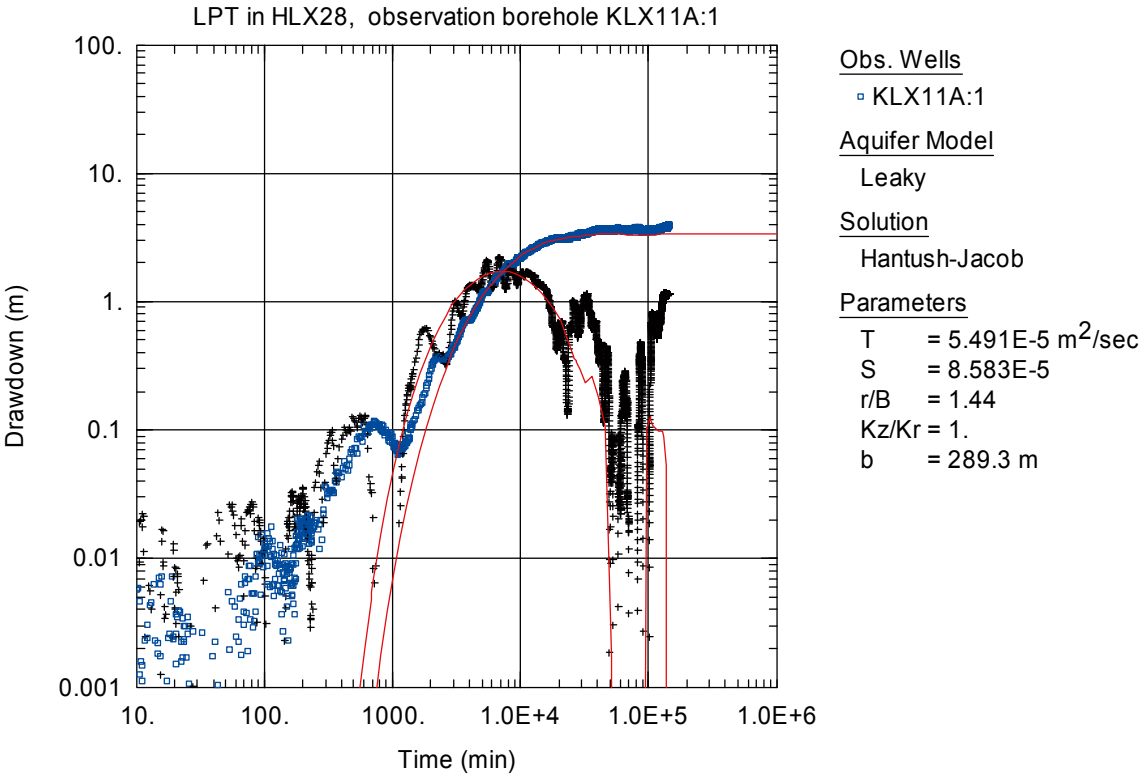

Figure A6-45. *Log-log plot of drawdown (▫) and drawdown derivative, ds/d(ln t) (+), versus time in KLX11A:1 during the interference test in HLX28. Transient evaluation is based on the first part of the drawdown period.*

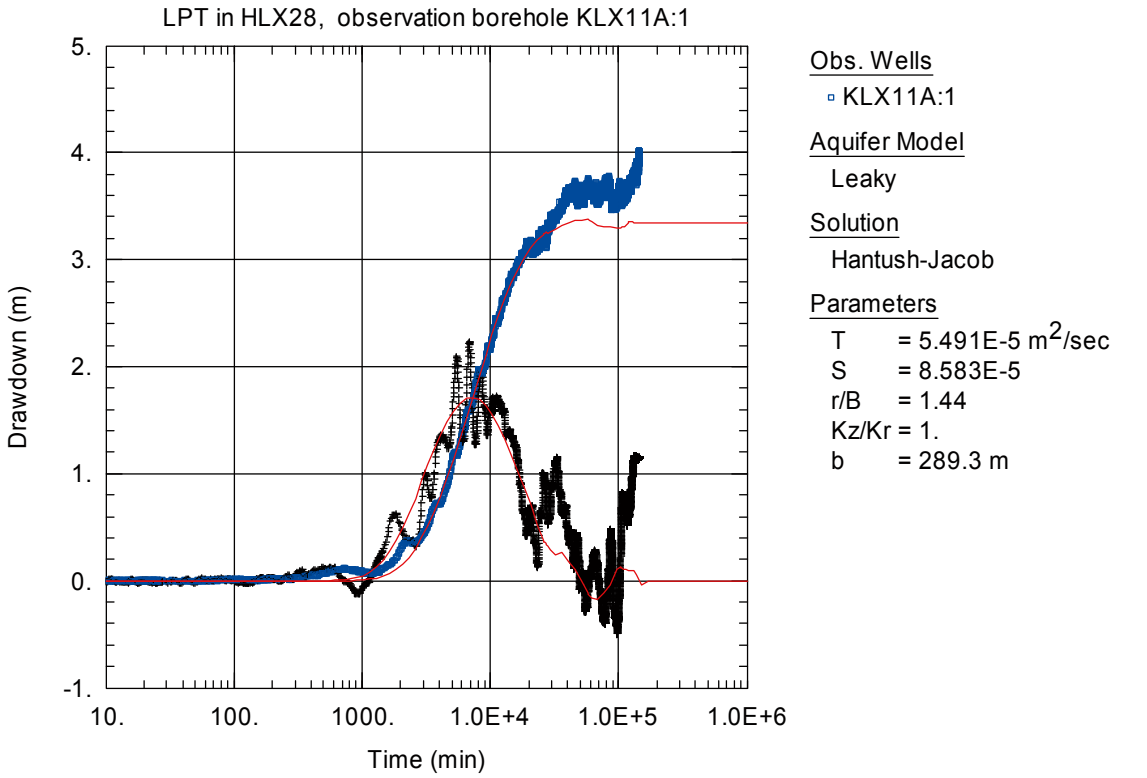

Figure A6-46. *Lin-log plot of drawdown (▫) and drawdown derivative, ds/d(ln t) (+), versus time in KLX11A:1 during the interference test in HLX28. Transient evaluation is based on the first part of the drawdown period.*

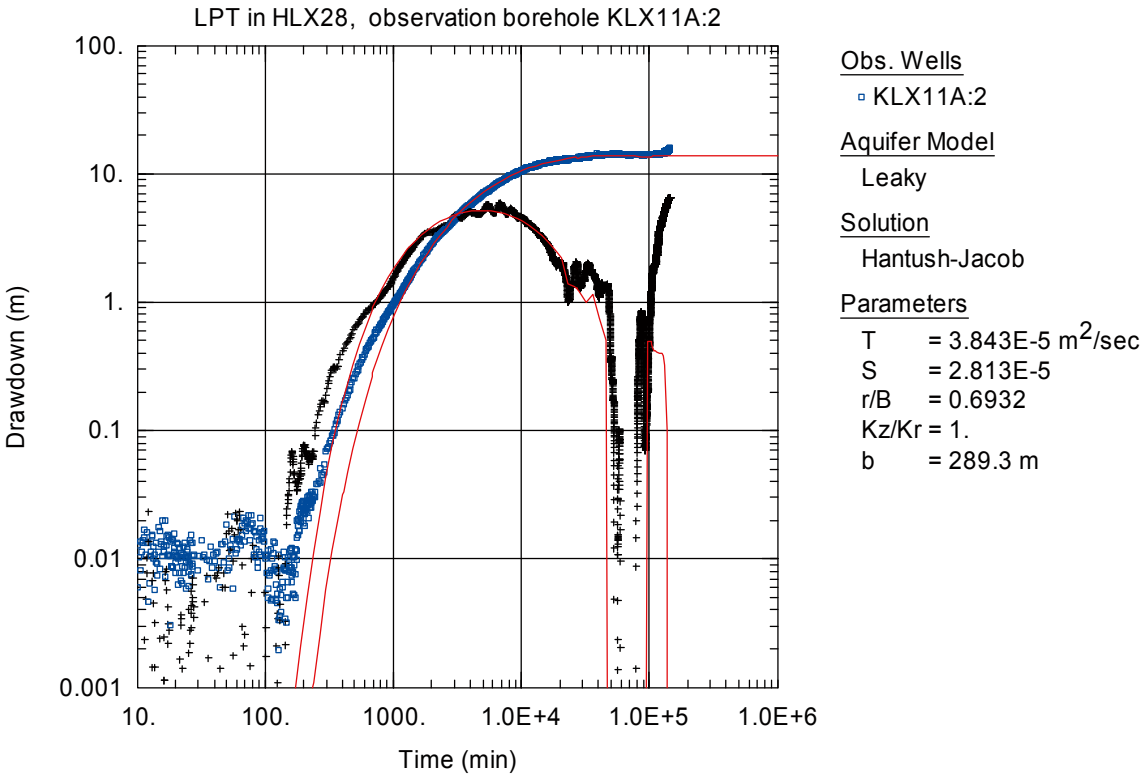

Figure A6-47. *Log-log plot of drawdown (▫) and drawdown derivative, ds/d(ln t) (+), versus time in KLX11A:2 during the interference test in HLX28. Transient evaluation is based on the first part of the drawdown period.*

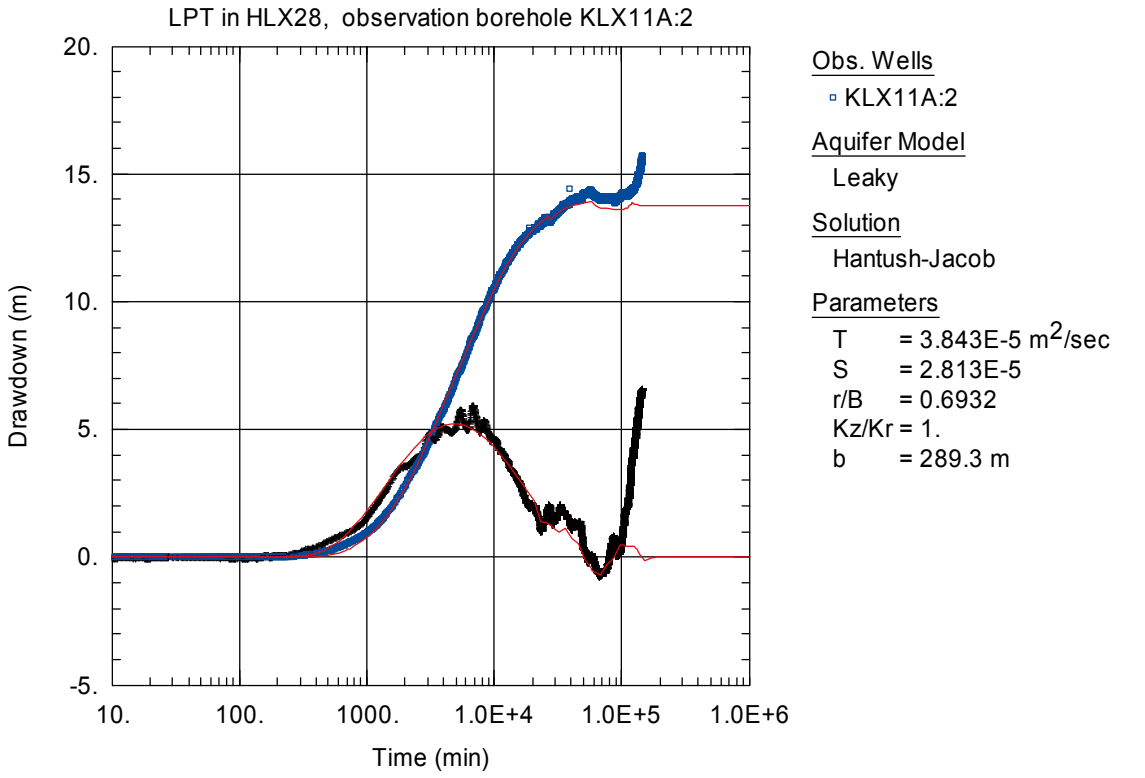

Figure A6-48. *Lin-log plot of drawdown (▫) and drawdown derivative, ds/d(ln t) (+), versus time in KLX11A:2 during the interference test in HLX28. Transient evaluation is based on the first part of the drawdown period.*

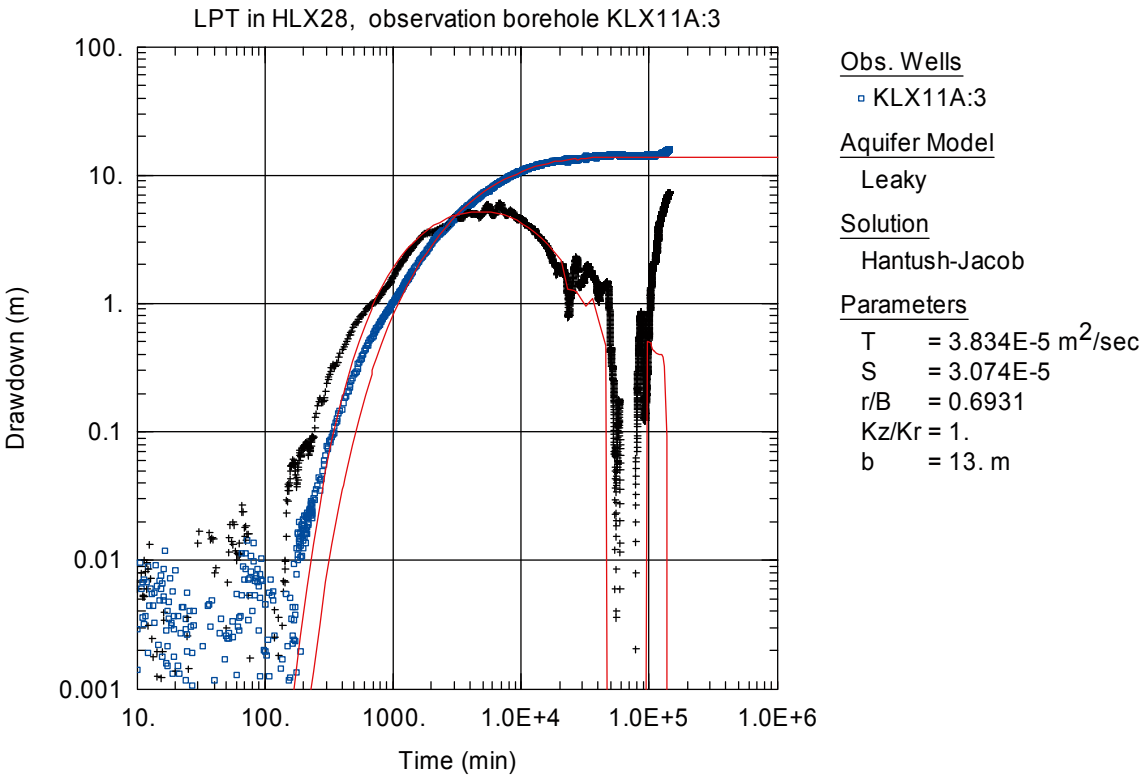

Figure A6-49. *Log-log plot of drawdown (▫) and drawdown derivative, ds/d(ln t) (+), versus time in KLX11A:3 during the interference test in HLX28. Transient evaluation is based on the first part of the drawdown period. The section was used for tracer injection.*

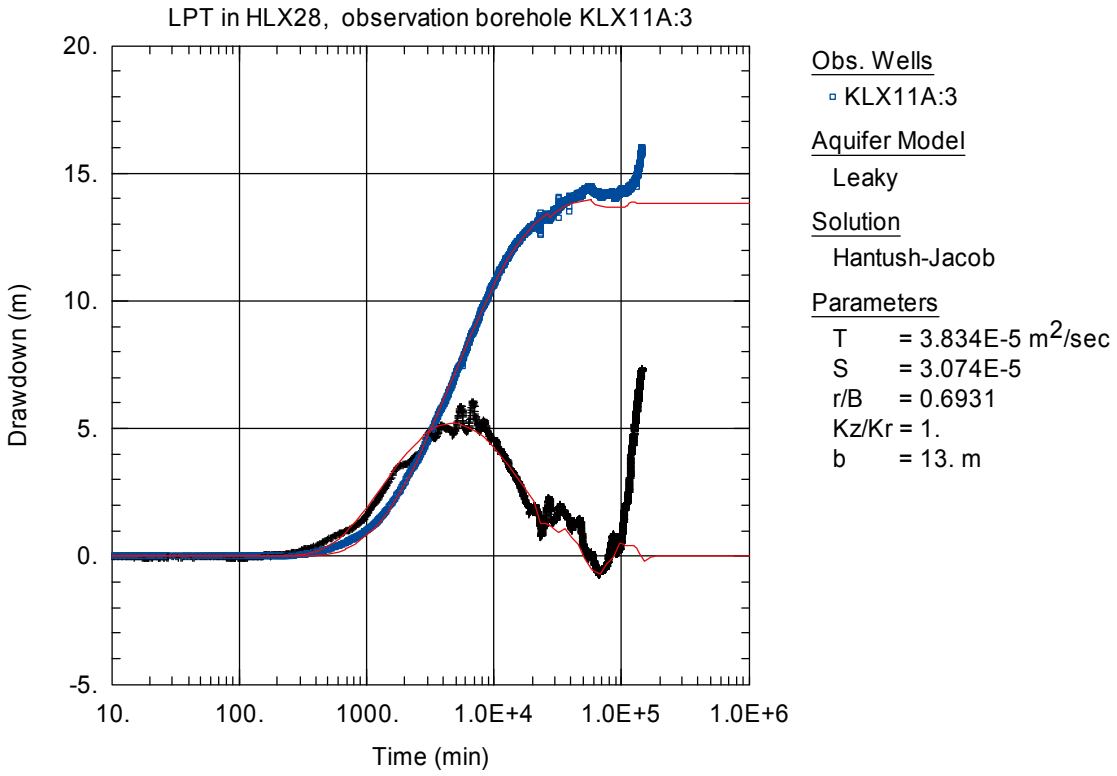

Figure A6-50. *Lin-log plot of drawdown (▫) and drawdown derivative, ds/d(ln t) (+), versus time in KLX11A:3 during the interference test in HLX28. Transient evaluation is based on the first part of the drawdown period. The section was used for tracer injection.*

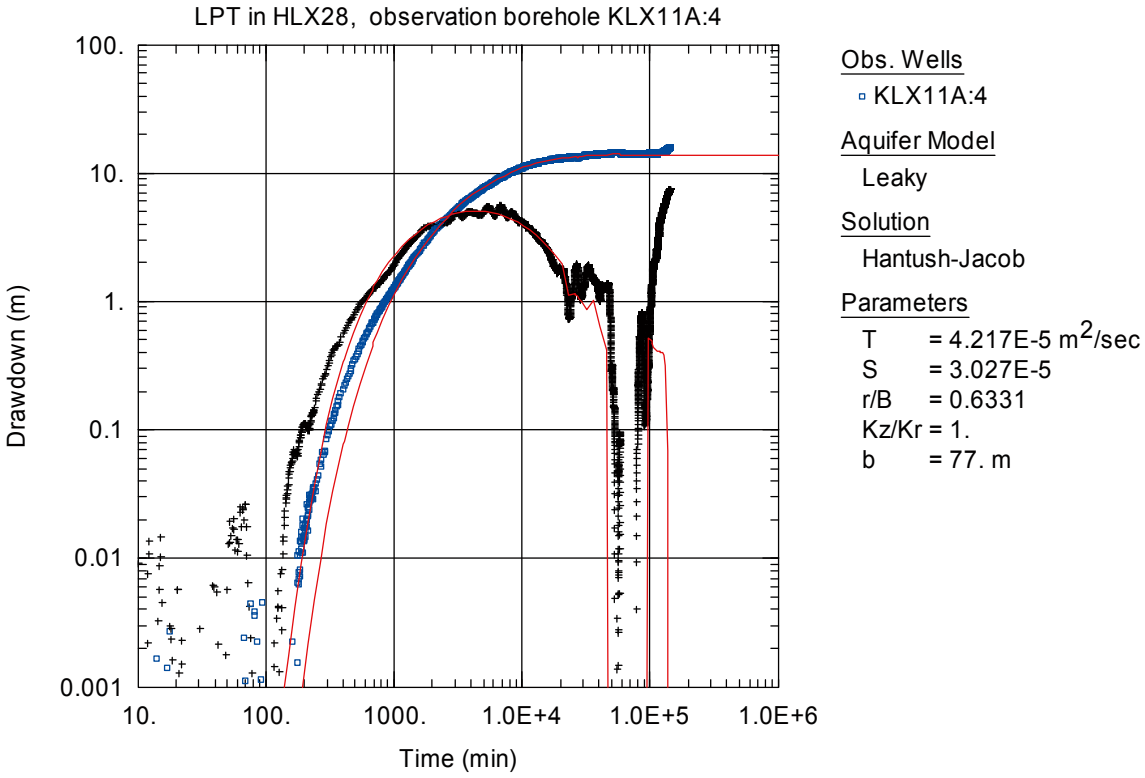

Figure A6-51. *Log-log plot of drawdown (▫) and drawdown derivative, ds/d(ln t) (+), versus time in KLX11A:4 during the interference test in HLX28. Transient evaluation is based on the first part of the drawdown period.*

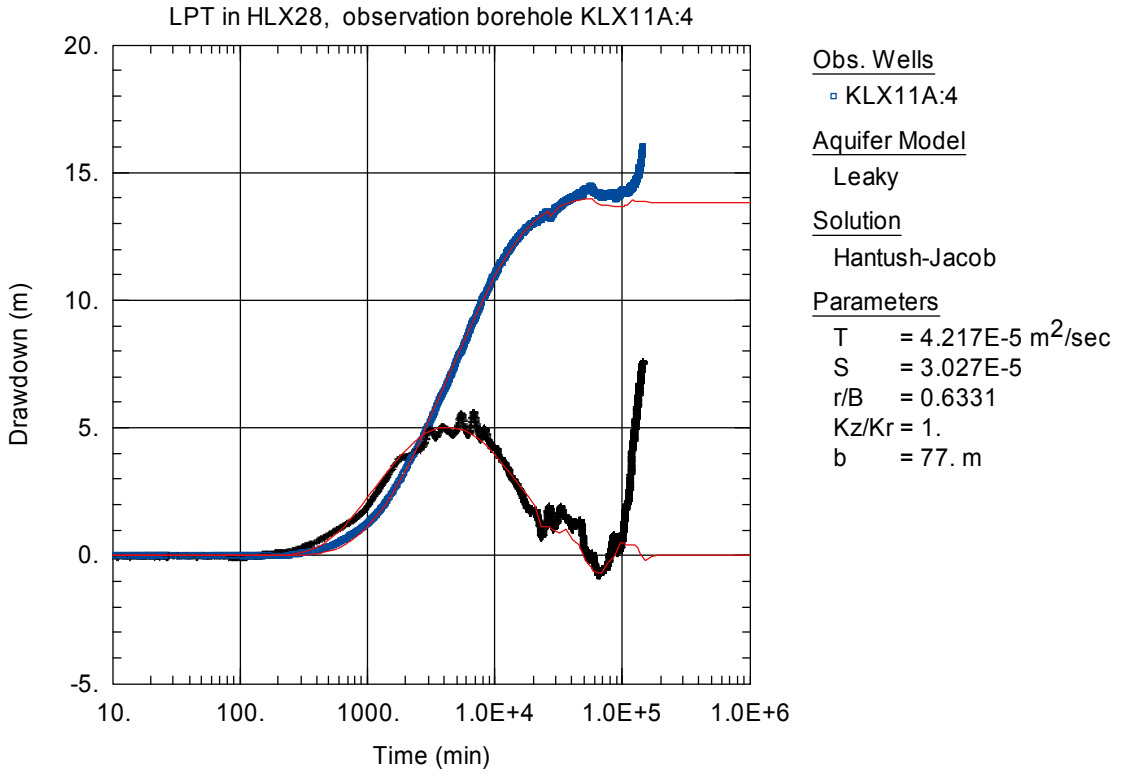

Figure A6-52. *Lin-log plot of drawdown (▫) and drawdown derivative, ds/d(ln t) (+), versus time in KLX11A:4 during the interference test in HLX28. Transient evaluation is based on the first part of the drawdown period.*

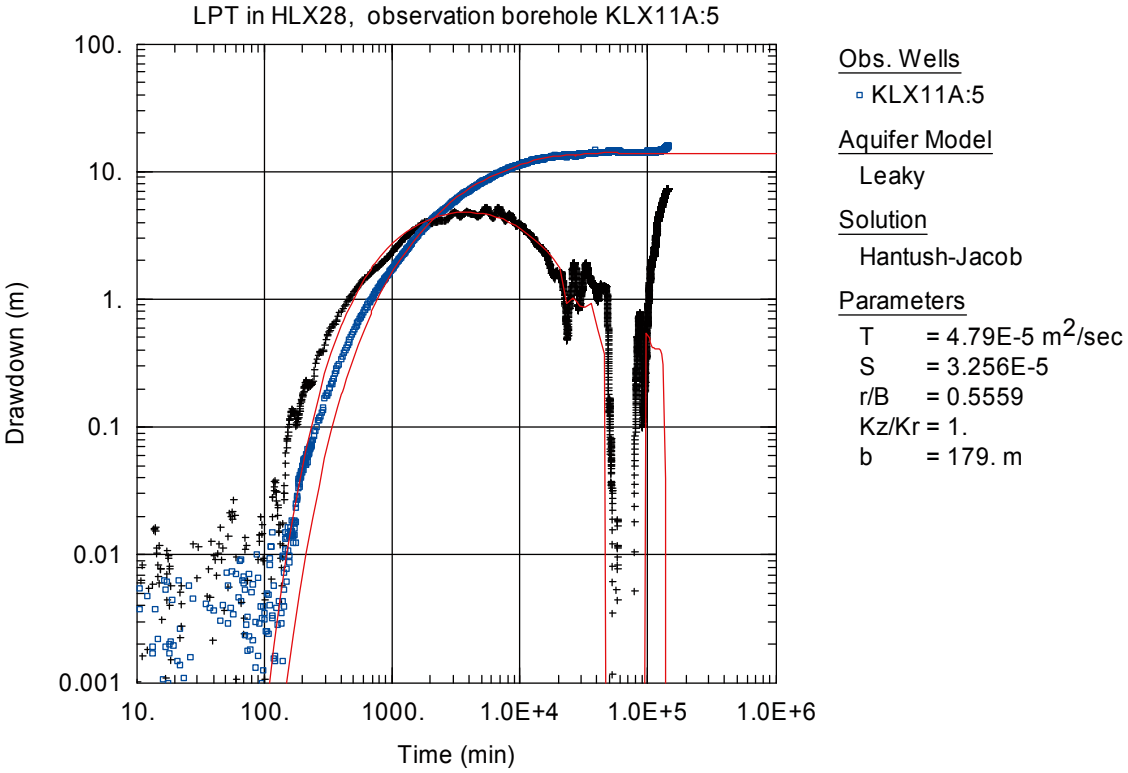

Figure A6-53. *Log-log plot of drawdown (▫) and drawdown derivative, ds/d(ln t) (+), versus time in KLX11A:5 during the interference test in HLX28. Transient evaluation is based on the first part of the drawdown period.*

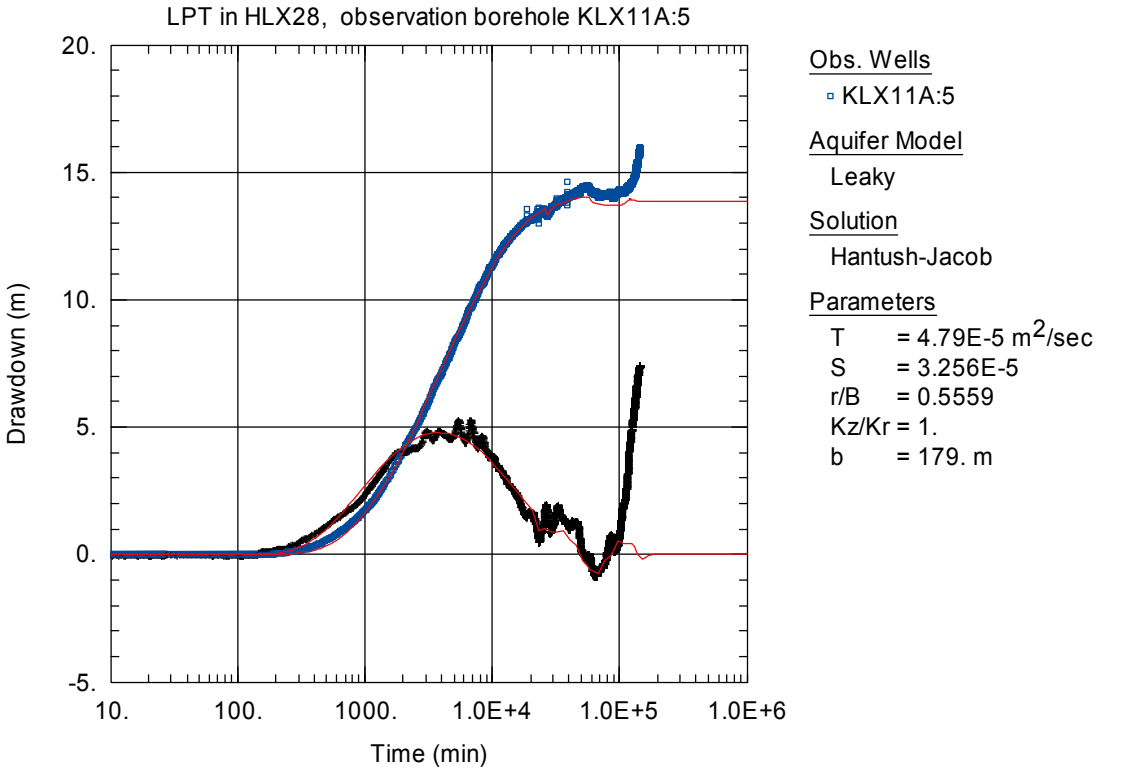

Figure A6-54. *Lin-log plot of drawdown (▫) and drawdown derivative, ds/d(ln t) (+), versus time in KLX11A:5 during the interference test in HLX28. Transient evaluation is based on the first part of the drawdown period.*

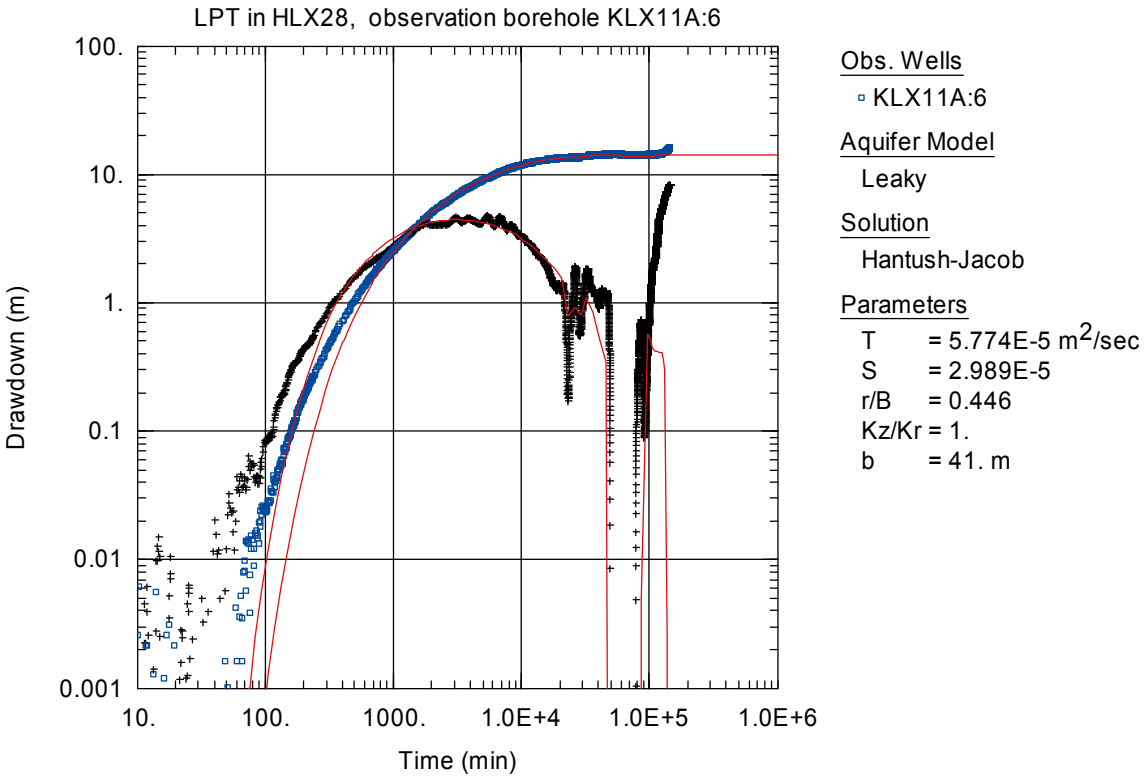

Figure A6-55. *Log-log plot of drawdown (▫) and drawdown derivative, ds/d(ln t) (+), versus time in KLX11A:6 during the interference test in HLX28. Transient evaluation is based on the first part of the drawdown period.*

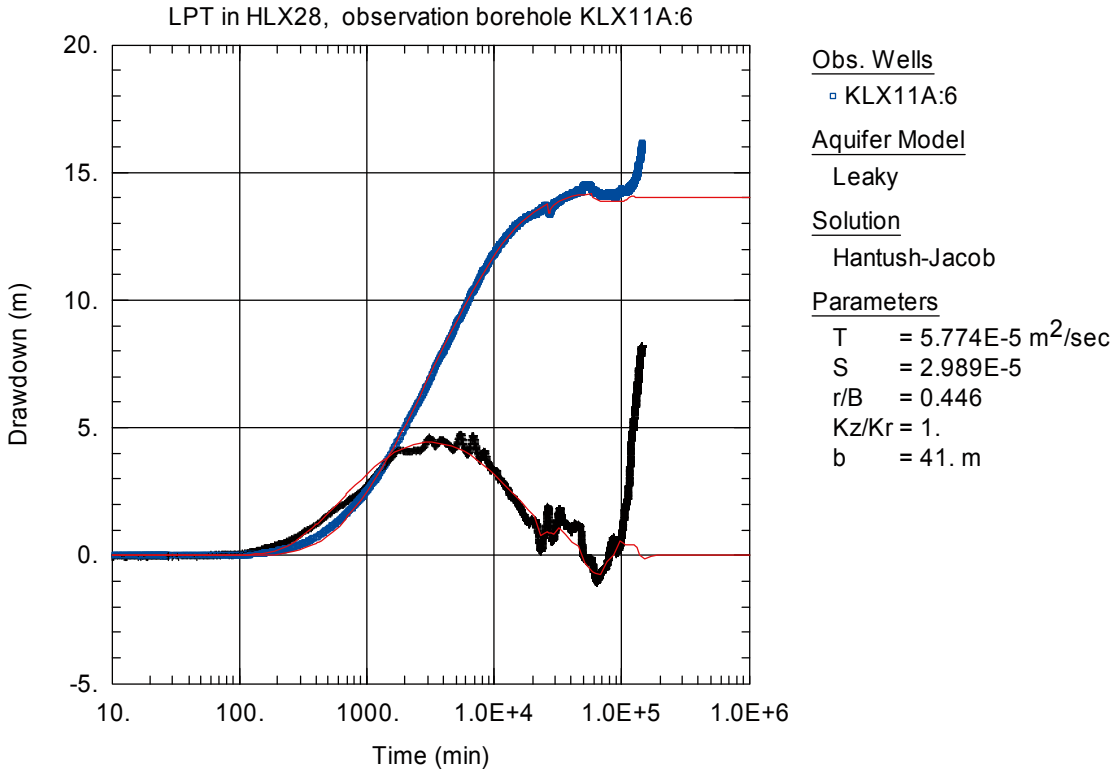

Figure A6-56. *Lin-log plot of drawdown (▫) and drawdown derivative, ds/d(ln t) (+), versus time in KLX11A:6during the interference test in HLX28. Transient evaluation is based on the first part of the drawdown period.*

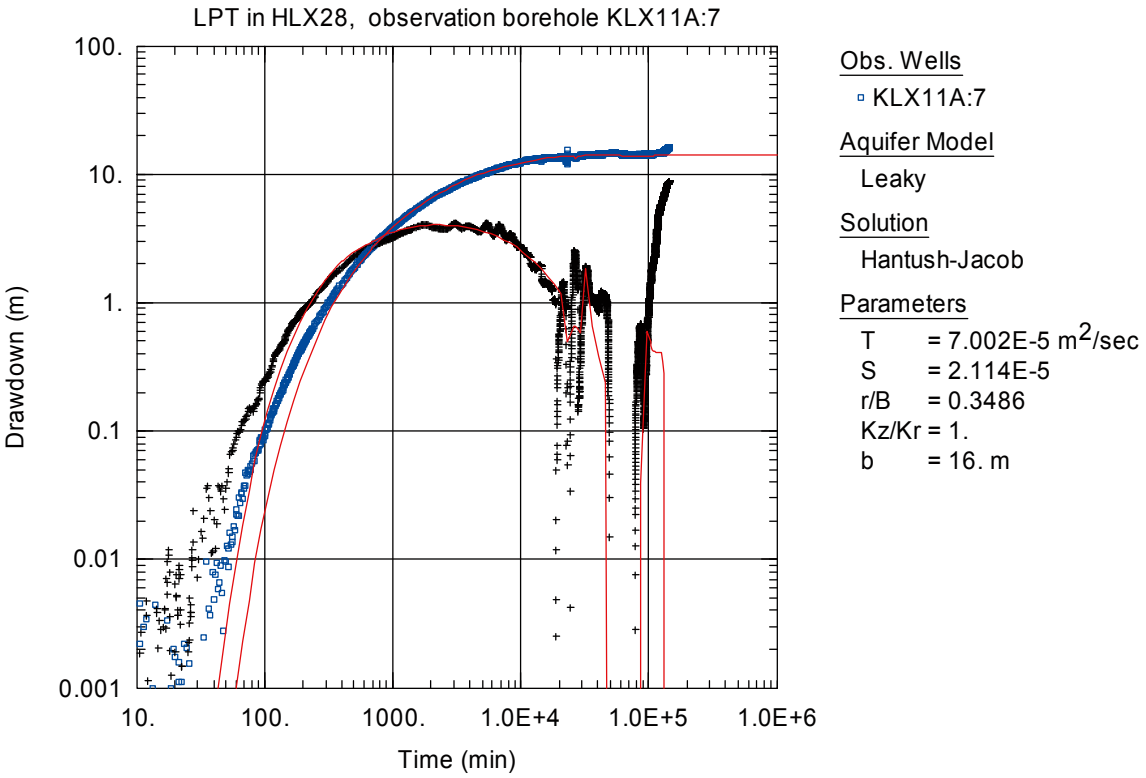

Figure A6-57. *Log-log plot of drawdown (▫) and drawdown derivative, ds/d(ln t) (+), versus time in KLX11A:7 during the interference test in HLX28. Transient evaluation is based on the first part of the drawdown period.*

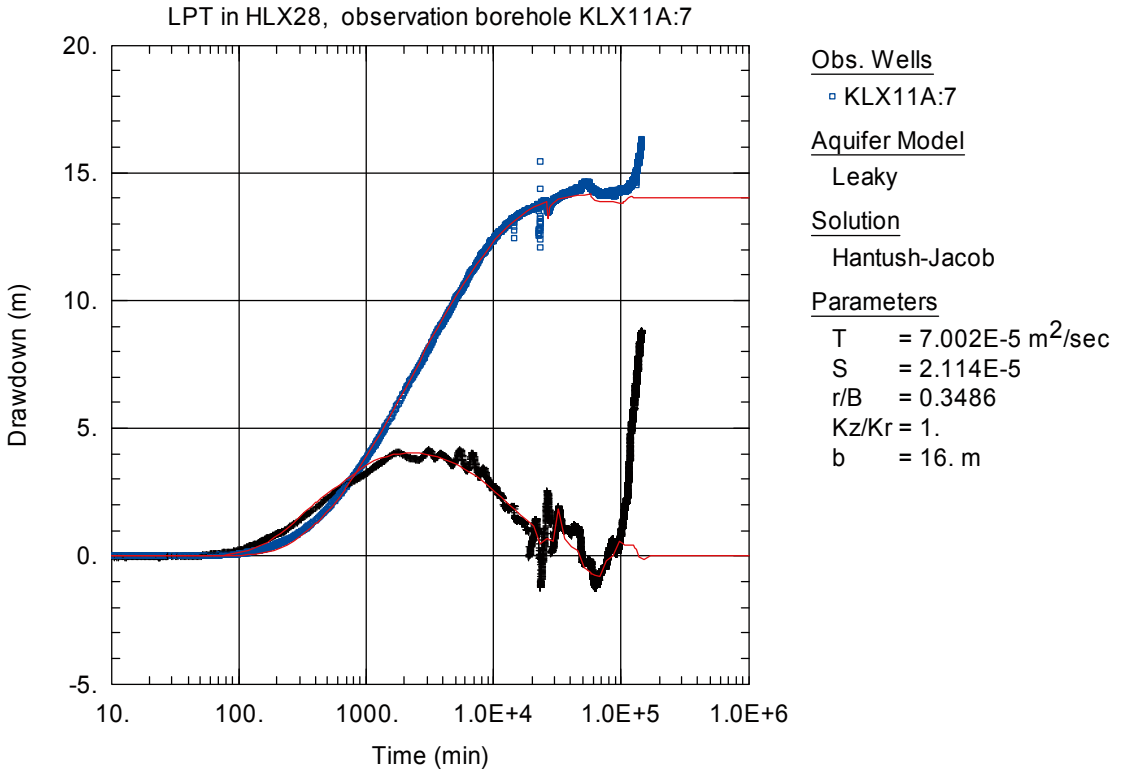

Figure A6-58. *Lin-log plot of drawdown (▫) and drawdown derivative, ds/d(ln t) (+), versus time in KLX11A:7 during the interference test in HLX28. Transient evaluation is based on the first part of the drawdown period.*

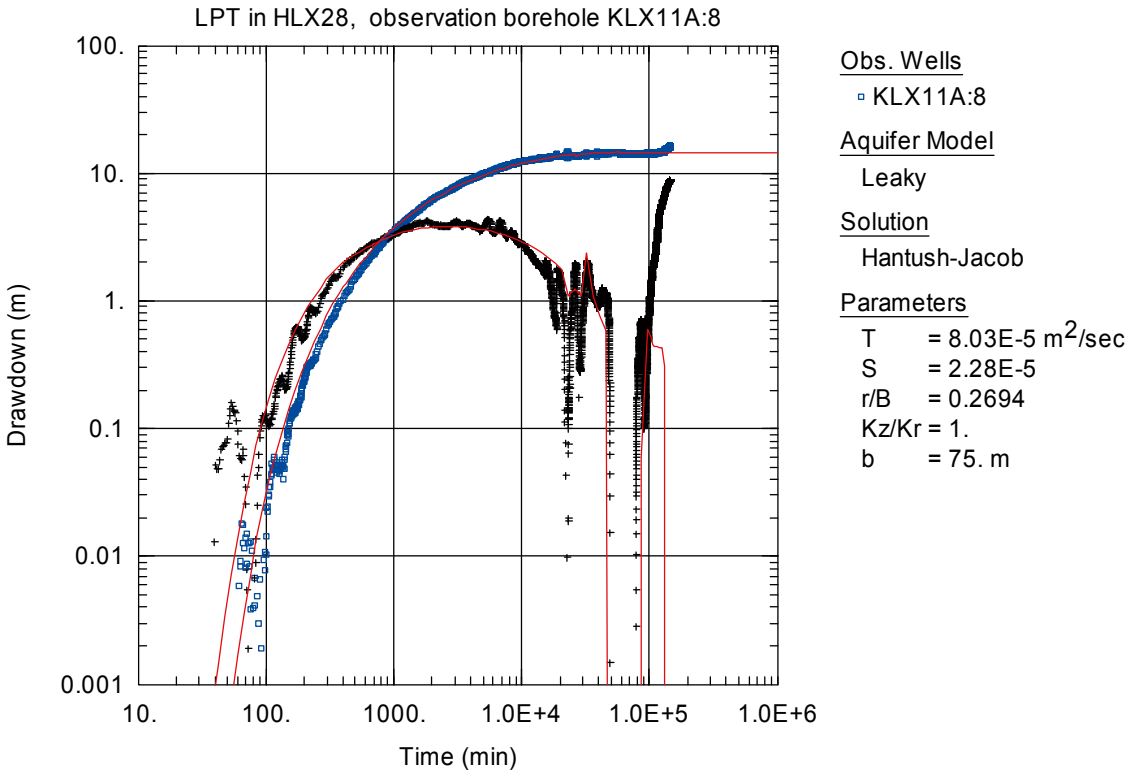

Figure A6-59. *Log-log plot of drawdown (▫) and drawdown derivative, ds/d(ln t) (+), versus time in KLX11A:8 during the interference test in HLX28. Transient evaluation is based on the first part of the drawdown period.*

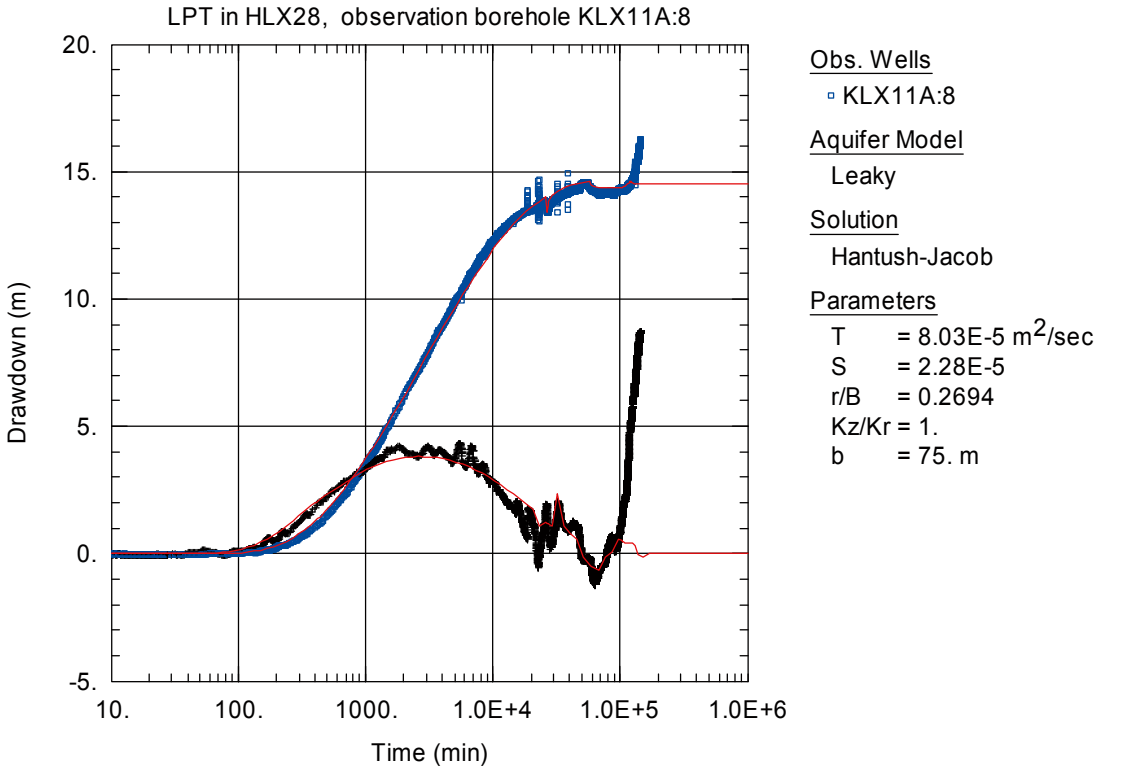

Figure A6-60. *Lin-log plot of drawdown (▫) and drawdown derivative, ds/d(ln t) (+), versus time in KLX11A:8 during the interference test in HLX28. Transient evaluation is based on the first part of the drawdown period.*

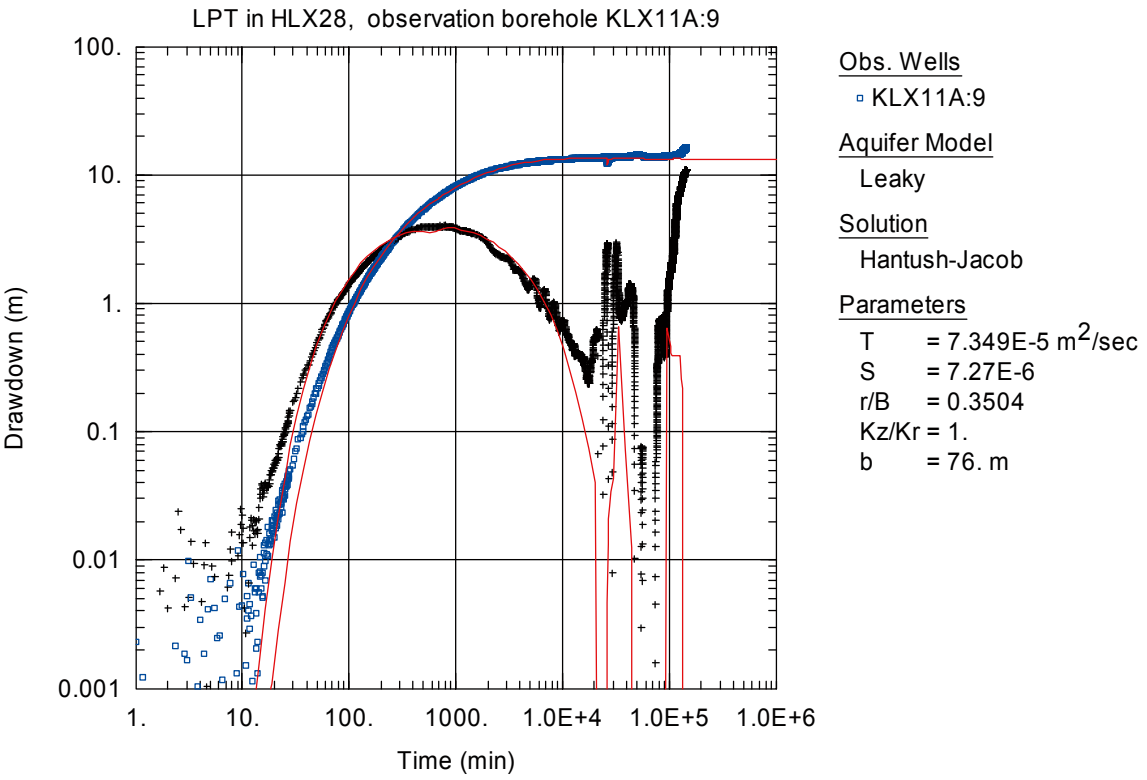

Figure A6-61. *Log-log plot of drawdown (▫) and drawdown derivative, ds/d(ln t) (+), versus time in KLX11A:9 during the interference test in HLX28. Transient evaluation is based on the first part of the drawdown period.*

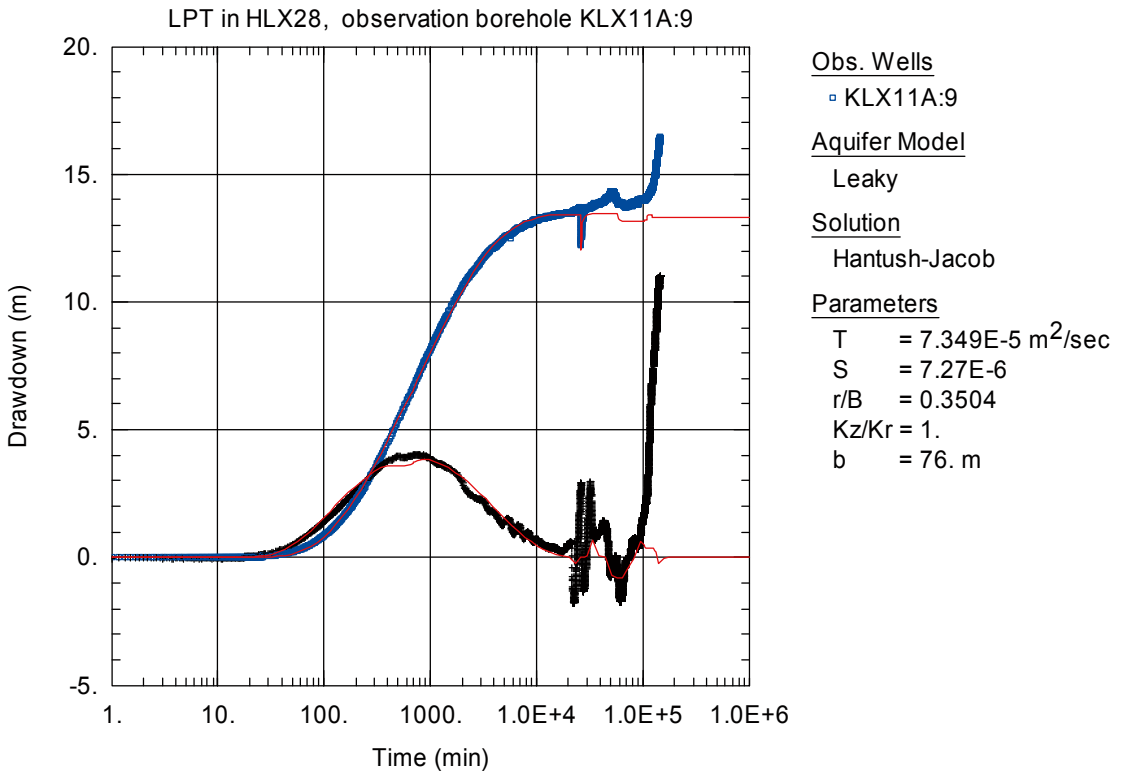

Figure A6-62. *Lin-log plot of drawdown (▫) and drawdown derivative, ds/d(ln t) (+), versus time in KLX11A:9 during the interference test in HLX28. Transient evaluation is based on the first part of the drawdown period.*

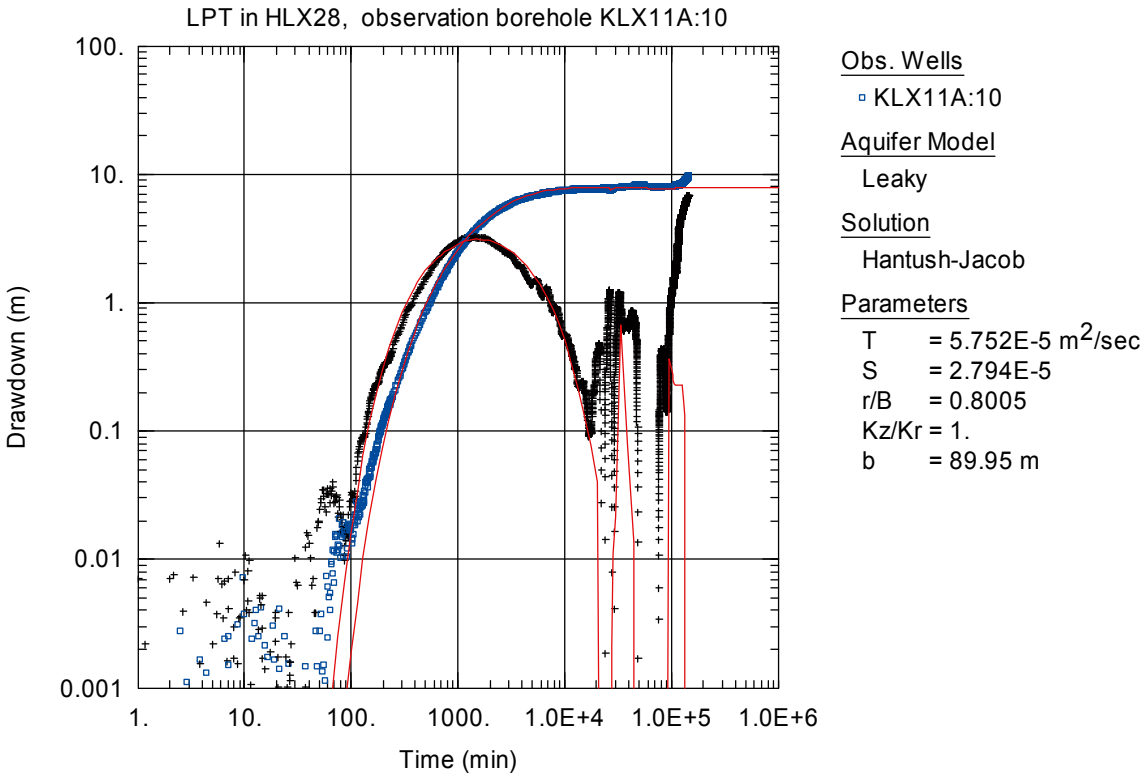

Figure A6-63. *Log-log plot of drawdown (▫) and drawdown derivative, ds/d(ln t) (+), versus time in KLX11A:10 during the interference test in HLX28. Transient evaluation is based on the first part of the drawdown period.*

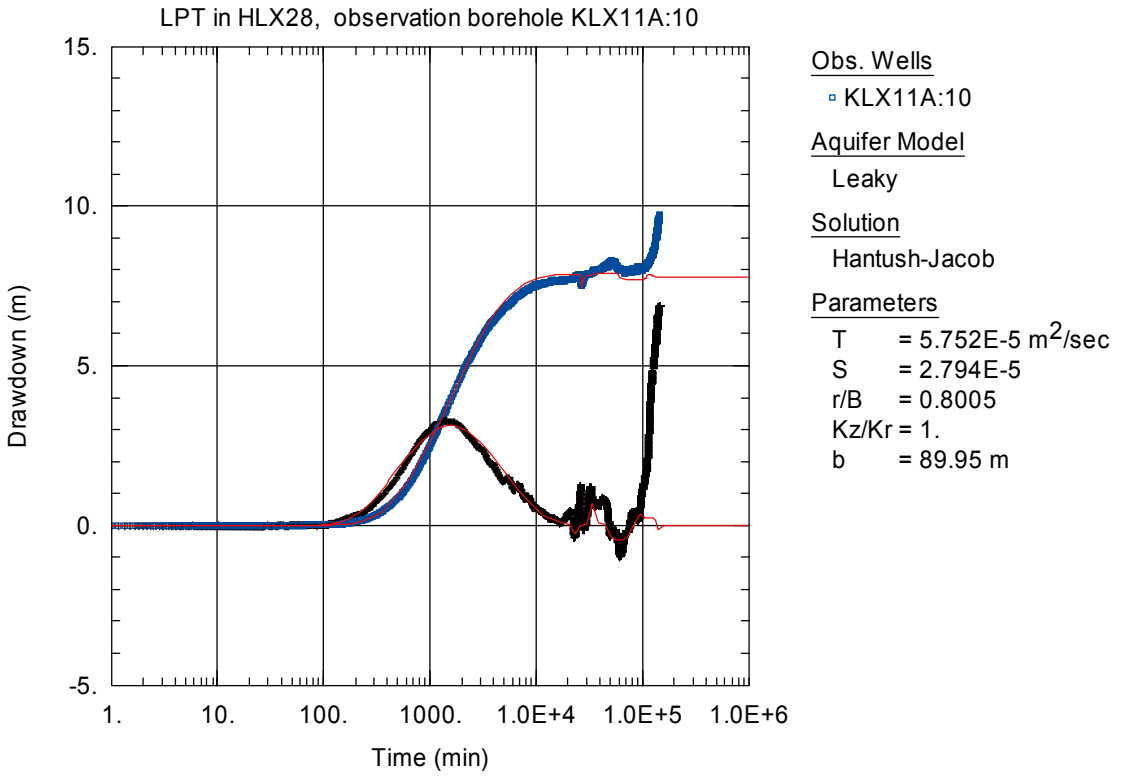

Figure A6-64. *Lin-log plot of drawdown (▫) and drawdown derivative, ds/d(ln t) (+), versus time in KLX11A:10 during the interference test in HLX28. Transient evaluation is based on the first part of the drawdown period.*

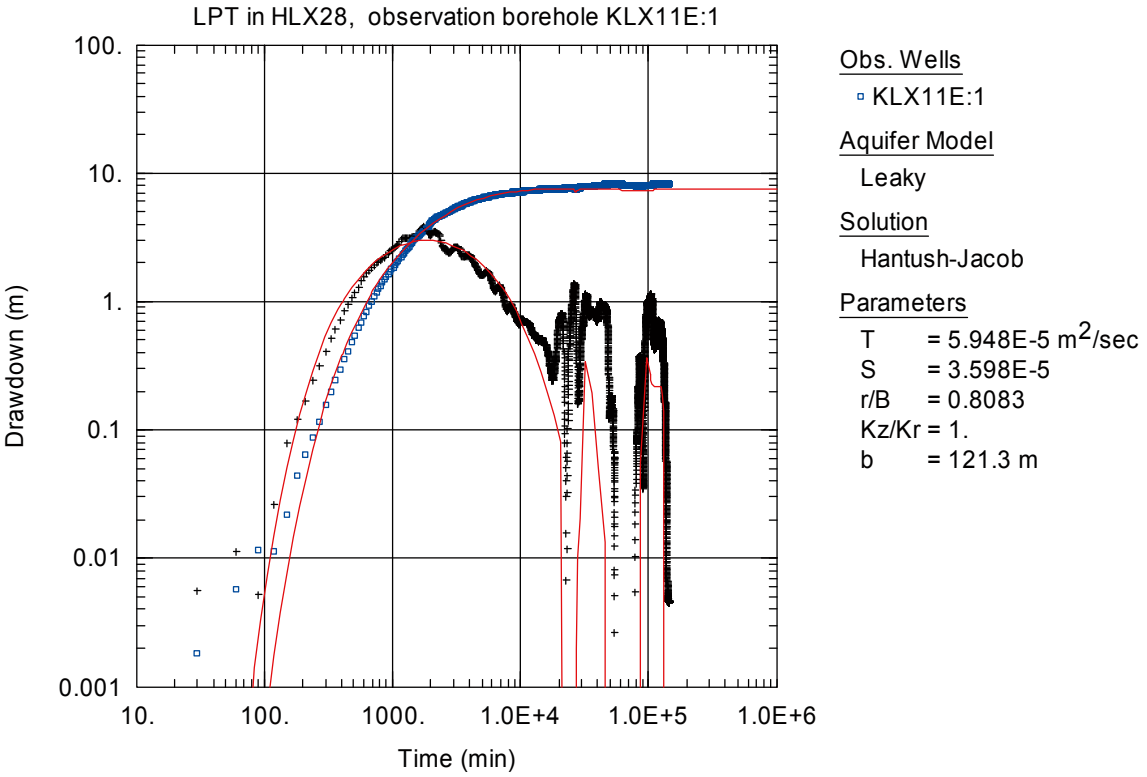

Figure A6-65. *Log-log plot of drawdown (▫) and drawdown derivative, ds/d(ln t) (+), versus time in KLX11E:1 during the interference test in HLX28. Transient evaluation is based on the first part of the drawdown period.*

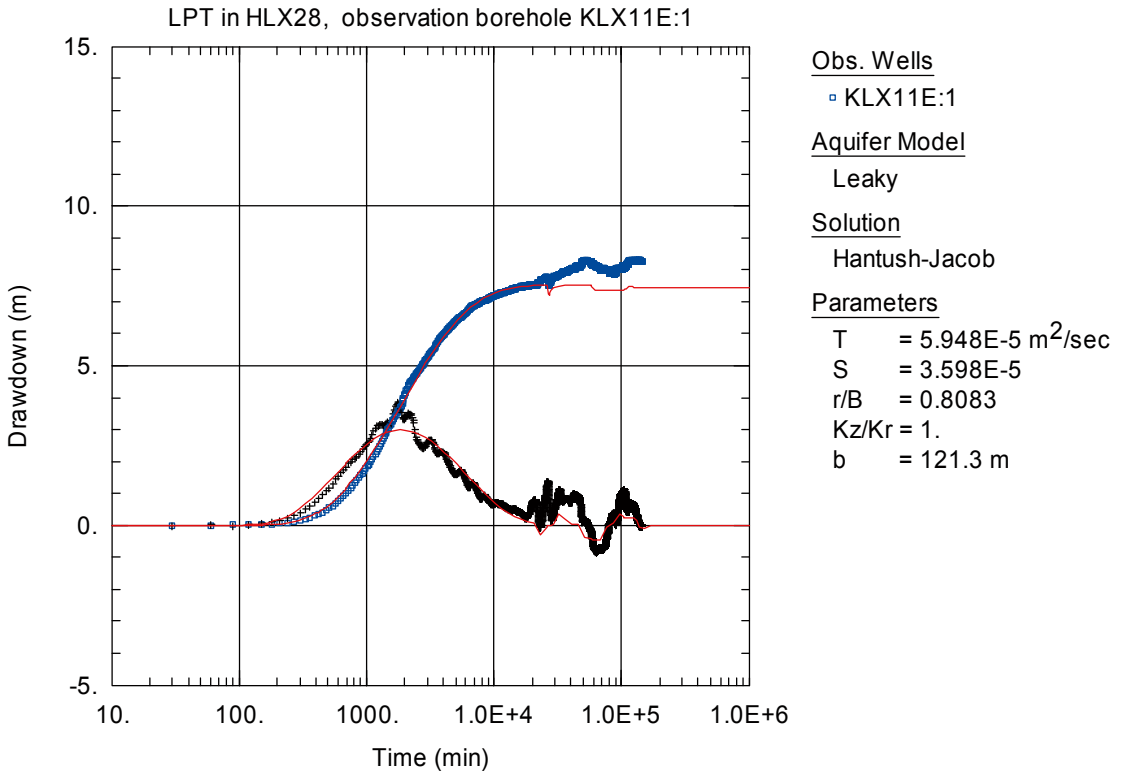

Figure A6-66. *Lin-log plot of drawdown (▫) and drawdown derivative, ds/d(ln t) (+), versus time in KLX11E:1 during the interference test in HLX28. Transient evaluation is based on the first part of the drawdown period.*

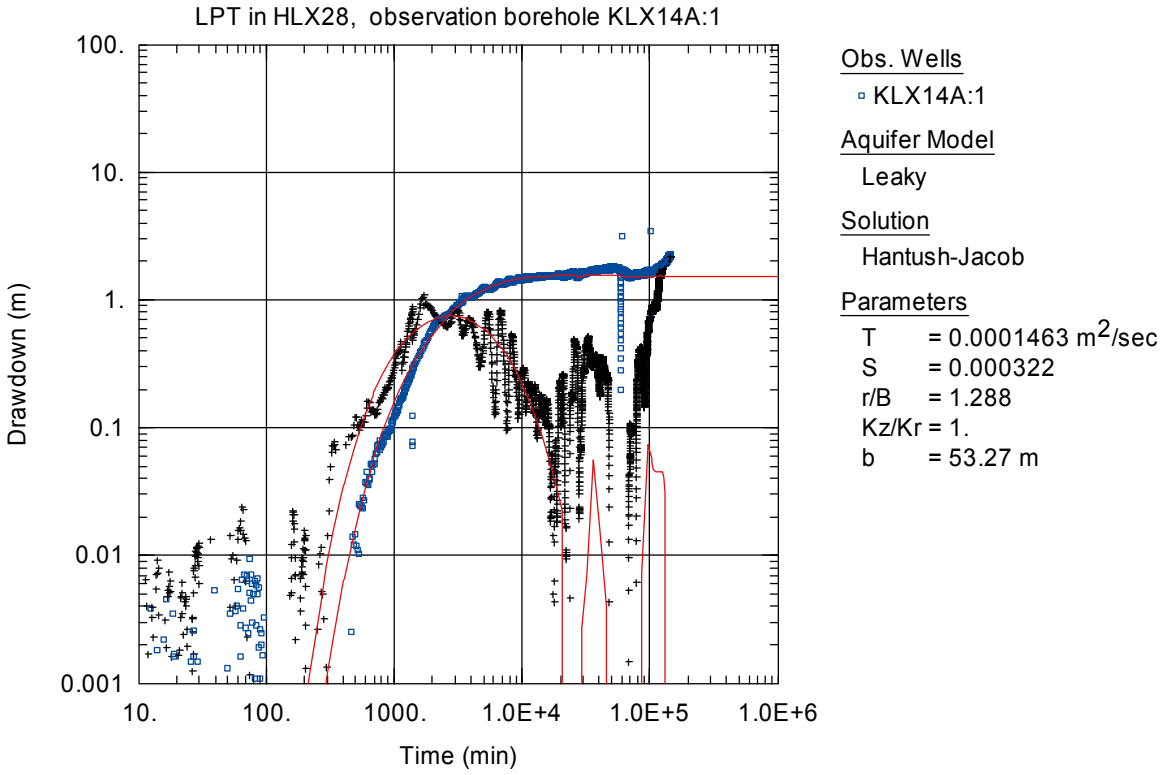

Figure A6-67. *Log-log plot of drawdown (▫) and drawdown derivative, ds/d(ln t) (+), versus time in KLX14A:1 during the interference test in HLX28. Transient evaluation is based on the first part of the drawdown period.*

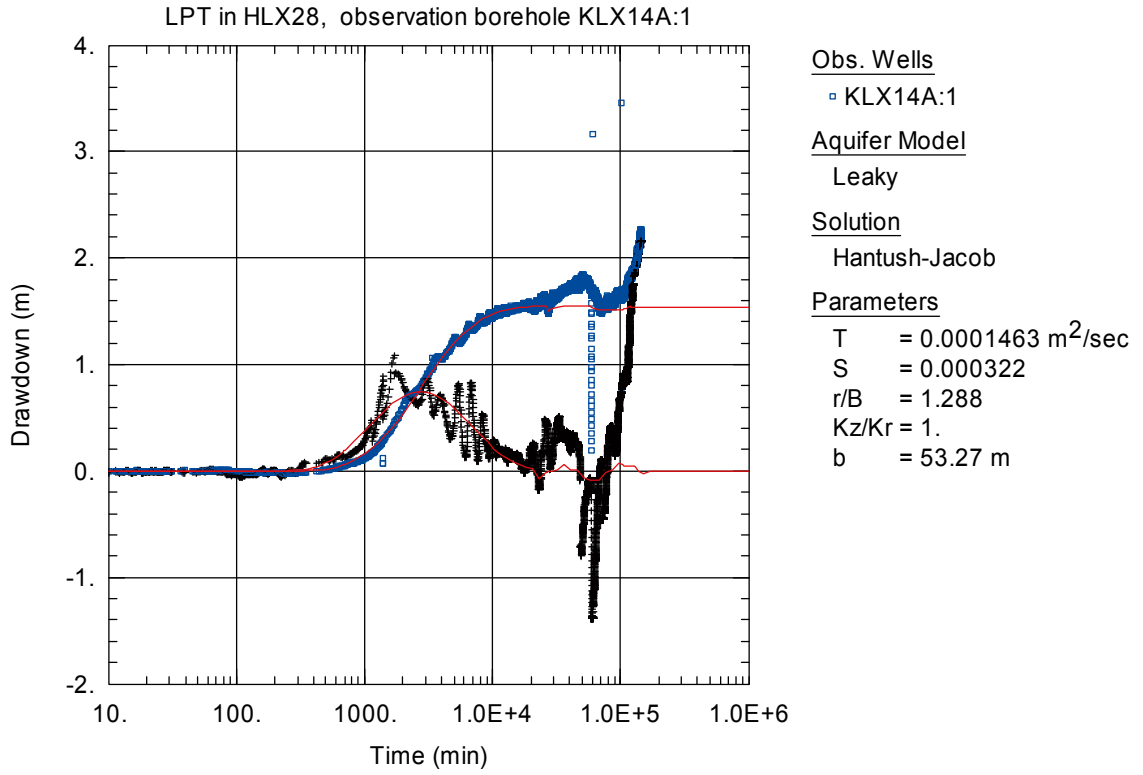

Figure A6-68. *Lin-log plot of drawdown (▫) and drawdown derivative, ds/d(ln t) (+), versus time in KLX14A:1 during the interference test in HLX28. Transient evaluation is based on the first part of the drawdown period.*

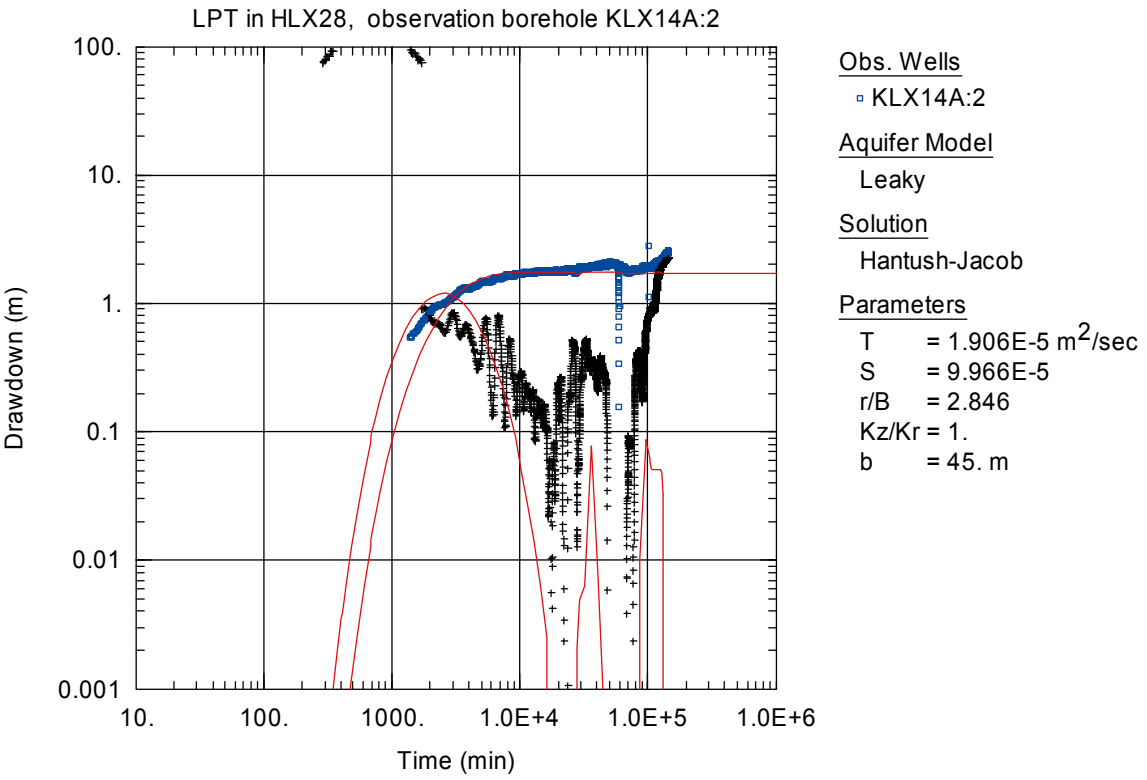

Figure A6-69. *Log-log plot of drawdown (▫) and drawdown derivative, ds/d(ln t) (+), versus time in KLX14A:2 during the interference test in HLX28. No unambiguous transient evaluation could be made for this section due to missing data in the beginning. The presented evaluation is only an example of possible evaluations.*

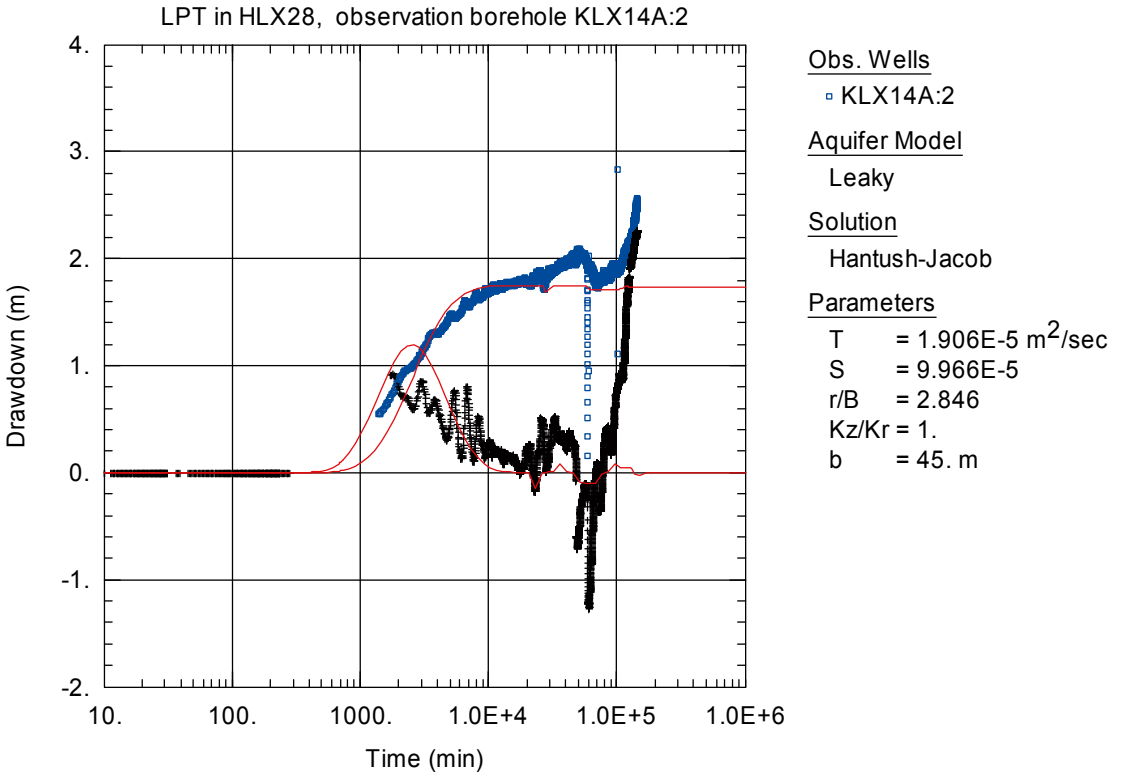

Figure A6-70. *Lin-log plot of drawdown (▫) and drawdown derivative, ds/d(ln t) (+), versus time in KLX14A:2 during the interference test in HLX28. No unambiguous transient evaluation could be made for this section due to missing data in the beginning.*

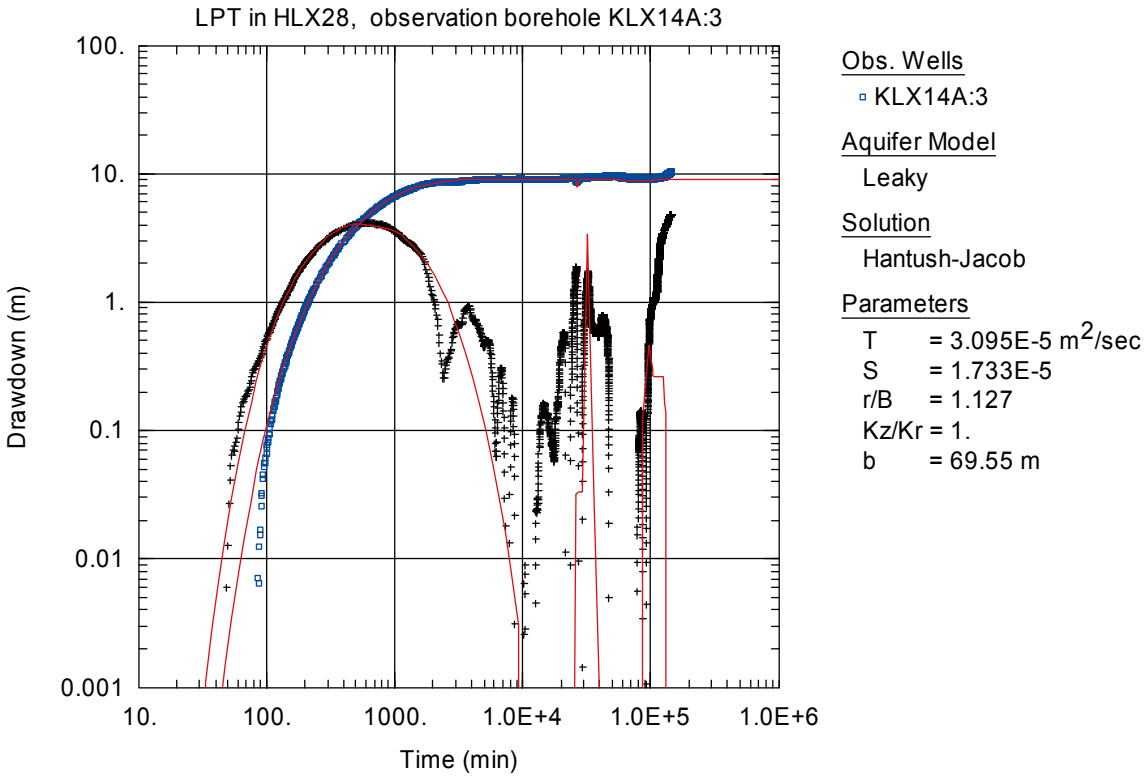

Figure A6-71. *Log-log plot of drawdown (▫) and drawdown derivative, ds/d(ln t) (+), versus time in KLX14A:3 during the interference test in HLX28. Transient evaluation is based on the first part of the drawdown period.*

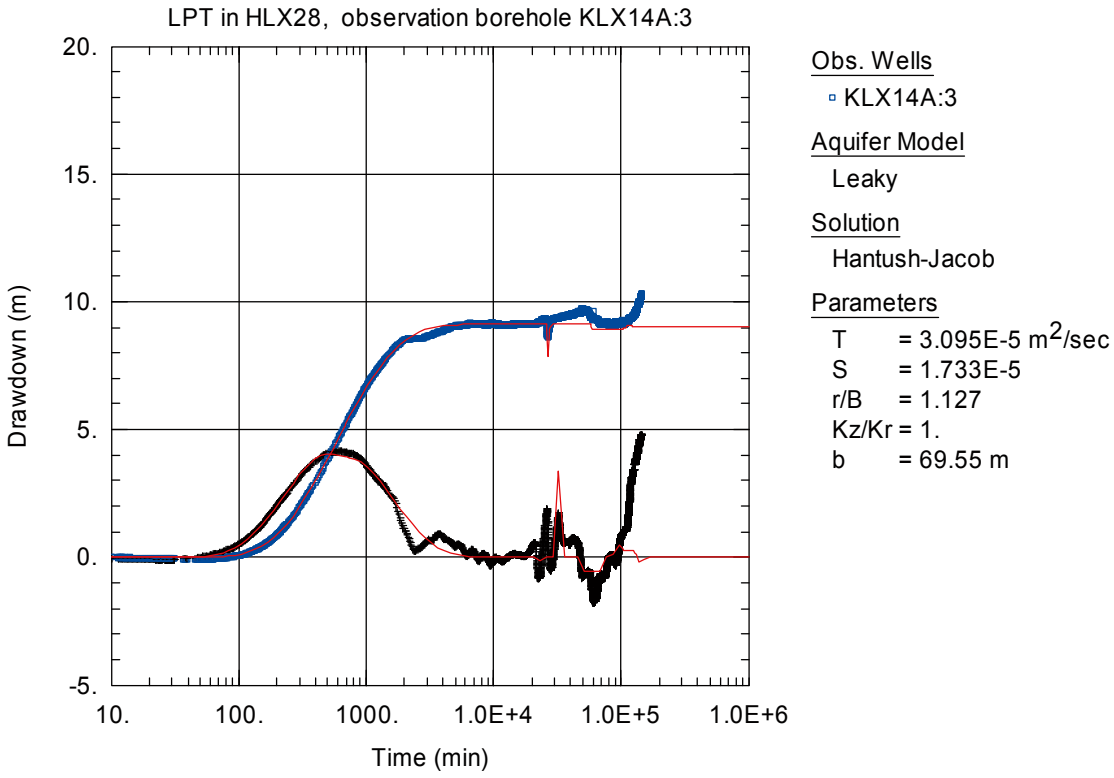

Figure A6-72. *Lin-log plot of drawdown (▫) and drawdown derivative, ds/d(ln t) (+), versus time in KLX14A:3 during the interference test in HLX28. Transient evaluation is based on the first part of the drawdown period.*

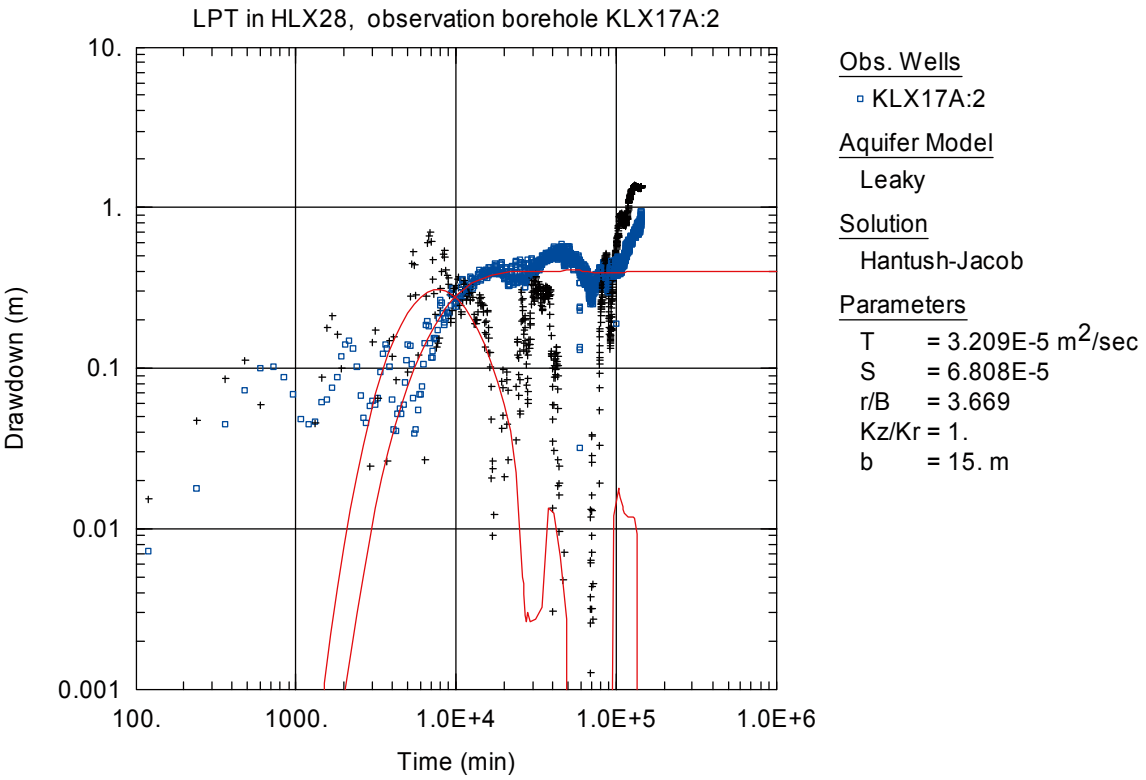

Figure A6-73. *Log-log plot of drawdown (▫) and drawdown derivative, ds/d(ln t) (+), versus time in KLX17A:2 during the interference test in HLX28. Transient evaluation is based on the first part of the drawdown period.*

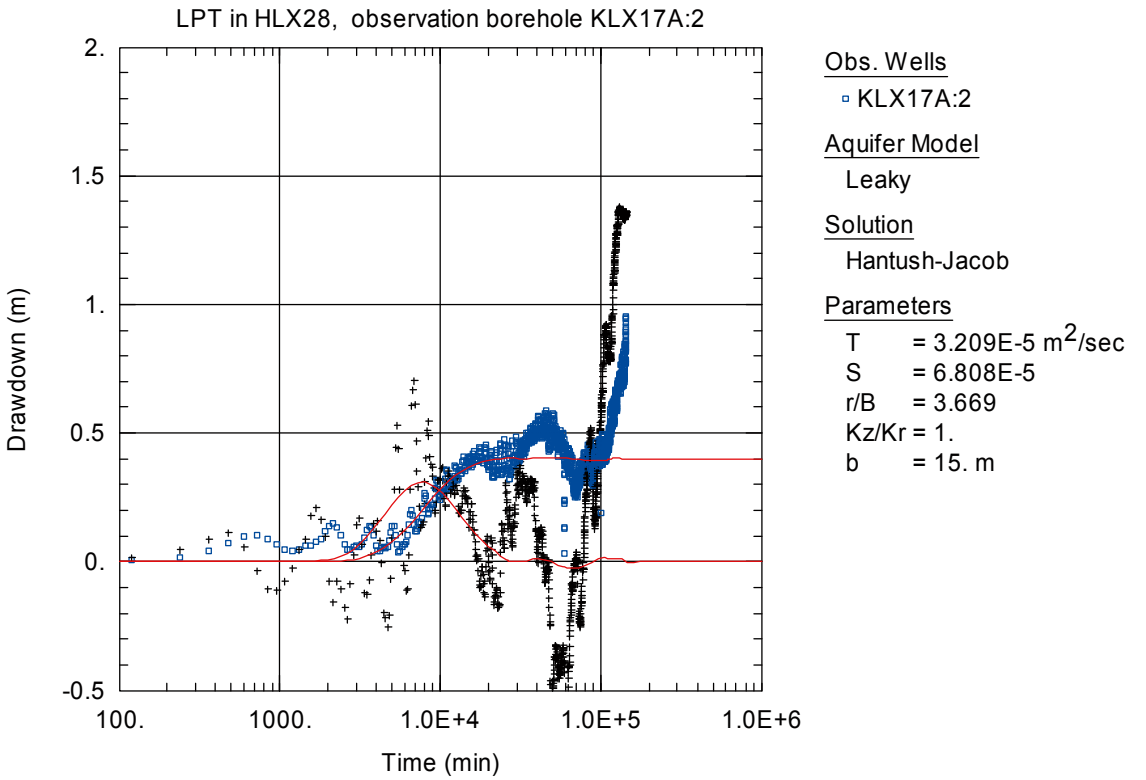

Figure A6-74. *Lin-log plot of drawdown (▫) and drawdown derivative, ds/d(ln t) (+), versus time in KLX17A:2 during the interference test in HLX28. Transient evaluation is based on the first part of the drawdown period.*

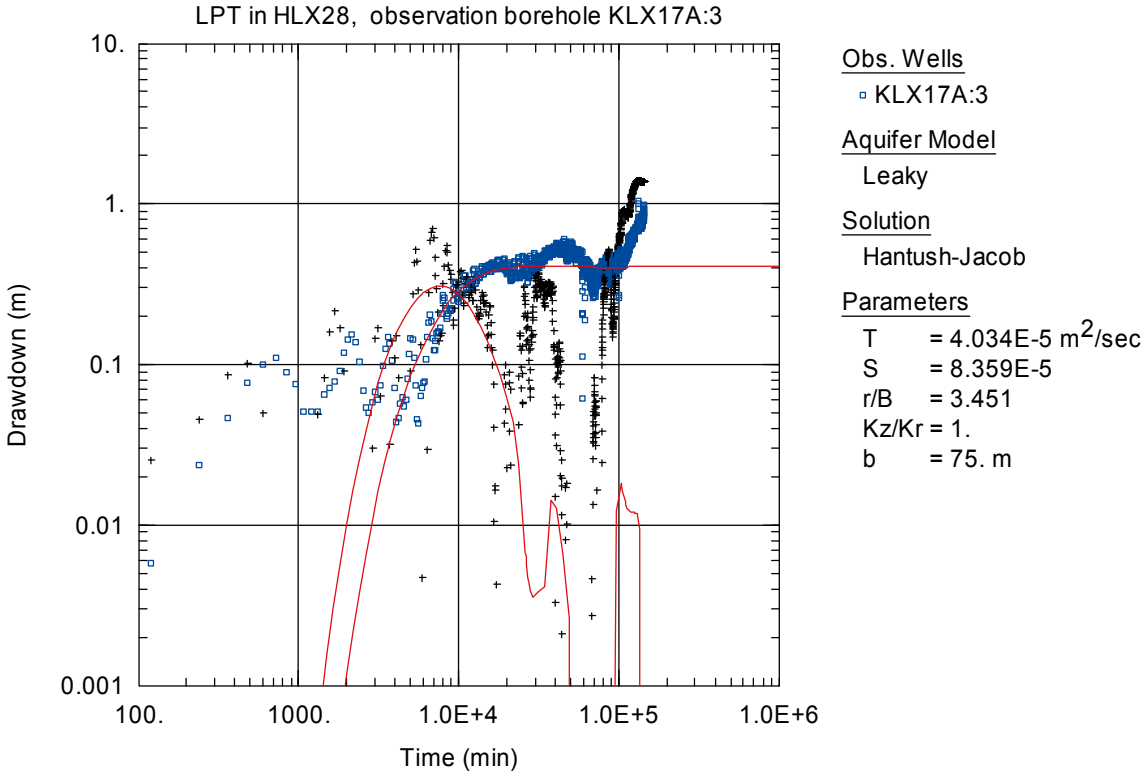

Figure A6-75. *Log-log plot of drawdown (▫) and drawdown derivative, ds/d(ln t) (+), versus time in KLX17A:3 during the interference test in HLX28. Transient evaluation is based on the first part of the drawdown period.*

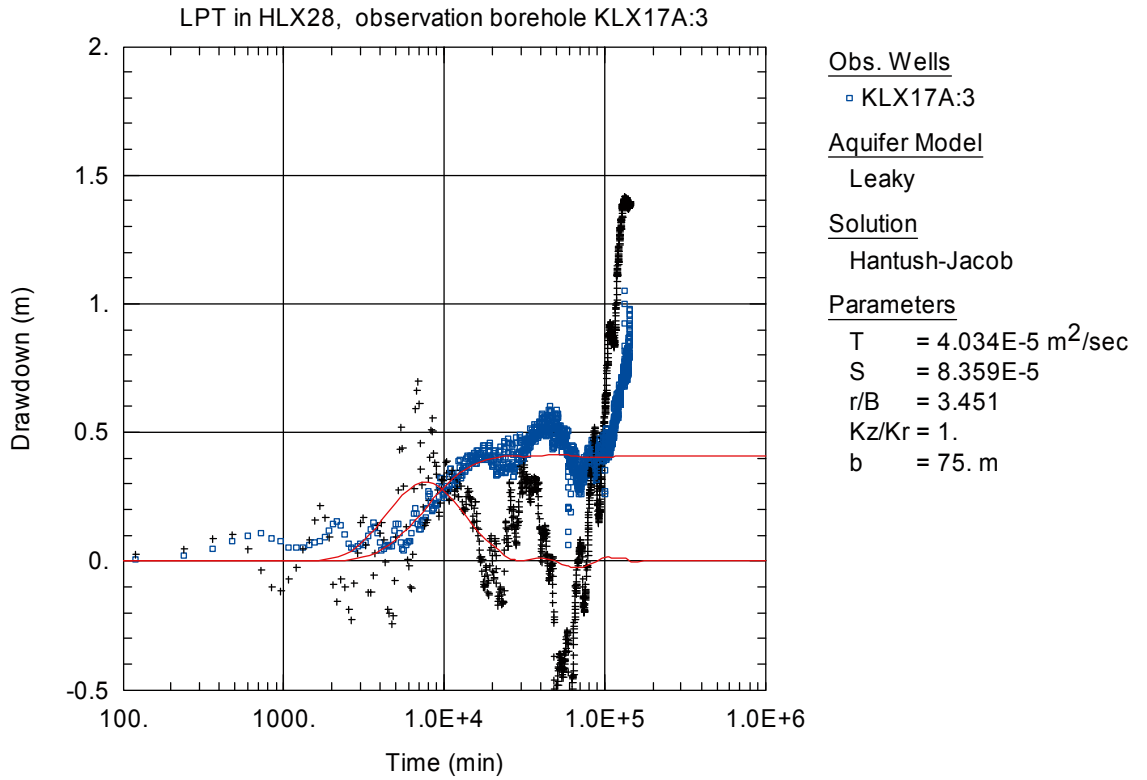

Figure A6-76. *Lin-log plot of drawdown (▫) and drawdown derivative, ds/d(ln t) (+), versus time in KLX17A:3 during the interference test in HLX28. Transient evaluation is based on the first part of the drawdown period.*

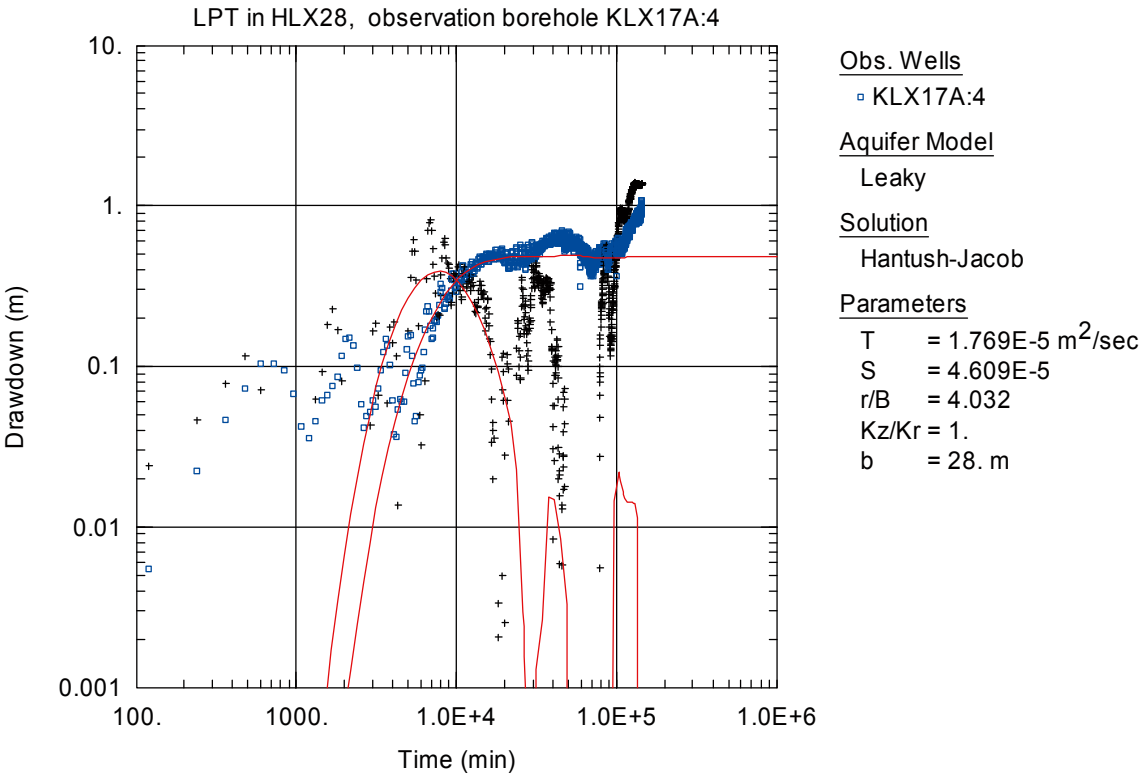

Figure A6-77. *Log-log plot of drawdown (▫) and drawdown derivative, ds/d(ln t) (+), versus time in KLX17A:4 during the interference test in HLX28. Transient evaluation is based on the first part of the drawdown period.*

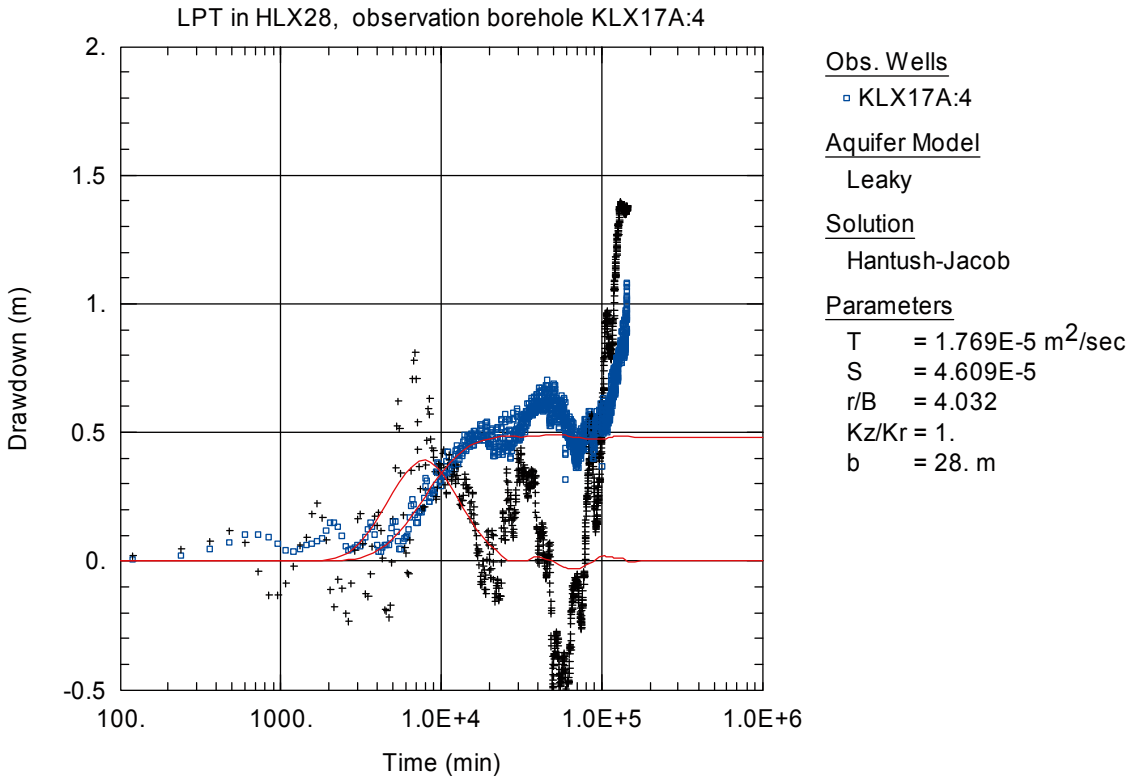

Figure A6-78. *Lin-log plot of drawdown (▫) and drawdown derivative, ds/d(ln t) (+), versus time in KLX17A:4 during the interference test in HLX28. Transient evaluation is based on the first part of the drawdown period.*

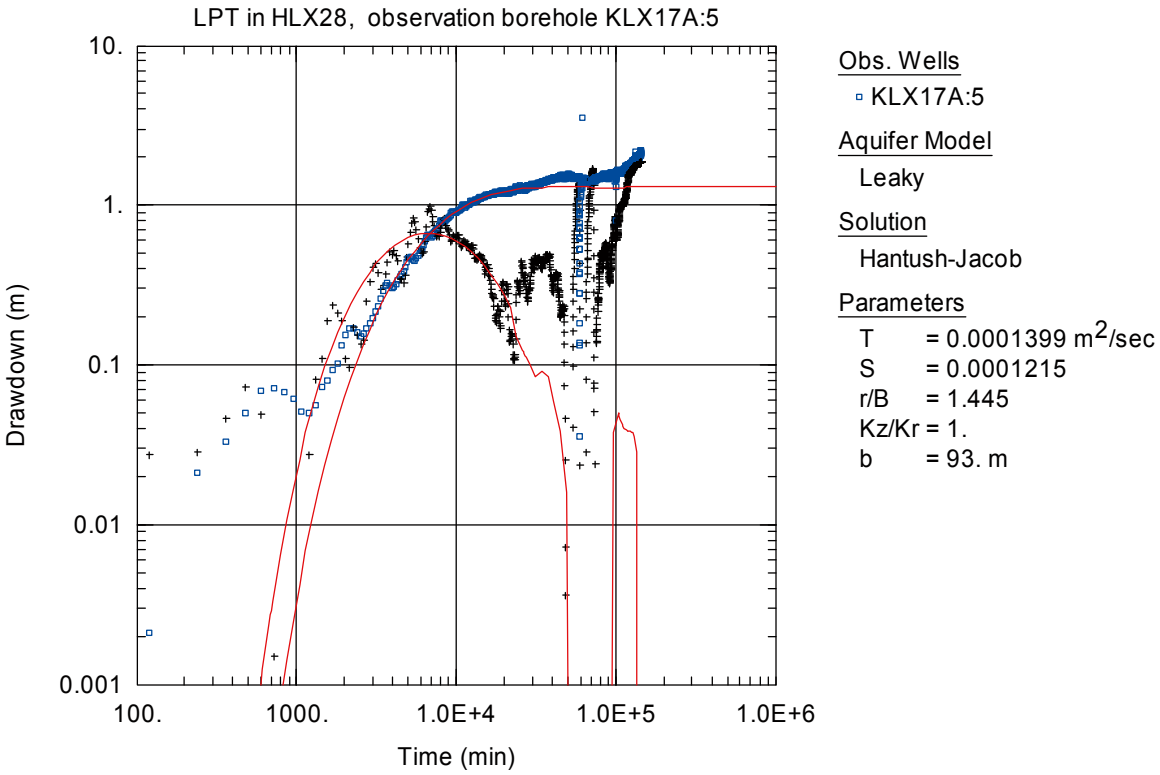

Figure A6-79. *Log-log plot of drawdown (▫) and drawdown derivative, ds/d(ln t) (+), versus time in KLX17A:5 during the interference test in HLX28. Transient evaluation is based on the first part of the drawdown period.*

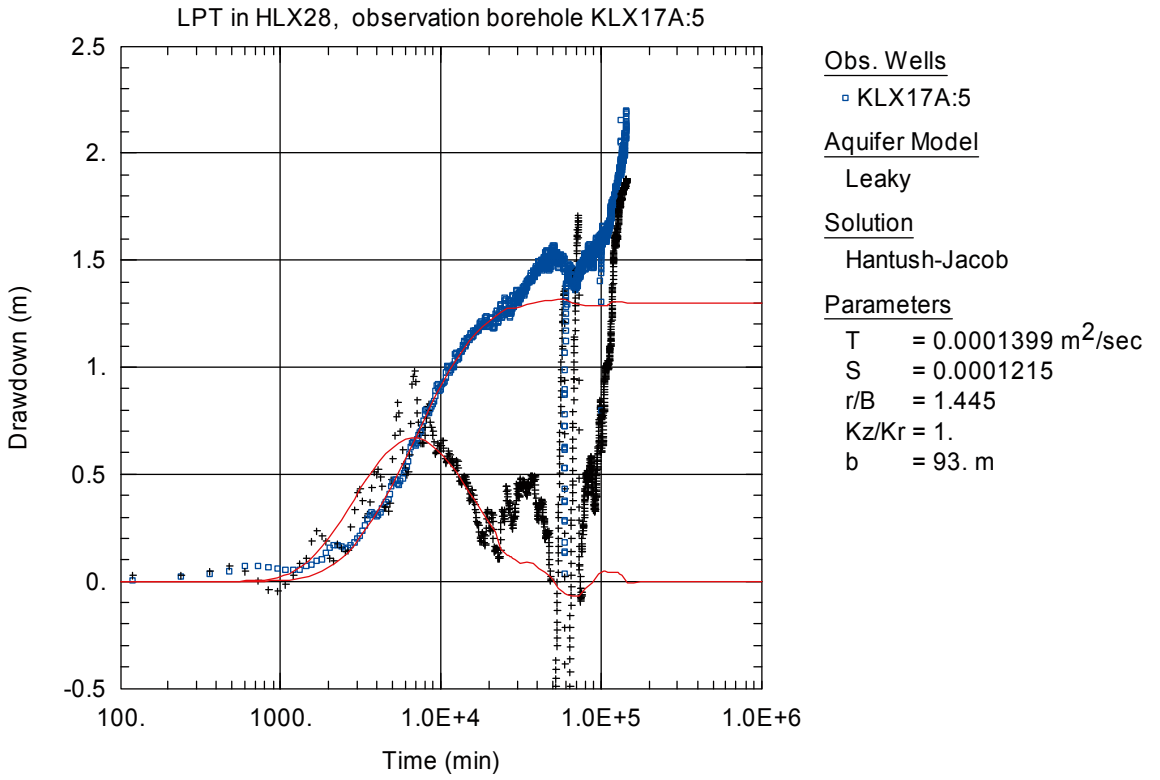

Figure A6-80. *Lin-log plot of drawdown (▫) and drawdown derivative, ds/d(ln t) (+), versus time in KLX17A:5 during the interference test in HLX28. Transient evaluation is based on the first part of the drawdown period.*

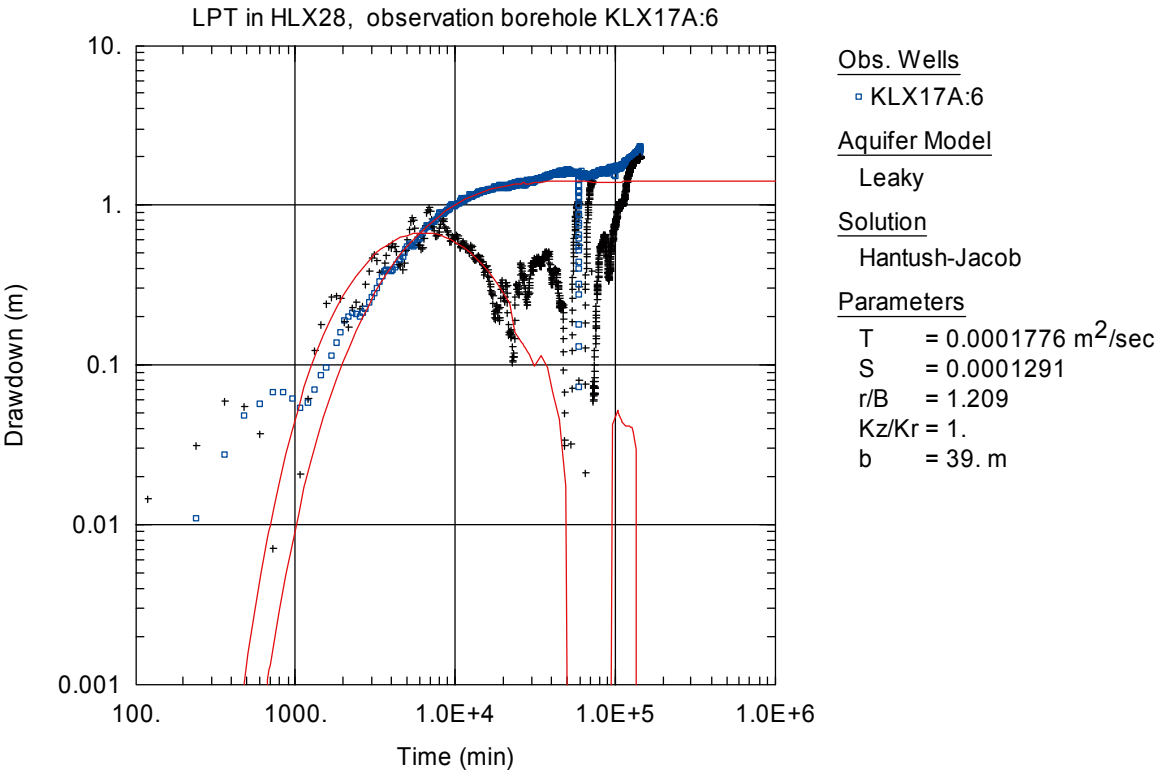

Figure A6-81. *Log-log plot of drawdown (▫) and drawdown derivative, ds/d(ln t) (+), versus time in KLX17A:6 during the interference test in HLX28. Transient evaluation is based on the first part of the drawdown period.*

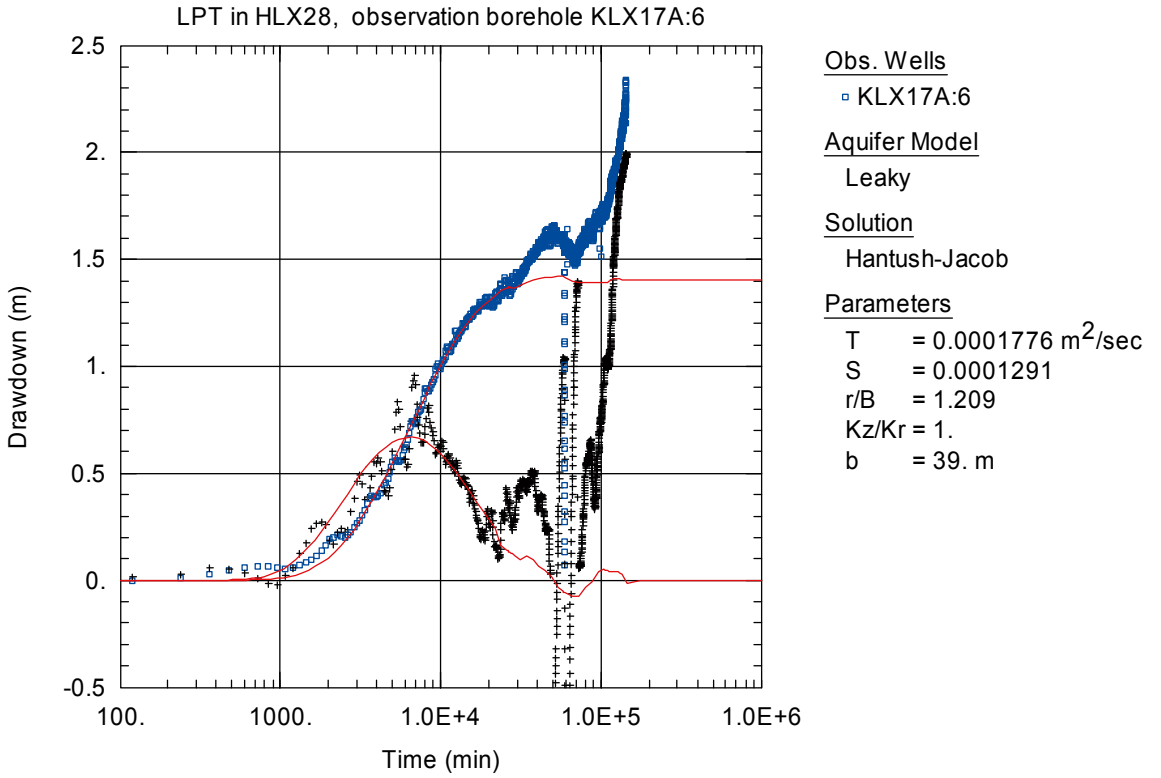

Figure A6-82. *Lin-log plot of drawdown (▫) and drawdown derivative, ds/d(ln t) (+), versus time in KLX17A:6 during the interference test in HLX28. Transient evaluation is based on the first part of the drawdown period.*

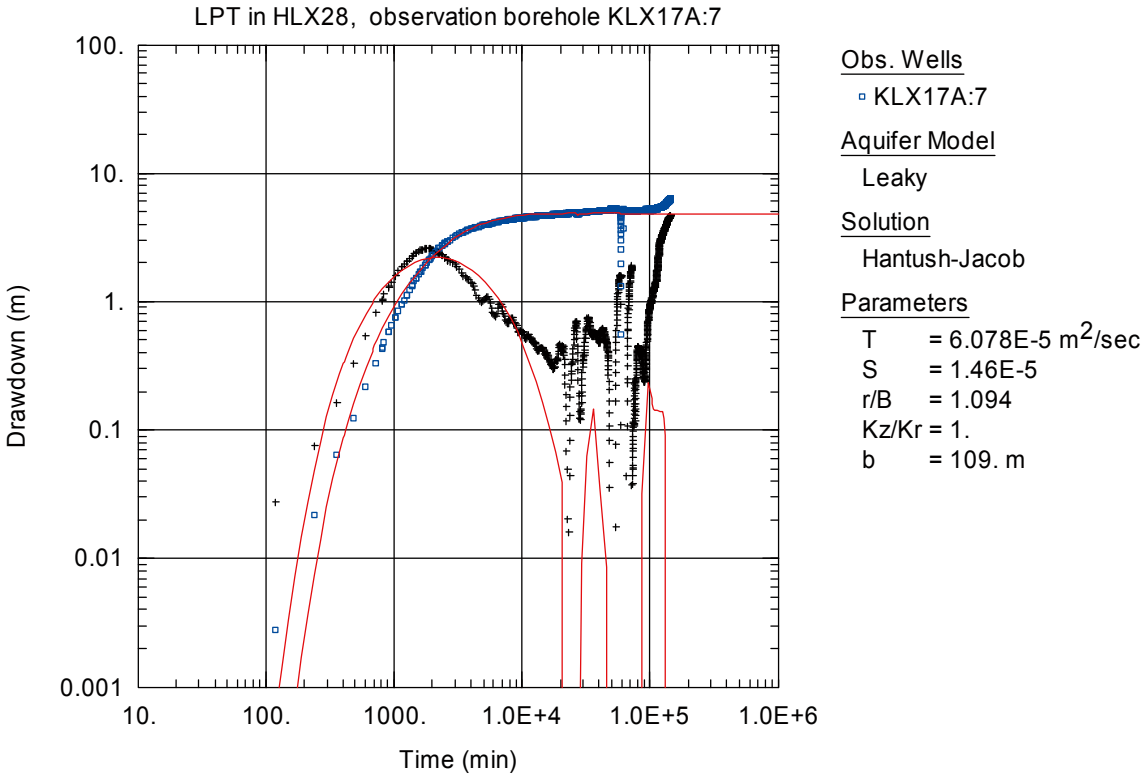

Figure A6-83. *Log-log plot of drawdown (▫) and drawdown derivative, ds/d(ln t) (+), versus time in KLX17A:7 during the interference test in HLX28. Transient evaluation is based on the first part of the drawdown period.*

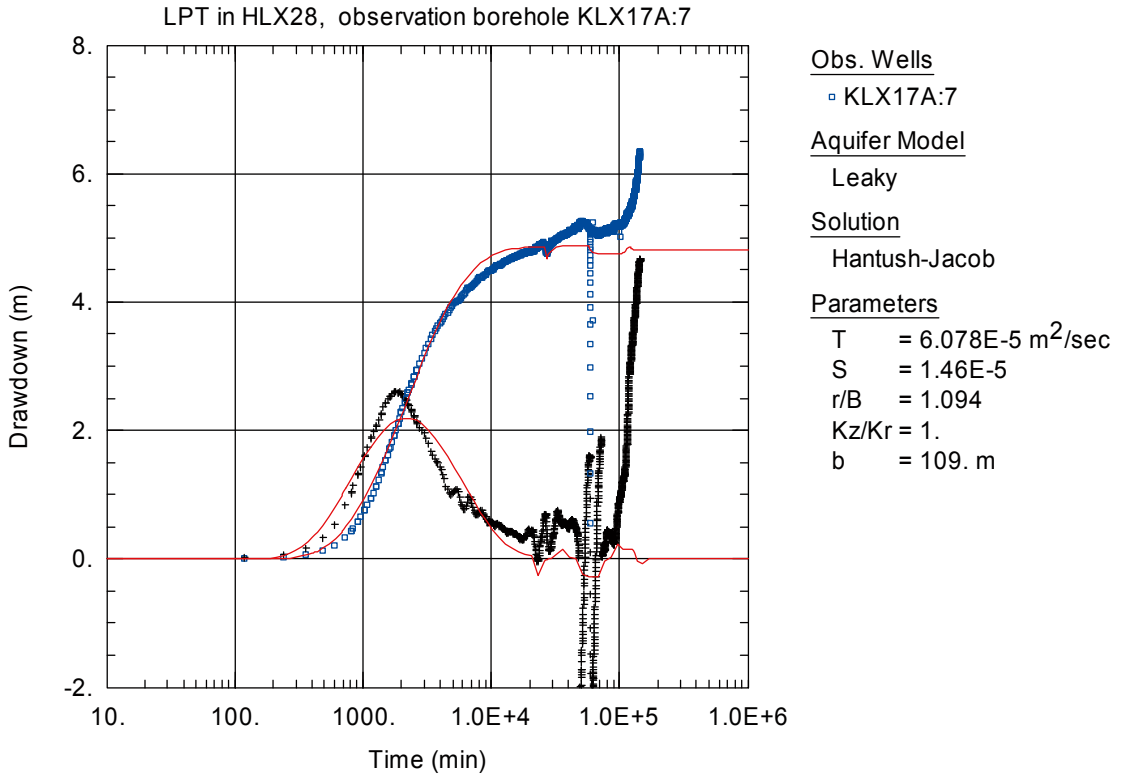

Figure A6-84. *Lin-log plot of drawdown (▫) and drawdown derivative, ds/d(ln t) (+), versus time in KLX17A:7 during the interference test in HLX28. Transient evaluation is based on the first part of the drawdown period.*

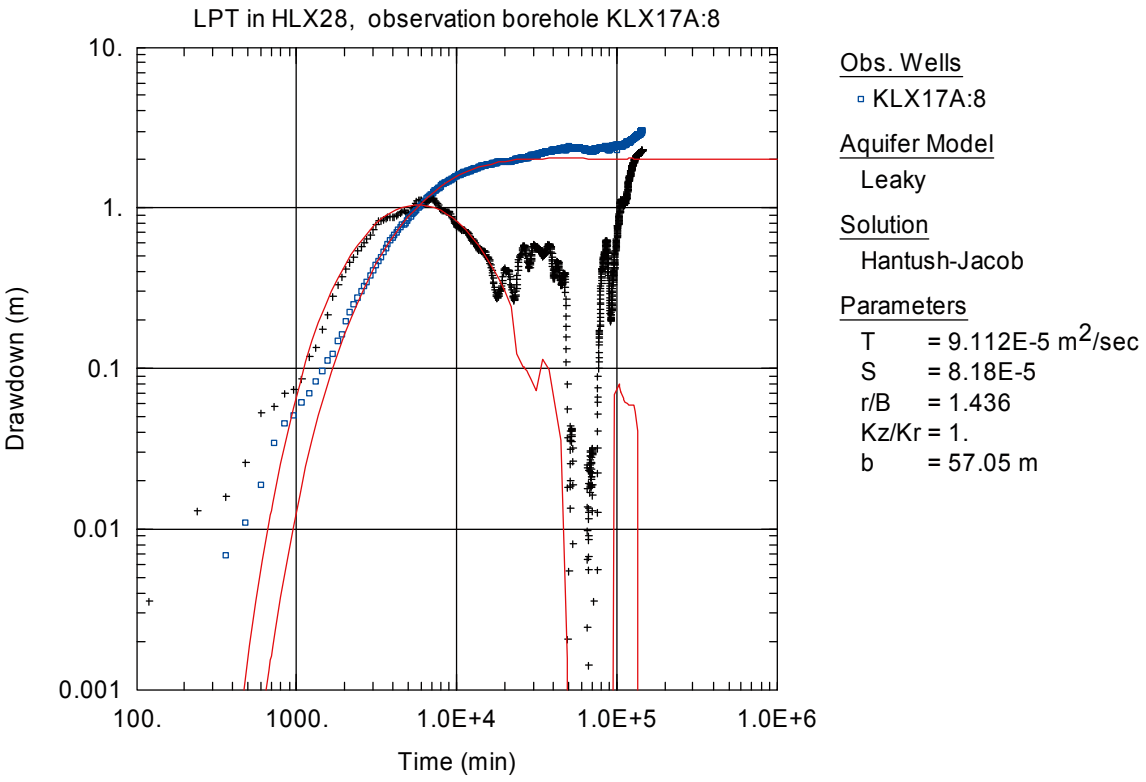

Figure A6-85. *Log-log plot of drawdown (▫) and drawdown derivative, ds/d(ln t) (+), versus time in KLX17A:8 during the interference test in HLX28. Transient evaluation is based on the first part of the drawdown period.*

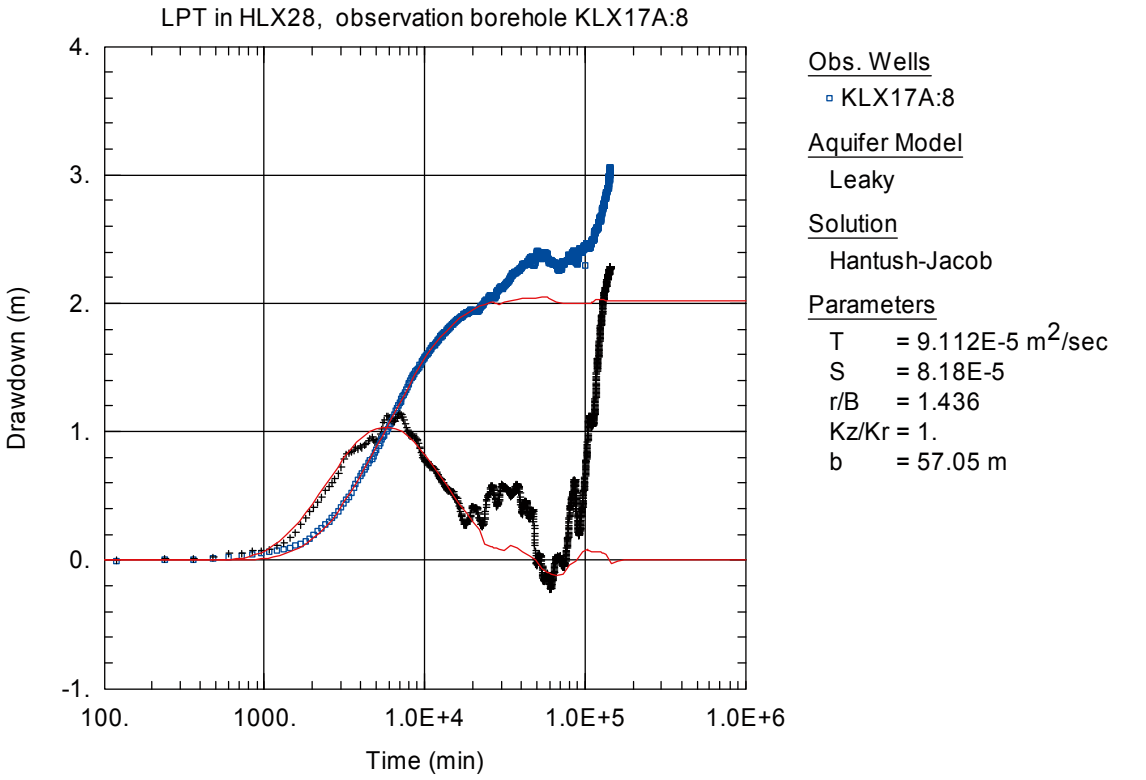

Figure A6-86. *Lin-log plot of drawdown (▫) and drawdown derivative, ds/d(ln t) (+), versus time in KLX17A:8 during the interference test in HLX28. Transient evaluation is based on the first part of the drawdown period.*

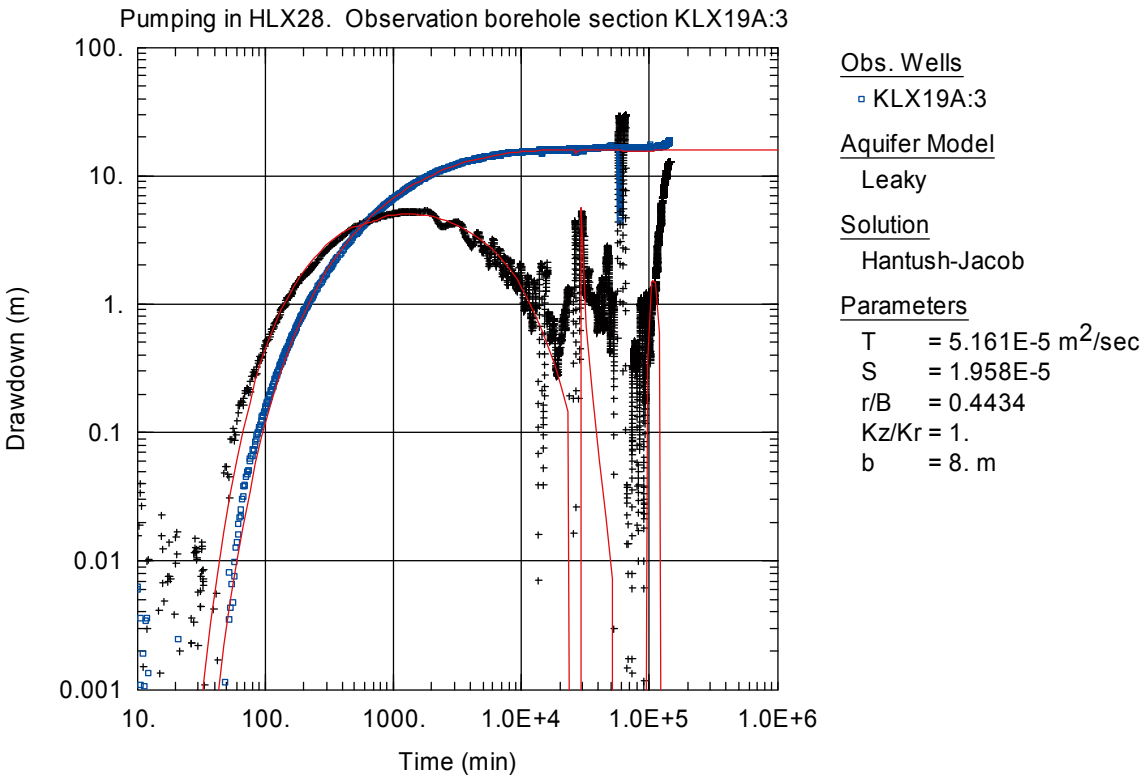

Figure A6-87. *Log-log plot of drawdown (▫) and drawdown derivative, ds/d(ln t) (+), versus time in KLX19A:3 during the interference test in HLX28. Transient evaluation is based on the first part of the drawdown period.*

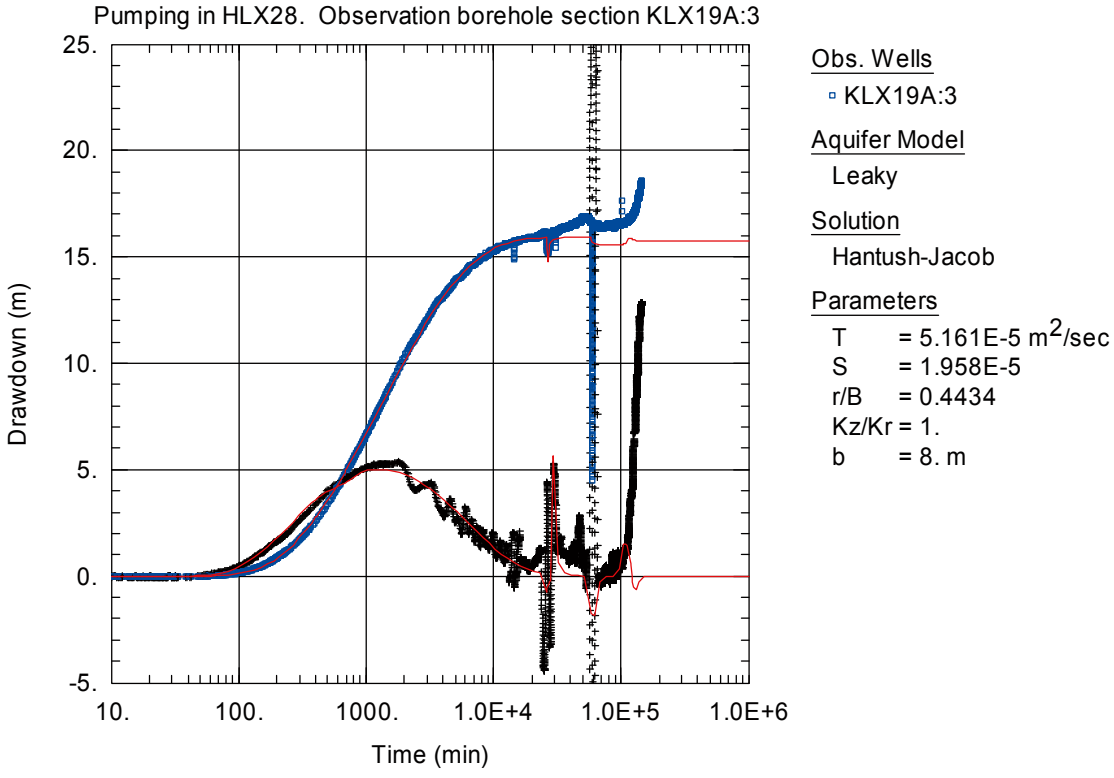

Figure A6-88. *Lin-log plot of drawdown (▫) and drawdown derivative, ds/d(ln t) (+), versus time in KLX19A:3 during the interference test in HLX28. Transient evaluation is based on the first part of the drawdown period.*

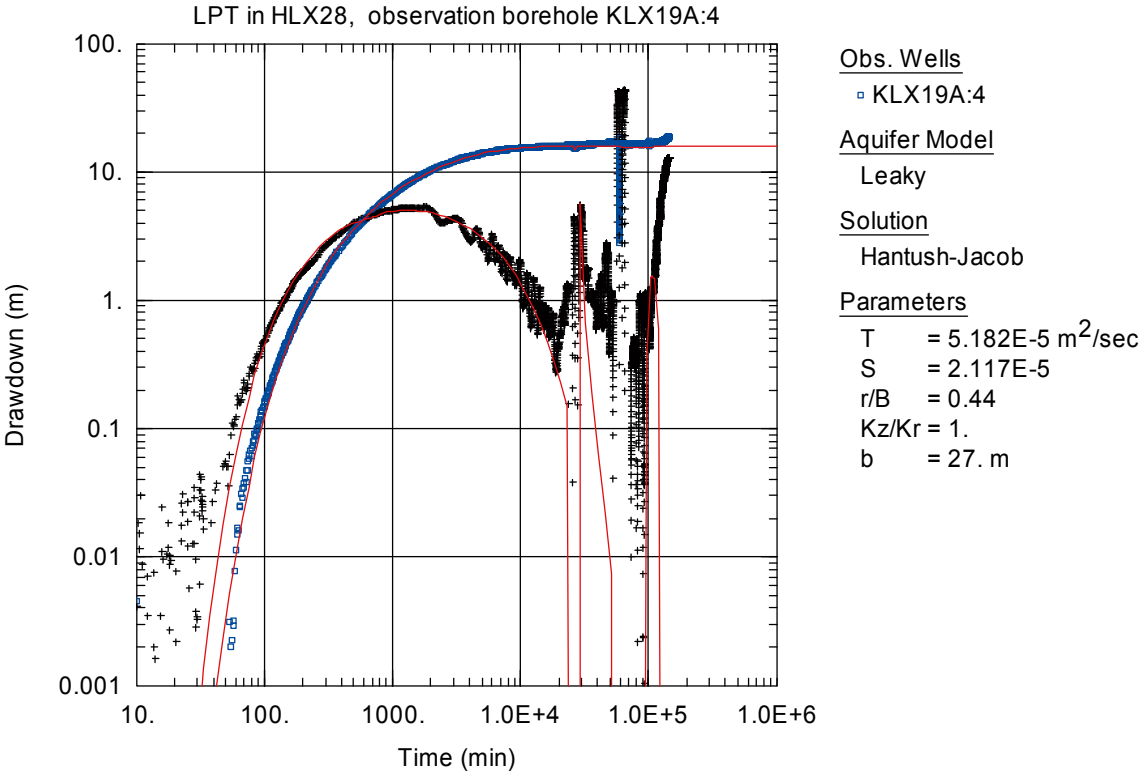

Figure A6-89. *Log-log plot of drawdown (▫) and drawdown derivative, ds/d(ln t) (+), versus time in KLX19A:4 during the interference test in HLX28. Transient evaluation is based on the first part of the drawdown period.*

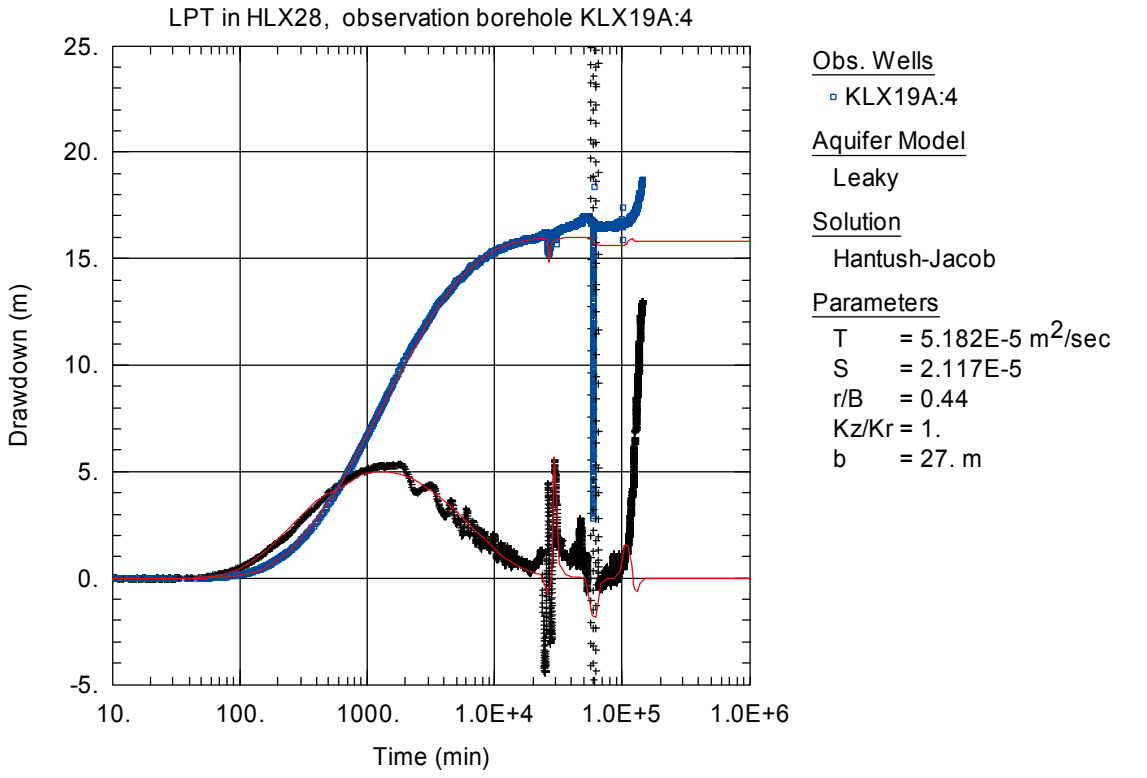

Figure A6-90. *Lin-log plot of drawdown (▫) and drawdown derivative, ds/d(ln t) (+), versus time in KLX19A:4 during the interference test in HLX28. Transient evaluation is based on the first part of the drawdown period.*

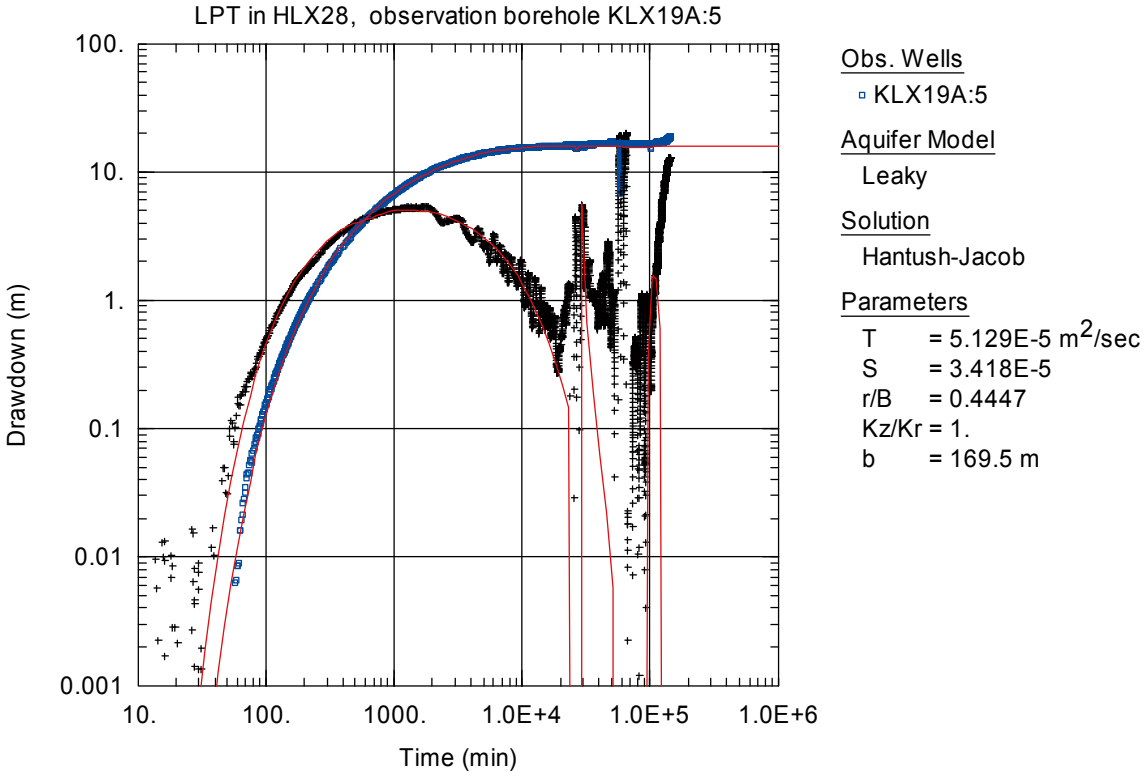

Figure A6-91. *Log-log plot of drawdown (▫) and drawdown derivative, ds/d(ln t) (+), versus time in KLX19A:5 during the interference test in HLX28. Transient evaluation is based on the first part of the drawdown period.*

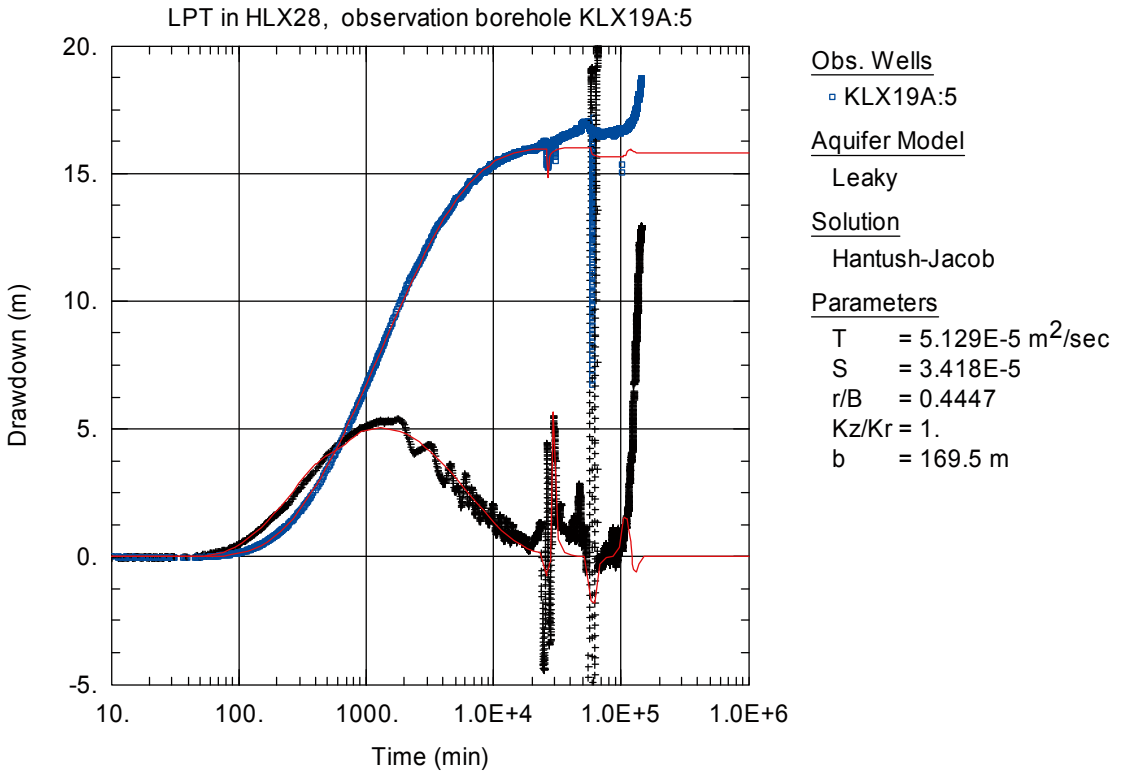

Figure A6-92. *Lin-log plot of drawdown (▫) and drawdown derivative, ds/d(ln t) (+), versus time in KLX19A:5 during the interference test in HLX28. Transient evaluation is based on the first part of the drawdown period.*

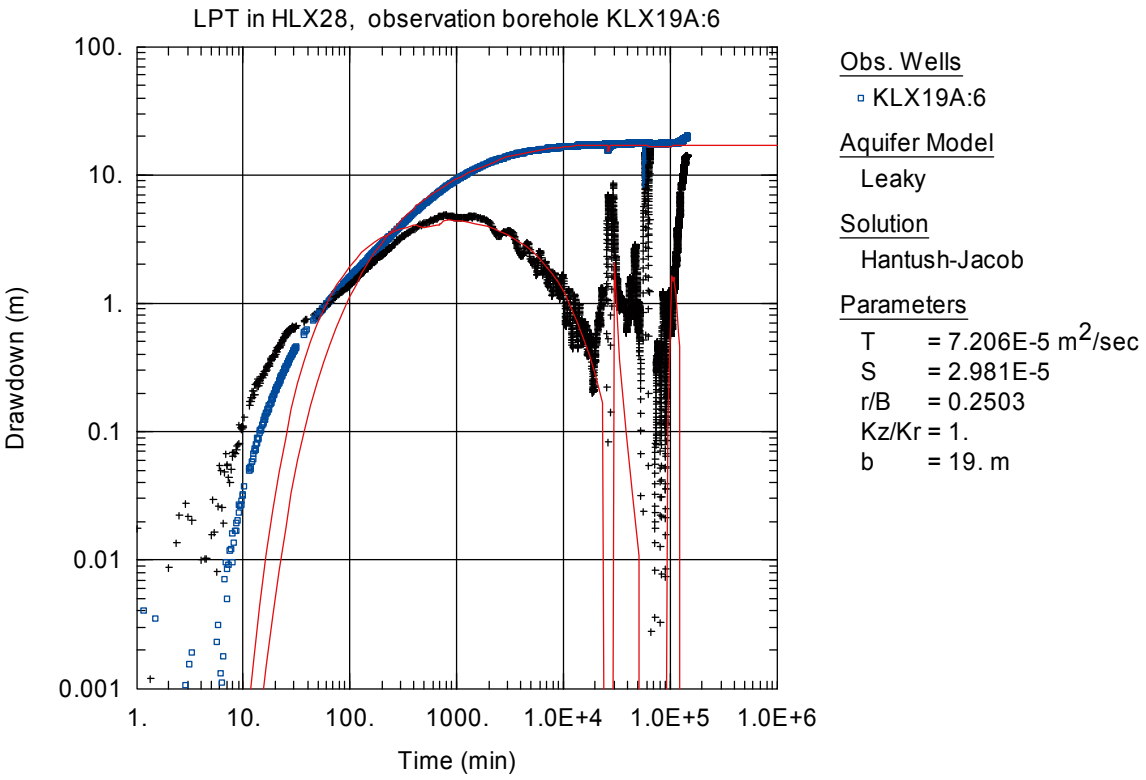

Figure A6-93. *Log-log plot of drawdown (▫) and drawdown derivative, ds/d(ln t) (+), versus time in KLX19A:6 during the interference test in HLX28. Transient evaluation is based on the first part of the drawdown period.*

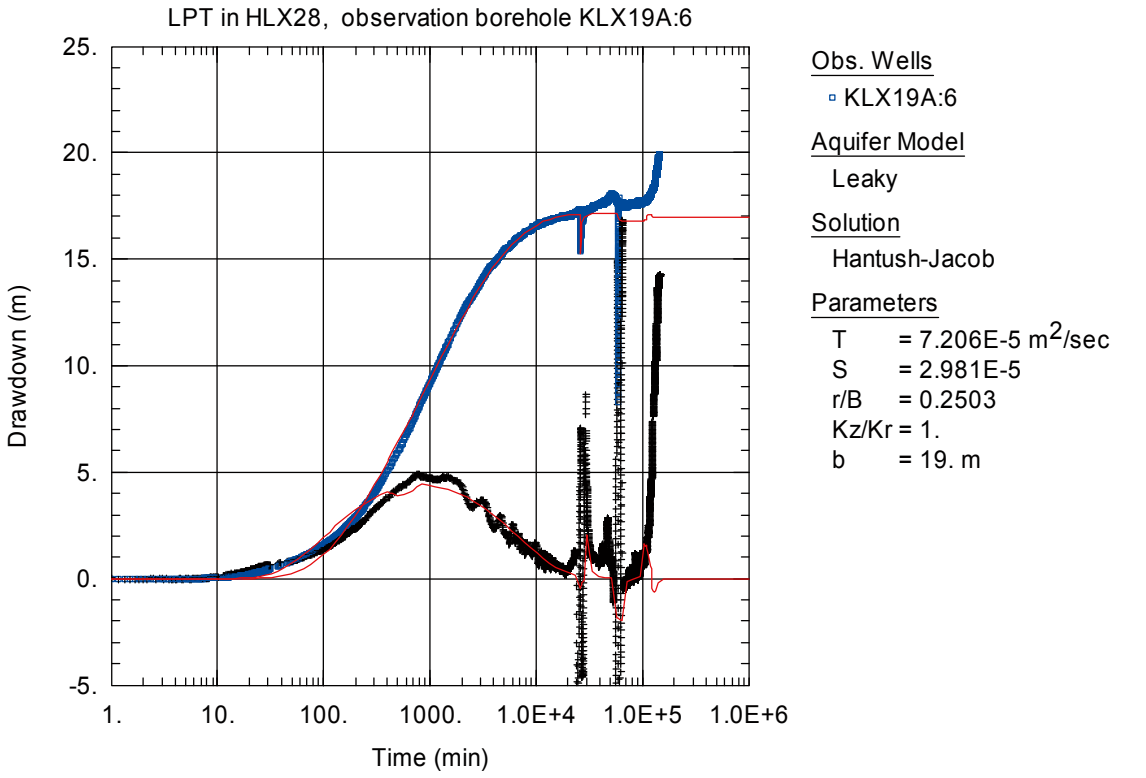

Figure A6-94. *Lin-log plot of drawdown (▫) and drawdown derivative, ds/d(ln t) (+), versus time in KLX19A:6 during the interference test in HLX28. Transient evaluation is based on the first part of the drawdown period.*

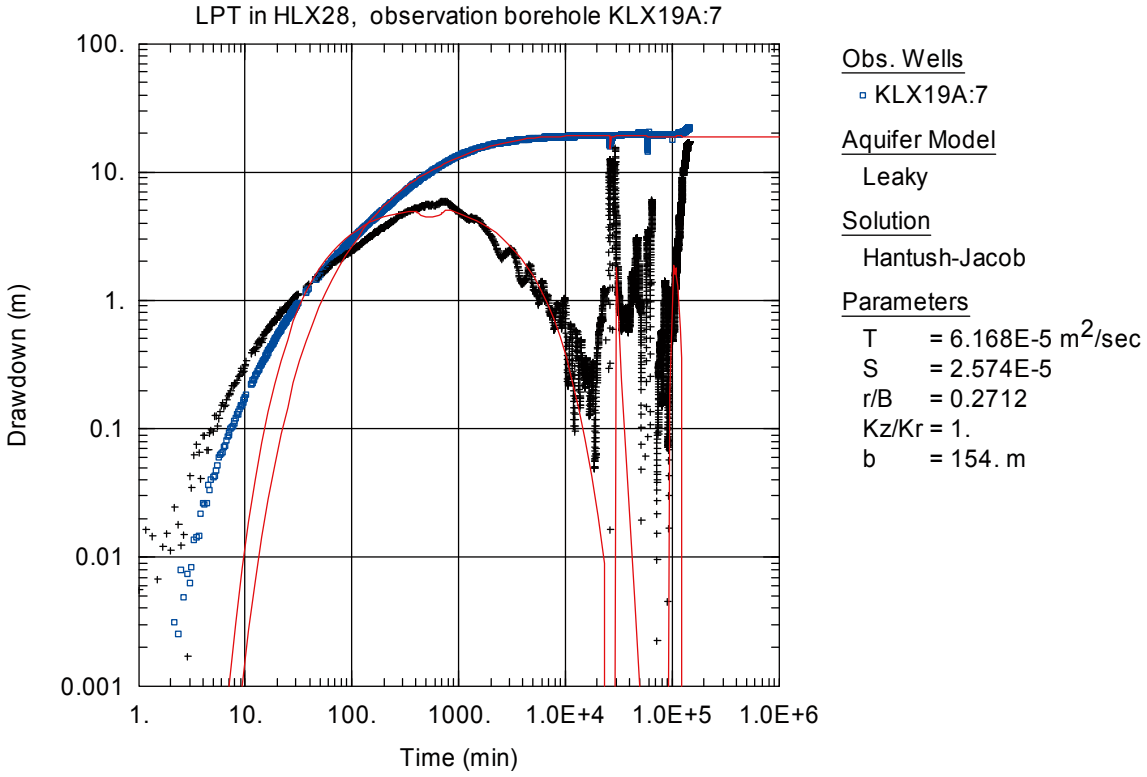

Figure A6-95. *Log-log plot of drawdown (▫) and drawdown derivative, ds/d(ln t) (+), versus time in KLX19A:7 during the interference test in HLX28. Transient evaluation is based on the first part of the drawdown period.*

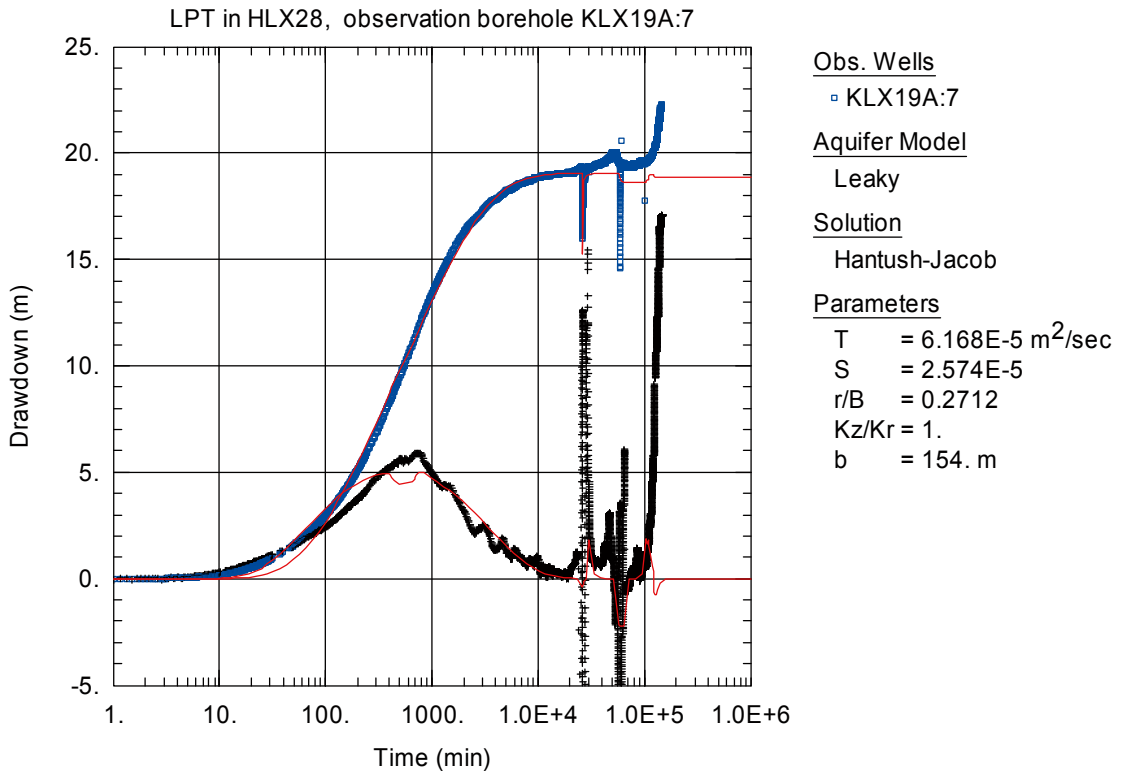

Figure A6-96. *Lin-log plot of drawdown (▫) and drawdown derivative, ds/d(ln t) (+), versus time in KLX19A:7 during the interference test in HLX28. Transient evaluation is based on the first part of the drawdown period.*

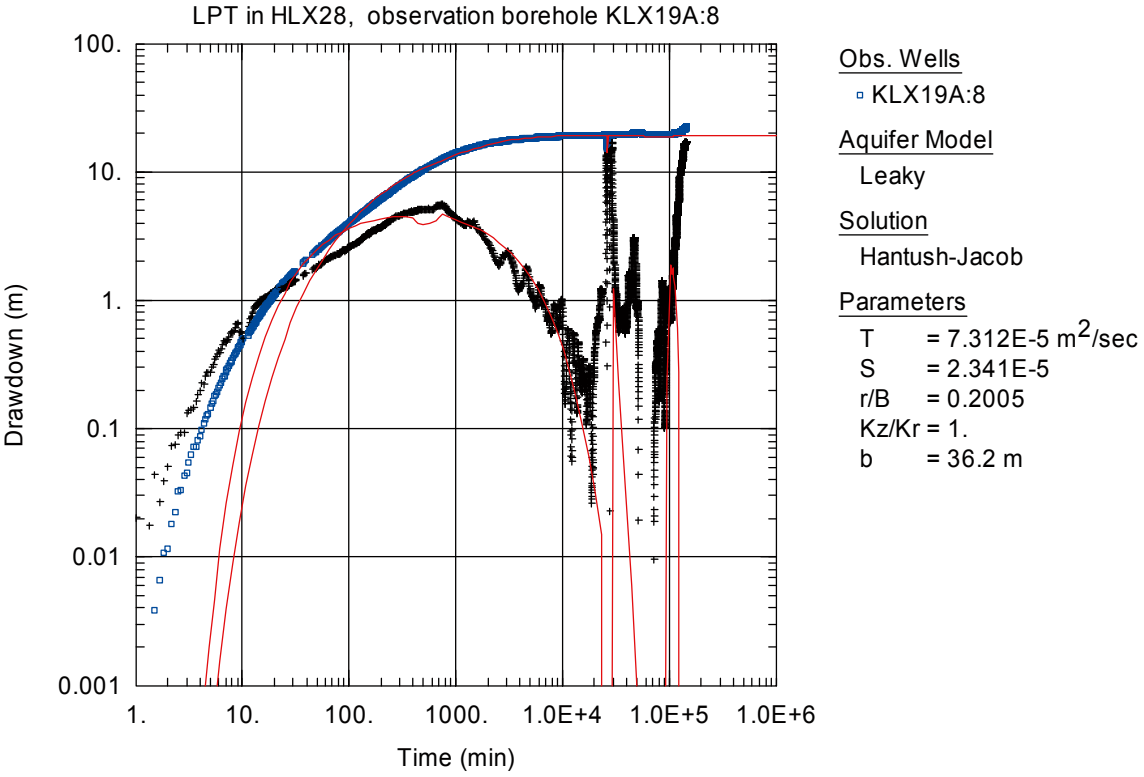

Figure A6-97. *Log-log plot of drawdown (▫) and drawdown derivative, ds/d(ln t) (+), versus time in KLX19A:8 during the interference test in HLX28. Transient evaluation is based on the first part of the drawdown period.*

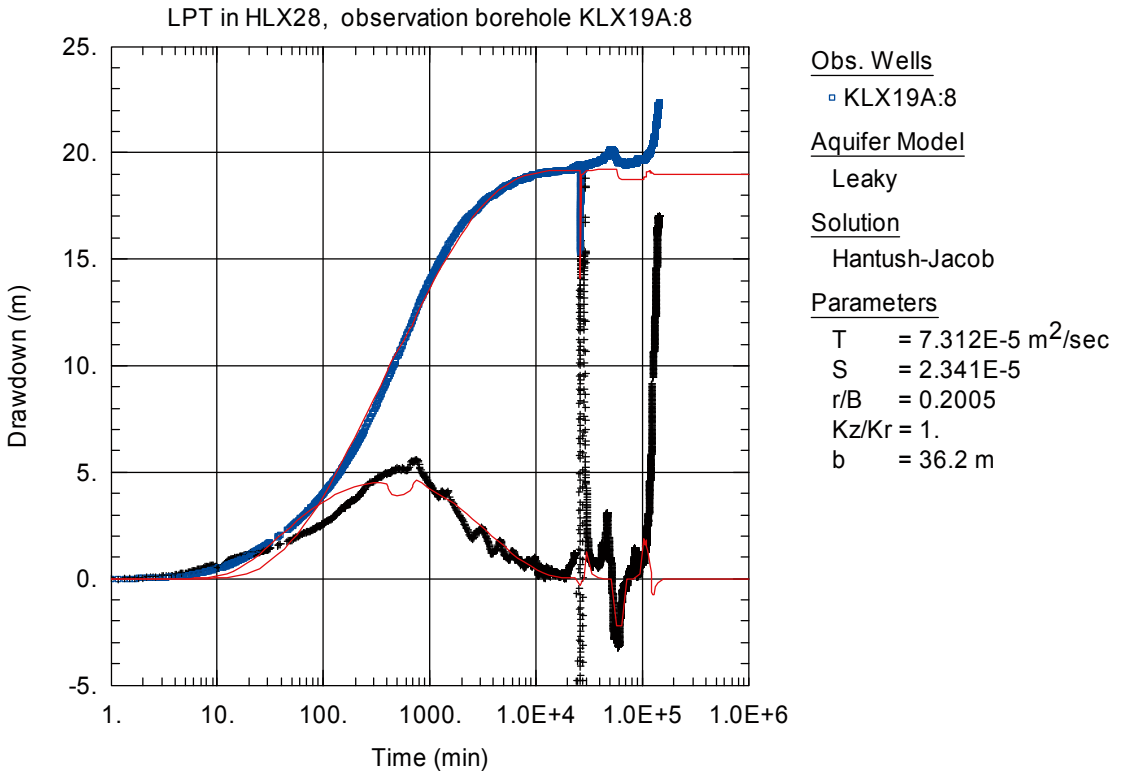

Figure A6-98. *Lin-log plot of drawdown (▫) and drawdown derivative, ds/d(ln t) (+), versus time in KLX19A:8 during the interference test in HLX28. Transient evaluation is based on the first part of the drawdown period.*

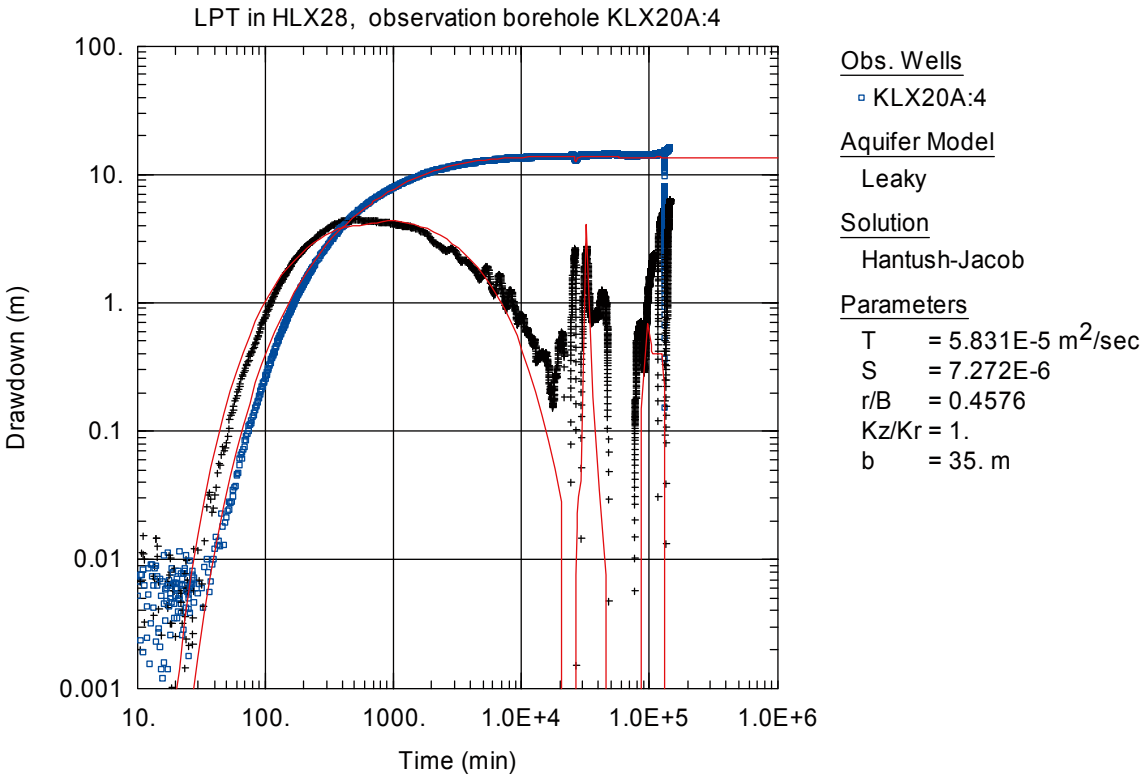

Figure A6-99. *Log-log plot of drawdown (▫) and drawdown derivative, ds/d(ln t) (+), versus time in KLX20A:4 during the interference test in HLX28. Transient evaluation is based on the first part of the drawdown period.*

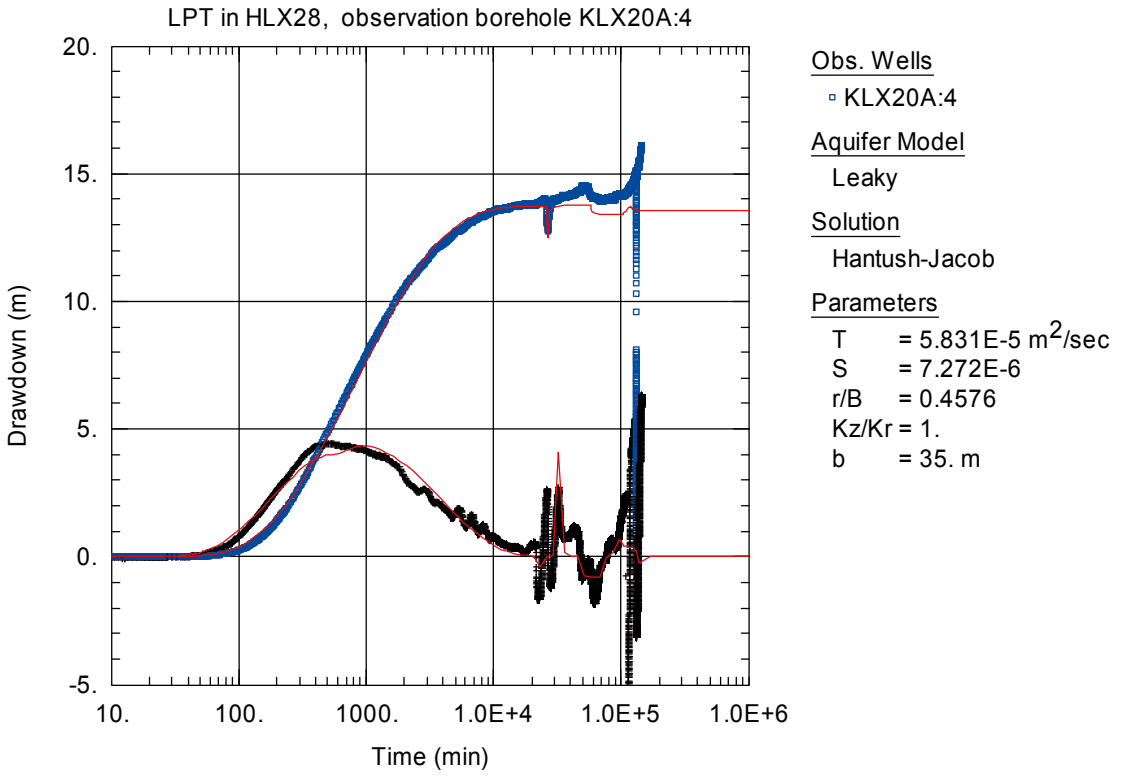

Figure A6-100. *Lin-log plot of drawdown (▫) and drawdown derivative, ds/d(ln t) (+), versus time in KLX20A:4 during the interference test in HLX28. Transient evaluation is based on the first part of the drawdown period.*

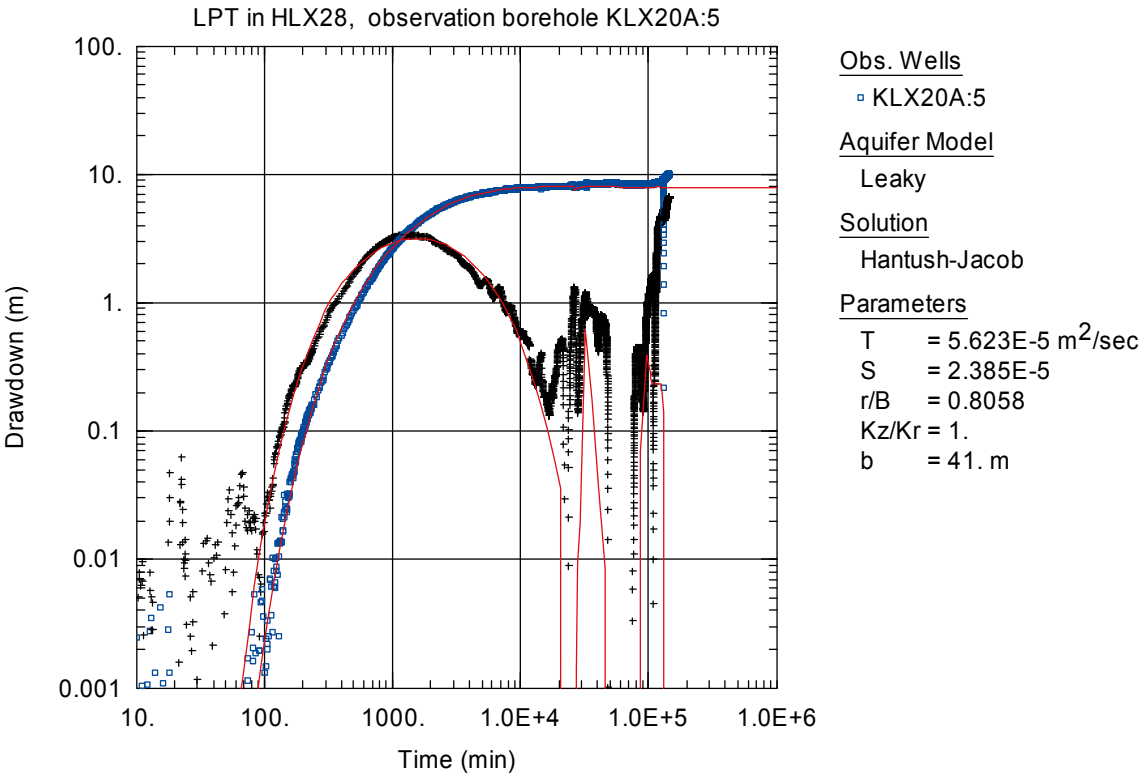

Figure A6-101. *Log-log plot of drawdown (▫) and drawdown derivative, ds/d(ln t) (+), versus time in KLX20A:5 during the interference test in HLX28. Transient evaluation is based on the first part of the drawdown period. Tracer injection section.*

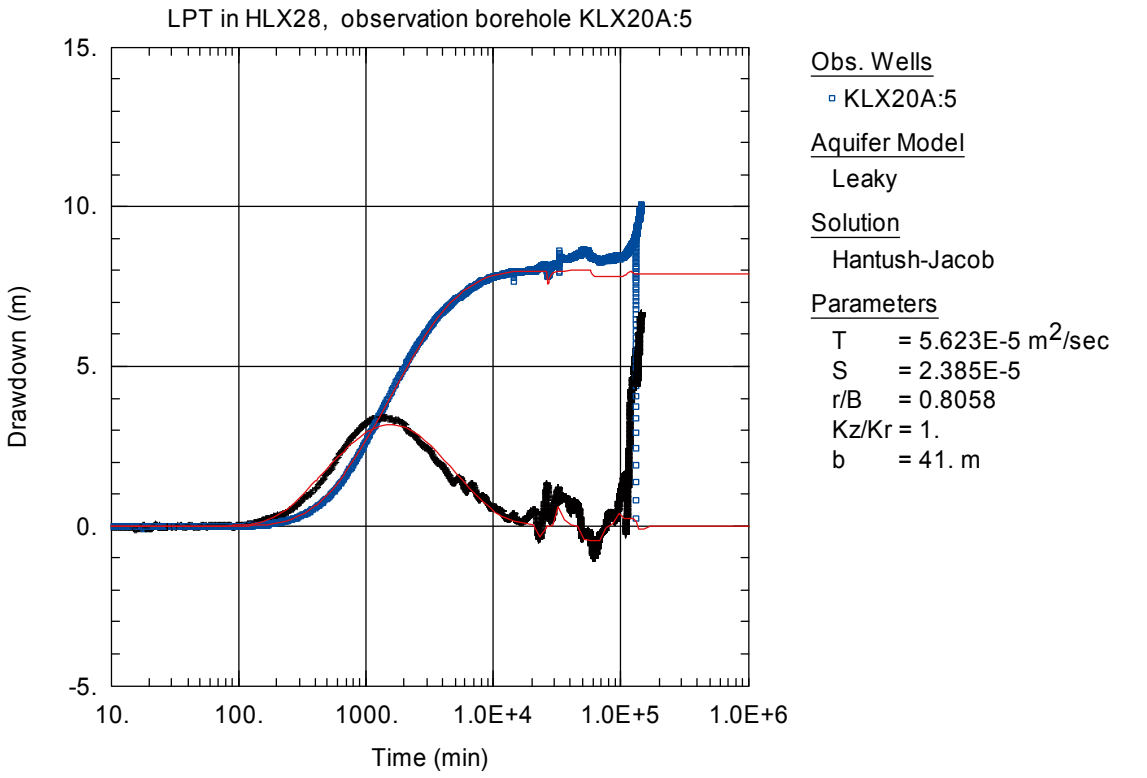

Figure A6-102. *Lin-log plot of drawdown (▫) and drawdown derivative, ds/d(ln t) (+), versus time in KLX20A:5 during the interference test in HLX28. Transient evaluation is based on the first part of the drawdown period. Tracer injection section.*

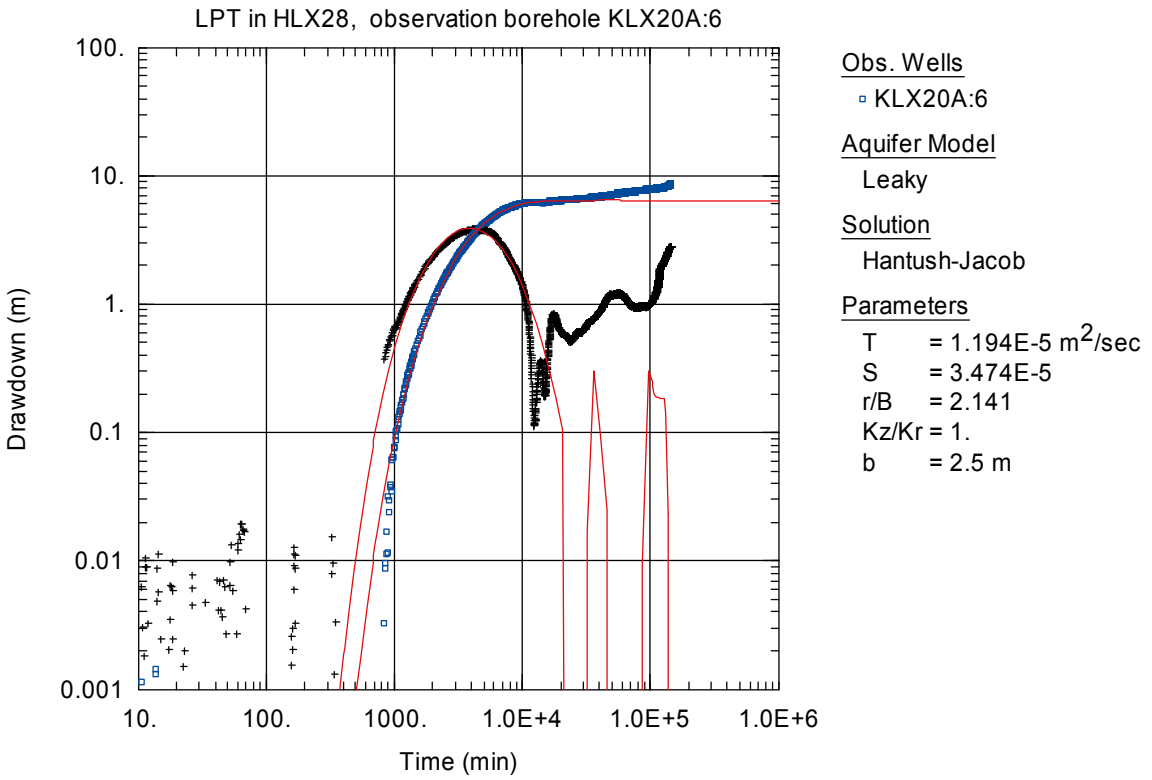

Figure A6-103. *Log-log plot of drawdown (▫) and drawdown derivative, ds/d(ln t) (+), versus time in KLX20A:6 during the interference test in HLX28. Transient evaluation is based on the first part of the drawdown period. Somewhat uncertain transient evaluation due to rising groundwater level in the section before start of pumping.*

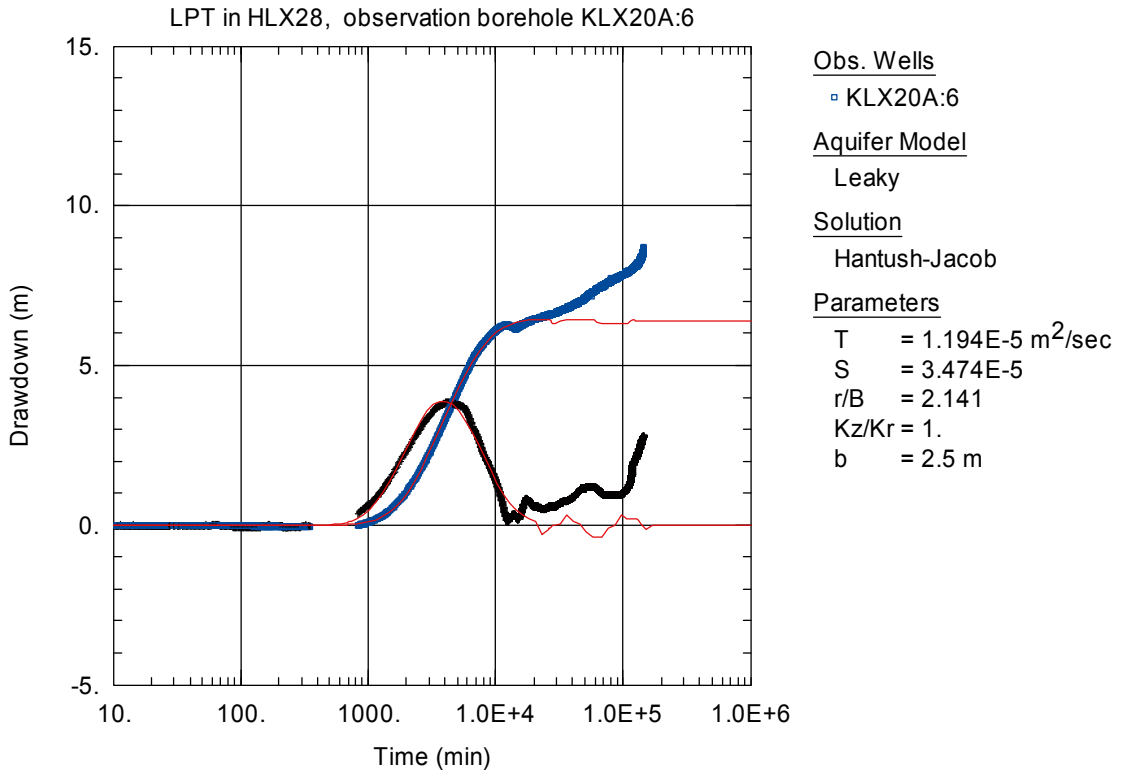

Figure A6-104. *Lin-log plot of drawdown (▫) and drawdown derivative, ds/d(ln t) (+), versus time in KLX20A:6 during the interference test in HLX28. Transient evaluation is based on the first part of the drawdown period. Somewhat uncertain transient evaluation, see above.*

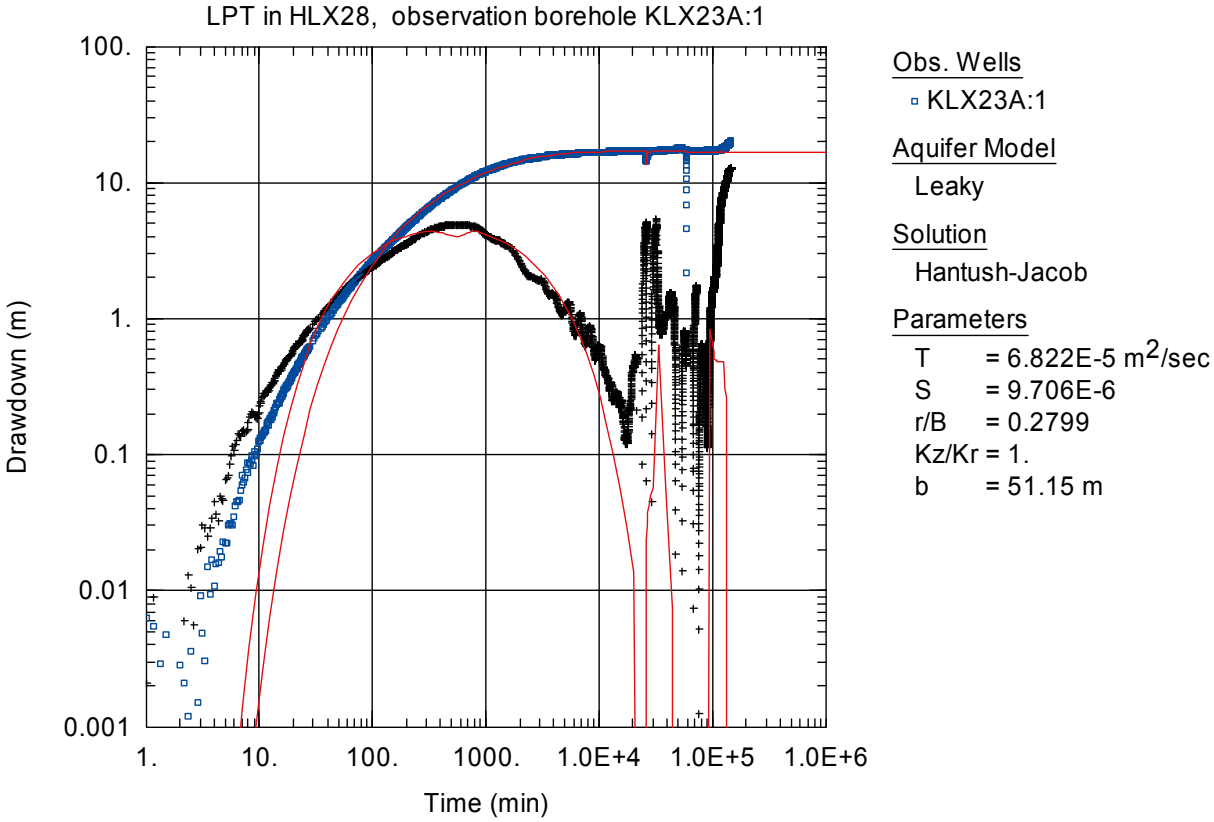

Figure A6-105. *Log-log plot of drawdown (▫) and drawdown derivative, ds/d(ln t) (+), versus time in KLX23A:1 during the interference test in HLX28. Transient evaluation is based on the first part of the drawdown period.*

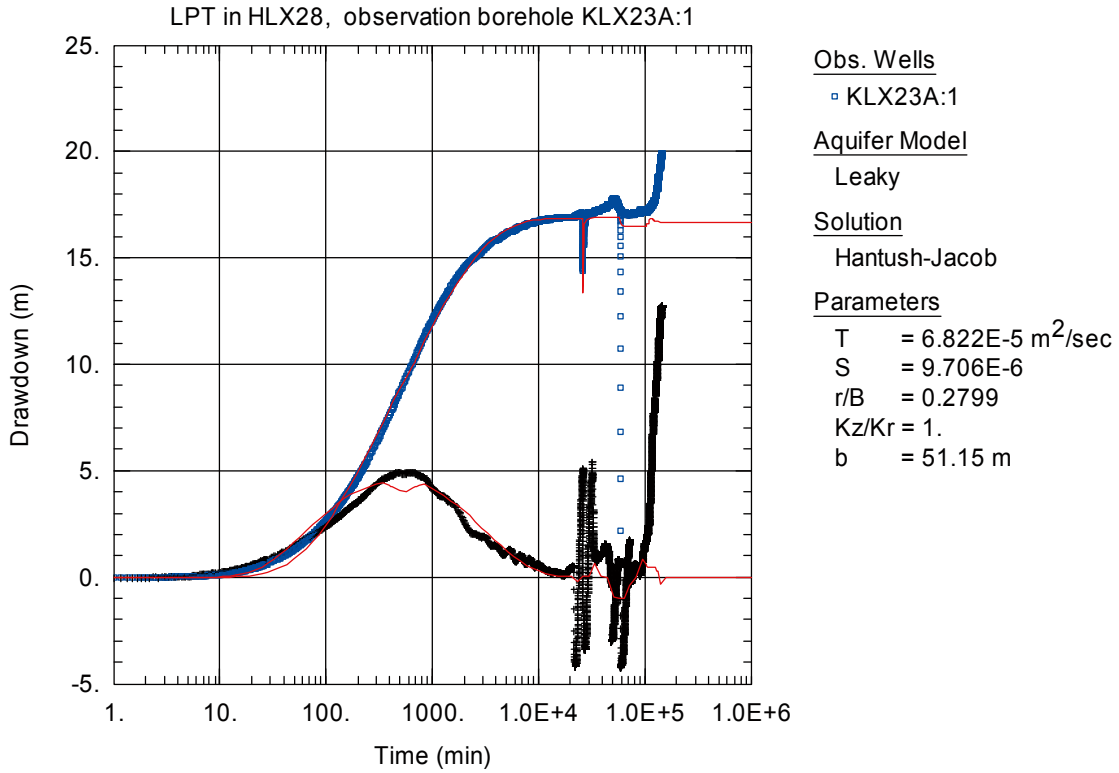

Figure A6-106. *Lin-log plot of drawdown (▫) and drawdown derivative, ds/d(ln t) (+), versus time in KLX23A:1 during the interference test in HLX28. Transient evaluation is based on the first part of the drawdown period.*

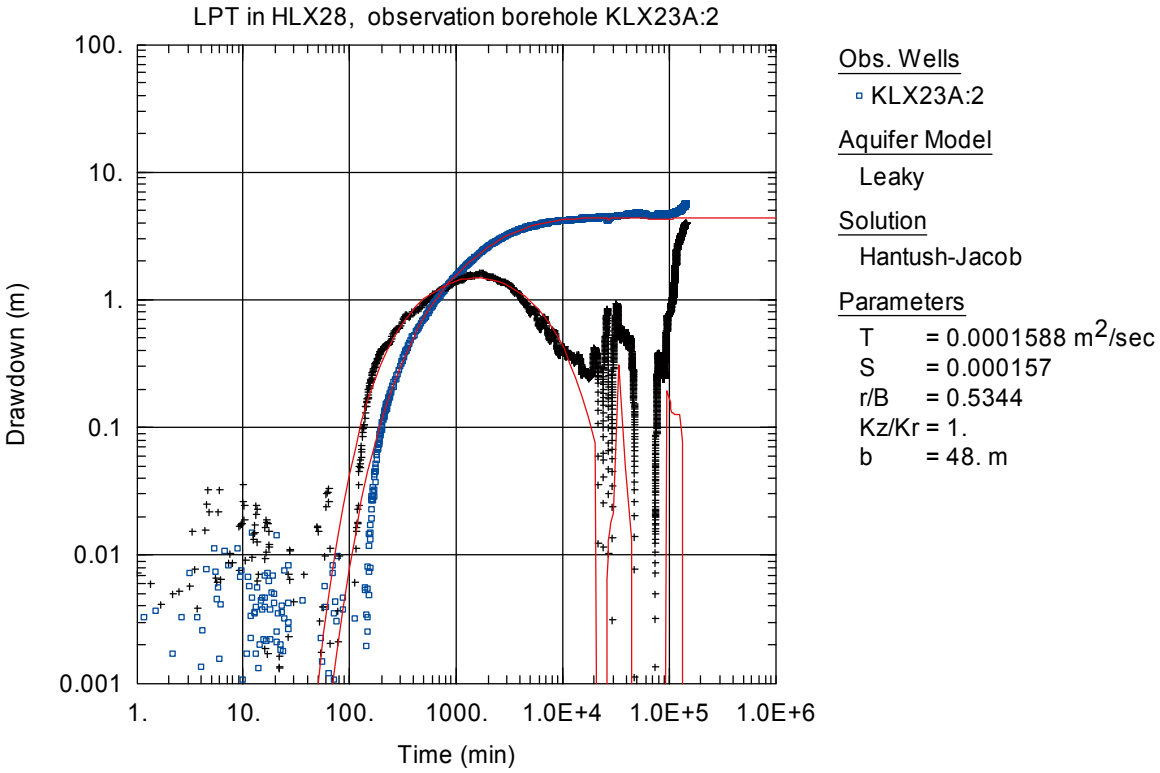

Figure A6-107. *Log-log plot of drawdown (▫) and drawdown derivative, ds/d(ln t) (+), versus time in KLX23A:2 during the interference test in HLX28. Transient evaluation is based on the first part of the drawdown period.*

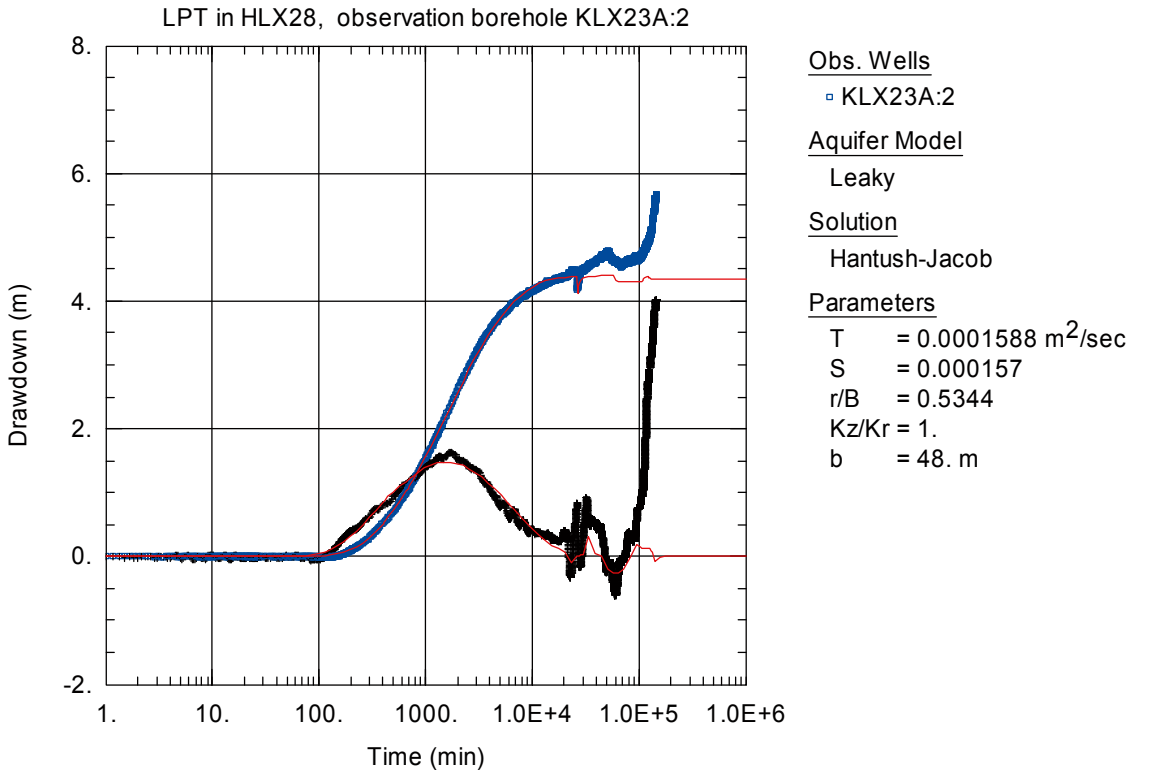

Figure A6-108. *Lin-log plot of drawdown (▫) and drawdown derivative, ds/d(ln t) (+), versus time in KLX23A:2 during the interference test in HLX28. Transient evaluation is based on the first part of the drawdown period.*

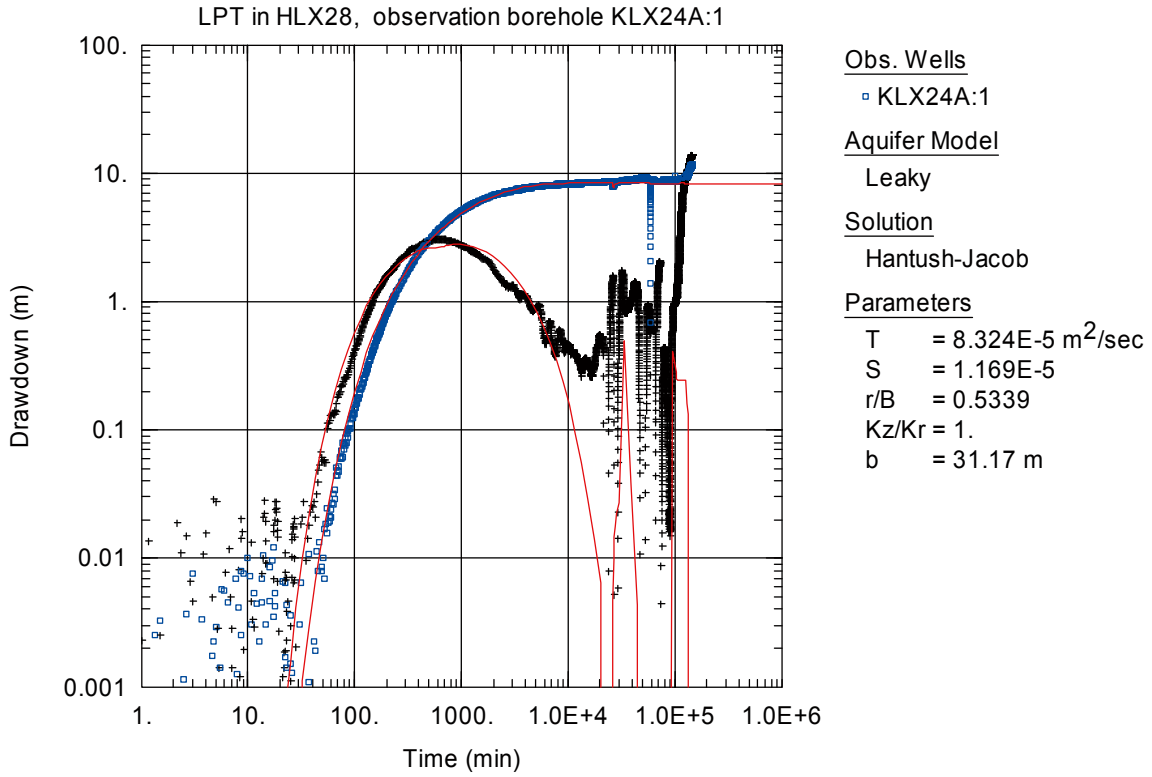

Figure A6-109. *Log-log plot of drawdown (▫) and drawdown derivative, ds/d(ln t) (+), versus time in KLX24A:1 during the interference test in HLX28. Transient evaluation is based on the first part of the drawdown period.*

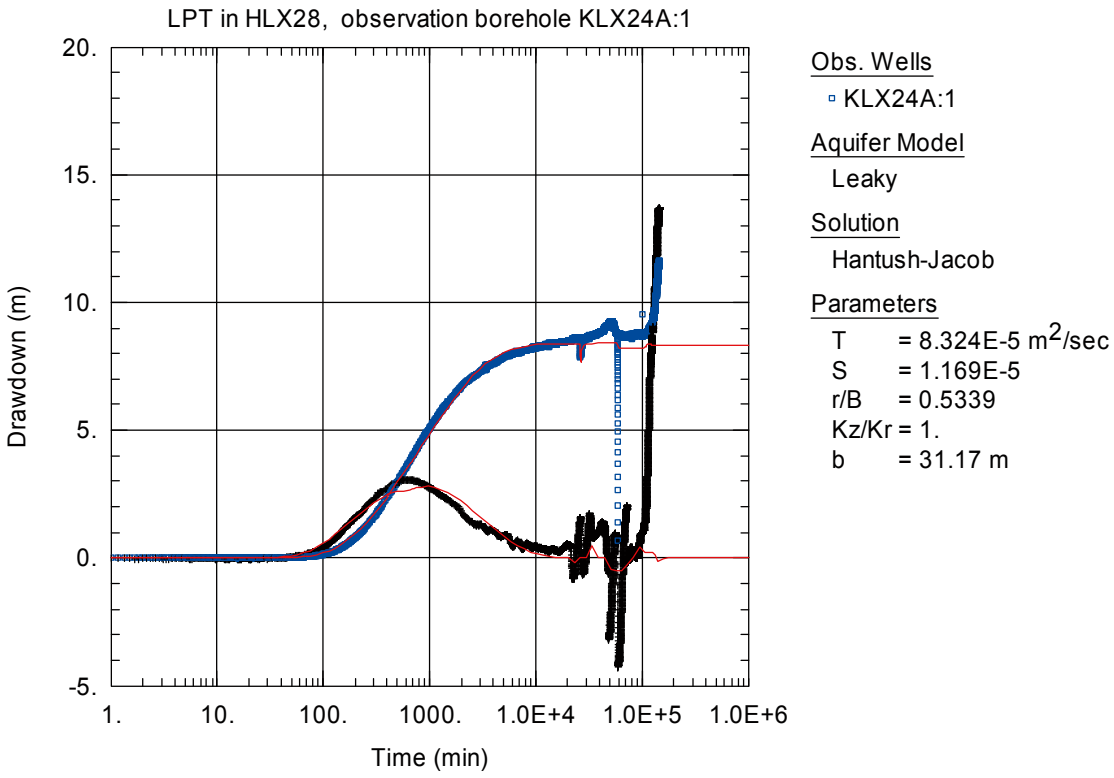

Figure A6-110. *Lin-log plot of drawdown (▫) and drawdown derivative, ds/d(ln t) (+), versus time in KLX24A:1 during the interference test in HLX28. Transient evaluation is based on the first part of the drawdown period.*

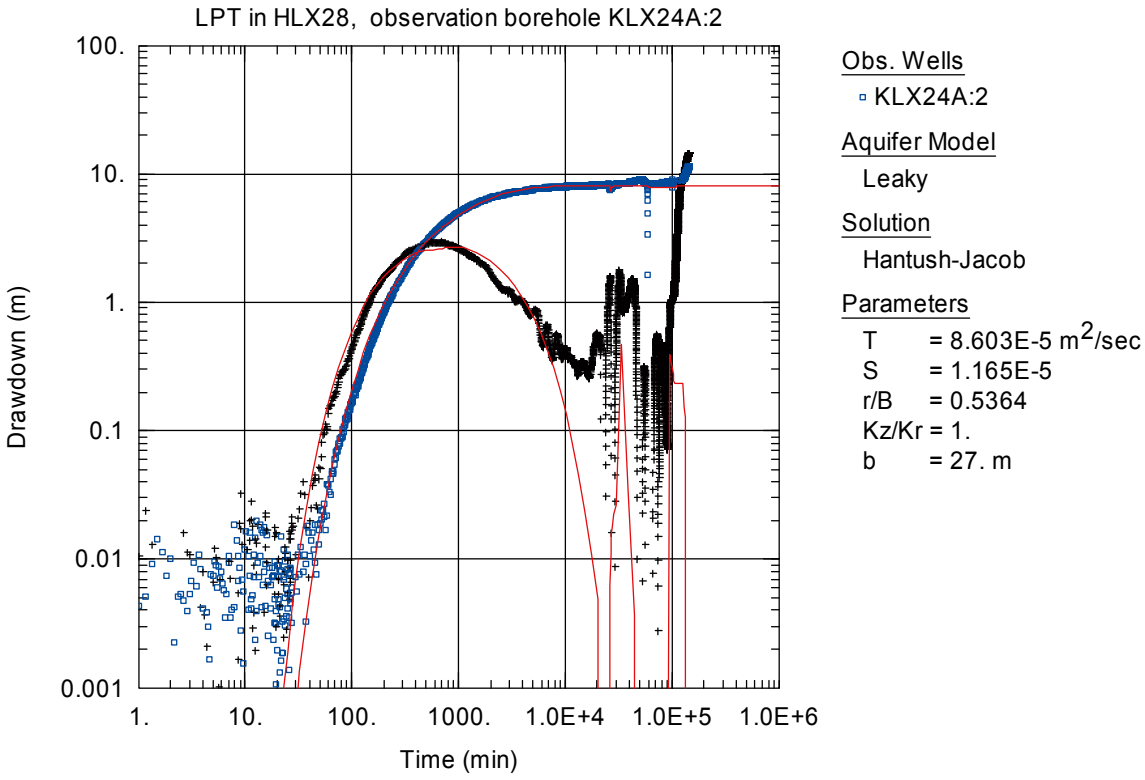

Figure A6-111. *Log-log plot of drawdown (▫) and drawdown derivative, ds/d(ln t) (+), versus time in KLX24A:2 during the interference test in HLX28. Transient evaluation is based on the first part of the drawdown period.*

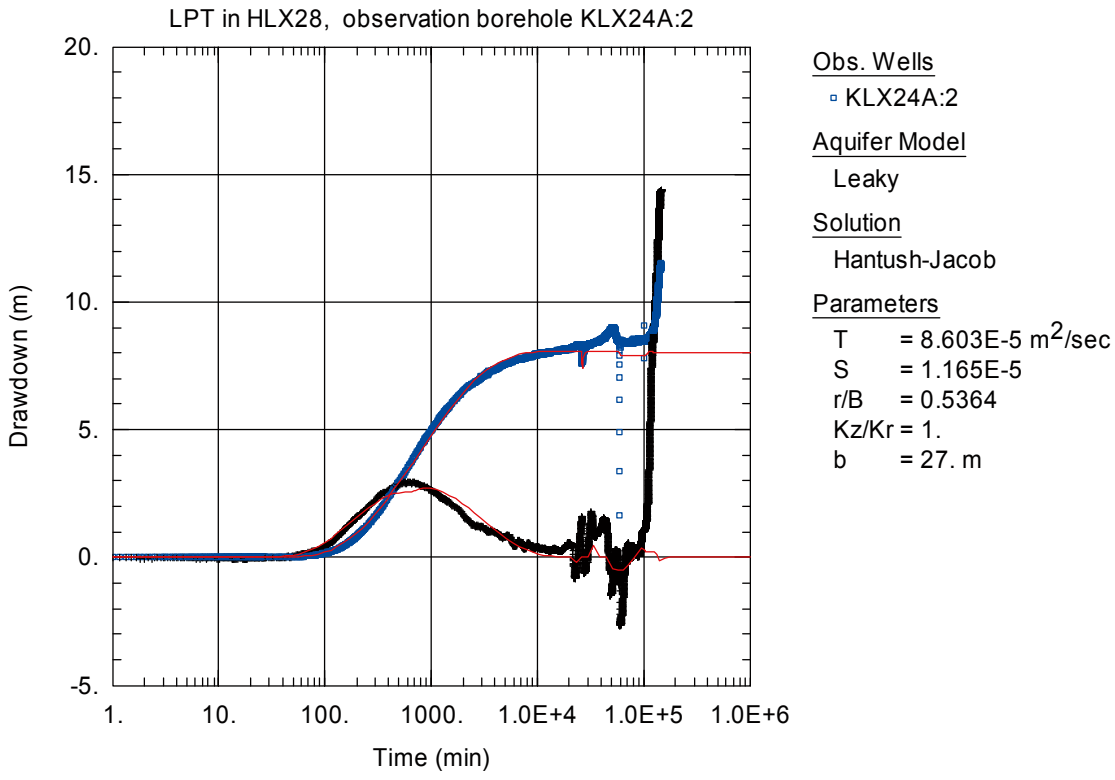

Figure A6-112. *Lin-log plot of drawdown (▫) and drawdown derivative, ds/d(ln t) (+), versus time in KLX24A:2 during the interference test in HLX28. Transient evaluation is based on the first part of the drawdown period.*

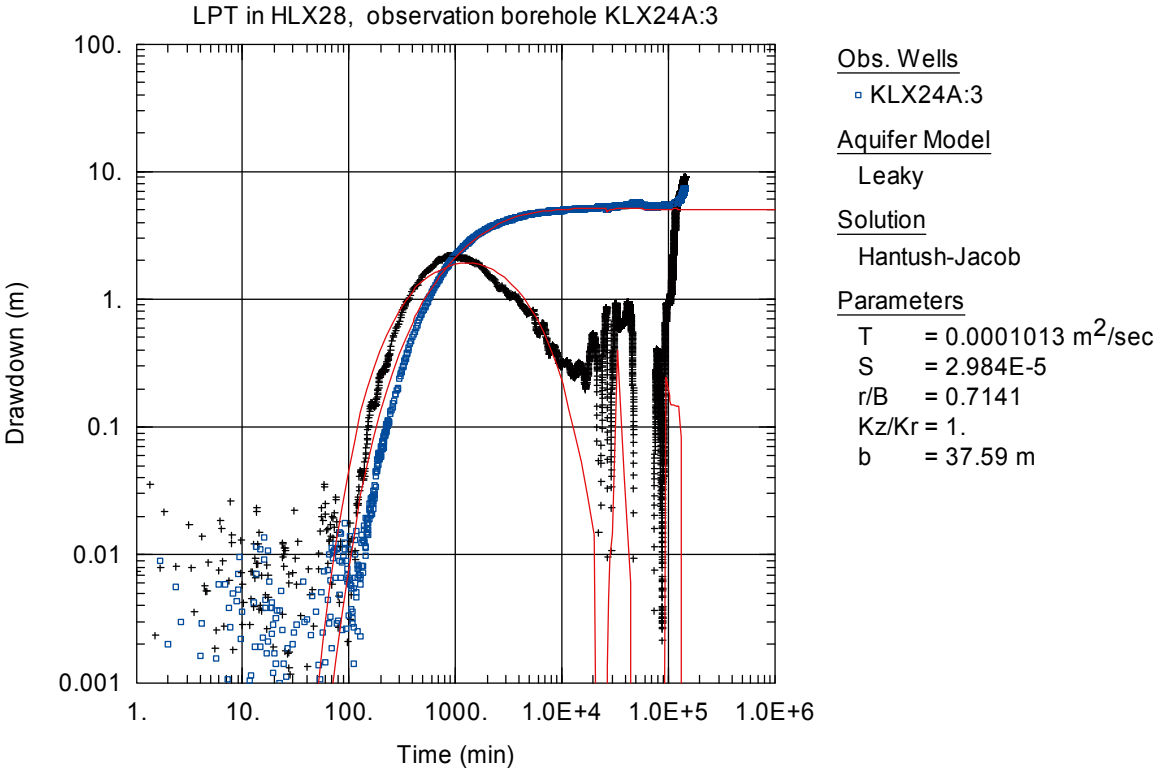

Figure A6-113. *Log-log plot of drawdown (▫) and drawdown derivative, ds/d(ln t) (+), versus time in KLX24A:3 during the interference test in HLX28. Transient evaluation is based on the first part of the drawdown period.*

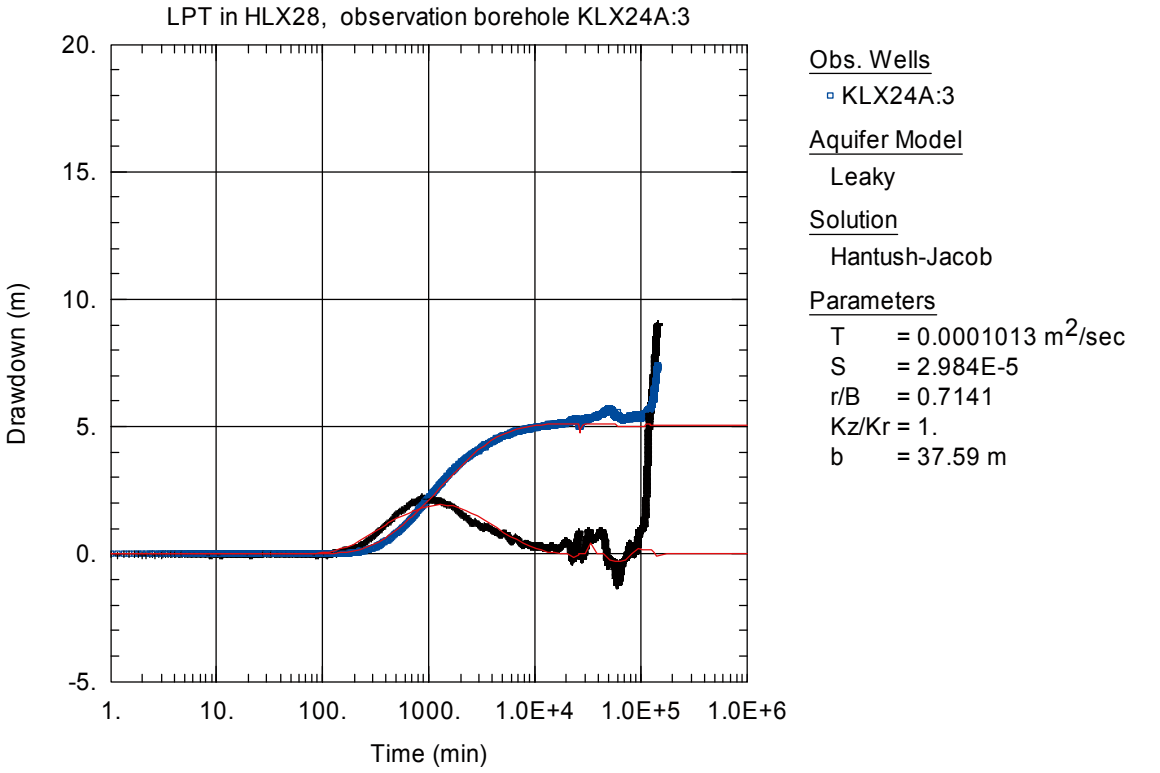

Figure A6-114. *Lin-log plot of drawdown (▫) and drawdown derivative, ds/d(ln t) (+), versus time in KLX24A:3 during the interference test in HLX28. Transient evaluation is based on the first part of the drawdown period.*

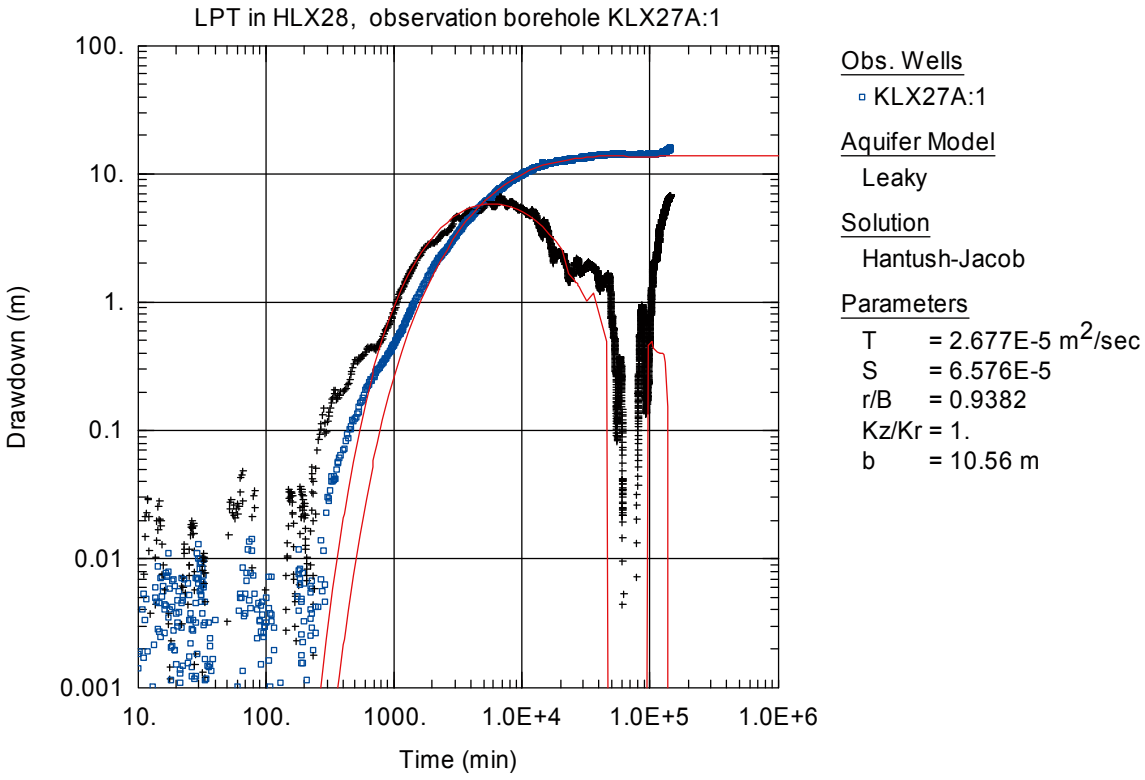

Figure A6-115. *Log-log plot of drawdown (▫) and drawdown derivative, ds/d(ln t) (+), versus time in KLX27A:1 during the interference test in HLX28. Transient evaluation is based on the first part of the drawdown period.*

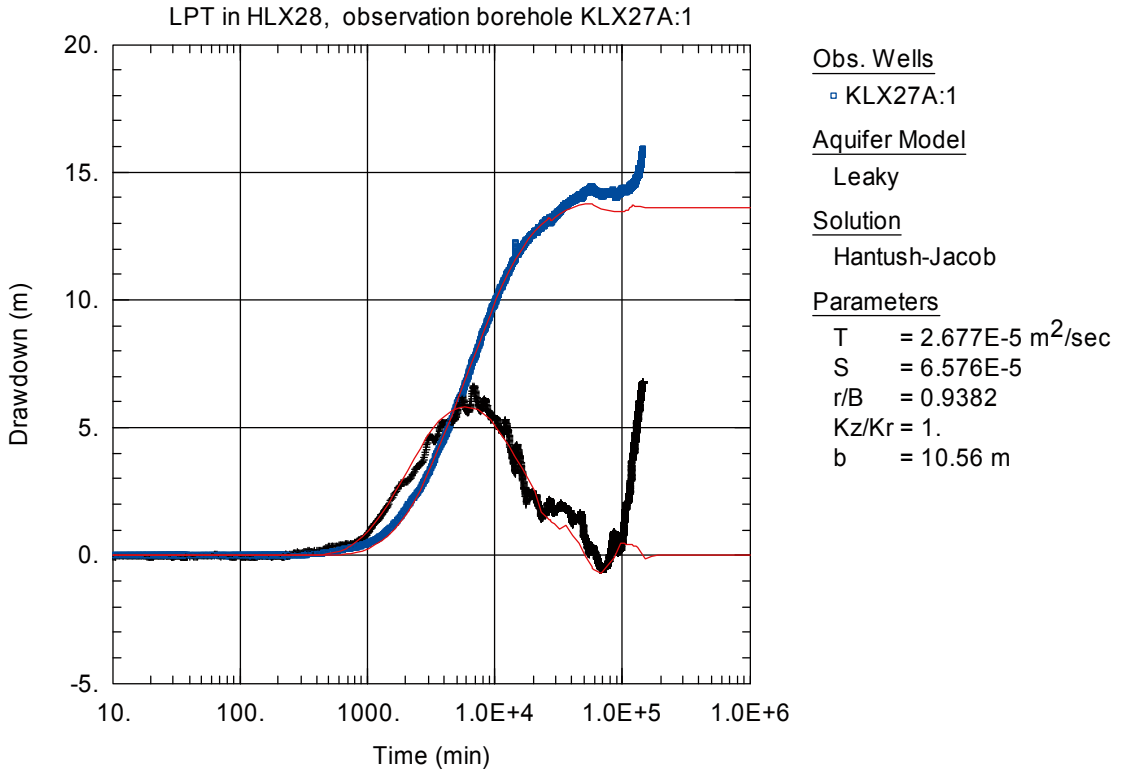

Figure A6-116. *Lin-log plot of drawdown (▫) and drawdown derivative, ds/d(ln t) (+), versus time in KLX27A:1 during the interference test in HLX28. Transient evaluation is based on the first part of the drawdown period.*

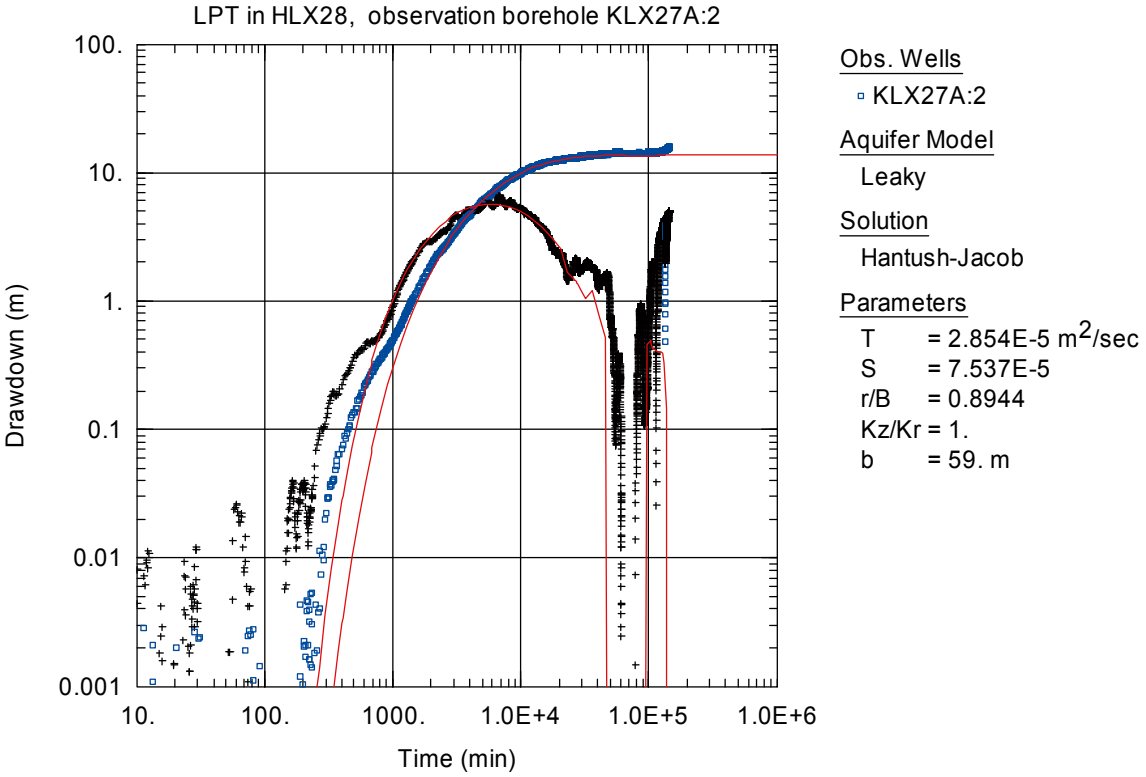

Figure A6-117. *Log-log plot of drawdown (▫) and drawdown derivative, ds/d(ln t) (+), versus time in KLX27A:2 during the interference test in HLX28. Transient evaluation is based on the first part of the drawdown period.*

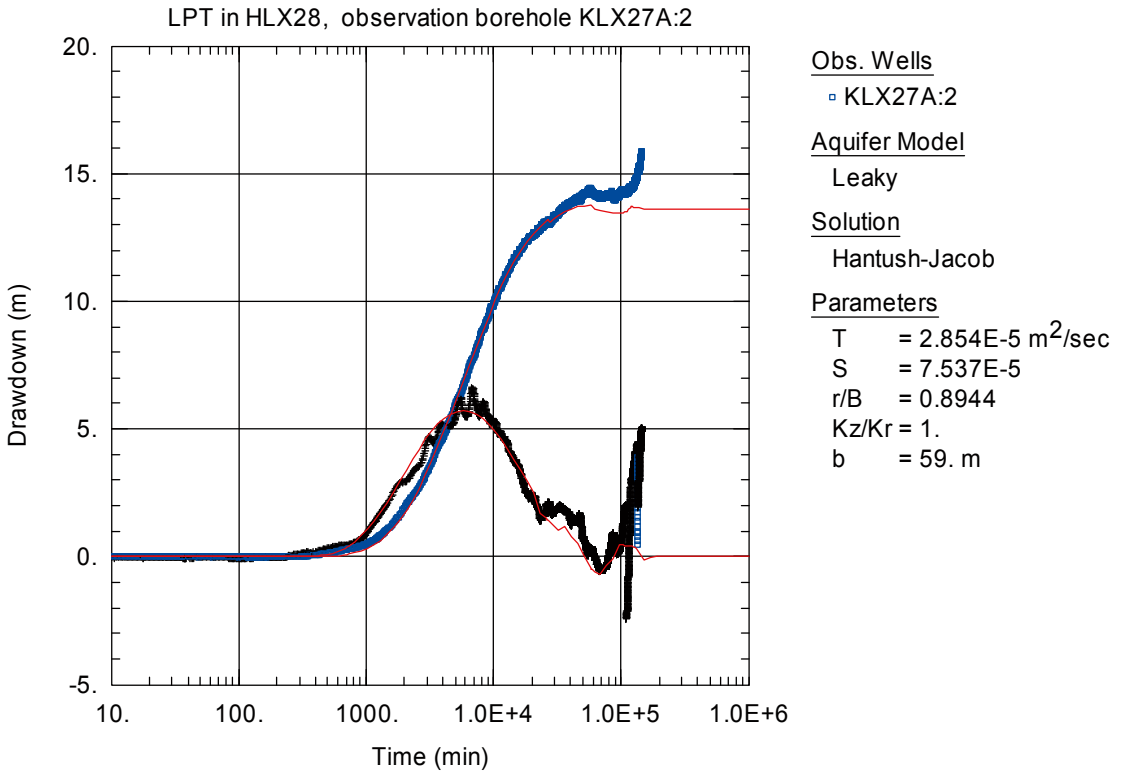

Figure A6-118. *Lin-log plot of drawdown (▫) and drawdown derivative, ds/d(ln t) (+), versus time in KLX27A:2 during the interference test in HLX28. Transient evaluation is based on the first part of the drawdown period.*

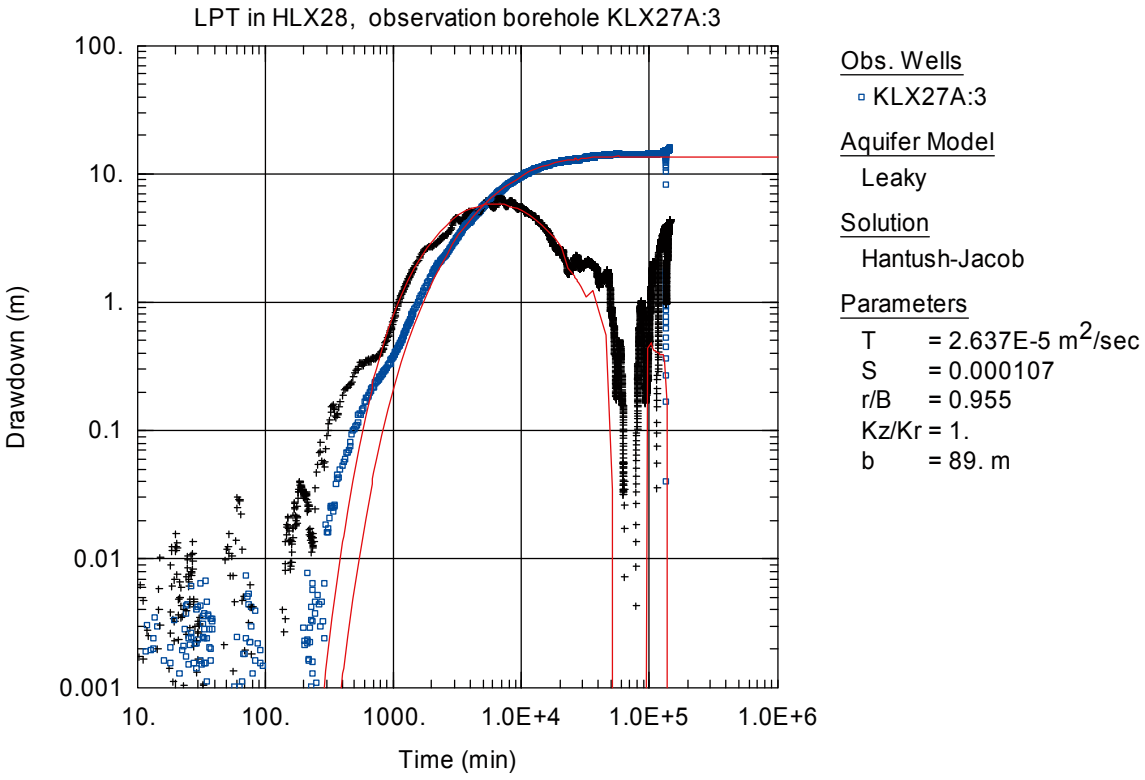

Figure A6-119. *Log-log plot of drawdown (▫) and drawdown derivative, ds/d(ln t) (+), versus time in KLX27A:3 during the interference test in HLX28. Transient evaluation is based on the first part of the drawdown period.*

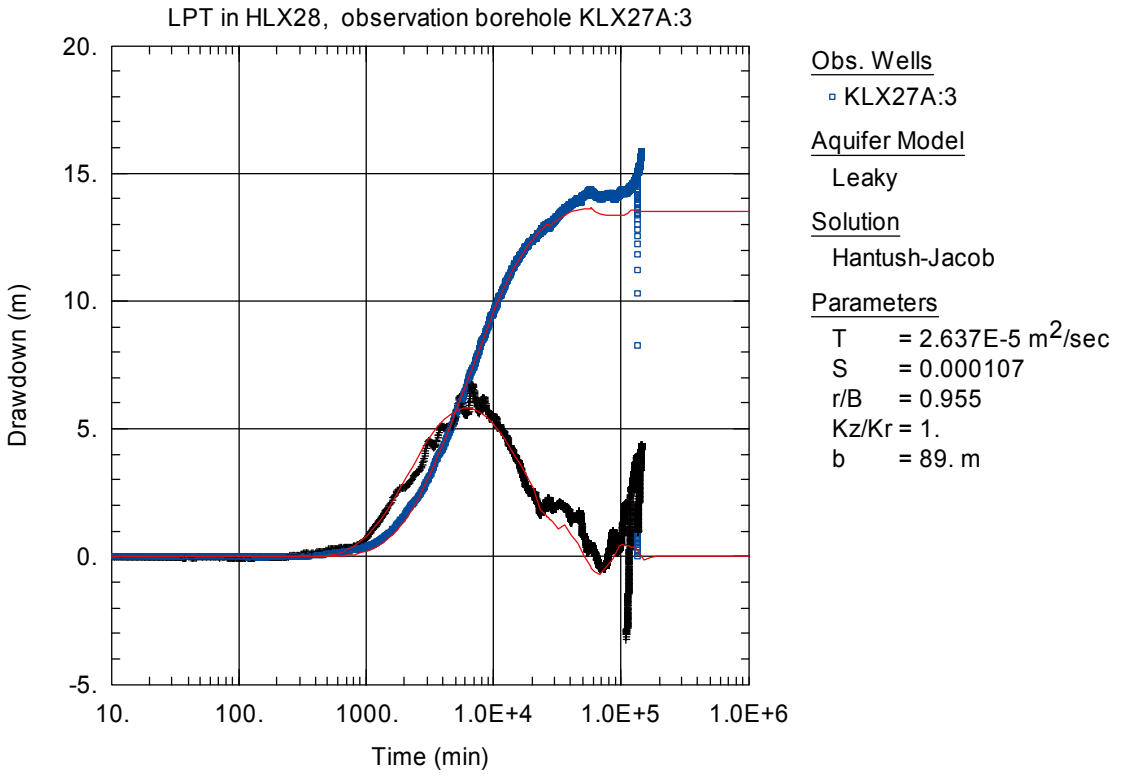

Figure A6-120. *Lin-log plot of drawdown (▫) and drawdown derivative, ds/d(ln t) (+), versus time in KLX27A:3 during the interference test in HLX28. Transient evaluation is based on the first part of the drawdown period.*

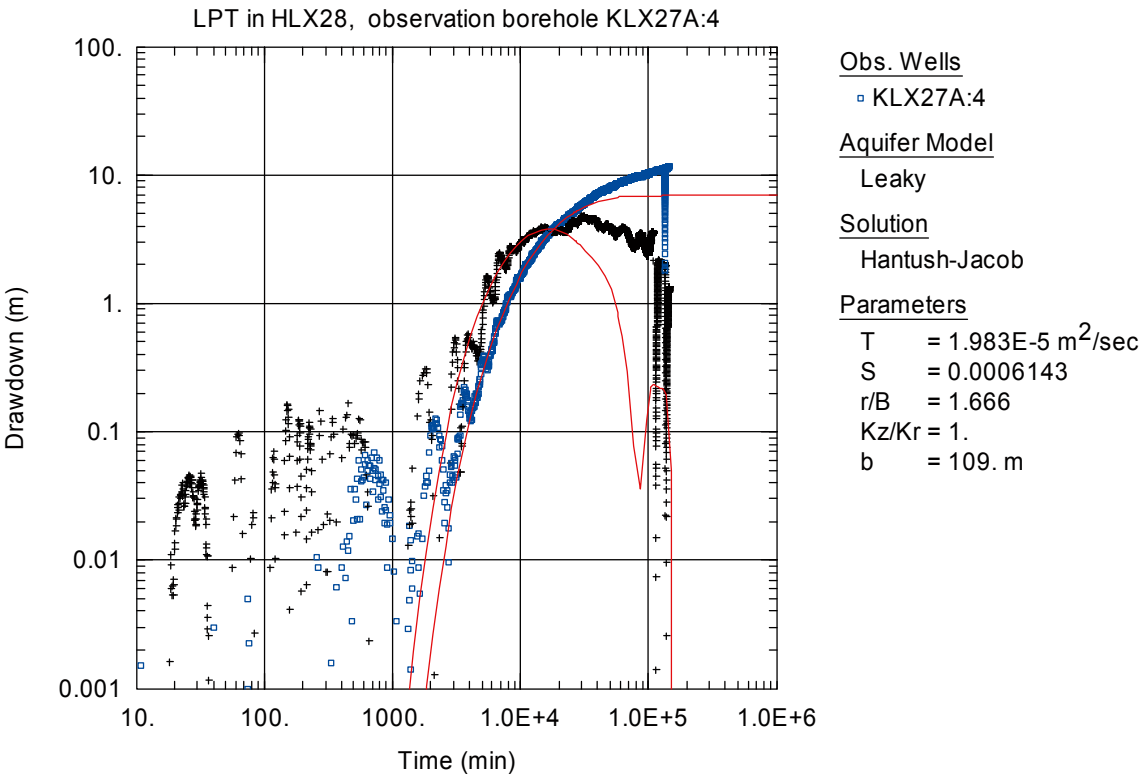

Figure A6-121. *Log-log plot of drawdown (▫) and drawdown derivative, ds/d(ln t) (+), versus time in KLX27A:4 during the interference test in HLX28. Transient evaluation is based on the first part of the drawdown period.*

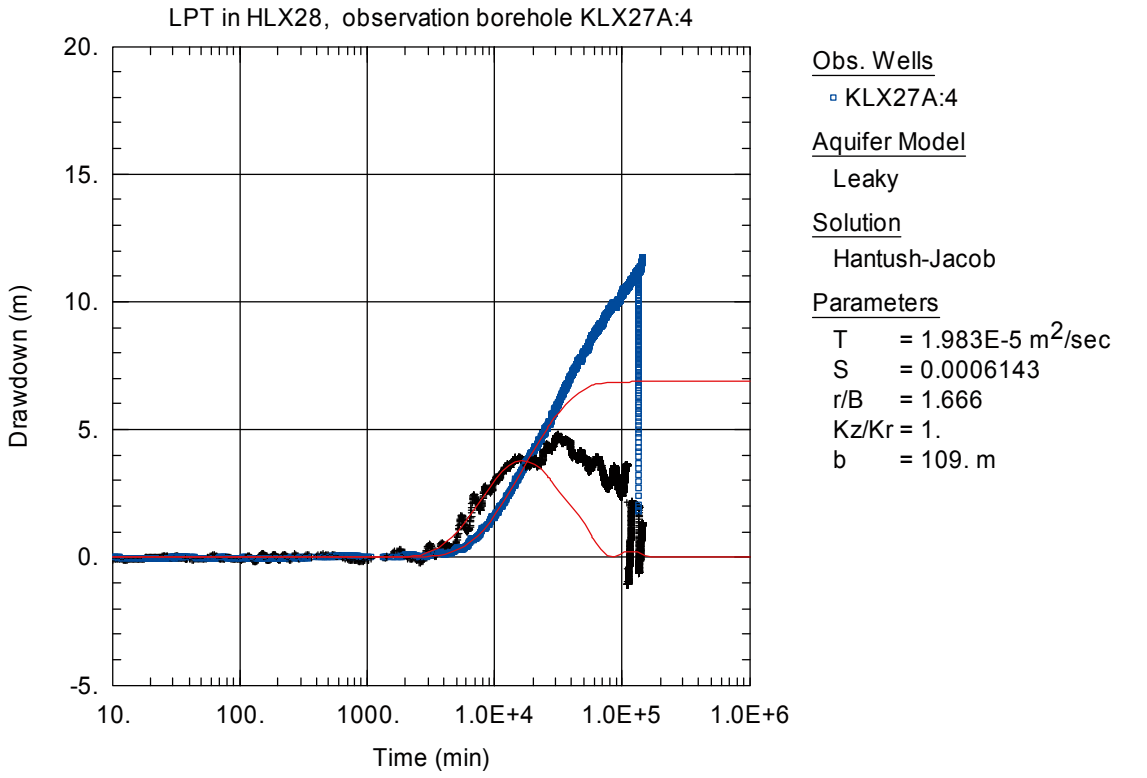

Figure A6-122. *Lin-log plot of drawdown (▫) and drawdown derivative, ds/d(ln t) (+), versus time in KLX27A:4 during the interference test in HLX28. Transient evaluation is based on the first part of the drawdown period.*

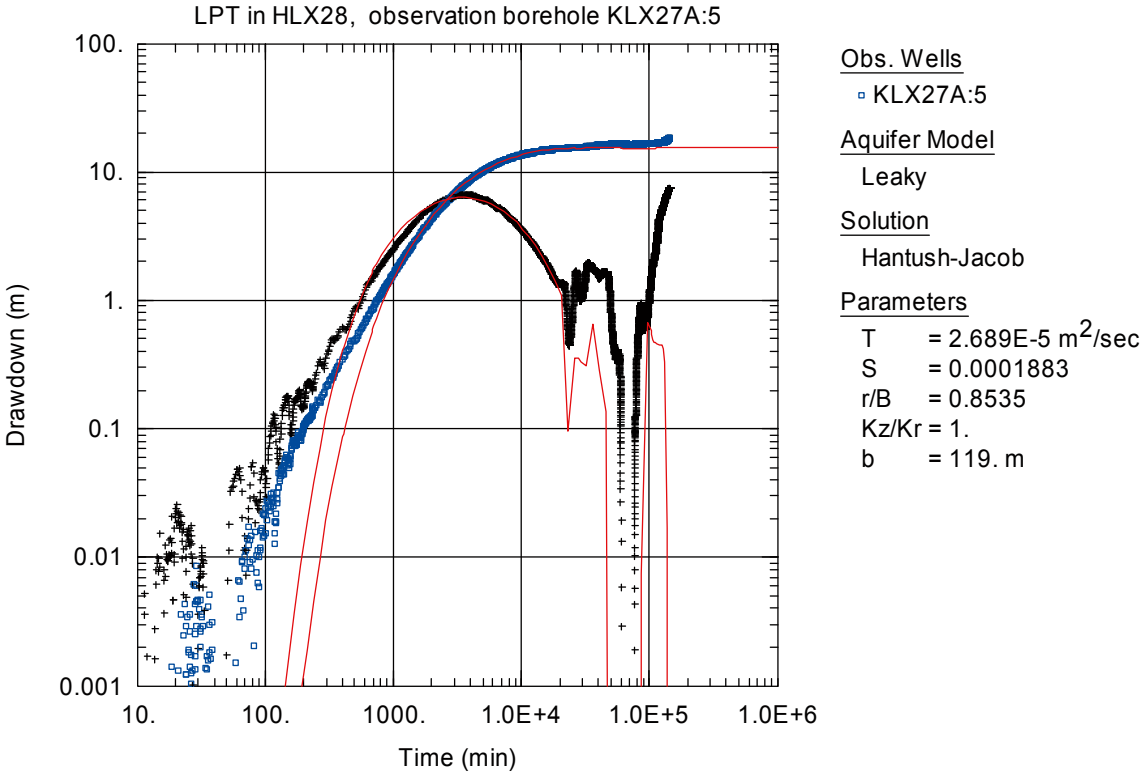

Figure A6-123. *Log-log plot of drawdown (▫) and drawdown derivative, ds/d(ln t) (+), versus time in KLX27A:5 during the interference test in HLX28. Transient evaluation is based on the first part of the drawdown period.*

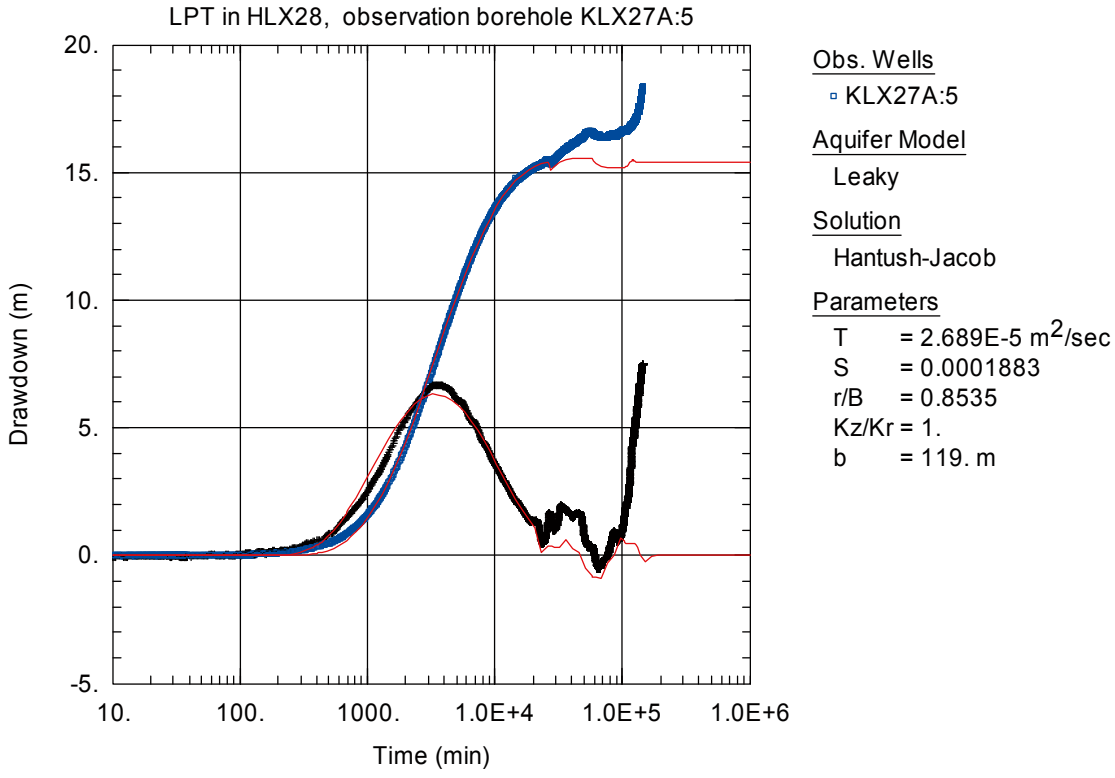

Figure A6-124. *Lin-log plot of drawdown (▫) and drawdown derivative, ds/d(ln t) (+), versus time in KLX27A:5 during the interference test in HLX28. Transient evaluation is based on the first part of the drawdown period.*

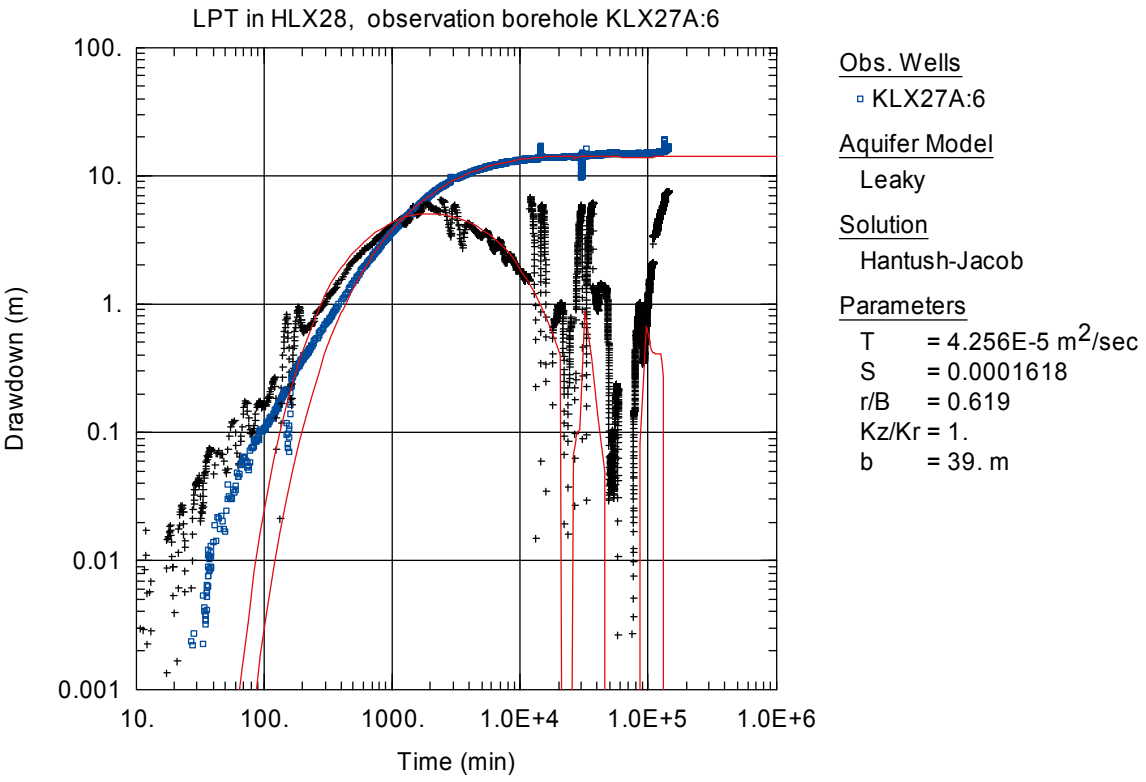

Figure A6-125. *Log-log plot of drawdown (▫) and drawdown derivative, ds/d(ln t) (+), versus time in KLX27A:6 during the interference test in HLX28. Transient evaluation is based on the first part of the drawdown period. The section was used for tracer injection.*

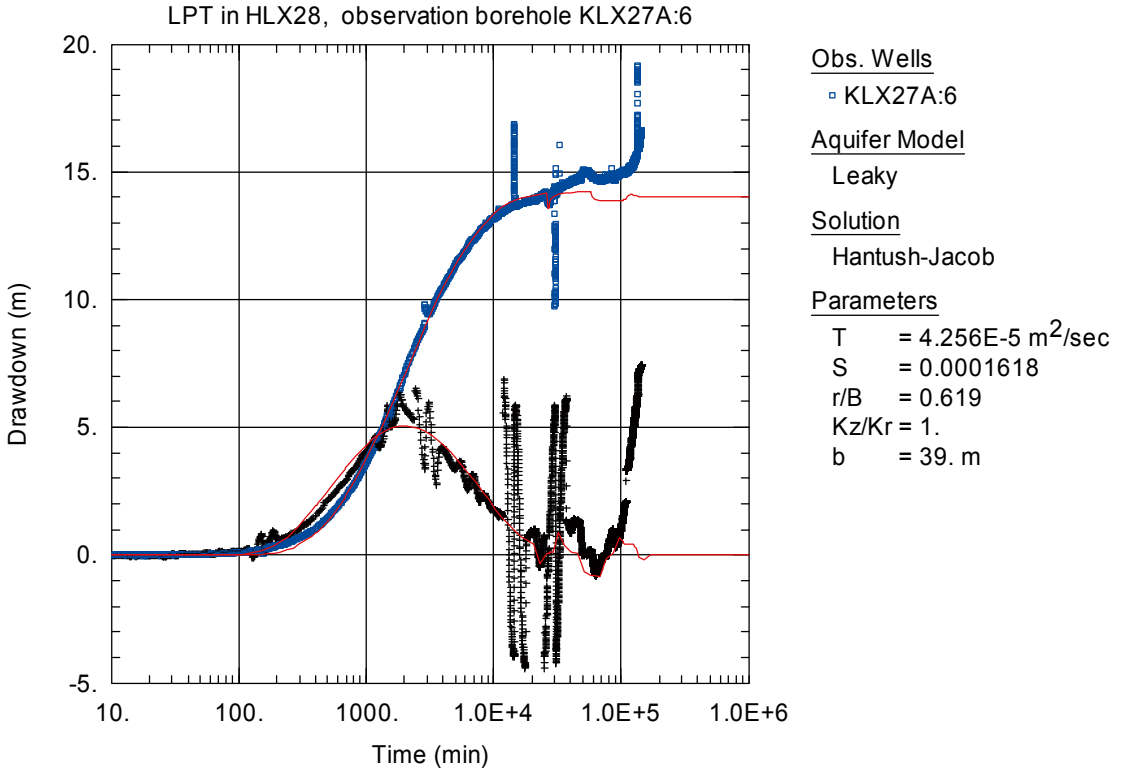

Figure A6-126. *Lin-log plot of drawdown (▫) and drawdown derivative, ds/d(ln t) (+), versus time in KLX27A:6 during the interference test in HLX28. Transient evaluation is based on the first part of the drawdown period. The section was used for tracer injection.*

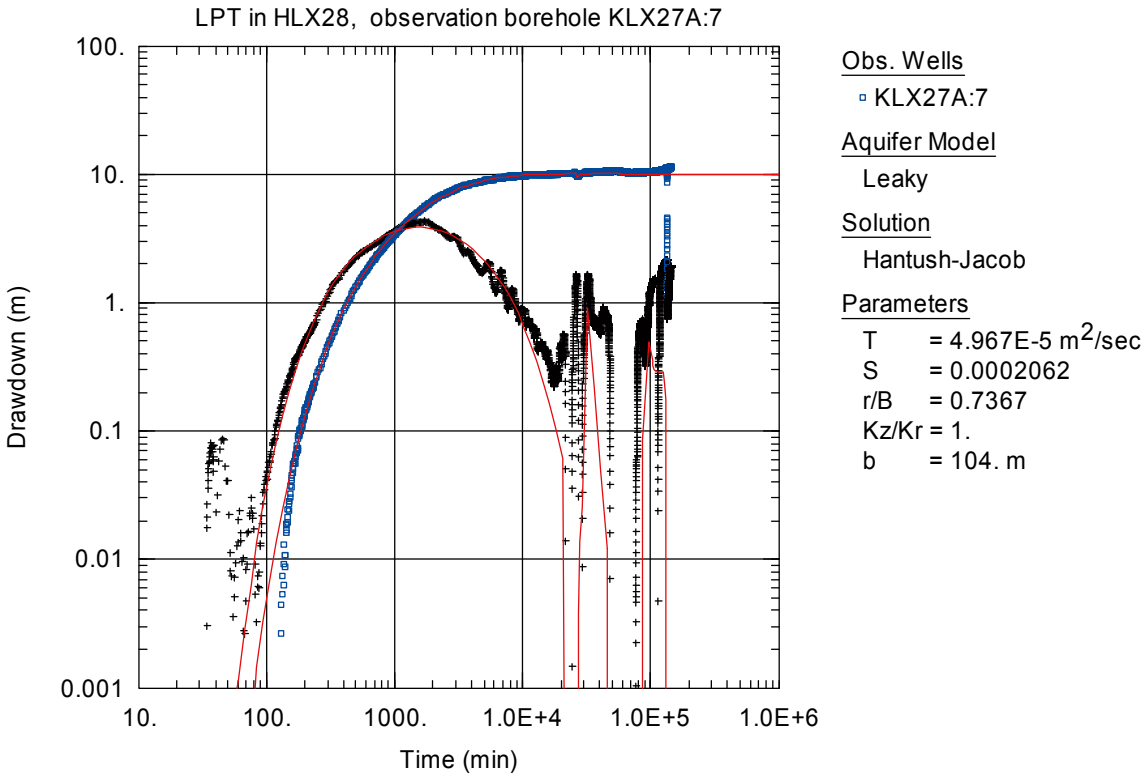

Figure A6-127. *Log-log plot of drawdown (▫) and drawdown derivative, ds/d(ln t) (+), versus time in KLX27A:7 during the interference test in HLX28. Transient evaluation is based on the first part of the drawdown period.*

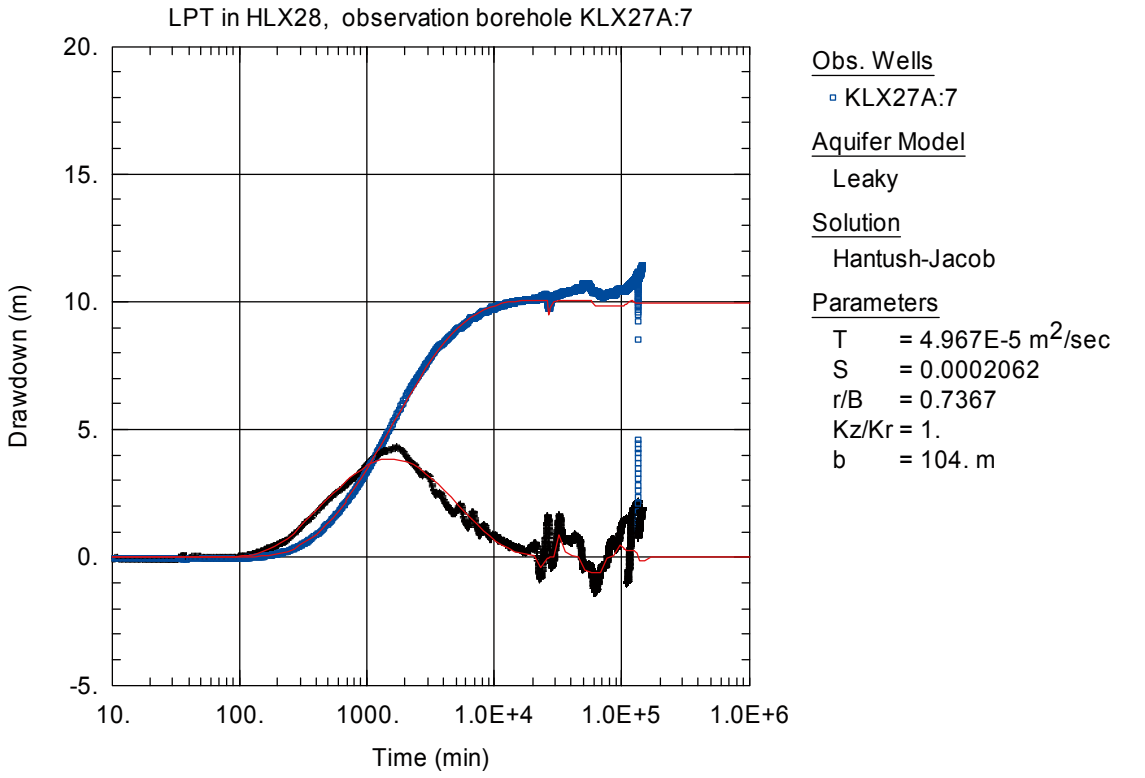

Figure A6-128. *Lin-log plot of drawdown (▫) and drawdown derivative, ds/d(ln t) (+), versus time in KLX27A:7 during the interference test in HLX28. Transient evaluation is based on the first part of the drawdown period.*

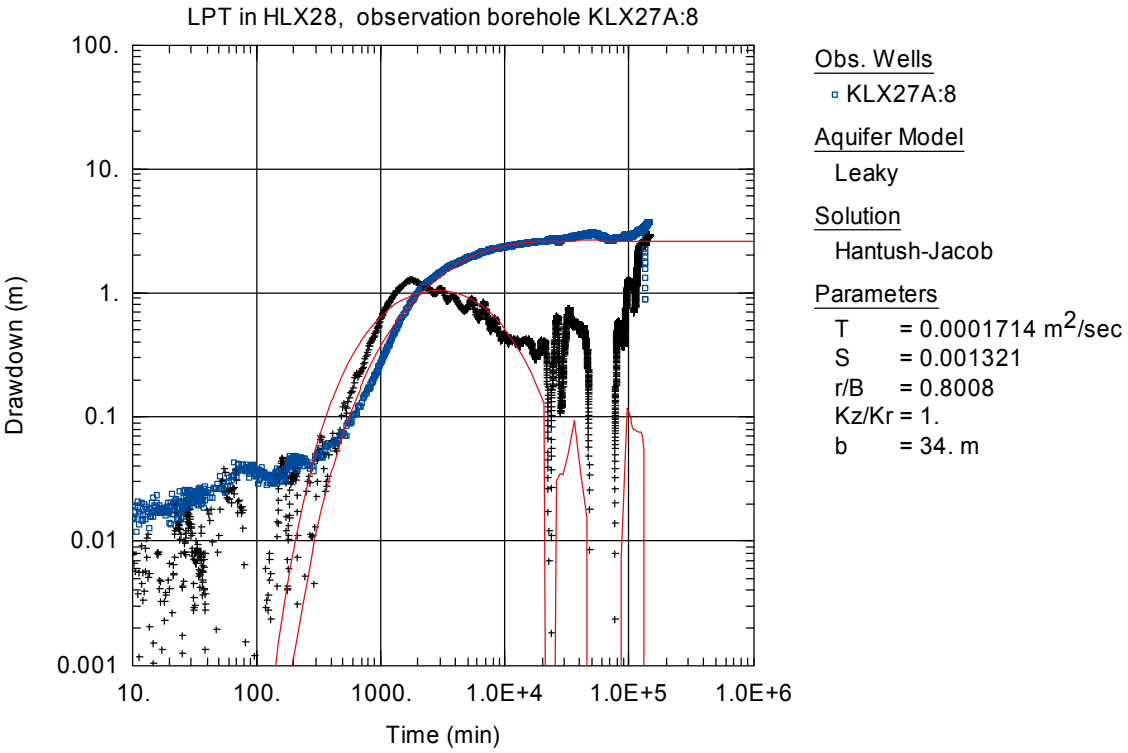

Figure A6-129. *Log-log plot of drawdown (▫) and drawdown derivative, ds/d(ln t) (+), versus time in KLX27A:8 during the interference test in HLX28. Transient evaluation is based on the first part of the drawdown period. Slightly decreasing groundwater level in the section after start of pumping.*

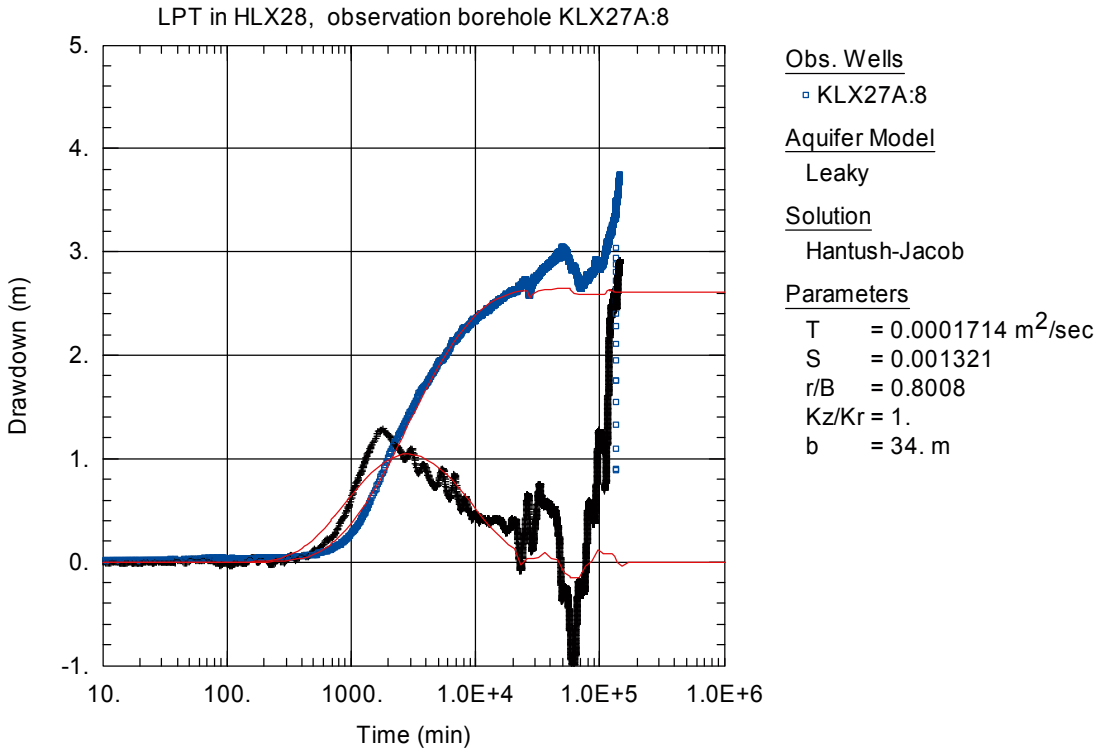

Figure A6-130. *Lin-log plot of drawdown (▫) and drawdown derivative, ds/d(ln t) (+), versus time in KLX27A:8 during the interference test in HLX28. Transient evaluation is based on the first part of the drawdown period. Slightly decreasing groundwater level in the section after start of pumping.*

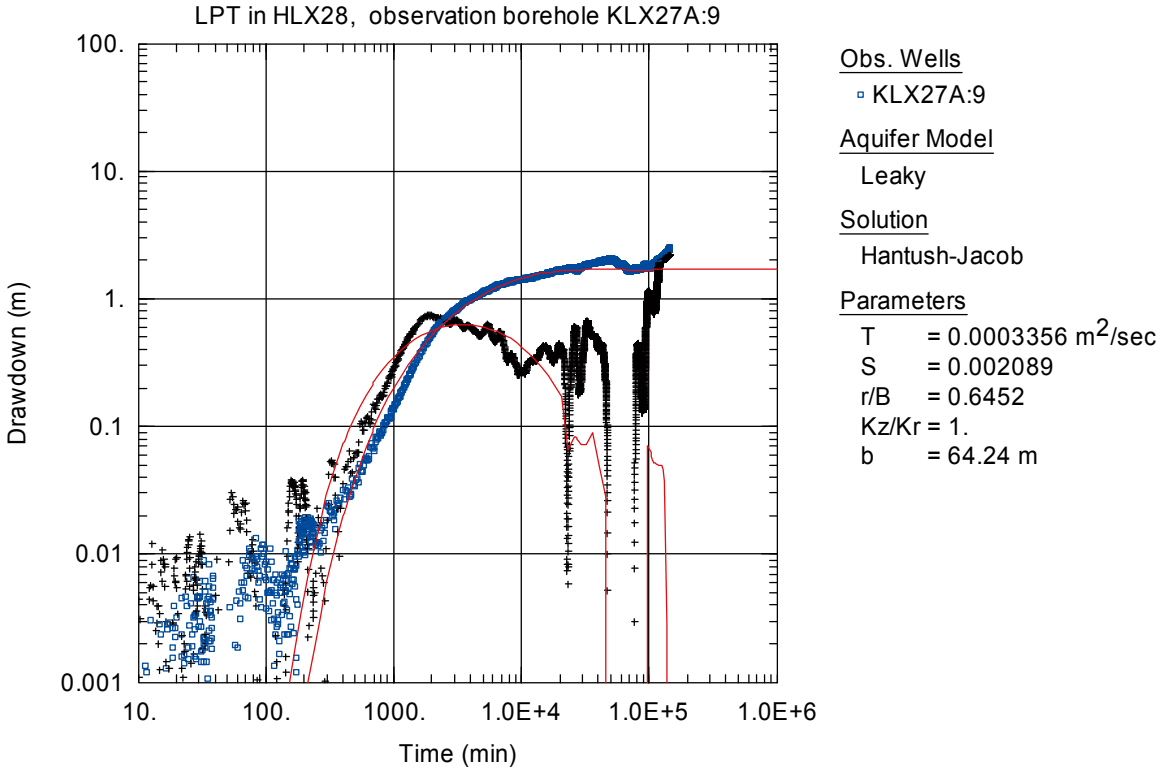

Figure A6-131. *Log-log plot of drawdown (▫) and drawdown derivative, ds/d(ln t) (+), versus time in KLX27A:9 during the interference test in HLX28. Transient evaluation is based on the first part of the drawdown period.*

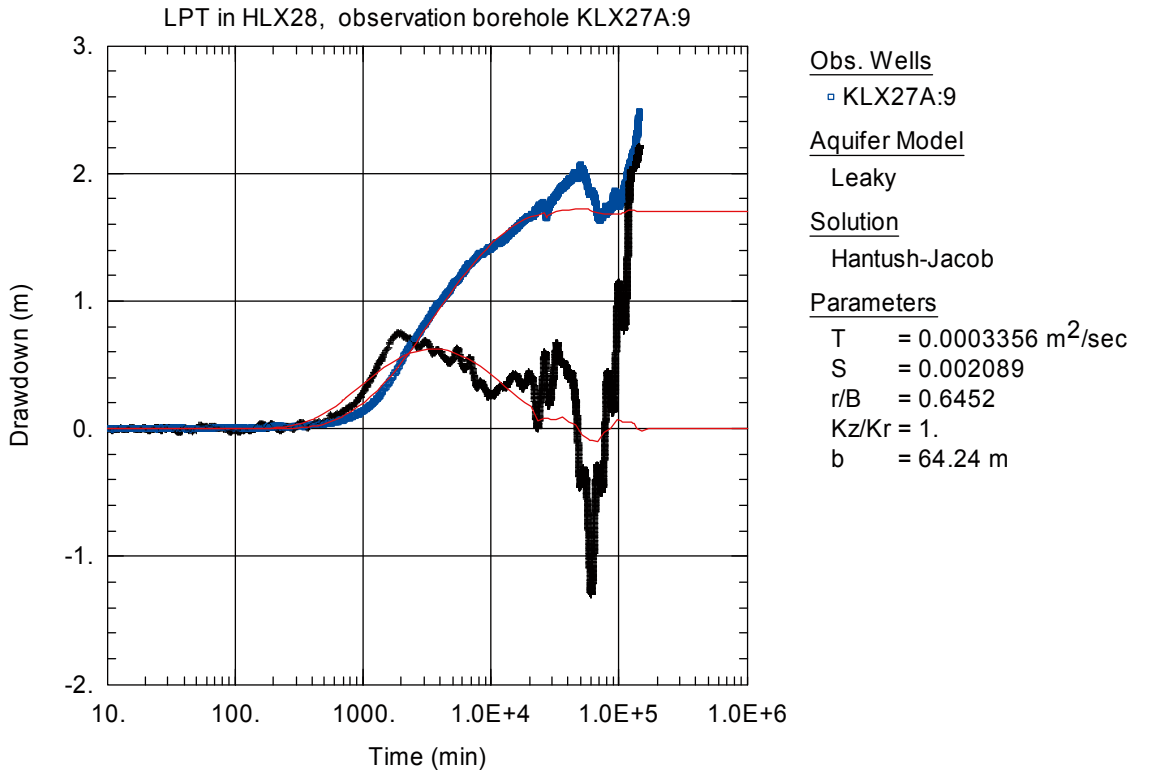

Figure A6-132. *Lin-log plot of drawdown (▫) and drawdown derivative, ds/d(ln t) (+), versus time in KLX27A:9 during the interference test in HLX28. Transient evaluation is based on the first part of the drawdown period.*